Doctoral theses at NTNU, 2024:187

Øystein Gullbrekken

Coupled Transport in Li-ion Battery Electrolytes

Doctoral thesis

NTNU
Norwegian University of Science and Technology
Thesis for the Degree of
Philosophiae Doctor
Faculty of Natural Sciences
Department of Materials Science and Engineering

NTNU
Norwegian University of
Science and Technology

Øystein Gullbrekken

Coupled Transport in Li-ion Battery Electrolytes

Thesis for the Degree of Philosophiae Doctor

Trondheim, May 2024

Norwegian University of Science and Technology
Faculty of Natural Sciences
Department of Materials Science and Engineering

NTNU
Norwegian University of
Science and Technology

NTNU
Norwegian University of Science and Technology

Thesis for the Degree of Philosophiae Doctor

Faculty of Natural Sciences
Department of Materials Science and Engineering

ISBN 978-82-326-7966-9 (printed ver.)
ISBN 978-82-326-7965-2 (electronic ver.)
ISSN 1503-8181 (printed ver.)
ISSN 2703-8084 (online ver.)

Doctoral theses at NTNU, 2024:187

Printed by NTNU Grafisk senter

Preface

This thesis is submitted to the Department of Materials Science and Engineering at the Norwegian University of Science and Technology (NTNU) as a partial fulfillment of the requirements for the degree of Philosophiae Doctor (PhD). The PhD period lasted from May 2020 to May 2024.

The Research Council of Norway is acknowledged for the support to the Norwegian Micro- and Nano-Fabrication Facility, NorFab, project number 295864. Computational resources were provided by Sigma2 - the National Infrastructure for High Performance Computing and Data Storage in Norway through the projects NN9264K and NN9414K, and by the NTNU IDUN/EPIC computing cluster. The main supervisor was Prof. Sverre Magnus Selbach (NTNU) and the co-supervisor was Ass. Prof. Sondre Kvalvåg Schnell (NTNU).

Øystein Gullbrekken
Trondheim, April 2024

List of Articles

Articles included in this thesis

I. **Ø. Gullbrekken**, I. T. Røe, S. M. Selbach, and S. K. Schnell,

Charge Transport in Water-NaCl Electrolytes with Molecular Dynamics Simulations,

Journal of Physical Chemistry B **127**:12 2729-2738 (2023).
DOI: 10.1021/acs.jpcb.2c08047

Contribution: I performed MD simulations, data analysis, paper drafting, review and editing.

II. **Ø. Gullbrekken** and S. K. Schnell,

Coupled ion transport in concentrated PEO-LiTFSI polymer electrolytes,

New Journal of Chemistry **47**:44 20344-20357 (2023).
DOI: 10.1039/D3NJ04065H

Contribution: I performed MD simulations, data analysis, paper drafting, review and editing.

III. **S. Kjelstrup**, A. F. Gunnarshaug, Ø. Gullbrekken S. K. Schnell, and A. Lervik,

Transport coefficients for ion and solvent coupling. The case of the lithium-ion battery electrolyte,

Journal of Chemical Physics **159**:3 034104 (2023).
DOI: 10.1063/5.0158623

Contribution: I performed MD simulations, data analysis, paper review and editing.

IV. **Ø. Gullbrekken**, A. F. Gunnarshaug, A. Lervik, S. Kjelstrup, and S. K. Schnell,
Effect of the Ion, Solvent, and Thermal Interaction Coefficients on Battery Voltage,
Journal of the American Chemical Society **146**:7 4592–4604 (2024).
DOI: 10.1021/jacs.3c11589

Contribution: I performed equilibrium MD simulations, data analysis, paper drafting, review and editing.

Manuscripts not included in this thesis

I. **Ø. Gullbrekken**, K. Eggestad, M. Tsoutsouva, B. A. D. Williamson, D. Rettenwander, S. K. Schnell, M. A. Einarsrud, and S. M. Selbach,
Phase evolution and thermodynamics of cubic $Li_{6.25}Al_{0.25}La_3Zr_2O_{12}$ studied by high-temperature X-ray diffraction,

Contribution: I synthesized oxide powders, and performed X-ray diffraction, thermal characterization, data analysis and paper drafting.

II. **Ø. Gullbrekken**, F. Bresme, S. M. Selbach, and S. K. Schnell,
Electric Double Layer Studies of Li electrode - PEO-LiTFSI electrolyte by Constant Potential Simulations,

Contribution: I performed MD simulations, data analysis and paper drafting.

Acknowledgments

First and foremost, thank you to my supervisors Sverre M. Selbach and Sondre K. Schnell for guiding me through the PhD, for many interesting and helpful discussions and for keeping my spirits up. I also appreciate all the help from other Professors and Staff at the Department of Materials Science and Engineering.

Great acknowledgment goes to Anders Lervik, Astrid Fagertun Gunnarshaug and Signe Kjelstrup for the collaboration on studying the electrolyte effect on battery performance. Thank you to Ingeborg Røe Treu for helping me with molecular dynamics simulations, the analysis of correlations files and python programming. I also want to thank Kristoffer Eggestad and Benjamin Williamson for their help with doing and analyzing density functional theory calculations. Thank you to Maria Tsoutsouva for great help with high-temperature X-ray diffraction of oxide powders, and Kyyas Seyitmuhammedov for the help with ICP-MS analysis of said powders.

In the spring of 2023, I was lucky to visit Fernando Bresme and his research group at Imperial College in London for three months. Thank you to Fernando for being a great host to me and for his enthusiasm and interest in my research. Thank you to "Christiania Spigerverks og Gunnar Schjelderups legat til NTNU" and "Norges tekniske høgskoles fond" for scholarship support for the research stay in London.

Lastly, thank you to all my colleagues and friends at K1 for a great working and social environment, and thank you to my family and friends for always supporting me.

Summary

Lithium-ion batteries play a crucial role in the transition from a fossil fuel-based to a sustainable energy economy. They will be used primarily to electrify transport but also in stationary energy storage as a buffer for intermittent energy sources such as solar and wind. Better batteries with higher energy and power density are required for new, demanding applications like long-distance transport of goods by road, electric aircraft, and transport by sea. These batteries require new electrode materials that can store more lithium per weight and volume. New electrode materials must be accompanied by new electrolytes that are optimized for the electrodes. Additionally, it is desirable to be able to charge the batteries faster. The chemical energy inside the batteries cannot be fully converted to electrical energy during use. Charging and discharging of batteries, like all non-equilibrium processes, result in losses by entropy increase. The batteries should be designed and operated in such a way that these losses are minimized. Electrolytes with optimized transport properties are essential to meet all these criteria.

Central in all lithium-ion batteries is the electrolyte which transports electric charge (Li^+) in between the electrodes during charge-discharge cycles. The electrolyte in current lithium-ion batteries is a complex multi-component mixture composed of a lithium salt dissolved in several polar solvents. The transport (diffusion) of Li^+ is coupled to the movements of the other species in the mixture. Coupling also exists between transport of mass, charge and heat, all of which are prevalent in battery electrolytes. These coupling effects have a significant impact on the charge transport in the electrolyte and ultimately on the battery performance, i.e. the charge-discharge capabilities. Improving the understanding of coupling effects in battery electrolytes has been a major part of this work.

Li^+ ions face various barriers in their journey through the electrolyte. There is ohmic resistance due to finite conductivity of the electrolyte, and gradients in com-

ponent concentrations and temperature caused by mass transfer limitations and the reactions occurring at the electrode surfaces. These barriers constitute losses in the battery by reduction of the battery voltage and the resulting energy output. In this work, we have examined and quantified these losses, enabling a deeper understanding of the electrolyte transport mechanisms and facilitating a more accurate development and optimization of new electrolytes. A bottom-up understanding of the macroscopic transport properties of electrolytes due to the microscopic atomic and molecular motions is advantageous. The main tool for these studies, molecular dynamics simulations, provides the means for examining electrolytes from both these perspectives.

In this work we have studied several well-known electrolytes, water-NaCl, the polymer electrolyte PEO-LiTFSI, and common liquid carbonate-based electrolytes used in commercial lithium-ion batteries. All the time, we have focused on the coupling effects present in mass transport and their role in determining the transport properties. An example of such coupling is that transport of Li^+ leads to solvent segregation and polarization in mixed carbonate solvents. The coupling between transport of mass, charge and heat was also studied in the carbonate-based electrolytes. The transport in equilibrium simulations can be characterized using the Nernst-Einstein method, employing self-diffusion coefficients which give transport without gradients and coupling, or the Onsager coefficients which include coupling. The Nernst-Einstein method neglects all coupling phenomena and should be avoided, unless for comparison to the Onsager coefficients as a way of examining the ideality of the electrolyte. We find that coupling effects are important in all these electrolytes and need to be taken into account for a better understanding of the transport in these electrolytes.

Populærvitenskapelig sammendrag

Litium-ion-batterier spiller en viktig rolle i overgangen fra dagens fossilbaserte energiøkonomi til framtidas bærekraftige energiøkonomi. Vi trenger batterier for å elektrifisere transport, både til lands, vanns og i lufta og kutte bruken av olje, gass, bensin og diesel. Elbiler med Li-ion-batterier har blitt veldig populære i Norge og utgjør over 90 % av nye personbiler så langt i 2024 (kilde: OFV). Etter hvert som stadig mer energi kommer fra fornybare kilder som sol og vind vil det være behov for energilagring når sola ikke skinner og vinden ikke blåser. Her kan Li-ion-batterier også være et godt alternativ. For å muliggjøre elektriske lastebiler for langdistanse-transport og elektriske fly trengs det batterier med høyere energitetthet enn i dag. Dette krever utvikling av nye elektrodematerialer som kan lagre mer litium per vekt og volum. Nye elektrodematerialer må ledsages av nye elektrolytter som er tilpasset de nye elektrodene. Det er dessuten ønskelig at man kan lade batteriene raskere enn i dag for å spare tid. Elektrolytter med optimaliserte transportegenskaper er nødvendig for å oppnå alle disse målene.

Utladning og oppladning av batterier er eksempler på ikke-likevektsprosesser. Ikke-likevektsprosesser kjennetegnes ved at det skjer en endring i systemet. Endringer er irreversible, man kan aldri få tilbake den opprinnelige tilstanden når en endring først har skjedd. Dette er et resultat av termodynamikkens andre lov, at entropien øker i ikke-likevektsprosesser. Transportprosessene som skjer i et batteri under utladning og oppladning medfører alltid økning i entropien. Vi kan anse dette som tap i prosessen, vi klarer ikke å omvandle all kjemisk energi i batteriet til elektrisk energi. Om vi kan forstå hvordan disse tapene skjer kan vi designe og drifte batterier på en slik måte at tapene minimeres. Teorien for å forstå dette kalles ikke-likevekts termodynamikk og er mye brukt i dette arbeidet.

Elektrolytten er en essensiell del av et batteri. Den sørger for at elektrisk ladning kan transporteres (ved transport av Li^+ ioner) mellom elektrodene under utladning og op-

pladning av batteriet. Elektrolytten i dagens Li-ion-batterier er komplekse blandinger som består av et litium salt som er oppløst i en blanding av polare løsemidler. Ingen av komponentene i elektrolytten kan bevege seg uavhengig av de andre komponentene i blandingen — det er koblinger mellom dem. Dette betyr at transporten av en komponent vil bli påvirket av bevegelsene og transporten av andre komponenter i blandingen. Disse koblingseffektene kan ha en betydelig innvirkning på transporten av ladninger og dermed ytelsen til et Li-ion-batteri. I et batteri er det transport av masse, elektrisk ladning og varme. Det vil også være koblingseffekter mellom disse transport-typene. En stor del av denne avhandlingen handler om studier av slike koblinger og hvordan de kan påvirke batteriytelsen.

Vi har studert flere velkjente elektrolytter i dette arbeidet; saltvann (med NaCl-salt), polymer-elektrolytten PEO-LiTFSI, og vanlige karbonat-baserte flytende elektrolytter brukt i kommersielt tilgjengelige Li-ion-batterier. Hele tiden har vi fokusert på koblingseffektene som er tilstede i massetransport og hvordan de påvirker transportegenskapene. Det viser seg at disse koblingseffektene er signifikante og må tas hensyn til for å forstå transportegenskapene bedre. Dette har ikke alltid blitt gjort i tidligere elektrolytt-studier. Vi har beregnet Onsager-koeffisienter for å karakterisere og kvantifisere disse koblingseffektene. Verktøyet i våre studier har vært såkalte molekyldynamiske simuleringer. Med slike simuleringer kan vi beregne makroskopiske transportkoeffisienter og samtidig se på hvordan de mikroskopiske mekanismene mellom atomer og molekyler foregår. Å få innsikt i sammenhengen mellom makroskopiske størrelser og mikroskopiske mekanismer er svært verdifullt for å øke forståelsen av elektrolytter generelt, og for å forstå deres funksjon i Li-ion-batterier spesielt. Denne forståelsen kan brukes til å akselerere utviklingen av bedre elektrolytter i framtidige batterier.

Contents

1 Motivation and aim of work

1.1 Motivation

Sustainable energy use is essential for the continued survival and prosperity of our civilization. This means that we need to replace fossil fuels, which currently make up about 85 % of the global primary energy consumption [1], by energy sources which do not emit greenhouse gases and are renewable. Furthermore, avoiding potentially catastrophic climate change caused by burning of fossil fuels is one of the gravest and greatest challenges for humanity in the next decades [2]. The shift away from fossil fuels must be accelerated to reduce the total amount of greenhouse gases emitted. To enable sustainable transport without fossil fuels, we need technologies that can store energy in an effective manner. The lithium-ion battery is currently the rechargeable battery with highest energy density and has been an enormously successful technology since it was commercialized by Sony in 1991 [3]. In the coming years, lithium-ion batteries will likely become even more important to reduce emissions of greenhouse gases and make transport sustainable.

To accelerate the adoption of lithium-ion batteries for existing applications like electric vehicles, and new applications such as long-distance transport by trucks and electric aviation, the rate performance of the batteries must be improved, especially during charging. The United States Department of Energy has set a target for next-generation batteries of less than 15 minutes charging time to reach 80 % state of charge [4]. New electrolytes that can transport lithium ions faster are needed to achieve this goal. In addition, next-generation batteries with higher energy density using new electrode materials also require new electrolytes [5–7]. A fundamental understanding of the transport and interface properties of electrolytes is highly beneficial for the development of new electrolytes and for optimal operation of current batteries. The ability to relate the microscopic mechanisms and interactions to macroscopic properties and

performance could potentially enable molecular level design of new electrolytes to achieve specific goals with respect to transport and other electrolyte properties. This could accelerate the development of better Li-ion batteries.

1.2 Aim of work

The aim of this work was to contribute to a more fundamental understanding of the transport properties of lithium-ion battery electrolytes and how they impact battery operation and performance. The charge transport in the electrolyte influences the energy conversion in lithium-ion batteries, both the efficiency and the rate at which the energy can be converted. As lithium-ion batteries become increasingly important in today's society, even small improvements to the batteries in terms of energy density, charge-discharge capabilities and rate performance can have a significant importance. A deeper understanding of the transport properties of relevant electrolytes for lithium-ion batteries can facilitate such improvements. Additionally, a better understanding of transport in electrolytes is beneficial when designing new electrolytes for next-generation batteries. We have used molecular dynamics simulations to study several electrolytes which allow us to compute macroscopic transport properties while examining the microscopic molecular mechanisms that govern them. This connection is valuable to promote the understanding.

In particular, we have focused on the effects of various forms of coupling in the electrolytes. Electrolytes for modern lithium-ion batteries are multi-component mixtures where transport and motion of one species is inevitably linked to the transport of other species in the mixture. The coupling can be quantified by Onsager transport coefficients that are obtained directly from molecular simulations. We have examined the coupling effects in mass transport, but also the coupling between transport of mass, charge and heat that occur in the battery electrolyte. From the coefficients that characterize the transport and coupling effects, we have quantified their effect on the battery performance.

2 Lithium-ion batteries

In this chapter we will introduce important concepts and theories for understanding transport in lithium-ion battery electrolytes. We will start, however, by introducing the operating mechanisms of lithium-ion batteries and the materials used in them.

2.1 Working principle

The electrochemical cell makes up the core of lithium-ion and other rechargeable batteries. The cell contains two electrodes, an anode and a cathode, separated by an electrolyte which is electronically insulating but conducts electric current by ionic motion. When the cell supplies energy, chemical energy stored in the cell is converted to electrical energy by means of redox reactions occurring at the anode and cathode. The oxidation reaction occurs at the anode and the reduction reaction occurs at the cathode.

In a lithium-ion battery, one redox reaction corresponds to one lithium leaving or entering the anode or cathode, and one electron going from the anode to the cathode through an outer circuit powering an external device. Upon charging of the battery, the reactions are reversed and the oxidation and reduction reactions occur at opposite electrodes in comparison to discharging. The behavior at discharging is the convention for naming the electrodes anode (negative electrode) and cathode (positive electrode). The driving force for the discharge process is the electrochemical potential difference of the lithium ions in the anode and the cathode [8]. The electrochemical potential of an ion i is defined as the sum of its chemical potential, μ_i, and electrostatic (Maxwell) potential ψ multiplied by the Faraday constant F and the charge valency z_i [9]:

$$\tilde{\mu}_{\mathrm{Li}^+} = \mu_{\mathrm{Li}^+} + z_{\mathrm{Li}^+} F\psi. \tag{2.1}$$

In short, the lithium ion prefers to be in the cathode due to the stronger chemical bond-

ing there than in the anode. The journey of a lithium ion consists of diffusion/migration in the electrode materials, transfer across the electrode/electrolyte interfaces, and diffusion/migration in the electrolyte [10]. Several electrochemical cells are connected to make a lithium-ion battery. A schematic of the different parts of a Li-ion battery cell is shown in Figure 2.1.

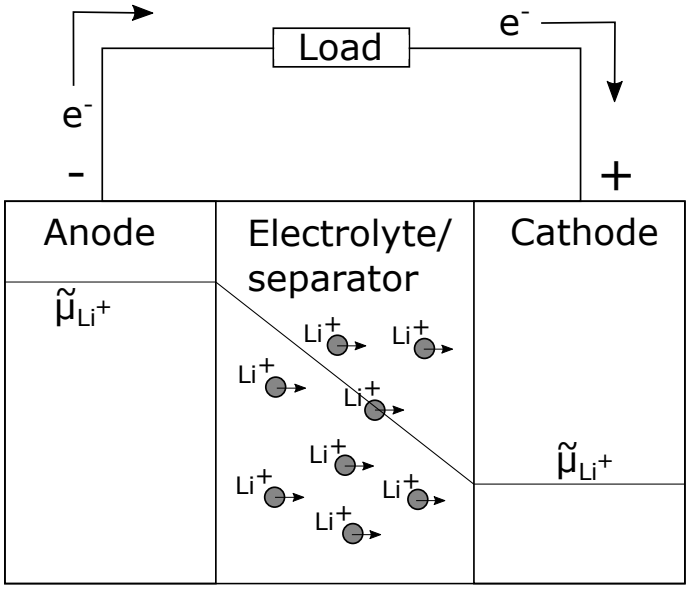

Figure 2.1: Schematic of Li-ion battery cell showing direction of electrons and lithium ions during discharge. The electrochemical potential profile of Li^+, $\tilde{\mu}_{Li^+}$, through the battery cell is shown.

The energy density of the battery is given by the specific capacity C of the electrodes and the voltage difference V:

$$E = CV. \tag{2.2}$$

The specific capacity of an electrode is directly related to the number of lithium atoms which can be reversibly extracted from and inserted into the electrode, and is usually denoted by mAh per g. The cell voltage is given by the energy difference of the redox energies of the anode and cathode [11] or the difference in oxidation and reduction potentials of the anode and cathode. This voltage is called the open-circuit potential and reflects the amount of energy released by the redox reaction (reaction Gibbs energy), but it depends on the state of charge [12]. Polarization of the battery influences the voltage during battery operation meaning that the cell voltage will vary with respect to the state of charge and the rate at which energy is withdrawn. Polarization here refers

to various gradients occurring in different parts of the battery and the activation energy for the electrochemical reaction [13]. In the electrolyte, concentration gradients of components can arise due to mass transfer limitations and coupling effects, and temperature gradients due to differences in heat generation at the anode and cathode [14, 15]. There can be concentration gradients of Li^+ in the electrode materials caused by slow diffusion [16, 17] and different material phases present at different states of charge which might also influence transport of lithium [18–21]. These distinct phenomena can interact as well and all can influence the battery voltage and performance.

2.2 Materials in lithium-ion batteries

The electrodes of current lithium-ion batteries are made up of active material particles held together by a polymer binder that are coated onto a thin metal current collector foil. Typically, graphite is used as the anode active material. At the cathode there are several options, e.g. $LiCoO_2$ [22] which is common in consumer electronics, lithium nickel manganese cobalt oxides ($LiNi_xMn_yCo_{1-x-y}O_2$, NMC [23–25]) which is used in long-range electric vehicles and stationary storage, and lithium iron phosphate ($LiFePO_4$, LFP [18]), increasingly used in smaller electric vehicles and stationary storage [26, 27].

In order to make batteries with higher energy density, new electrode materials are required. Graphite has the highest gravimetric capacity of the above materials, so the focus has been on improving the cathode material. Increasing the nickel content in NMC materials has been a strategy for enhancing the energy density by increasing the capacity of the cathode [28]. Further into the future, entirely new cathode materials are necessary to continue increasing the energy density [29, 30].

On the anode side silicon is a promising material, with ten times higher gravimetric capacity than graphite [31]. The ultimate anode material, sometimes called the "the holy grail" of lithium-based batteries, is lithium metal due to having the highest theoretical capacity and lowest electrochemical potential [32]. Using pure lithium as anode in rechargeable batteries is difficult due its high reactivity and uneven lithium deposition, causing continuous electrolyte decomposition and dendrite formation which can lead to short-circuiting [33, 34]. Stabilizing lithium and controlling the deposition of lithium at the anode over many cycles at high charging and discharging rates are major challenges.

The electrolyte is thermodynamically unstable at the low/high redox potentials of the cathode/anode, causing electrolyte decomposition [35–38]. The electrolyte de-

composition products are solid and adhere to the electrode surfaces, and ideally the resulting interphases passivate the electrode surface and prevent further reaction between the electrode and electrolyte. The interphases on the anode and cathode are called the solid electrolyte interphase (SEI) and cathode electrolyte interphase (CEI), respectively.

The electrolyte electrochemically connects the anode and cathode inside the battery, enabling transport of lithium ions while blocking electrons. Currently, the majority of electrolytes used in commercial batteries are composed of the salt $LiPF_6$ dissolved in a mixture of cyclic and linear carbonates with small amounts of additives to stabilize the solid electrolyte interphase layers on the electrodes made up of electrolyte decomposition products [39–41]. The motivation for using a mixture of solvents is two-fold, the solvent should effectively dissociate the lithium salt (i.e. have a high dielectric constant) and at the same time have low viscosity to ensure rapid transport of ions. The former property is usually obtained by a cyclic carbonate (e.g. ethylene carbonate, EC) and the latter by a linear carbonate (e.g. diethyl carbonate, DEC) [39].

Polymer electrolytes are also used in some commercial batteries, often based on poly(ethylene oxide) (PEO) with lithium bis(trifluoromethanesulfonyl)imide (LiTFSI) salt. PEO-LiTFSI and other polymer electrolytes have improved interfacial and electrochemical stability with lithium metal compared to common liquid electrolytes [42–45]. These electrolytes have rather poor conductivity at room temperature due to the slow segmental motion of the polymer [44, 46, 47], so they require heating to achieve high enough conductivity ($\geq$1 mS cm^{-1}) for commercial applications [48]. A common way of improving the conductivity of polymer electrolytes is to add liquid plasticizers, e.g. organic solvents or low-molecular weight PEO, in so-called gel-polymer electrolytes [44, 49].

2.3 Transport in lithium-ion battery electrolytes

Lithium-ion battery electrolytes facilitate transport of lithium ions from the anode to the cathode during discharge of the battery and enable the conversion of chemical to electrical energy. The transport properties of the electrolyte, together with the transport processes occurring in other parts of the battery, contribute to determining how quickly and efficiently energy can be withdrawn from the battery. The transport processes in liquid and polymer electrolytes lead to the build-up of gradients in concentration and chemical potential of the electrolyte components, and potentially even temperature

gradients inside the battery. Such gradients represent thermodynamic forces that may influence the work required for charge transport (by changing the voltage). The extra work corresponds to energy loss which is made unavailable for the external source powered by the battery. The magnitude of the gradients, and consequently the efficiency of the battery, are determined by the ion-, solvent- and thermal interactions [50]. Examples of fully developed chemical potential gradients in the stationary state are given in Figure 5.6b.

2.4 Lithium-ion battery electrolytes

Electrolytes are materials containing mobile charge carriers — ions. Often, electrolytes are composed of one or more salts dissolved in polar solvents. Strong and long-range electrostatic interactions are significant in such mixtures and play a big part in determining the properties of electrolytes. As a result, electrolytes are highly complex and no theory exists which can fully predict the properties of electrolytes from the electrolyte constituents [51]. Electrolytes can be characterized as dilute or concentrated depending on the concentration of the ions. There are no strict distinctions between the two, however electrolytes where the ions are so abundant that they influence each other can be called concentrated. Electrolytes for batteries are so concentrated that ion pairing and direct ion-ion contact occurs, in addition to solvent-ion coordination. A snapshot of the molecular structure of a common liquid electrolyte used in lithium-ion batteries is shown in Figure 2.2. Two types of transport mechanisms are relevant for Li^+ ions in electrolytes; structural diffusion and vehicular diffusion [52, 53]. The former involves Li^+ changing its coordination environment and the latter is when Li^+ is moving together with its solvation environment. Both types occur in liquid and polymer electrolytes. Structural diffusion dominates in solid-state electrolytes [54].

Two transport properties are highly important for the performance of a lithium-ion battery electrolyte: the ionic conductivity and the lithium-ion transport number (also called transference number [55–57]). The ionic conductivity is the ability of the electrolyte to carry electric current (by ion motion) in a unit electric field, with unit Siemens per meter equal to inverse resistance or $\mathrm{A V^{-1} m^{-1}}$ (Ohm's law):

$$\kappa = -\left(\frac{j}{\nabla\varphi}\right)_{\nabla T=0,\nabla\mu_i=0}, \tag{2.3}$$

where j is current density and $\nabla\varphi$ is the measurable electric potential gradient. The

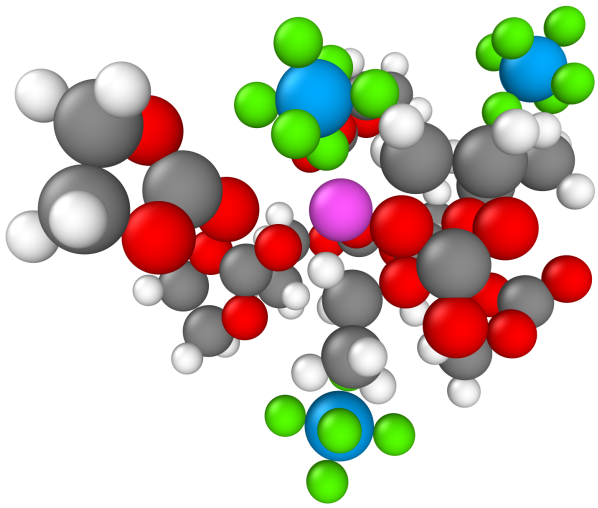

Figure 2.2: Molecular dynamics snapshot showing the electrolyte structure surrounding a lithium ion in an electrolyte composed of $LiPF_6$ dissolved in ethylene carbonate and diethyl carbonate. Color legend: lithium is purple, carbon is grey, oxygen is red, hydrogen is white, phosphorous is blue and fluorine is green.

subscripts indicate requirements for the expression, i.e. no gradients in temperature or chemical potentials. The lithium-ion transport number is the fraction of the total electric current carried by the lithium-ion:

$$t_+ = \frac{u_+}{u_+ + u_-}, \tag{2.4}$$

where u_i is the electrophoretic mobility of ion i (absolute velocity in unit electric field) and it is assumed that there is only one type of monovalent cation and anion in the electrolyte. Both quantities are defined in the absence of gradients in chemical potentials and temperature [55]. The electrodes of a lithium-ion battery are only active to the lithium ions, i.e. the anion and the solvent of liquid and polymer electrolytes can not (ideally) enter the electrodes and so they are confined within the electrolyte volume. A lithium-ion transport number below unity will therefore lead to net anion motion in the opposite direction during battery operation and a concentration gradient of the anion in the electrolyte. Due to the strong electrostatic attraction between oppositely charged cations and anions, charge neutrality must be maintained in the bulk phase of the electrolyte within a distance where the interaction energy corresponds to the thermal energy, $k_B T$. This distance is called the Bjerrum length [58] and is normally well below 1 nm. Consequently, a concentration gradient of the anion leads to a similar salt

concentration gradient. It is clear that the salt concentration gradient inside a lithium-ion battery electrolyte must be directly linked to the lithium-ion transport number. A very low lithium-ion transport number (below 0.2) will result in a steep concentration gradient, and potentially depletion of the cations at the cathode interface during discharge at high rates. The current density and salt diffusion coefficient determine how quickly the salt concentration gradient develops [56, 59, 60].

A study by Doyle, Fuller and Newman [61] showed that the battery performance will benefit considerably by increasing the lithium-ion transport number, even at the expense of lower ionic conductivity. It is perhaps more important to find ways of improving the lithium-ion transport number than the ionic conductivity in order to enhance the rate performance of next-generation electrolytes. This is challenging, however, as the lithium ion is quite small, has a high charge density, and therefore strongly attract solvent and anions to create a large solvation shell. This significantly reduces its mobility. The effective size of the lithium ion (including the solvation shell) in a battery electrolyte is larger than for common anions, even though the anions themselves are bigger than a lithium ion [62]. As a result, the lithium-ion transport number is well below 0.5 in most liquid and polymer electrolytes. The positive aspect is that even a minor improvement of the lithium-ion transport number can have a noticeable impact on the rate performance of a battery. We believe it is key to understand the ion-solvent, cation-anion, cation-cation, and anion-anion interactions, i.e. the various coupling effects, in order to realize such improvements.

2.4.1 Experimental determination of electrolyte transport properties

The conductivity of electrolytes is routinely measured by electrochemical impedance spectroscopy. The determination of transport numbers, however, is much less trivial. Several experimental methods exist for measuring the transport number in liquid electrolytes, e.g. the Hittorf method, moving boundary method [63], steady-state Bruce-Vincent method [64] and using self-diffusion coefficients obtained by pulsed-field gradient nuclear magnetic resonance (pfg-NMR) [57]. All the methods have benefits and disadvantages. In the Hittorf experiment, a known current is passed through a cell of initially uniform composition with electrodes active to one of the ionic species. Salt will accumulate on one side during the experiment. After a while, the compartments of the cell are separated and analyzed to find the amount of salt which has been transported per mole of electric charge (faraday) that passed through the cell. Sectioning the cell while avoiding contamination with sticky polymer electrolytes is challenging

and so the Hittorf method has not been much used to analyze such electrolytes. Also, the difference in salt concentration in the compartments is normally small which leads to large uncertainty [65, 66].

In the Bruce-Vincent method, a small voltage is applied to a symmetric cell with electrodes active to the cation. Initially, the composition is uniform and the cations and anions migrate only due to the electric field. As the anion is confined within the electrolyte volume it will accumulate on the anode side, resulting in a concentration gradient of the anion and salt. At steady-state, the diffusion of the anion due to the concentration gradient and the migration due to the electric field balance out and the net anion motion is zero. Only the cation motion contributes to the steady-state current when the concentration gradient is linear (see Figure 2.3). The Bruce-Vincent cation transport number is then simply the ratio between the steady-state current, i_{SS}, and the initial current, i_0:

$$t_+ = \frac{i_{SS}}{i_0}, \tag{2.5}$$

The changing resistance of the interphases during the experiment with lithium electrodes are accounted for by:

$$t_+ = \frac{i_{SS}\Delta V - i_0 R_{CT}^0}{i_0 \Delta V - i_{SS} R_{CT}^{SS}}, \tag{2.6}$$

where ΔV is the applied voltage, and R_{CT}^0 and R_{CT}^{SS} are interphasial resistances at initial and steady states, respectively. The Bruce-Vincent cation transport number is only correct if we assume that the concentration gradient of the salt does not influence the cation transport, i.e. by assuming no coupling between the anions and cations in the electrolyte. In the dilute limit, there is no concentration gradient at steady state. Both the Bruce-Vincent method and using self-diffusion coefficients to determine transport numbers assume ideal or dilute electrolytes.

Newman and colleagues developed a method to determine the transport number in concentrated electrolytes [56, 68] but this is rarely used as it involves three separate experiments, one of which must be repeated for many different concentrations [56]. The uncertainty by combining all the measurement data is significant. In addition, the transport number by Newman is determined in the solvent-velocity frame of reference, which might complicate the interpretation.

The observation of negative lithium-ion transport numbers in PEO-LiTFSI polymer electrolytes [57] triggered several studies trying to explain such behavior [69–71]. Mistry et al. [72] discovered that the main reason for the negative transport numbers was

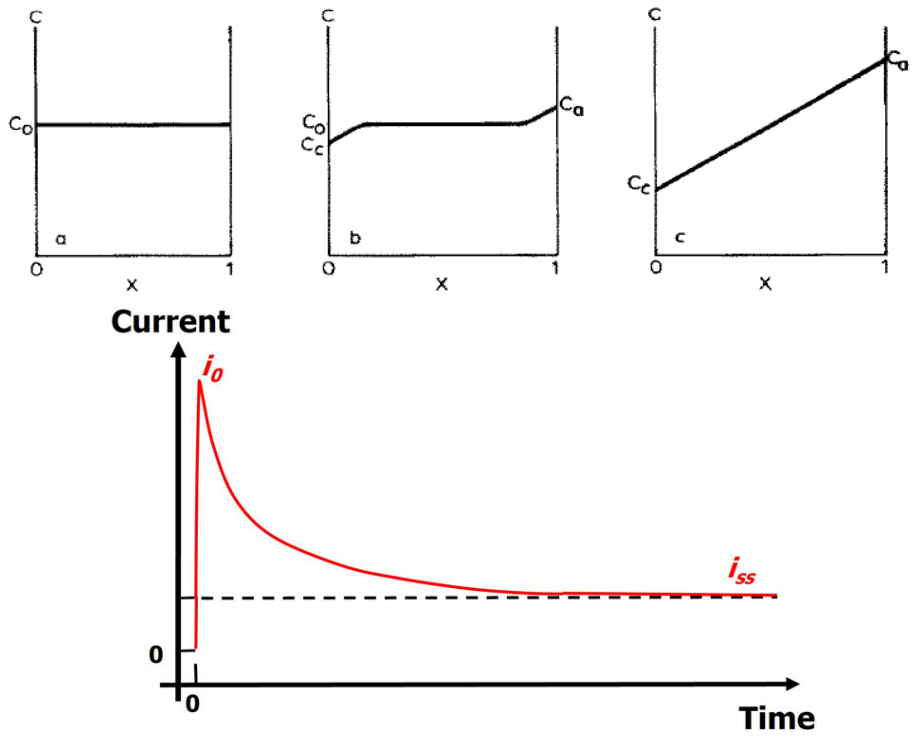

Figure 2.3: Top: Salt concentration profiles of cell during Bruce-Vincent steady-state experiment. Initial concentration to the left, intermediate concentration in the middle and concentration profile at steady-state to the right. Reproduced with permission from ref. [64]. Copyright 1987 Journal of Electroanalytical Chemistry. Bottom: Evolution of current during Bruce-Vincent steady-state experiment. i_0 is initial current and i_{SS} is the steady-state current. Obtained from ref. [67] by Kang Xu under the CC BY 4.0 (`http://creativecommons.org/licenses/by/4.0`) license.

the use of the solvent-velocity frame of reference, as the solvent was found to move significantly in the concentrated electrolytes during passage of current. The lithium-ion transport number was positive when the electrode/electrolyte interface was used as the frame of reference instead. We will come back to the importance of the frame of reference in chapter 4.1.

Electrophoretic NMR (eNMR) allows the direct measurement of electrophoretic mobilities (u) of species under electric fields for determination of transport numbers and has become popular [73–76]. eNMR can be readily used to characterize transport numbers in dilute and concentrated electrolytes. The transport numbers obtained by eNMR are defined with respect to the laboratory frame of reference. Potential challenges related to using eNMR are that the mobilities might depend on the electric field

strength [73] and the presence of convection caused by joule heating due to the rapid migration in the strong electric field [74]. Finally, transport coefficients and numbers can be determined from molecular simulations which we will elaborate more on later.

2.4.2 Solid-state electrolytes

Ceramic solid-state electrolytes are promising for next-generation lithium-ion batteries because they are non-flammable and safer than current carbonate-based liquid electrolytes. The transport mechanisms in solid-state electrolytes are fundamentally different than in liquid electrolytes. The crystal structure framework is composed of anions and cations that are believed to be mostly immobile. The lithium sub-lattice is highly disordered and lithium ions can jump from site to site by solid-state diffusion mechanisms characterized by migration energy barriers. The lithium-ion transport number of such electrolytes can be close to unity [77]. As a consequence, the rate performance of batteries with solid-state electrolytes can be better than with liquid electrolytes, even if the ionic conductivity of the solid-state electrolyte is lower [54].

A promising ceramic electrolyte is the oxide LLZO ($Li_7La_3Zr_2O_{12}$) due to its high ionic conductivity and its stability against Li metal and high voltage cathodes [78, 79]. Monroe and Newman showed that an isotropic solid electrolyte with sufficiently high shear modulus (twice that of Li metal) should suppress dendrite initiation and growth [80] which could potentially enable use of Li metal anodes. LLZO has more than 10 times higher shear modulus than Li metal and could thus be able to stop dendrites [81]. In practice, dendrites can still form in ceramic electrolytes (including LLZO) due to the presence of defects at imperfect solid-solid interfaces causing current focusing, crack opening and propagation [82]. It has even been shown that dendrites can form inside the LLZO by reduction of Li^+ due to the non-negligible electronic conductivity of the electrolyte [83].

The interfaces between the solid-state electrolyte and electrodes are critical in solid-state batteries. It is challenging to maintain stable solid-solid interfaces with high contact area using electrodes that expand and contract during battery operation [84]. A possible solution is to make a composite where the flexibility and ductility of polymer electrolytes is combined with the high ionic conductivity of ceramic electrolytes (e.g. LLZO). The flexible polymer can ensure good contact with e.g. lithium metal over time. In composite electrolytes, however, new interfaces appear between the polymer and ceramic that create new challenges. Particularly, it is difficult to ensure efficient transport of lithium ions between the polymer and ceramic electrolytes in order to utilize

both phases of the composite [85, 86]. A close-contact interface between the cathode particles and the solid-state electrolyte is usually achieved by high-temperature co-sintering, resulting in interdiffusion between the cathode and electrolyte and possible side reactions. The diffusion interlayer normally represents a major interfacial resistance [87–89].

3 Non-equilibrium thermodynamics and Onsager coefficients

The theory of non-equilibrium thermodynamics (NET) is useful for understanding transport in lithium-ion battery electrolytes during battery operation and other systems that are out of global equilibrium. According to the theory, each flux J_i is a linear combination of all forces X_j:

$$J_i = \sum_j L_{ij} X_j, \tag{3.1}$$

where the phenomenological Onsager coefficients L_{ij} obey $L_{ij} = L_{ji}$. The theory of NET assumes local equilibrium, which means that the Gibbs equation is valid locally for any small volume element, even if the total system is out of global equilibrium [90] (see Figure 3.1). The net rate of change for the process is assumed to be small compared to the two rates in opposite directions in the dynamic equilibrium, i.e. there is microscopic reversibility [91]. Many irreversible processes obey local equilibrium [91, 92], even shock waves [93]. By knowledge of all relevant Onsager coefficients, we can precisely determine the flux of cations, anions, solvents, and heat inside an electrolyte for known thermodynamic forces. Notably, the L_{ij} quantify the coupling of i and j when they are different. Coupling can occur for diffusion processes in multi-component mixtures when the transport of one component causes diffusion of another. There will also be coupling between different types of transport processes. Examples of such coupling are the Seebeck effect, when a temperature gradient results in a voltage and electric current, and the Dufour effect, when a concentration gradient brings about heat transport, the reciprocal phenomenon of the Soret effect [94]. All these transport processes follow equation (3.1). Irreversible processes increase the entropy in the system according to

the product sum of conjugate fluxes and forces and the second law of thermodynamics:

$$\sigma = \sum_i J_i X_i \geq 0. \tag{3.2}$$

The values of the fluxes and Onsager coefficients depend on the chosen frame of reference. The entropy production (σ) is independent of the frame of reference. Importantly, L_{ij} is assumed to be independent of the magnitude of the force or gradient [94]. The critical point to understanding the processes occurring during charging or discharging of batteries is to determine the relevant Onsager coefficients. In this work, we have utilized the fluctuation-dissipation theorem to determine the Onsager coefficients.

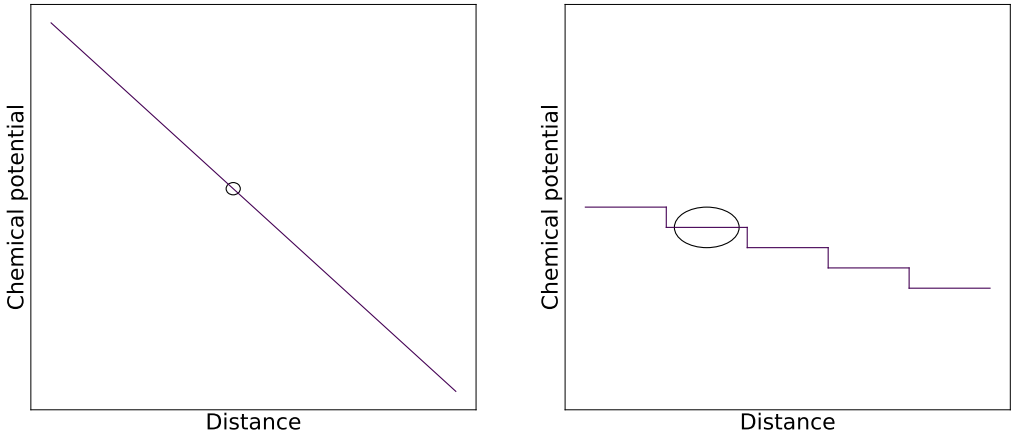

Figure 3.1: Left: Macroscopic chemical potential gradient in system out of global equilibrium with a microscopic volume element marked. Right: Zoom-in on the microscopic volume element assuming local equilibrium inside the volume element.

3.1 Fluctuation-dissipation theorems

The fluctuation-dissipation theorem is an important result in statistical mechanics based on Onsager's regression hypothesis. The hypothesis assumes microscopic reversibility and states that the relaxation of a macroscopic gradient (dissipation) is governed by the same mechanisms as the regression of corresponding spontaneous microscopic fluctuations [94], illustrated in Figure 3.2. Onsager used it to derive his reciprocal relations. Later, Callen and Welton [95], Green [96, 97], Kubo [98] and Helfand [99] worked out the mathematical expressions which enable us to compute transport coefficients from microscopic fluctuations that we can probe in equilibrium molecular

dynamics simulations. The results apply for systems in the linear response regime, i.e. for systems that obey non-equilibrium thermodynamics and equation (3.1). Diffusion coefficients are obtained by sampling velocity correlations with the Green-Kubo relations, or by sampling displacement correlations with the Einstein relations [60]. The two methods are formally equivalent, however in practice there are some differences. A linear relation between the mean squared displacement and time will be realized for sufficiently long times with the Einstein relations, when the system is in the diffusive regime, corresponding to a slope of 1 in a log-log plot. This criterion is used to identify the minimum simulation length. With the Green-Kubo method, there is no such clear indication of a minimum simulation length, as the tail of the velocity-correlation functions slowly decays towards zero [100]. In this work, we have only used the Einstein relations. When we compute interdiffusion coefficients L_{ij} from equilibrium molecular dynamics simulations using appropriate force fields to describe atomic and ionic interactions, we obtain the transport of species i in a chemical potential gradient of species j.

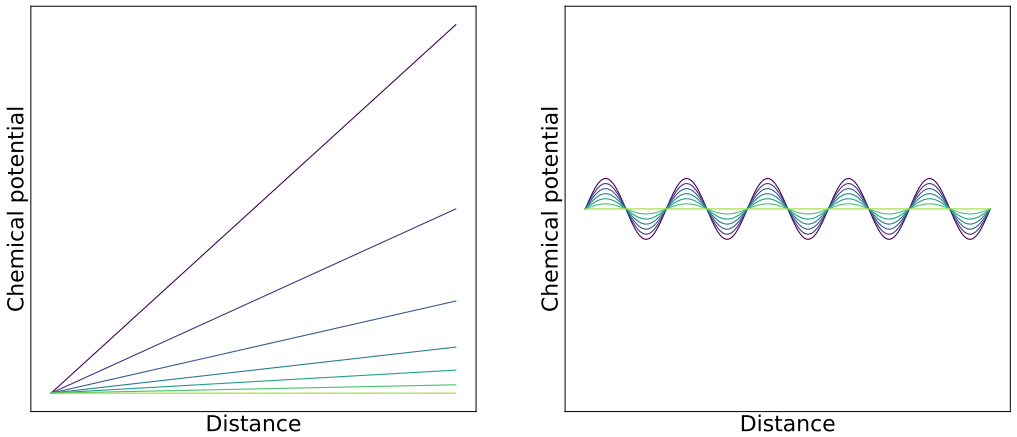

Figure 3.2: Left: Macroscopic chemical potential gradient dissipating towards equilibrium. Right: Microscopic fluctuations of chemical potential at equilibrium.

There are two ways of computing the mass transport properties of electrolytes by the fluctuation-dissipation theorems; by the Nernst-Einstein (NE) approximation and the Onsager coefficients. We mention the former because the Nernst-Einstein approximation has been used in many simulation studies [71, 101–106]. The main difference between the two is that NE is based on self-diffusion coefficients, which describe transport in the absence of gradients, and do not take coupling effects into account, while the Onsager coefficients include coupling. For dilute and ideal electrolytes, both

methods should give the same result. However, coupling effects are important in concentrated electrolytes and we argue that an appropriate way of characterizing such electrolytes is by using the Onsager coefficients. The equation for the self-diffusion coefficient of species i is

$$D_{i,\text{self}} = \frac{1}{6N_i} \lim_{t\to\infty} \frac{\mathrm{d}}{\mathrm{d}t} \Big\langle \sum_{k=1}^{N_i} \big(\mathbf{r}_{k,i}(t) - \mathbf{r}_{k,i}(0)\big)^2 \Big\rangle, \tag{3.3}$$

where $\mathbf{r}$ is the particle position vector, t is time, N_i is the number of particles of type i and the $\langle\cdots\rangle$ denote the ensemble average. The expression for the Onsager coefficient L_{ij}, giving transport of species i in a chemical potential gradient of species j is

$$L_{ij} = \frac{1}{6N} \lim_{t\to\infty} \frac{\mathrm{d}}{\mathrm{d}t} \Big\langle \Big(\sum_{k=1}^{N_i} \big[\mathbf{r}_{k,i}(t) - \mathbf{r}_{k,i}(0)\big] \Big) \Big(\sum_{l=1}^{N_j} \big[\mathbf{r}_{l,j}(t) - \mathbf{r}_{l,j}(0)\big] \Big) \Big\rangle, \tag{3.4}$$

in which N_i and N_j are the numbers of particles of i and j, respectively.

Onsager coefficients for both charged and neutral species are obtained from equilibrium simulations. Operationally defined properties are closer related to measurable quantities and are needed for thermodynamic modelling. These are related to the transport properties of neutral components [107]. The transformation of coefficients for charged and neutral species (ions and solvents) to just neutral species (salt and solvents) is necessary to perform the modelling [90]. We obtain Onsager coefficients for mass transfer (interdiffusion) and coupling effects in mass transfer, coupling between mass transfer and electric potential gradients (related to transference coefficients), coupling between electric potential and temperature gradients (Seebeck effect, from experiments), and coupling between mass transfer and temperature gradients (Soret effect) [90]. These coefficients are useful for battery modeling.

3.1.1 Onsager transport coefficients in electrolytes

The use of Onsager coefficients obtained from equilibrium molecular simulations by the fluctuation-dissipation theorem to characterize transport properties and transport numbers in electrolytes has seen a revival recently, for example in several papers by Fong, Bergstrom, McCloskey, Persson and colleagues [60, 74, 105, 108, 109] focusing on ion correlations, and in other articles [110]. We will here summarize some of these important recent works.

Fong and colleagues analyzed the transport in polyelectrolyte solutions, a type

of electrolyte composed of polymer chains with covalently bonded anions and free lithium cations dissolved in a non-aqueous solvent [108, 109]. Such electrolytes were called single-ion conductors, as the anion was believed to be immobilized at the polymer. Early studies based on the self-diffusion coefficients (obtained by pfg-NMR) of polyelectrolytes suggested they had very high Li^+ transport numbers of close to one [111, 112]. However, deeper investigations of the transport mechanisms by molecular dynamics simulations revealed that ion correlations played an important role in these polyelectrolytes, largely invalidating self-diffusion coefficients as useful indicators of the true transport number. In order to quantify the importance of ion correlations, they split the expression for L_{ii} (3.4) into a self term, L_{ii}^{self}, considering only the displacement of similar particles $k = l$ (equivalent to the self diffusion coefficient), and a distinct term, L_{ii}^{distinct}, considering only the displacement of different particles $k \neq l$ of the same type. They found that the anion distinct term, L_{--}^{distinct}, dominated for longer polymer chains, not surprising given that all the anions on the same chain must move in the same direction. L_{+-} also increased with longer chains due to more ion aggregation, causing decreased conductivity. Upon taking the ion correlations into account, the cation transport numbers were dramatically reduced for longer chains, even going to negative values. The different ion correlations are displayed in Figure 3.3.

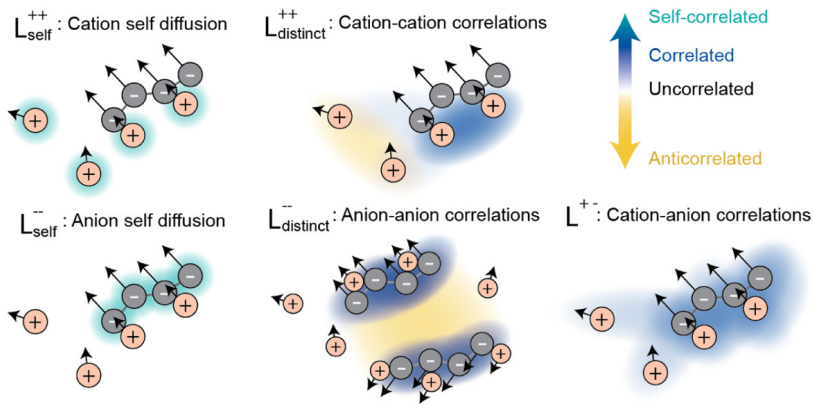

Figure 3.3: Schematic illustration of the different types of ion correlations in a polyelectrolyte. The solvent is present but not shown. Reprinted (adapted) with permission from ref. [108]. Copyright 2020 American Chemical Society.

Ionic liquids (IL) are liquid salts at close to ambient temperature. They are composed only of cations and anions without any solvent. The research interest in ionic liquids has been high in the last two decades due to their many interesting and promising properties for use in electrochemical processes, like batteries [113–115]. An IL made

up of one salt has two species. The Onsager transport coefficients L_{++}, L_{+-} and L_{--} are then interdependent due to the constraint of momentum conservation, $\sum_i M_i L_{ij} = 0$. As a consequence of charge neutrality, the concentration of cations and anions must be similar everywhere in the electrolyte and the interpretation of the transport numbers becomes meaningless. Hence, the ionic conductivity is the only independent transport property in simple ionic liquids [105].

Shao and Gudla et al. studied the ion transport in PEO-LiTFSI polymer electrolytes [116, 117]. In ref. [116] they investigated the effect of varying the solvent polarity (dielectric constant) to obtain different degrees of ion pairing in simulations. The lifetime of ion pairs reached a minimum for a solvent dielectric constant of 3-4, corresponding to maximum ionic conductivity and a positive contribution of the cation-anion correlation to conductivity. The solvent polarity had a large impact on the ion pair lifetime, and short lifetimes were necessary for improving the transport properties in PEO-LiTFSI electrolytes. The combination of Onsager transport coefficients (dynamic properties), radial distribution functions (static properties) and pair lifetime correlations unravelling the dynamics of the coordination environments of e.g. Li^+ ions is potent for characterizing and understanding of transport in electrolyte mixtures.

Recently, highly concentrated electrolytes have been investigated experimentally by Bergstrom and McCloskey [74] to determine Onsager coefficients. Such electrolytes have received increasing attention in the last decade because of their ability to form stable solid electrolyte interphases on lithium metal anodes among other things. Clear disadvantages are their lower conductivity caused by high viscosity and the cost of salt making them expensive. The Li^+ transport number was found to increase with higher concentration, attributed to enhanced cation-cation correlation as Li^+ is mostly coordinated by anions, creating anion-Li^+-anion coordination paths. Structural (hopping) diffusion of Li^+ becomes more important with increasing salt concentration. Localized high concentration electrolytes contain non-solvating diluents to reduce the viscosity and increase conductivity while maintaining the beneficial anion-rich solvation of Li^+ which promotes stable SEI formation [118]. The presence of the diluents, however, apparently disrupt the cation coordination site network, harming the transport of Li^+, and lowering the Li^+ ion transport number [74].

3.2 Relation to other coefficients

Maxwell-Stefan diffusivities have traditionally been used to characterize transport due to chemical potential gradients in multi-component mixtures. The M-S coefficients are independent of the frame of reference since they are defined using velocity differences [94]. While the Onsager coefficients act as a proportionality constant between the flux and force, the M-S coefficients are inversely proportional to the driving force and can be interpreted as inverse drag coefficients [119]. This potentially makes the M-S diffusivity values less intuitive than Onsager coefficients, and they can also diverge to negative or positive infinity [53, 59, 60, 110]. M-S coefficients and Onsager coefficients are formally equivalent as both include coupling effects and both can be used to describe transport in electrolytes.

Fick's diffusion coefficients are perhaps most common as they describe diffusion due to concentration gradients which are readily available from experiments. As previously mentioned, electrolytes are complex and characterized by strong and diverse interatomic forces. We cannot expect simple concentration gradients to fully capture the driving forces for the ion- and solvent motion in electrolytes. The electrolyte species move according to the variations in the electrochemical potential. Concentrations and chemical potentials are related by the thermodynamic factors which can be used to convert Onsager coefficients obtained in simulations to Fick's coefficients in order to compare to experimental results. The Darken or Vignes equations can be used to predict M-S diffusivities due to chemical potential gradients from self-diffusivities or binary diffusion coefficients that are easier to obtain [120]. The generalized Darken equation to predict M-S diffusivities in multi-component systems is:

$$Đ_{ij} = \frac{x_i}{x_i + x_j} D_{j,\text{self}} + \frac{x_j}{x_i + x_j} D_{i,\text{self}}, \tag{3.5}$$

where x_i is the mole fraction of species i. The equation is an approximation, and exact only when $x_i \to 1$ or $x_j \to 1$.

Finally, we note that it is not yet possible to measure the chemical potential of species experimentally, and so it is not straightforward to obtain Onsager coefficients directly from experiments. It is however possible to estimate Onsager coefficients from experimentally measured quantities [60, 74, 110, 121–123], specifically using the variation of the salt activity coefficient with respect to salt concentration, the salt diffusion coefficient, the ionic conductivity and the ion transport numbers.

4 Molecular Dynamics

Molecular Dynamics (MD) was the primary tool in this work. In classical Molecular Dynamics, the pairwise interactions between atoms and ions are described using simple potential energy functions, e.g. harmonic oscillators for covalent bonds and angles, Lennard-Jones functions for repulsion-dispersion interactions, and Coulomb's law for electrostatic interactions. These energy functions are efficiently evaluated on computers which allow us to study large systems containing thousands or millions of atoms over longer time spans (>50 ns) with femtosecond time resolution. Electrons are treated implicitly in the energy functions. The total energy of the system is the sum of the potential and kinetic energy. In the original microcanonical ensemble the total energy is conserved, i.e. the energy can only change between potential and kinetic. For every time step, the forces acting on each atom are computed from the potential energy functions and the particle positions. A time integrator is used to update the positions and velocities of all particles according to Newton's laws of motion. The system trajectory develops by repeating the above process many times. The temperature and pressure of the simulation can be controlled using thermostats and barostats, by adjusting the particle velocities and simulation box volume, respectively.

The accuracy of the potential energy functions and corresponding parameters describing the system determine the reliability of the results. The parametrization of any classical potential or force field describing a real system is always done against a limited number of physical properties. The choice of physical properties used in the parametrization process influences the transferability of the force field, i.e. the suitability of the force field for describing the system (atom, ion, molecule, crystal) in different chemical environments and under different conditions. As a consequence, there will always be some uncertainty in the accuracy of the force field and the simulation results. To minimize the uncertainty and make us more confident in our results, we compare our simulation results to experimental data when available.

$$U = \sum_i \text{bonds} + \sum_i \text{bends/angles} + \sum_i \text{rotations/dihedrals} + \sum_{i<j} (\text{electrostatics} + \text{Lennard-Jones}) \tag{4.1}$$

$$U(\mathbf{r}^{\mathrm{N}}) = \sum_{i=1}^{\mathrm{N_{bond}}} \frac{1}{2} k_{b,i} (\mathbf{r}_i - \mathbf{r}_{0,i})^2 + \sum_{i=1}^{\mathrm{N_{angle}}} \frac{1}{2} k_{\theta,i} (\theta - \theta_{0,i})^2 + \sum_{i=1}^{\mathrm{N_{torsion}}} \frac{1}{2} \left(V_{1,i}(1 + \cos(\varphi_i)) + V_{2,i}(1 - \cos(2\varphi_i)) + V_{3,i}(1 + \cos(3\varphi_i)) + V_{4,i}(1 - \cos(4\varphi_i)) \right) + \sum_{i<j} \left\{ \frac{q_i q_j e^2}{r_{ij}} + 4\epsilon_{ij} \left[\left(\frac{\sigma_{ij}}{r_{ij}} \right)^{12} - \left(\frac{\sigma_{ij}}{r_{ij}} \right)^{6} \right] \right\}. \tag{4.2}$$

The above equation (4.2) or similar expressions give the potential energy for molecular systems in several common force fields, e.g. the optimized potential for liquid simulations (OPLS) [124, 125], GROMOS [126], AMBER [127] and CHARMM [128]. The potential energy is the sum of the intramolecular interactions (bonds, angles, torsions) and the intermolecular (non-bonded) interactions; Lennard-Jones potential and electrostatics. The parameters describing the system are the bond force constants (k_b) and equilibrium bond lengths ($\mathbf{r}_0$), angle force constants (k_θ) and equilibrium angles (θ_0), torsion force constants (V), partial atomic charges (q) and Lennard-Jones parameters (ϵ and σ). The potential energy for a specific system depends only on the particle positions, $\mathbf{r}^{\mathrm{N}}$.

A clear simplification in many classical force fields is the use of atomic partial static point charges positioned in the center of the atoms, called non-polarizable force fields. Other effects such as charge transfer are also normally neglected. Several studies have shown that ion-ion interactions in electrolytes and ionic liquids are exaggerated in non-polarizable force fields [129–132]. As a result, the transport of species is inhibited and transport properties are underestimated. A simple empirical way of improving the accuracy of the simulations is to scale the ion charges by a factor of 0.7 to 0.8 [130] to emulate the softer interactions of polarizable atoms and charge transfer [133–136]. Explicitly including atomic polarizability in the force field would naturally be preferred but the many-body effect of polarizability potentially makes the simulations much more computationally expensive [137, 138]. We also find that the availability of po-

larizable force fields for electrolytes is still quite limited relative to the availability of non-polarizable force fields. Including polarizability in the force field does not guarantee that the model will better represent the real material in all cases. The accuracy of the model depends both on the energy functions included and the parametrization process.

Molecular dynamics simulations allow us to compute macroscopic transport properties while providing a view of the underlying microscopic mechanisms. Transport properties can be examined either in non-equilibrium MD simulations by creating a gradient or applying a field and directly measuring the resulting transport, or via the fluctuation-dissipation theorems in equilibrium simulations. Both methods have pros and cons. Considerable gradients or fields must be employed to establish species fluxes during the short time spans of non-equilibrium MD simulations. Large fields or gradients can give rise to anomalies, for example the transport can depend on the magnitude of the field [139–141]. Several simulations with varying field strengths are necessary to ensure that the system response is in the linear regime. Most thermostats are derived for equilibrium systems and might not work as intended in non-equilibrium simulations [142].

Equilibrium simulations sampled by the fluctuation-dissipation theorems potentially suffer from the stochastic nature of the fluctuations causing significant variance in the measured properties. The systems must be sufficiently large and the simulations should be long to reduce the uncertainty. Several replicas should be examined to quantify the uncertainty. Still, we prefer equilibrium simulations due to the reduced risk of anomalies and the fluctuation-dissipation theorems providing more data on the underlying correlations governing the transport [138]. In equilibrium simulations we can compute radial distribution functions and coordination numbers which gives a picture of the average coordination environments of the ions. Kirkwood-Buff integrals of radial distribution functions are related to many interesting thermodynamic variables, such as compressibility, partial molar volumes and thermodynamic factors [143–145]. Pair lifetime correlation functions can be used to determine residence times which gives us information about the dynamics of the coordination environments [109, 146]. Particle trajectories can be studied visually to facilitate the understanding of the mentioned properties. This makes molecular dynamics a powerful tool for studying and understanding transport in electrolytes.

In this work, we used the MD software package LAMMPS [147] to perform the simulations. It is based on a customizable open-source platform and anyone can contribute

new features, bug fixes and documentation to the associated Github project.

4.1 Frame of reference

Transport must be measured relative to a frame of reference. The importance of the frame of reference has been a point of discussion in numerous recent articles [72, 117, 138, 148, 149]. This has perhaps become more relevant in recent years due to the rise in popularity of analyzing transport properties by molecular dynamics. The natural frame of reference in simulations (barycentric) is different than the natural frame of reference in experiments (solvent velocity [10, 56] or laboratory). Care must therefore be taken when comparing simulation results with experimental results, which in practice means converting data sets to the same frame of reference [94, 117, 138, 150] in order to make a direct comparison. The significance of the frame of reference was examined by Shao et al. in [117]. The lithium-ion transport number and Onsager coefficients of PEO-LiTFSI electrolytes were shown to be highly sensitive to the frame of reference. They showed that lithium-ion transport numbers obtained in simulations in the barycentric frame of reference were positive, and became negative upon converting them to the solvent-velocity frame of reference. The lithium-ion transport number in the solvent-velocity frame of reference was found to depend on the anion mass and anion-anion correlation.

The choice of frame of reference should be considered in relation to which properties you want to investigate. For example, in battery electrolytes we are usually interested in the motion of lithium ions from one electrode to the other. The electrode surface would perhaps be the optimal choice of frame of reference in this scenario. This can be challenging to use in practice, particularly because the electrode surface also can move during charging or discharging of a battery [72]. It is easier to interpret the results if the motion of the frame of reference is known, i.e. external frames of reference outside the system might be preferable to internal frames of reference that are part of the system [149].

5 Summary of articles

An important aim of this work was to contribute to improved understanding of transport in lithium-ion battery electrolytes, particularly the coupling effects. We have used molecular dynamics simulations to investigate the transport in a well-studied model electrolyte (water-NaCl), in polymer electrolytes (PEO-LiTFSI) and in conventional liquid carbonate-based electrolytes (EC:DEC/DMC + $LiPF_6$). We have used the Onsager theoretical framework as a basis in all the studies to quantify the coupling effects. The results have been published in four articles in peer-reviewed journals.

5.1 Article I

In the first article we compared several methods to study charge transport in a well-known electrolyte, water with NaCl. We studied two models, a non-polarizable of SPC/E water [151] with a NaCl model designed for use in concentrated water solutions [152], and a polarizable of SWM4-NDP water [153] with polarizable Na^+ and Cl^- [154] which had not previously been studied by these methods. The charge transport in equilibrium simulations was examined by the fluctuation-dissipation theorems. We compared the Nernst-Einstein method employing self-diffusion coefficients to Onsager coefficients. Surprisingly, the NE conductivity of the non-polarizable model was closer to experimental values than the Onsager conductivity which was about 30 to 50 % too low. However, we believe that the Onsager conductivity gave a better representation of the conductivity of the model. As mentioned in chapter 4, it is generally known that non-polarizable models underestimate the transport due to excessive interionic interactions.

The transport numbers of the non-polarizable model as a function of salt concentration derived directly from simulations deviated from the experimental data. Here, we illustrate the importance of considering the frame of reference when comparing

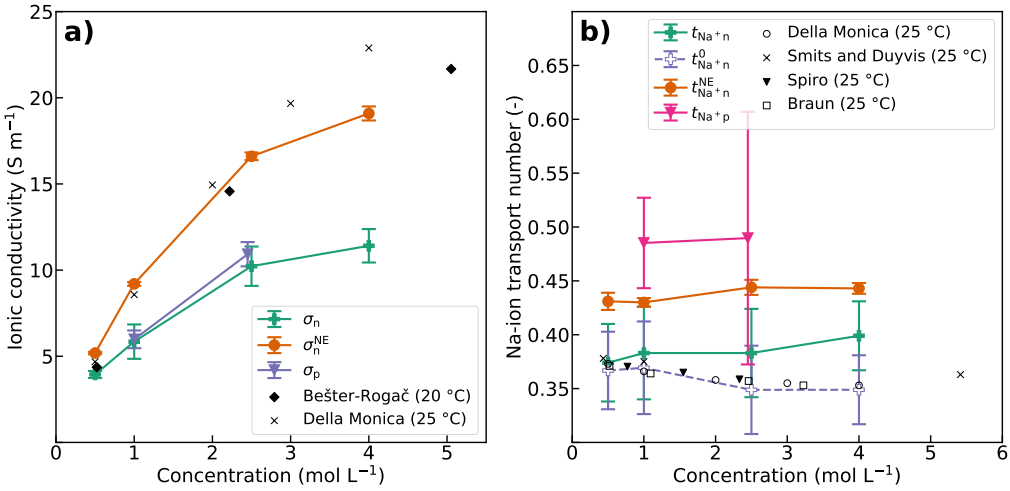

Figure 5.1: (a) Ionic conductivity and (b) Na-ion transport number as a function of salt concentration from equilibrium MD simulations of the systems with SPC/E and SWM4-NDP water molecules compared to experimental data. The results from non-polarizable (SPC/E water) and polarizable (SWM4-NDP water) simulations are denoted with subscript n and p, respectively. The computed ionic conductivities are compared to experimental data by Bešter-Rogač et al. [155] and Della Monica et al. [156]. The computed transport numbers in the barycentric and solvent velocity reference frames are displayed, the latter denoted with superscript 0. The computed Na-ion transport numbers are compared to experimental data by Della Monica et al. [156], Smits and Duyvis [157], Spiro [158] and Braun [159]. Reproduced from ref. [138].

simulated and experimental data. The simulated data are measured in the barycentric frame of reference, while most of the experimental data are measured in the solvent-velocity frame of reference. In order to make proper comparison, we converted the simulated data to the solvent-velocity frame of reference, and obtained very good agreement with the experimental values. This also shows that non-polarizable models can reproduce the relative transport of species (e.g. transport numbers) in a precise manner, even though the absolute values (conductivity) are off. The NE transport numbers are less accurate than the Onsager transport numbers. We also studied a Drude-style polarizable NaCl-water model, SWM4-NDP with Na^+ and Cl^-, to compare its transport properties to the non-polarizable model. The polarizable model did not exhibit more accurate charge transport than the non-polarizable model. We believe the most important reason is that the polarizable model was not specifically parametrized for concentrated salt water solutions like the non-polarizable model. The conductivity and Na-ion transport numbers of the systems are shown in Figure 5.1.

We compared the transport in non-equilibrium simulations with transport in equi-

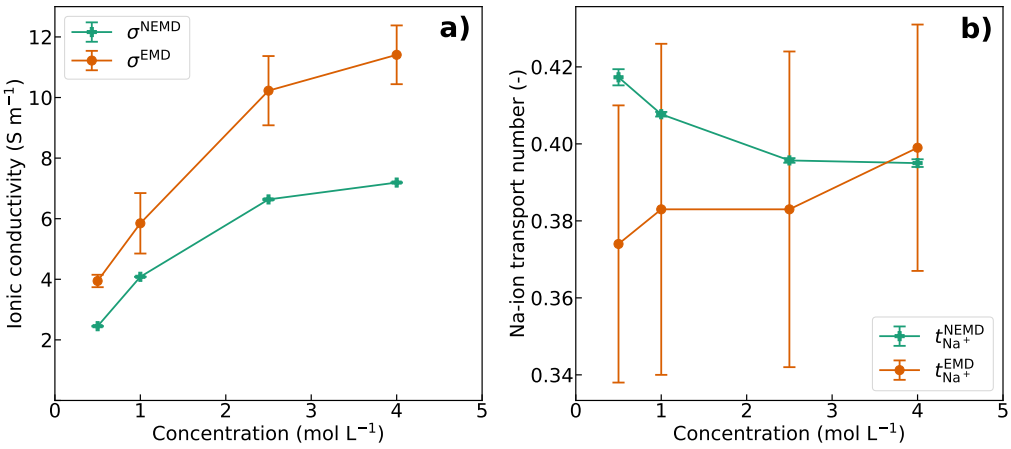

Figure 5.2: (a) Ionic conductivity and (b) Na-ion transport number as function of salt concentration in the system with SPC/E water molecules in non-equilibrium simulations (NEMD) using an electric field strength of 0.03 V Å^{-1}. The values are compared to the equilibrium results (EMD) for the same systems. Reproduced from ref. [138].

librium simulations using the non-polarizable model. Non-equilibrium simulations were performed by applying a uniform electric field to the simulation box and letting the ions and water molecules drift through the box. The displacement of the ions as a function of field strength was used to compute ionic conductivity and transport numbers. The conductivity was lower and the transport numbers were higher than in the equilibrium simulations, as shown in Figure 5.2. Notably, we found that the temperature of the simulation changed due to the field. We argue that the rigid SPC/E water molecules are restrained in the field, effectively reducing the number of degrees of freedom which results in a lower temperature. The effect was not observed for flexible water models. We believe the main reason for the lower conductivity, however, is the reduced diffusivity and rotational motion of the polarized water molecule in the strong field. The equilibrium simulations gave more accurate results than the non-equilibrium simulations for this system.

5.2 Article II

In the second article, we examine transport and thermodynamic properties of a well-studied polymer electrolyte, PEO-LiTFSI, as a function of salt concentration and PEO chain length. We use equilibrium simulations and compare the transport properties with the NE methodology and with Onsager coefficients. It is clear that PEO-LiTFSI is a

non-ideal electrolyte even at quite low salt concentrations, and that the Onsager coefficients are necessary for studying transport and coupling effects. The non-polarizable model gives quite accurate results compared to experimental data.

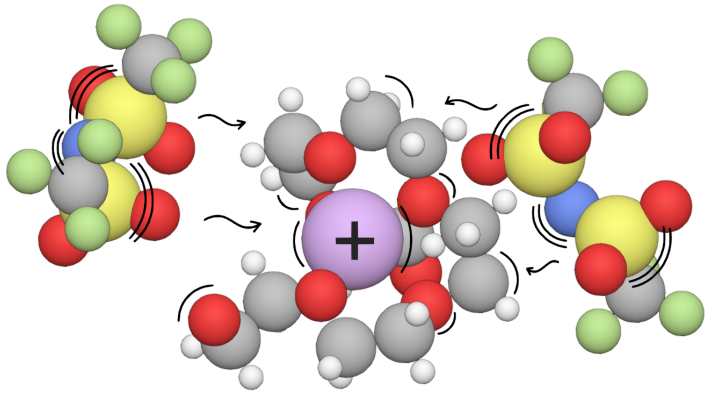

Figure 5.3: Illustration of the proposed mechanism for how the flexibility of the $TFSI^-$ anion imparts greater mobility of the PEO chains, making the Li^+ ions move faster. Reproduced from ref. [149].

The most interesting property of these electrolytes is the L_{+-} coupling coefficient which relates how the cations and anions are moving relative to each other — it is negative (see Figure 5.4). A negative L_{+-} enhances the ionic conductivity. The negative L_{+-} combined with a quite high L_{++} relative to the self diffusion coefficient D_{Li} results in super-ionicity, meaning ionicity values above one. The ionicity is defined as the ratio of the Onsager conductivity and the NE conductivity. Super-ionicity is rarely encountered in electrolytes. The exact cause of super-ionicity in PEO-LiTFSI is not known, but one hypothesis proposes that the flexibility of the $TFSI^-$ anion promotes segmental mobility of the PEO chains which ultimately facilitates Li^+ jumping and motion through the polymer, as illustrated in Figure 5.3. Further, the improved PEO chain mobility creates more voids for the $TFSI^-$ anion to move into. Our analysis of the distribution of residence times for different Li^+ in super-concentrated PEO-LiTFSI indicates that Li^+ that are coordinated by more $TFSI^-$ move faster than Li^+ that are coordinated by fewer $TFSI^-$. We also find that the Onsager Li-ion transport number increases with increasing salt concentration, in contrast to the NE Li-ion transport number which is non-monotonic. It appears that the Li^+ ions to a greater degree than the $TFSI^-$ ions

are moving in the same direction ("marching") in the electrolyte as the self diffusion coefficient for $TFSI^-$ is consistently higher than for Li^+.

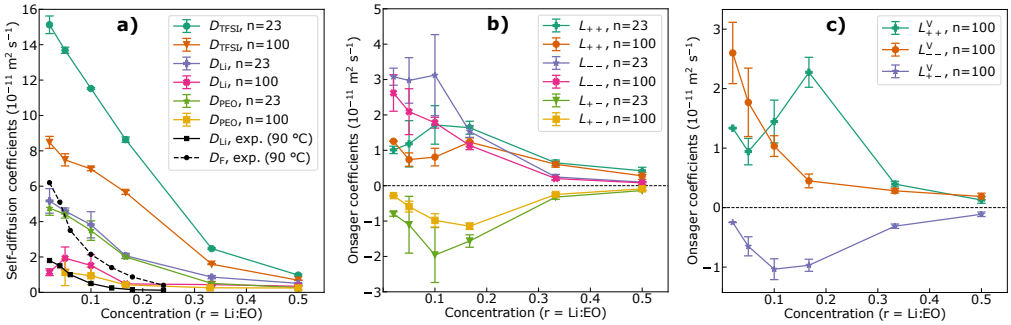

Figure 5.4: (a) Self-diffusion coefficients, (b) Onsager coefficients in the barycentric reference frame, and (c) Onsager coefficients in the volume-fixed reference frame as a function of salt concentration and chain length. The error in the volume-fixed coefficients was calculated using uncertainty propagation rules. Experimental self-diffusion coefficients by Timachova [160]. Reproduced from ref. [149].

Several studies have suggested that PEO-LiTFSI electrolytes exhibit negative Li^+ transport numbers [56, 57, 59], meaning that Li^+ moves in the "wrong direction" inside a battery. Recent studies have shown that this surprising finding is partly caused by the use of the solvent-velocity frame of reference [72]. In concentrated electrolytes, it is possible that motion of charged species can cause net solvent transport [161]. The solvent is an internal frame of reference and usually used in dilute systems where the solvent is the major component. We argue that using an external frame of reference might be beneficial in cases where the internal frame of reference is moving significantly compared to the other species. We convert the Onsager coefficients from the barycentric to the volume-fixed frame of reference, which is similar to the laboratory frame of reference (an external frame of reference) for incompressible electrolytes [148, 162, 163]. Analysis of the partial molar volumes of the components as a function of salt concentration supports that PEO-LiTFSI is close to incompressible. The trends and absolute values of the Onsager coefficients are quite similar in the barycentric and volume-fixed frames of reference. Importantly, super-ionicity and increasing Li-ion transport numbers with increasing salt concentration are also observed in the volume-fixed frame of reference. Finally, we compute the thermodynamic factors from Kirkwood-Buff integrals and observe good agreement with experimental data and clear signs of non-ideality already at low salt concentrations.

5.3 Article III

The third and fourth articles are related to the effect of the ion, solvent and thermal interactions in the electrolyte on the battery voltage. In the third paper, we present the theory necessary to relate ion, and solvent transport coefficients to parameters relevant for cell modelling. A key ingredient is the transformation of coefficients obtained from MD simulations, of charged and neutral species, to operationally defined quantities, involving only neutral components. Operationally defined properties are usually obtained from experiments and are relevant for thermodynamic modelling. The transformation is called Rules for Coupling of Fluxes [90] and is schematically illustrated in Figure 5.5. The set of rules is based on entropy production invariance, when the electrolyte is viewed as a mixture of charged and neutral species (ions and solvents) or if the electrolyte is considered as a mixture of neutral components (salt and solvents) only. The procedure is as follows. Onsager coefficients obtained from equilibrium simulations in the barycentric frame of reference are converted to the solvent frame of reference using Gibbs-Duhem's equation, thereby reducing the number of unknown coefficients. The coefficients for the mixed scenario of charged and neutral species are then converted to describe a scenario of neutral-only components using the Rules for Coupling of Fluxes. Expressions for conductivity, transference coefficients, and transport numbers from Onsager coefficients are presented. We show how to relate Onsager and Fickian diffusion coefficients by thermodynamic factors. We can now model the electric potential gradient across the electrolyte of the cell using the above values.

5.4 Article IV

In the fourth paper, we use the theory from the third paper and show how to compute the electrolyte effect on battery voltage for practical lithium-ion battery electrolytes. We simulate standard ternary liquid electrolytes composed of ethylene carbonate (EC) and diethyl/dimethyl carbonate (DEC/DMC) with 1 M $LiPF_6$. Using the Rules for Coupling of Fluxes, we convert the simulated coefficients to operationally defined properties. Gradients in temperature, and in chemical potentials of components influence the electric potential gradient. The ohmic loss is always present. Upon starting charging or discharging of the battery, the electric potential gradient will evolve from an initial point with no chemical potential or temperature gradients. Intermediate scenarios can only be numerically solved, but in the stationary state with linear gradients it is possi-

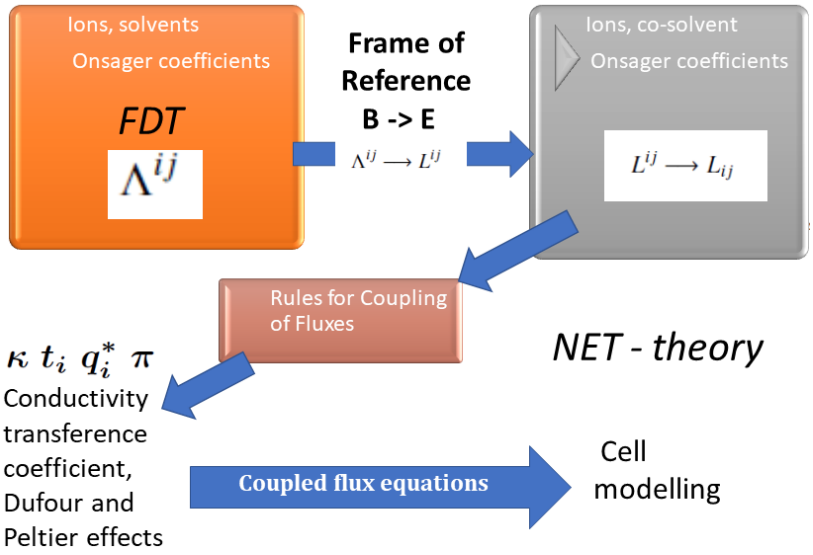

Figure 5.5: Procedure for calculation of diffusion coefficients, transference coefficients and conductivities for cell modelling from Onsager coefficients obtained from MD using the Rules for Coupling of Fluxes. Reproduced with permission from ref. [90]. Copyright 2023 The Journal of Chemical Physics.

ble to calculate the electric potential gradient exactly. We perform the calculation at stationary state and quantify the various contributions. We find that the salt concentration gradient contributes the most, followed by the ohmic loss and solvent polarization. All contributions are relevant. Solvent polarization, caused by the transport of Li^+ and the non-symmetric solvation environment of Li^+, has so far not been taken into account in state-of-the-art cell level models [164, 165]. The isothermal contributions are all found by MD simulations using the fluctuation-dissipation theorems and they are shown in Figure 5.6.

Temperature gradients may also form in the electrolyte causing a thermal contribution to the electric potential gradient via the Seebeck effect. We have determined the Seebeck coefficient of the electrolyte by placing liquid electrolytes between Li metal electrodes thermostatted to different temperatures and measuring the resulting voltage response. After subtracting the electrode contributions to the Peltier heat, we obtain the Seebeck coefficient for the electrolyte alone. The time evolution of the electric potential difference suggests a small Soret effect, which is confirmed by non-equilibrium MD simulations. The Soret effect can be neglected without loss of precision. We find the thermal polarization to be limited, but in the case of an applied interelectrode thermal force it becomes significant. The type of linear carbonate has a significant impact

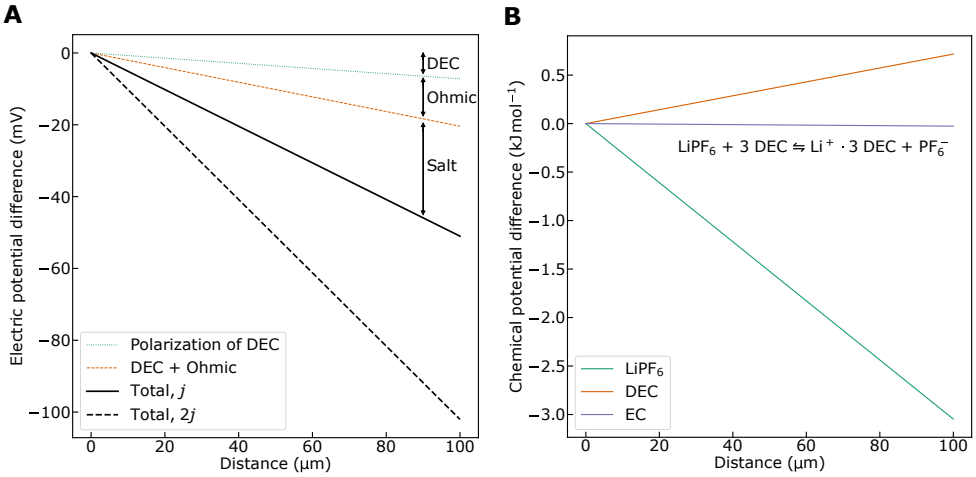

Figure 5.6: (a) Isothermal electrolyte contributions to electric potential difference in the stationary state as a function of distance from the anode during discharge. Contributions are shown for a current density corresponding to a discharge time of 1 h (1 C rate). The total polarization for a current density corresponding to a discharge time of 0.5 h (2 C rate) is also shown. Interface resistances are not taken into account. (b) Chemical potential gradients of the three components in the stationary state as a function of distance from the anode during discharge. The chemical potential gradient of $LiPF_6$ is negative and it is slightly positive for DEC. In the EC frame of reference, the chemical potential of EC is constant. Only relative differences matter, i.e. the starting point is arbitrary. Interface resistances are neglected.

on the voltage as the total polarization is reduced by almost 50 % by replacing DEC with the shorter linear carbonate DMC.

6 Conclusion and Perspectives

This work is a contribution to the increasing body of electrolyte studies by molecular dynamics simulations. We have focused on various types of coupling effects in electrolytes characterized by Onsager coefficients, L_{ij}, i.e. coupling between different components in the electrolyte in mass transport, the coupling between mass transport and electric potential (transference), between heat and mass transport (Soret effect), and between heat transport and electric potential (Seebeck effect). All types of coupling in mass transport can be examined from equilibrium fluctuations alone. The coupling effects are shown to be significant, and must be taken into account for an improved understanding of battery operation and performance.

6.1 Further work

Understanding transport in common electrolytes by molecular dynamics simulations is interesting and a natural starting point as experimental data is readily available to support our models and findings. The simulations are complementary to experiments as we can quantify coupling effects and directly examine microscopic mechanisms that evades most experimental techniques. The ability to predict transport properties based on the electrolyte components and structure is highly desirable. Still, this ability is lacking [51]. It is necessary to continue the studies of liquid and polymer electrolytes to increase our knowledge base and general understanding. To make better batteries, new electrolytes need to be designed and a bottom-up type molecular-level design approach is becoming more relevant, but requires a bottom-up understanding — from microscopic mechanisms to macroscopic properties. Electrolytes for next-generation batteries are potentially more complex than the current electrolytes. Up until now, mostly quite simple electrolytes have been investigated, but we also need to understand the transport in ternary and quaternary electrolytes, containing several solvents

and salts, and the coupling effects present in these. This should be a focus for future work.

The method that we present and apply in articles III and IV can be utilized directly to evaluate any other battery electrolyte and its effect on the voltage, given that accurate molecular models exist. It could be useful for characterization and evaluation of new electrolytes. We also believe the framework is a better starting point for improved modelling of battery cells than the current state-of-the-art models [164, 165]. The development and optimization of molecular force fields of new electrolytes, including effects like polarizability and charge transfer, needs to continue to improve the models used in simulations. Machine-learned potentials that potentially can combine ab-initio accuracy with classical MD computational efficiency are promising in this respect [166–170].

The interface between the electrode and electrolyte is the location of the electrochemical reactions and is the most important part of a battery or any electrochemical process. Understanding these interfaces is challenging, but highly valuable and perhaps necessary to enable next-generation battery technologies like lithium metal batteries. The properties of the interface can be dramatically different than the adjacent bulk phases [94]. The nature of the interfaces, e.g. their size, dynamics, and composition, render them difficult if not impossible to examine experimentally. Computer simulations can be a useful complementary technique for studying and understanding the interface. Simulating the spontaneously formed electric double layer at the interface is possible [171–173]. Such simulations can provide important information about the charge transfer, mass transfer, desolvation and reduction of Li^+, formation of SEI layer [174, 175], and deposition mechanisms of Li which determine the morphology of Li metal anodes [176]. Including the interface next to the electrode is a natural extension to the homogeneous simulations we have performed in this work.

References

[1] *Global direct primary energy consumption.*
https://ourworldindata.org/grapher/global-primary-energy.
Accessed: January 2024.

[2] U. N. E. Programme.
Global Environment Outlook – GEO-6: Healthy Planet, Healthy People. 2019.

[3] G. E. Blomgren. "The Development and Future of Lithium Ion Batteries".
Journal of The Electrochemical Society **164** (2016), A5019.
DOI: 10.1149/2.0251701jes.

[4] D. Howell, S. Boyd, B. Cunningham, S. Gillard, and L. Slezak.
Enabling fast charging: a technology gap assessment. Tech. rep.
Accessed: 2023-01-08.
https://www.energy.gov/sites/default/files/2017/10/f38/XFC%20Technology%20Gap%20Assessment%20Report_FINAL_10202017.pdf.
US Department of Energy, 2017.

[5] X. Fan and C. Wang.
"High-voltage liquid electrolytes for Li batteries: progress and perspectives".
Chem. Soc. Rev. **50** (18 2021), pp. 10486–10566. DOI: 10.1039/D1CS00450F.

[6] V. Thangadurai and B. Chen.
"Solid Li- and Na-Ion Electrolytes for Next Generation Rechargeable Batteries".
Chemistry of Materials **34** (2022), pp. 6637–6658.
DOI: 10.1021/acs.chemmater.2c01475.

[7] M. Forsyth, L. Porcarelli, X. Wang, N. Goujon, and D. Mecerreyes.
"Innovative Electrolytes Based on Ionic Liquids and Polymers for
Next-Generation Solid-State Batteries".

Accounts of Chemical Research **52** (2019), pp. 686–694.
DOI: 10.1021/acs.accounts.8b00566.

[8] A. Urban, D.-H. Seo, and G. Ceder.
"Computational understanding of Li-ion batteries".
npj Computational Materials **2** (2016), p. 16002.
DOI: 10.1038/npjcompumats.2016.2.

[9] E. A. Guggenheim. "The Conceptions of Electrical Potential Difference between Two Phases and the Individual Activities of Ions".
The Journal of Physical Chemistry **33** (1929), pp. 842–849.
DOI: 10.1021/j150300a003.

[10] J. Newman, K. E. Thomas, H. Hafezi, and D. R. Wheeler.
"Modeling of lithium-ion batteries".
Journal of Power Sources **119-121** (2003). Selected papers presented at the 11th International Meeting on Lithium Batteries, pp. 838–843.
DOI: https://doi.org/10.1016/S0378-7753(03)00282-9.

[11] A. Manthiram. "A reflection on lithium-ion battery cathode chemistry".
Nature Communications **11** (2020), p. 1550.
DOI: 10.1038/s41467-020-15355-0.

[12] S. Lee, J. Kim, J. Lee, and B. Cho. "State-of-charge and capacity estimation of lithium-ion battery using a new open-circuit voltage versus state-of-charge".
Journal of Power Sources **185** (2008), pp. 1367–1373.
DOI: https://doi.org/10.1016/j.jpowsour.2008.08.103.

[13] A. Nyman, T. G. Zavalis, R. Elger, M. Behm, and G. Lindbergh.
"Analysis of the Polarization in a Li-Ion Battery Cell by Numerical Simulations".
Journal of The Electrochemical Society **157** (2010), A1236.
DOI: 10.1149/1.3486161.

[14] L. Spitthoff, A. F. Gunnarshaug, D. Bedeaux, O. Burheim, and S. Kjelstrup.
"Peltier effects in lithium-ion battery modeling".
The Journal of Chemical Physics **154** (2021), p. 114705.
DOI: 10.1063/5.0038168.

[15] A. F. Gunnarshaug, P. J. S. Vie, and S. Kjelstrup.
"Review—Reversible Heat Effects in Cells Relevant for Lithium-Ion Batteries".

Journal of The Electrochemical Society **168** (2021), p. 050522.
DOI: 10.1149/1945-7111/abfd73.

[16] K. P. C. Yao, J. S. Okasinski, K. Kalaga, I. A. Shkrob, and D. P. Abraham. "Quantifying lithium concentration gradients in the graphite electrode of Li-ion cells using operando energy dispersive X-ray diffraction". *Energy Environ. Sci.* **12** (2 2019), pp. 656–665. DOI: 10.1039/C8EE02373E.

[17] M. R. Roberts, A. Madsen, C. Nicklin, J. Rawle, M. G. Palmer, J. R. Owen, and A. L. Hector. "Direct Observation of Active Material Concentration Gradients and Crystallinity Breakdown in $LiFePO_4$ Electrodes During Charge/Discharge Cycling of Lithium Batteries". *The Journal of Physical Chemistry C* **118** (2014). PMID: 24790684, pp. 6548–6557. DOI: 10.1021/jp411152s.

[18] A. K. Padhi, K. S. Nanjundaswamy, and J. B. Goodenough. "Phospho-olivines as Positive-Electrode Materials for Rechargeable Lithium Batteries". *Journal of The Electrochemical Society* **144** (1997), p. 1188. DOI: 10.1149/1.1837571.

[19] J. R. Dahn. "Phase diagram of Li_xC_6". *Phys. Rev. B* **44** (17 1991), pp. 9170–9177. DOI: 10.1103/PhysRevB.44.9170.

[20] H. Fujimoto, T. Yamaki, K. Shimoda, S. Fujinami, T. Nakatani, G. Kano, M. Kawasaki, Z. Ogumi, and T. Abe. "Phase Diagram of Li-Graphite Intercalation Compound Formed by the Charge/Discharge Reaction in Li-Ion Battery". *Journal of The Electrochemical Society* **169** (2022), p. 070507. DOI: 10.1149/1945-7111/ac7e77.

[21] S.-I. Pyun and Y.-G. Ryu. "Lithium transport through graphite electrodes that contain two stage phases". *Journal of Power Sources* **70** (1998), pp. 34–39. DOI: https://doi.org/10.1016/S0378-7753(97)02616-5.

[22] K. Mizushima, P. Jones, P. Wiseman, and J. Goodenough. "Li_xCoO_2 (0<x<-1): A new cathode material for batteries of high energy density". *Materials Research Bulletin* **15** (1980), pp. 783–789. DOI: https://doi.org/10.1016/0025-5408(80)90012-4.

[23] K. Numata, C. Sakaki, and S. Yamanaka. “Synthesis and characterization of layer structured solid solutions in the system of $LiCoO_2$–Li_2MnO_3”. *Solid State Ionics* **117** (1999), pp. 257–263. DOI: https://doi.org/10.1016/S0167-2738(98)00417-2.

[24] Z. Lu, D. D. MacNeil, and J. R. Dahn. “Layered Cathode Materials $Li[Ni_xLi_{(1/3-2x/3)}Mn_{(2/3-x/3)}]O_2$ for Lithium-Ion Batteries”. *Electrochemical and Solid-State Letters* **4** (2001), A191. DOI: 10.1149/1.1407994.

[25] N. Yabuuchi and T. Ohzuku. “Novel lithium insertion material of $LiCo_{1/3}Ni_{1/3}Mn_{1/3}O_2$ for advanced lithium-ion batteries”. *Journal of Power Sources* **119-121** (2003). Selected papers presented at the 11th International Meeting on Lithium Batteries, pp. 171–174. DOI: https://doi.org/10.1016/S0378-7753(03)00173-3.

[26] J. Quan, S. Zhao, D. Song, T. Wang, W. He, and G. Li. “Comparative life cycle assessment of LFP and NCM batteries including the secondary use and different recycling technologies”. *Science of The Total Environment* **819** (2022), p. 153105. DOI: https://doi.org/10.1016/j.scitotenv.2022.153105.

[27] T. Fan, W. Liang, W. Guo, T. Feng, and W. Li. “Life cycle assessment of electric vehicles’ lithium-ion batteries reused for energy storage”. *Journal of Energy Storage* **71** (2023), p. 108126. DOI: https://doi.org/10.1016/j.est.2023.108126.

[28] S.-T. Myung, F. Maglia, K.-J. Park, C. S. Yoon, P. Lamp, S.-J. Kim, and Y.-K. Sun. “Nickel-Rich Layered Cathode Materials for Automotive Lithium-Ion Batteries: Achievements and Perspectives”. *ACS Energy Letters* **2** (2017), pp. 196–223. DOI: 10.1021/acsenergylett.6b00594.

[29] M. Kotal, S. Jakhar, S. Roy, and H. K. Sharma. “Cathode materials for rechargeable lithium batteries: Recent progress and future prospects”. *Journal of Energy Storage* **47** (2022), p. 103534. DOI: https://doi.org/10.1016/j.est.2021.103534.

[30] J. Xu, S. Dou, H. Liu, and L. Dai. “Cathode materials for next generation lithium ion batteries”. *Nano Energy* **2** (2013), pp. 439–442. DOI: https://doi.org/10.1016/j.nanoen.2013.05.013.

[31] Y. Jin, B. Zhu, Z. Lu, N. Liu, and J. Zhu. “Challenges and Recent Progress in the Development of Si Anodes for Lithium-Ion Battery”. *Advanced Energy Materials* **7** (2017), p. 1700715. DOI: https://doi.org/10.1002/aenm.201700715.

[32] D. Lin, Y. Liu, and Y. Cui. “Reviving the lithium metal anode for high-energy batteries”. *Nature Nanotechnology* **12** (2017), pp. 194–206. DOI: 10.1038/nnano.2017.16.

[33] J. Liu, Z. Bao, Y. Cui, E. J. Dufek, J. B. Goodenough, P. Khalifah, Q. Li, B. Y. Liaw, P. Liu, A. Manthiram, Y. S. Meng, V. R. Subramanian, M. F. Toney, V. V. Viswanathan, M. S. Whittingham, J. Xiao, W. Xu, J. Yang, X.-Q. Yang, and J.-G. Zhang. “Pathways for practical high-energy long-cycling lithium metal batteries”. *Nature Energy* **4** (2019), pp. 180–186. DOI: 10.1038/s41560-019-0338-x.

[34] B. Liu, J.-G. Zhang, and W. Xu. “Advancing Lithium Metal Batteries”. *Joule* **2** (2018), pp. 833–845. DOI: https://doi.org/10.1016/j.joule.2018.03.008.

[35] A. Wang, S. Kadam, H. Li, S. Shi, and Y. Qi. “Review on modeling of the anode solid electrolyte interphase (SEI) for lithium-ion batteries”. *npj Computational Materials* **4** (2018), p. 15. DOI: 10.1038/s41524-018-0064-0.

[36] E. Peled and S. Menkin. “Review—SEI: Past, Present and Future”. *Journal of The Electrochemical Society* **164** (2017), A1703. DOI: 10.1149/2.1441707jes.

[37] E. Peled, D. Golodnitsky, and G. Ardel. “Advanced Model for Solid Electrolyte Interphase Electrodes in Liquid and Polymer Electrolytes”. *Journal of The Electrochemical Society* **144** (1997), p. L208. DOI: 10.1149/1.1837858.

[38] P. Verma, P. Maire, and P. Novák. “A review of the features and analyses of the solid electrolyte interphase in Li-ion batteries”. *Electrochimica Acta* **55** (2010), pp. 6332–6341. DOI: https://doi.org/10.1016/j.electacta.2010.05.072.

[39] K. Xu.
"Nonaqueous Liquid Electrolytes for Lithium-Based Rechargeable Batteries".
Chemical Reviews **104** (2004). PMID: 15669157, pp. 4303–4418.
DOI: 10.1021/cr030203g.

[40] S. S. Zhang. "A review on electrolyte additives for lithium-ion batteries".
Journal of Power Sources **162** (2006). Special issue including selected papers from the International Power Sources Symposium 2005 together with regular papers, pp. 1379–1394.
DOI: https://doi.org/10.1016/j.jpowsour.2006.07.074.

[41] A. M. Haregewoin, A. S. Wotango, and B.-J. Hwang. "Electrolyte additives for lithium ion battery electrodes: progress and perspectives".
Energy Environ. Sci. **9** (6 2016), pp. 1955–1988. DOI: 10.1039/C6EE00123H.

[42] Q. Liu, Y. Liu, X. Jiao, Z. Song, M. Sadd, X. Xu, A. Matic, S. Xiong, and J. Song.
"Enhanced ionic conductivity and interface stability of hybrid solid-state polymer electrolyte for rechargeable lithium metal batteries".
Energy Storage Materials **23** (2019), pp. 105–111.
DOI: https://doi.org/10.1016/j.ensm.2019.05.023.

[43] J.-H. Shin, W. Henderson, G. Appetecchi, F. Alessandrini, and S. Passerini.
"Recent developments in the ENEA lithium metal battery project".
Electrochimica Acta **50** (2005). Polymer Electrolytes, pp. 3859–3865.
DOI: https://doi.org/10.1016/j.electacta.2005.02.049.

[44] Z. Xue, D. He, and X. Xie.
"Poly(ethylene oxide)-based electrolytes for lithium-ion batteries".
Journal of Materials Chemistry A **3** (2015), pp. 19218–19253.
DOI: 10.1039/c5ta03471j.

[45] D. Zhou, D. Shanmukaraj, A. Tkacheva, M. Armand, and G. Wang.
"Polymer Electrolytes for Lithium-Based Batteries: Advances and Prospects".
Chem **5** (2019), pp. 2326–2352.
DOI: https://doi.org/10.1016/j.chempr.2019.05.009.

[46] K. Pożyczka, M. Marzantowicz, J. Dygas, and F. Krok.
"IONIC CONDUCTIVITY AND LITHIUM TRANSFERENCE NUMBER OF POLY(ETHYLENE OXIDE):LiTFSI SYSTEM".
Electrochimica Acta **227** (2017), pp. 127–135.
DOI: https://doi.org/10.1016/j.electacta.2016.12.172.

[47] H. Zhang, C. Liu, L. Zheng, F. Xu, W. Feng, H. Li, X. Huang, M. Armand, J. Nie, and Z. Zhou.
"Lithium bis(fluorosulfonyl)imide/poly(ethylene oxide) polymer electrolyte".
Electrochimica Acta **133** (2014), pp. 529–538.
DOI: https://doi.org/10.1016/j.electacta.2014.04.099.

[48] M. Wetjen, G.-T. Kim, M. Joost, G. B. Appetecchi, M. Winter, and S. Passerini.
"Thermal and electrochemical properties of PEO-LiTFSI-Pyr_{14}TFSI-based composite cathodes, incorporating 4 V-class cathode active materials".
Journal of Power Sources **246** (2014), pp. 846–857.
DOI: https://doi.org/10.1016/j.jpowsour.2013.08.037.

[49] I. Kelly, J. Owen, and B. Steele. "Mixed polyether lithium-ion conductors".
Journal of Electroanalytical Chemistry and Interfacial Electrochemistry **168** (1984), pp. 467–478.
DOI: https://doi.org/10.1016/0368-1874(84)87116-6.

[50] Ø. Gullbrekken, A. F. Gunnarshaug, A. Lervik, S. Kjelstrup, and S. K. Schnell.
"Effect of the Ion, Solvent, and Thermal Interaction Coefficients on Battery Voltage". *Journal of the American Chemical Society* **146** (2024). PMID: 38340142, pp. 4592–4604. DOI: 10.1021/jacs.3c11589.

[51] A. Mistry, Z. Yu, B. L. Peters, C. Fang, R. Wang, L. A. Curtiss, N. P. Balsara, L. Cheng, and V. Srinivasan. "Toward Bottom-Up Understanding of Transport in Concentrated Battery Electrolytes".
ACS Central Science **8** (2022), pp. 880–890.
DOI: 10.1021/acscentsci.2c00348.

[52] B. Dereka, N. H. C. Lewis, Y. Zhang, N. T. Hahn, J. H. Keim, S. A. Snyder, E. J. Maginn, and A. Tokmakoff.
"Exchange-Mediated Transport in Battery Electrolytes: Ultrafast or Ultraslow?"
Journal of the American Chemical Society **144** (2022). PMID: 35470669, pp. 8591–8604. DOI: 10.1021/jacs.2c00154.

[53] A. Mistry, Z. Yu, L. Cheng, and V. Srinivasan. "On Relative Importance of Vehicular and Structural Motions in Defining Electrolyte Transport".
Journal of The Electrochemical Society **170** (2023), p. 110536.
DOI: 10.1149/1945-7111/ad0c66.

[54] J. C. Bachman, S. Muy, A. Grimaud, H.-H. Chang, N. Pour, S. F. Lux, O. Paschos, F. Maglia, S. Lupart, P. Lamp, L. Giordano, and Y. Shao-Horn. "Inorganic Solid-State Electrolytes for Lithium Batteries: Mechanisms and Properties Governing Ion Conduction". *Chemical Reviews* **116** (2016). PMID: 26713396, pp. 140–162. DOI: 10.1021/acs.chemrev.5b00563.

[55] J. Newman. *Electrochemical Systems*. Second. Prentice-Hall, 1991.

[56] Y. Ma, M. Doyle, T. F. Fuller, M. M. Doeff, L. C. D. Jonghe, and J. Newman. "The Measurement of a Complete Set of Transport Properties for a Concentrated Solid Polymer Electrolyte Solution". *Journal of The Electrochemical Society* **142** (1995), pp. 1859–1868. DOI: 10.1149/1.2044206.

[57] D. M. Pesko, K. Timachova, R. Bhattacharya, M. C. Smith, I. Villaluenga, J. Newman, and N. P. Balsara. "Negative Transference Numbers in Poly(ethylene oxide)-Based Electrolytes". *Journal of The Electrochemical Society* **164** (2017), E3569–E3575. DOI: 10.1149/2.0581711jes.

[58] A. A. Lee, C. S. Perez-Martinez, A. M. Smith, and S. Perkin. "Scaling Analysis of the Screening Length in Concentrated Electrolytes". *Phys. Rev. Lett.* **119** (2 2017), p. 026002. DOI: 10.1103/PhysRevLett.119.026002.

[59] I. Villaluenga, D. M. Pesko, K. Timachova, Z. Feng, J. Newman, V. Srinivasan, and N. P. Balsara. "Negative Stefan-Maxwell Diffusion Coefficients and Complete Electrochemical Transport Characterization of Homopolymer and Block Copolymer Electrolytes". *Journal of The Electrochemical Society* **165** (2018), A2766–A2773. DOI: 10.1149/2.0641811jes.

[60] K. D. Fong, H. K. Bergstrom, B. D. McCloskey, and K. K. Mandadapu. "Transport phenomena in electrolyte solutions: Nonequilibrium thermodynamics and statistical mechanics". *AIChE Journal* **66** (2020), e17091. DOI: https://doi.org/10.1002/aic.17091.

[61] M. Doyle, T. F. Fuller, and J. Newman. "The importance of the lithium ion transference number in lithium/polymer cells".

Electrochimica Acta **39** (1994), pp. 2073–2081.
DOI: https://doi.org/10.1016/0013-4686(94)85091-7.

[62] K. M. Diederichsen, E. J. McShane, and B. D. McCloskey. “Promising Routes to a High Li^+ Transference Number Electrolyte for Lithium Ion Batteries”. *ACS Energy Letters* **2** (2017), pp. 2563–2575.
DOI: 10.1021/acsenergylett.7b00792.

[63] G. S. Hartley. “A new method for the determination of transport numbers. Part I.—Theory of the method”. *Trans. Faraday Soc.* **30** (0 1934), pp. 648–653.
DOI: 10.1039/TF9343000648.

[64] P. G. Bruce and C. A. Vincent.
“Steady state current flow in solid binary electrolyte cells”.
Journal of Electroanalytical Chemistry and Interfacial Electrochemistry **225** (1987), pp. 1–17. DOI: https://doi.org/10.1016/0022-0728(87)80001-3.

[65] P. G. Bruce, M. T. Hardgrave, and C. A. Vincent. “The determination of transference numbers in solid polymer electrolytes using the Hittorf method”. *Solid State Ionics* **53-56** (1992), pp. 1087–1094.
DOI: https://doi.org/10.1016/0167-2738(92)90295-Z.

[66] A. A. Wang, S. Greenbank, G. Li, D. A. Howey, and C. W. Monroe.
“Current-driven solvent segregation in lithium-ion electrolytes”.
Cell Reports Physical Science **3** (2022), p. 101047.
DOI: https://doi.org/10.1016/j.xcrp.2022.101047.

[67] K. Xu. “Navigating the minefield of battery literature”.
Communications Materials **3** (2022), p. 31.
DOI: 10.1038/s43246-022-00251-5.

[68] D. M. Pesko, S. Sawhney, J. Newman, and N. P. Balsara.
“Comparing Two Electrochemical Approaches for Measuring Transference Numbers in Concentrated Electrolytes”.
Journal of The Electrochemical Society **165** (2018), A3014–A3021.
DOI: 10.1149/2.0231813jes.

[69] P. Kang, L. Wu, D. Chen, Y. Su, Y. Zhu, J. Lan, X. Yang, and G. Sui.
“Dynamical Ion Association and Transport Properties in PEO–LiTFSI Electrolytes: Effect of Salt Concentration”. *The Journal of Physical Chemistry B*

126 (2022). PMID: 35695471, pp. 4531–4542.
DOI: 10.1021/acs.jpcb.2c01523.

[70] N. Molinari, J. P. Mailoa, and B. Kozinsky.
"Effect of Salt Concentration on Ion Clustering and Transport in Polymer Solid Electrolytes: A Molecular Dynamics Study of PEO–LiTFSI".
Chemistry of Materials **30** (2018), pp. 6298–6306.
DOI: 10.1021/acs.chemmater.8b01955.

[71] A. France-Lanord and J. C. Grossman.
"Correlations from Ion Pairing and the Nernst-Einstein Equation".
Phys. Rev. Lett. **122** (13 2019), p. 136001.
DOI: 10.1103/PhysRevLett.122.136001.

[72] A. Mistry, L. S. Grundy, D. M. Halat, J. Newman, N. P. Balsara, and V. Srinivasan.
"Effect of Solvent Motion on Ion Transport in Electrolytes".
Journal of The Electrochemical Society **169** (2022), p. 040524.
DOI: 10.1149/1945-7111/ac6329.

[73] M. P. Rosenwinkel and M. Schönhoff. "Lithium Transference Numbers in PEO/LiTFSA Electrolytes Determined by Electrophoretic NMR".
Journal of The Electrochemical Society **166** (2019), A1977.
DOI: 10.1149/2.0831910jes.

[74] H. K. Bergstrom and B. D. McCloskey. "Ion Transport in (Localized) High Concentration Electrolytes for Li-Based Batteries".
ACS Energy Letters **0** (0000), pp. 373–380.
DOI: 10.1021/acsenergylett.3c01662.

[75] C. Fang, D. M. Halat, A. Mistry, J. A. Reimer, N. P. Balsara, and R. Wang.
"Quantifying selective solvent transport under an electric field in mixed-solvent electrolytes". *Chem. Sci.* **14** (20 2023), pp. 5332–5339.
DOI: 10.1039/D3SC01158E.

[76] M. Lorenz, F. Kilchert, P. Nürnberg, M. Schammer, A. Latz, B. Horstmann, and M. Schönhoff. "Local Volume Conservation in Concentrated Electrolytes Is Governing Charge Transport in Electric Fields". *The Journal of Physical Chemistry Letters* **13** (2022). PMID: 36102654, pp. 8761–8767.
DOI: 10.1021/acs.jpclett.2c02398.

[77] L. Fan, S. Wei, S. Li, Q. Li, and Y. Lu. “Recent Progress of the Solid-State Electrolytes for High-Energy Metal-Based Batteries”. *Advanced Energy Materials* **8** (2018), p. 1702657. DOI: https://doi.org/10.1002/aenm.201702657.

[78] A. Manthiram, X. Yu, and S. Wang. “Lithium battery chemistries enabled by solid-state electrolytes”. *Nature Reviews Materials* **2** (2017), p. 16103. DOI: 10.1038/natrevmats.2016.103.

[79] C. Wang, K. Fu, S. P. Kammampata, D. W. McOwen, A. J. Samson, L. Zhang, G. T. Hitz, A. M. Nolan, E. D. Wachsman, Y. Mo, V. Thangadurai, and L. Hu. “Garnet-Type Solid-State Electrolytes: Materials, Interfaces, and Batteries”. *Chemical Reviews* **120** (2020). PMID: 32271022, pp. 4257–4300. DOI: 10.1021/acs.chemrev.9b00427.

[80] C. Monroe and J. Newman. “The Impact of Elastic Deformation on Deposition Kinetics at Lithium/Polymer Interfaces”. *Journal of The Electrochemical Society* **152** (2005), A396. DOI: 10.1149/1.1850854.

[81] S. Yu, R. D. Schmidt, R. Garcia-Mendez, E. Herbert, N. J. Dudney, J. B. Wolfenstine, J. Sakamoto, and D. J. Siegel. “Elastic Properties of the Solid Electrolyte $Li_7La_3Zr_2O_{12}$ (LLZO)”. *Chemistry of Materials* **28** (2016), pp. 197–206. DOI: 10.1021/acs.chemmater.5b03854.

[82] L. Porz, T. Swamy, B. W. Sheldon, D. Rettenwander, T. Frömling, H. L. Thaman, S. Berendts, R. Uecker, W. C. Carter, and Y.-M. Chiang. “Mechanism of Lithium Metal Penetration through Inorganic Solid Electrolytes”. *Advanced Energy Materials* **7** (2017), p. 1701003. DOI: https://doi.org/10.1002/aenm.201701003.

[83] F. Han, A. S. Westover, J. Yue, X. Fan, F. Wang, M. Chi, D. N. Leonard, N. J. Dudney, H. Wang, and C. Wang. “High electronic conductivity as the origin of lithium dendrite formation within solid electrolytes”. *Nature Energy* **4** (2019), pp. 187–196. DOI: 10.1038/s41560-018-0312-z.

[84] S. Lou, F. Zhang, C. Fu, M. Chen, Y. Ma, G. Yin, and J. Wang. “Interface Issues and Challenges in All-Solid-State Batteries: Lithium, Sodium, and Beyond”.

Advanced Materials **33** (2021), p. 2000721.
DOI: https://doi.org/10.1002/adma.202000721.

[85] A. Gupta and J. Sakamoto.
"Controlling Ionic Transport through the PEO-LiTFSI/LLZTO Interface".
The Electrochemical Society Interface **28** (2019), p. 63.
DOI: 10.1149/2.F06192if.

[86] M. R. Bonilla, F. A. García Daza, H. A. Cortés, J. Carrasco, and E. Akhmatskaya.
"On the interfacial lithium dynamics in $Li_7La_3Zr_2O_{12}$:poly(ethylene oxide) (LiTFSI) composite polymer-ceramic solid electrolytes under strong polymer phase confinement".
Journal of Colloid and Interface Science **623** (2022), pp. 870–882.
DOI: https://doi.org/10.1016/j.jcis.2022.05.069.

[87] K. Nie, Y. Hong, J. Qiu, Q. Li, X. Yu, H. Li, and L. Chen.
"Interfaces Between Cathode and Electrolyte in Solid State Lithium Batteries: Challenges and Perspectives". *Frontiers in Chemistry* **6** (2018).
DOI: 10.3389/fchem.2018.00616.

[88] S. Su, J. Ma, L. Zhao, K. Lin, Q. Li, S. Lv, F. Kang, and Y.-B. He.
"Progress and perspective of the cathode/electrolyte interface construction in all-solid-state lithium batteries". *Carbon Energy* **3** (2021), pp. 866–894.
DOI: https://doi.org/10.1002/cey2.129.

[89] B. Gao, R. Jalem, Y. Ma, and Y. Tateyama. "Li^+ Transport Mechanism at the Heterogeneous Cathode/Solid Electrolyte Interface in an All-Solid-State Battery via the First-Principles Structure Prediction Scheme".
Chemistry of Materials **32** (2020), pp. 85–96.
DOI: 10.1021/acs.chemmater.9b02311.

[90] S. Kjelstrup, A. F. Gunnarshaug, Ø. Gullbrekken, S. K. Schnell, and A. Lervik.
"Transport coefficients for ion and solvent coupling. The case of the lithium-ion battery electrolyte".
The Journal of Chemical Physics **159** (2023), p. 034104.
DOI: 10.1063/5.0158623.

[91] K. Førland, T. Førland, and S. Kjelstrup Ratkje.
Irreversible thermodynamics. Theory and Applications. Wiley, Chichester, 1988.

[92] I. Prigogine. “The Equilibrium Hypothesis in Chemical Kinetics.” *The Journal of Physical Chemistry* **55** (1951), pp. 765–774. DOI: 10.1021/j150489a002.

[93] T. W. Maltby, B. Hafskjold, D. Bedeaux, S. Kjelstrup, and Ø. Wilhelmsen. “Local equilibrium in liquid phase shock waves”. *Phys. Rev. E* **107** (3 2023), p. 035108. DOI: 10.1103/PhysRevE.107.035108.

[94] S. Kjelstrup and D. Bedeaux. *Non-Equilibrium Thermodynamics of Heterogeneous Systems*. Singapore: World Scientific, 2008. DOI: 10.1142/6672.

[95] H. B. Callen and T. A. Welton. “Irreversibility and Generalized Noise”. *Phys. Rev.* **83** (1 1951), pp. 34–40. DOI: 10.1103/PhysRev.83.34.

[96] M. S. Green. “Markoff Random Processes and the Statistical Mechanics of Time-Dependent Phenomena”. *The Journal of Chemical Physics* **20** (2004), pp. 1281–1295. DOI: 10.1063/1.1700722.

[97] M. S. Green. “Markoff Random Processes and the Statistical Mechanics of Time-Dependent Phenomena. II. Irreversible Processes in Fluids”. *The Journal of Chemical Physics* **22** (2004), pp. 398–413. DOI: 10.1063/1.1740082.

[98] R. Kubo. “Statistical-Mechanical Theory of Irreversible Processes. I. General Theory and Simple Applications to Magnetic and Conduction Problems”. *Journal of the Physical Society of Japan* **12** (1957), pp. 570–586. DOI: 10.1143/JPSJ.12.570.

[99] E. Helfand. “Transport Coefficients from Dissipation in a Canonical Ensemble”. *Phys. Rev.* **119** (1 1960), pp. 1–9. DOI: 10.1103/PhysRev.119.1.

[100] S. H. Jamali, L. Wolff, T. M. Becker, M. de Groen, M. Ramdin, R. Hartkamp, A. Bardow, T. J. H. Vlugt, and O. A. Moultos. “OCTP: A Tool for On-the-Fly Calculation of Transport Properties of Fluids with the Order-n Algorithm in LAMMPS”. *Journal of Chemical Information and Modeling* **59** (2019), pp. 1290–1294. DOI: 10.1021/acs.jcim.8b00939.

[101] M. Ebadi, T. Eriksson, P. Mandal, L. T. Costa, C. M. Araujo, J. Mindemark, and D. Brandell. “Restricted Ion Transport by Plasticizing Side Chains in Polycarbonate-Based Solid Electrolytes”.
Macromolecules **53** (2020), pp. 764–774.
DOI: 10.1021/acs.macromol.9b01912.

[102] L. J. A. Siqueira and M. C. C. Ribeiro. “Molecular dynamics simulation of the polymer electrolyte poly(ethylene oxide)/$LiClO_4$. II. Dynamical properties”.
The Journal of Chemical Physics **125** (2006), p. 214903.
DOI: 10.1063/1.2400221.

[103] A. France-Lanord, Y. Wang, T. Xie, J. A. Johnson, Y. Shao-Horn, and J. C. Grossman. “Effect of Chemical Variations in the Structure of Poly(ethylene oxide)-Based Polymers on Lithium Transport in Concentrated Electrolytes”.
Chemistry of Materials **32** (2020), pp. 121–126.
DOI: 10.1021/acs.chemmater.9b02645.

[104] D. J. Brooks, B. V. Merinov, W. A. Goddard, B. Kozinsky, and J. Mailoa. “Atomistic Description of Ionic Diffusion in PEO–LiTFSI: Effect of Temperature, Molecular Weight, and Ionic Concentration”.
Macromolecules **51** (2018), pp. 8987–8995.
DOI: 10.1021/acs.macromol.8b01753.

[105] K. D. Fong, J. Self, B. D. McCloskey, and K. A. Persson. “Ion Correlations and Their Impact on Transport in Polymer-Based Electrolytes”.
Macromolecules **54** (2021), pp. 2575–2591.
DOI: 10.1021/acs.macromol.0c02545.

[106] C. Y. Son and Z.-G. Wang.
“Ion transport in small-molecule and polymer electrolytes”.
The Journal of Chemical Physics **153** (2020), p. 100903.
DOI: 10.1063/5.0016163.

[107] S. Kjelstrup, K. R. Kristiansen, A. F. Gunnarshaug, and D. Bedeaux.
“Seebeck, Peltier, and Soret effects: On different formalisms for transport equations in thermogalvanic cells”.
The Journal of Chemical Physics **158** (2023). 020901.
DOI: 10.1063/5.0131731.

[108] K. D. Fong, J. Self, B. D. McCloskey, and K. A. Persson.
"Onsager Transport Coefficients and Transference Numbers in Polyelectrolyte Solutions and Polymerized Ionic Liquids".
Macromolecules **53** (2020), pp. 9503–9512.
DOI: 10.1021/acs.macromol.0c02001.

[109] K. D. Fong, J. Self, K. M. Diederichsen, B. M. Wood, B. D. McCloskey, and K. A. Persson. "Ion Transport and the True Transference Number in Nonaqueous Polyelectrolyte Solutions for Lithium Ion Batteries".
ACS Central Science **5** (2019), pp. 1250–1260.
DOI: 10.1021/acscentsci.9b00406.

[110] N. M. Vargas-Barbosa and B. Roling. "Dynamic Ion Correlations in Solid and Liquid Electrolytes: How Do They Affect Charge and Mass Transport?"
ChemElectroChem **7** (2020), pp. 367–385.
DOI: https://doi.org/10.1002/celc.201901627.

[111] H. G. Buss, S. Y. Chan, N. A. Lynd, and B. D. McCloskey.
"Nonaqueous Polyelectrolyte Solutions as Liquid Electrolytes with High Lithium Ion Transference Number and Conductivity".
ACS Energy Letters **2** (2017), pp. 481–487.
DOI: 10.1021/acsenergylett.6b00724.

[112] K. M. Diederichsen, K. D. Fong, R. C. Terrell, K. A. Persson, and B. D. McCloskey.
"Investigation of Solvent Type and Salt Addition in High Transference Number Nonaqueous Polyelectrolyte Solutions for Lithium Ion Batteries".
Macromolecules **51** (2018), pp. 8761–8771.
DOI: 10.1021/acs.macromol.8b01696.

[113] A. Lewandowski and A. Świderska-Mocek. "Ionic liquids as electrolytes for Li-ion batteries—An overview of electrochemical studies".
Journal of Power Sources **194** (2009), pp. 601–609.
DOI: https://doi.org/10.1016/j.jpowsour.2009.06.089.

[114] M. Watanabe, M. L. Thomas, S. Zhang, K. Ueno, T. Yasuda, and K. Dokko.
"Application of Ionic Liquids to Energy Storage and Conversion Materials and Devices". *Chemical Reviews* **117** (2017). PMID: 28084733, pp. 7190–7239.
DOI: 10.1021/acs.chemrev.6b00504.

[115] Q. Yang, Z. Zhang, X.-G. Sun, Y.-S. Hu, H. Xing, and S. Dai. "Ionic liquids and derived materials for lithium and sodium batteries". *Chem. Soc. Rev.* **47** (6 2018), pp. 2020–2064. DOI: 10.1039/C7CS00464H.

[116] H. Gudla, Y. Shao, S. Phunnarungsi, D. Brandell, and C. Zhang. "Importance of the Ion-Pair Lifetime in Polymer Electrolytes". *The Journal of Physical Chemistry Letters* **12** (2021). PMID: 34449227, pp. 8460–8464. DOI: 10.1021/acs.jpclett.1c02474.

[117] Y. Shao, H. Gudla, D. Brandell, and C. Zhang. "Transference Number in Polymer Electrolytes: Mind the Reference-Frame Gap". *Journal of the American Chemical Society* **144** (2022), pp. 7583–7587. DOI: 10.1021/jacs.2c02389.

[118] X. Cao, H. Jia, W. Xu, and J.-G. Zhang. "Review—Localized High-Concentration Electrolytes for Lithium Batteries". *Journal of The Electrochemical Society* **168** (2021), p. 010522. DOI: 10.1149/1945-7111/abd60e.

[119] R. Krishna and J. Wesselingh. "The Maxwell-Stefan approach to mass transfer". *Chemical Engineering Science* **52** (1997), pp. 861–911. DOI: https://doi.org/10.1016/S0009-2509(96)00458-7.

[120] R. Krishna and J. M. van Baten. "The Darken Relation for Multicomponent Diffusion in Liquid Mixtures of Linear Alkanes: An Investigation Using Molecular Dynamics (MD) Simulations". *Industrial & Engineering Chemistry Research* **44** (2005), pp. 6939–6947. DOI: 10.1021/ie050146c.

[121] L. A. Woolf and K. R. Harris. "Velocity correlation coefficients as an expression of particle–particle interactions in (electrolyte) solutions". *J. Chem. Soc., Faraday Trans. 1* **74** (0 1978), pp. 933–947. DOI: 10.1039/F19787400933.

[122] D. Dong, F. Sälzer, B. Roling, and D. Bedrov. "How efficient is Li^+ ion transport in solvate ionic liquids under anion-blocking conditions in a battery?" *Phys. Chem. Chem. Phys.* **20** (46 2018), pp. 29174–29183. DOI: 10.1039/C8CP06214E.

[123] S. Pfeifer, F. Ackermann, F. Sälzer, M. Schönhoff, and B. Roling. "Quantification of cation–cation, anion–anion and cation–anion correlations in Li salt/glyme mixtures by combining very-low-frequency impedance spectroscopy with diffusion and electrophoretic NMR". *Phys. Chem. Chem. Phys.* **23** (1 2021), pp. 628–640. DOI: 10.1039/D0CP06147F.

[124] W. L. Jorgensen and J. Tirado-Rives. "Potential energy functions for atomic-level simulations of water and organic and biomolecular systems". *Proceedings of the National Academy of Sciences* **102** (2005), pp. 6665–6670. DOI: 10.1073/pnas.0408037102.

[125] W. L. Jorgensen, D. S. Maxwell, and J. Tirado-Rives. "Development and Testing of the OPLS All-Atom Force Field on Conformational Energetics and Properties of Organic Liquids". *Journal of the American Chemical Society* **118** (1996), pp. 11225–11236. DOI: 10.1021/ja9621760.

[126] C. Oostenbrink, A. Villa, A. E. Mark, and W. F. Van Gunsteren. "A biomolecular force field based on the free enthalpy of hydration and solvation: The GROMOS force-field parameter sets 53A5 and 53A6". *Journal of Computational Chemistry* **25** (2004), pp. 1656–1676. DOI: https://doi.org/10.1002/jcc.20090.

[127] Y. Duan, C. Wu, S. Chowdhury, M. C. Lee, G. Xiong, W. Zhang, R. Yang, P. Cieplak, R. Luo, T. Lee, J. Caldwell, J. Wang, and P. Kollman. "A point-charge force field for molecular mechanics simulations of proteins based on condensed-phase quantum mechanical calculations". *Journal of Computational Chemistry* **24** (2003), pp. 1999–2012. DOI: https://doi.org/10.1002/jcc.10349.

[128] A. D. J. MacKerell, D. Bashford, M. Bellott, R. L. J. Dunbrack, J. D. Evanseck, M. J. Field, S. Fischer, J. Gao, H. Guo, S. Ha, D. Joseph-McCarthy, L. Kuchnir, K. Kuczera, F. T. K. Lau, C. Mattos, S. Michnick, T. Ngo, D. T. Nguyen, B. Prodhom, W. E. Reiher, B. Roux, M. Schlenkrich, J. C. Smith, R. Stote, J. Straub, M. Watanabe, J. Wiórkiewicz-Kuczera, D. Yin, and M. Karplus. "All-Atom Empirical Potential for Molecular Modeling and Dynamics Studies of Proteins". *The Journal of Physical Chemistry B* **102** (1998). PMID: 24889800, pp. 3586–3616. DOI: 10.1021/jp973084f.

[129] I. V. Leontyev and A. A. Stuchebrukhov. “Polarizable molecular interactions in condensed phase and their equivalent nonpolarizable models”. *The Journal of Chemical Physics* **141** (2014), p. 014103. DOI: 10.1063/1.4884276.

[130] I. Leontyev and A. Stuchebrukhov. “Accounting for electronic polarization in non-polarizable force fields”. *Phys. Chem. Chem. Phys.* **13** (7 2011), pp. 2613–2626. DOI: 10.1039/C0CP01971B.

[131] V. Chaban. “Polarizability versus mobility: atomistic force field for ionic liquids”. *Phys. Chem. Chem. Phys.* **13** (35 2011), pp. 16055–16062. DOI: 10.1039/C1CP21379B.

[132] G. Saielli. “The effect of hydration on the stability of ionic liquid crystals: MD simulations of $[C_{14}C_1im]Cl$ and $[C_{14}C_1im]Cl \cdot H_2O$”. *Phys. Chem. Chem. Phys.* **23** (42 2021), pp. 24386–24395. DOI: 10.1039/D1CP03757A.

[133] K. Wendler, S. Zahn, F. Dommert, R. Berger, C. Holm, B. Kirchner, and L. Delle Site. “Locality and Fluctuations: Trends in Imidazolium-Based Ionic Liquids and Beyond”. *Journal of Chemical Theory and Computation* **7** (2011). PMID: 26598146, pp. 3040–3044. DOI: 10.1021/ct200375v.

[134] T. G. A. Youngs and C. Hardacre. “Application of Static Charge Transfer within an Ionic-Liquid Force Field and Its Effect on Structure and Dynamics”. *ChemPhysChem* **9** (2008), pp. 1548–1558. DOI: https://doi.org/10.1002/cphc.200800200.

[135] M. Bühl, A. Chaumont, R. Schurhammer, and G. Wipff. “Ab Initio Molecular Dynamics of Liquid 1,3-Dimethylimidazolium Chloride”. *The Journal of Physical Chemistry B* **109** (2005). PMID: 16853393, pp. 18591–18599. DOI: 10.1021/jp0518299.

[136] J. Schmidt, C. Krekeler, F. Dommert, Y. Zhao, R. Berger, L. D. Site, and C. Holm. “Ionic Charge Reduction and Atomic Partial Charges from First-Principles Calculations of 1,3-Dimethylimidazolium Chloride”. *The Journal of Physical Chemistry B* **114** (2010). PMID: 20397676, pp. 6150–6155. DOI: 10.1021/jp910771q.

[137] D. Bedrov, J.-P. Piquemal, O. Borodin, A. D. J. MacKerell, B. Roux, and C. Schröder. “Molecular Dynamics Simulations of Ionic Liquids and Electrolytes Using Polarizable Force Fields”. *Chemical Reviews* **119** (2019). PMID: 31141351, pp. 7940–7995. DOI: 10.1021/acs.chemrev.8b00763.

[138] Ø. Gullbrekken, I. T. Røe, S. M. Selbach, and S. K. Schnell. “Charge Transport in Water–NaCl Electrolytes with Molecular Dynamics Simulations”. *The Journal of Physical Chemistry B* **127** (2023). PMID: 36921121, pp. 2729–2738. DOI: 10.1021/acs.jpcb.2c08047.

[139] D. R. Wheeler and J. Newman. “Molecular Dynamics Simulations of Multicomponent Diffusion. 2. Nonequilibrium Method”. *The Journal of Physical Chemistry B* **108** (2004), pp. 18362–18367. DOI: 10.1021/jp047849c.

[140] D. MacGowan and D. J. Evans. “Heat and matter transport in binary liquid mixtures”. *Phys. Rev. A* **34** (3 1986), pp. 2133–2142. DOI: 10.1103/PhysRevA.34.2133.

[141] N. J. English and C. J. Waldron. “Perspectives on external electric fields in molecular simulation: progress, prospects and challenges”. *Phys. Chem. Chem. Phys.* **17** (19 2015), pp. 12407–12440. DOI: 10.1039/C5CP00629E.

[142] J. Ruiz-Franco, L. Rovigatti, and E. Zaccarelli. “On the effect of the thermostat in non-equilibrium molecular dynamics simulations”. *The European Physical Journal E* **41** (2018), p. 80. DOI: 10.1140/epje/i2018-11689-4.

[143] J. G. Kirkwood and F. P. Buff. “The Statistical Mechanical Theory of Solutions. I”. *The Journal of Chemical Physics* **19** (1951), pp. 774–777. DOI: 10.1063/1.1748352.

[144] A. T. Celebi, N. Dawass, O. A. Moultos, and T. J. H. Vlugt. “How sensitive are physical properties of choline chloride–urea mixtures to composition changes: Molecular dynamics simulations and Kirkwood–Buff theory”. *The Journal of Chemical Physics* **154** (2021), p. 184502. DOI: 10.1063/5.0049064.

[145] E. Ruckenstein and I. Shulgin. “Entrainer effect in supercritical mixtures”. *Fluid Phase Equilibria* **180** (2001), pp. 345–359. DOI: https://doi.org/10.1016/S0378-3812(01)00372-7.

[146] W. Zhao, F. Leroy, B. Heggen, S. Zahn, B. Kirchner, S. Balasubramanian, and F. Müller-Plathe. “Are There Stable Ion-Pairs in Room-Temperature Ionic Liquids? Molecular Dynamics Simulations of 1-n-Butyl-3-methylimidazolium Hexafluorophosphate”. *Journal of the American Chemical Society* **131** (2009), pp. 15825–15833. DOI: 10.1021/ja906337p.

[147] A. P. Thompson, H. M. Aktulga, R. Berger, D. S. Bolintineanu, W. M. Brown, P. S. Crozier, P. J. in ’t Veld, A. Kohlmeyer, S. G. Moore, T. D. Nguyen, R. Shan, M. J. Stevens, J. Tranchida, C. Trott, and S. J. Plimpton. “LAMMPS - a flexible simulation tool for particle-based materials modeling at the atomic, meso, and continuum scales”. *Comp. Phys. Comm.* **271** (2022), p. 108171. DOI: 10.1016/j.cpc.2021.108171.

[148] F. Kilchert, M. Lorenz, M. Schammer, P. Nürnberg, M. Schönhoff, A. Latz, and B. Horstmann. “A volume-based description of transport in incompressible liquid electrolytes and its application to ionic liquids”. *Phys. Chem. Chem. Phys.* **25** (38 2023), pp. 25965–25978. DOI: 10.1039/D2CP04423D.

[149] Ø. Gullbrekken and S. Kvalvåg Schnell. “Coupled ion transport in concentrated PEO–LiTFSI polymer electrolytes”. *New J. Chem.* **47** (44 2023), pp. 20344–20357. DOI: 10.1039/D3NJ04065H.

[150] S. de Groot and P. Mazur. *Non-equilibrium Thermodynamics*. North-Holland Publishing Company, 1962.

[151] H. J. C. Berendsen, J. R. Grigera, and T. P. Straatsma. “The Missing Term in Effective Pair Potentials”. *Journal of Physical Chemistry* **91** (1987), pp. 6269–6271. DOI: DOI10.1021/j100308a038.

[152] S. Weerasinghe and P. E. Smith. “A Kirkwood-Buff derived force field for sodium chloride in water”. *Journal of Chemical Physics* **119** (2003), pp. 11342–11349. DOI: 10.1063/1.1622372.

[153] G. Lamoureux, E. Harder, I. V. Vorobyov, B. Roux, and A. D. MacKerell. "A polarizable model of water for molecular dynamics simulations of biomolecules". *Chemical Physics Letters* **418** (2006), pp. 245–249. DOI: https://doi.org/10.1016/j.cplett.2005.10.135.

[154] H. Yu, T. W. Whitfield, E. Harder, G. Lamoureux, I. Vorobyov, V. M. Anisimov, A. D. J. MacKerell, and B. Roux. "Simulating Monovalent and Divalent Ions in Aqueous Solution Using a Drude Polarizable Force Field". *Journal of Chemical Theory and Computation* **6** (2010). PMID: 20300554, pp. 774–786. DOI: 10.1021/ct900576a.

[155] M. Bešter-Rogač, R. Neueder, and J. Barthel. "Conductivity of Sodium Chloride in Water + 1,4-Dioxane Mixtures from 5 to 35°C II. Concentrated Solution". *Journal of Solution Chemistry* **29** (2000), pp. 51–61. DOI: 10.1023/A:1005114500861.

[156] M. Della Monica, G. Petrella, A. Sacco, and S. Bufo. "Transference numbers in concentrated sodium chloride solutions". *Electrochimica Acta* **24** (1979), pp. 1013–1017. DOI: https://doi.org/10.1016/0013-4686(79)87099-1.

[157] L. J. M. Smits and E. M. Duyvis. "Transport Numbers of Concentrated Sodium Chloride Solutions at 25°". *The Journal of Physical Chemistry* **70** (1966), pp. 2747–2753. DOI: 10.1021/j100881a007.

[158] M. Spiro. "Volume Correction for the Indirect Moving-Boundary Method and the Transference Numbers of Concentrated Aqueous Sodium Chloride Solutions". *The Journal of Chemical Physics* **42** (1965), pp. 4060–4061. DOI: 10.1063/1.1695891.

[159] B. M. Braun. "Transference numbers of aqueous NaCl and Na_2SO_4 at 25°C from EMF measurements with sodium-selective glass electrodes". *Journal of Solution Chemistry* **14** (1985), pp. 675–686. DOI: 10.1007/BF00646059.

[160] K. Timachova. "Ion Diffusion and Electrochemically Driven Transport in Homogenous and Nanostructured Polymer Electrolytes". PhD thesis. University of California, Berkeley, 2018.

[161] J. Liu and C. W. Monroe. “Solute-volume effects in electrolyte transport”. *Electrochimica Acta* **135** (2014), pp. 447–460. DOI: https://doi.org/10.1016/j.electacta.2014.05.009.

[162] J. G. Kirkwood, R. L. Baldwin, P. J. Dunlop, L. J. Gosting, and G. Kegeles. “Flow Equations and Frames of Reference for Isothermal Diffusion in Liquids”. *The Journal of Chemical Physics* **33** (1960), pp. 1505–1513. DOI: 10.1063/1.1731433.

[163] Y. Zhou and G. H. Miller. “Green-Kubo Formulas for Mutual Diffusion Coefficients in Multicomponent Systems”. *The Journal of Physical Chemistry* **100** (1996), pp. 5516–5524. DOI: 10.1021/jp9533739.

[164] M. Andersson, M. Streb, J. Y. Ko, V. Löfqvist Klass, M. Klett, H. Ekström, M. Johansson, and G. Lindbergh. “Parametrization of physics-based battery models from input-output data: A review of methodology and current research”. *Journal of Power Sources* **521** (2022), p. 230859. DOI: https://doi.org/10.1016/j.jpowsour.2021.230859.

[165] A. A. Wang, S. E. J. O’Kane, F. B. Planella, J. L. Houx, K. O’Regan, M. Zyskin, J. Edge, C. W. Monroe, S. J. Cooper, D. A. Howey, E. Kendrick, and J. M. Foster. “Review of parameterisation and a novel database (LiionDB) for continuum Li-ion battery models”. *Progress in Energy* **4** (2022), p. 032004. DOI: 10.1088/2516-1083/ac692c.

[166] P.-L. Kang, C. Shang, and Z.-P. Liu. “Large-Scale Atomic Simulation via Machine Learning Potentials Constructed by Global Potential Energy Surface Exploration”. *Accounts of Chemical Research* **53** (2020). PMID: 32940999, pp. 2119–2129. DOI: 10.1021/acs.accounts.0c00472.

[167] G. Sivaraman, A. N. Krishnamoorthy, M. Baur, C. Holm, M. Stan, G. Csányi, C. Benmore, and Á. Vázquez-Mayagoitia. “Machine-learned interatomic potentials by active learning: amorphous and liquid hafnium dioxide”. *npj Computational Materials* **6** (2020), p. 104. DOI: 10.1038/s41524-020-00367-7.

[168] C. Verdi, F. Karsai, P. Liu, R. Jinnouchi, and G. Kresse.
"Thermal transport and phase transitions of zirconia by on-the-fly machine-learned interatomic potentials".
npj Computational Materials **7** (2021), p. 156.
DOI: 10.1038/s41524-021-00630-5.

[169] P. Friederich, F. Häse, J. Proppe, and A. Aspuru-Guzik.
"Machine-learned potentials for next-generation matter simulations".
Nature Materials **20** (2021), pp. 750–761. DOI: 10.1038/s41563-020-0777-6.

[170] Y. Shao, L. Knijff, F. M. Dietrich, K. Hermansson, and C. Zhang. "Modelling Bulk Electrolytes and Electrolyte Interfaces with Atomistic Machine Learning".
Batteries & Supercaps **4** (2021), pp. 585–595.
DOI: https://doi.org/10.1002/batt.202000262.

[171] J. I. Siepmann and M. Sprik. "Influence of surface topology and electrostatic potential on water/electrode systems".
The Journal of Chemical Physics **102** (1995), pp. 511–524.
DOI: 10.1063/1.469429.

[172] S. K. Reed, O. J. Lanning, and P. A. Madden. "Electrochemical interface between an ionic liquid and a model metallic electrode".
The Journal of Chemical Physics **126** (2007), p. 084704.
DOI: 10.1063/1.2464084.

[173] L. J. V. Ahrens-Iwers, M. Janssen, S. R. Tee, and R. H. Meißner.
"ELECTRODE: An electrochemistry package for atomistic simulations".
The Journal of Chemical Physics **157** (2022), p. 084801.
DOI: 10.1063/5.0099239.

[174] C. Yan, R. Xu, Y. Xiao, J.-F. Ding, L. Xu, B.-Q. Li, and J.-Q. Huang.
"Toward Critical Electrode/Electrolyte Interfaces in Rechargeable Batteries".
Advanced Functional Materials **30** (2020), p. 1909887.
DOI: https://doi.org/10.1002/adfm.201909887.

[175] Q. Wu, M. T. McDowell, and Y. Qi. "Effect of the Electric Double Layer (EDL) in Multicomponent Electrolyte Reduction and Solid Electrolyte Interphase (SEI) Formation in Lithium Batteries". *Journal of the American Chemical Society* **145** (2023). PMID: 36689617, pp. 2473–2484. DOI: 10.1021/jacs.2c11807.

[176] D. T. Boyle, S. C. Kim, S. T. Oyakhire, R. A. Vilá, Z. Huang, P. Sayavong, J. Qin, Z. Bao, and Y. Cui. “Correlating Kinetics to Cyclability Reveals Thermodynamic Origin of Lithium Anode Morphology in Liquid Electrolytes”. *Journal of the American Chemical Society* **144** (2022). PMID: 36318744, pp. 20717–20725. DOI: 10.1021/jacs.2c08182.

Articles

Article I

Ø. Gullbrekken, I. T. Røe, S. M. Selbach, and S. K. Schnell

Charge Transport in Water-NaCl Electrolytes with Molecular Dynamics Simulations,

The Journal of Physical Chemistry B **127**:12 2729-2738 (2023).
DOI: 10.1021/acs.jpcb.2c08047

Article I

Article I

THE JOURNAL OF PHYSICAL CHEMISTRY B
A JOURNAL OF THE AMERICAN CHEMICAL SOCIETY

pubs.acs.org/JPCB

Article

Charge Transport in Water−NaCl Electrolytes with Molecular Dynamics Simulations

Øystein Gullbrekken, Ingeborg Treu Røe, Sverre Magnus Selbach, and Sondre Kvalvåg Schnell*

Cite This: J. Phys. Chem. B 2023, 127, 2729−2738

Read Online

ACCESS | Metrics & More | Article Recommendations | Supporting Information

ABSTRACT: A systematic description of microscopic mechanisms is necessary to understand mass transport in solid and liquid electrolytes. From Molecular Dynamics (MD) simulations, transport properties can be computed and provide a detailed view of the molecular and ionic motions. In this work, ionic conductivity and transport numbers in electrolyte systems are computed from equilibrium and nonequilibrium MD simulations. Results from the two methods are compared with experimental results, and we discuss the significance of the frame of reference when determining and comparing transport numbers. Two ways of computing ionic conductivity from equilibrium simulations are presented: the Nernst−Einstein approximation or the Onsager coefficients. The Onsager coefficients take ionic correlations into account and are found to be more suitable for concentrated electrolytes. Main features and differences between equilibrium and nonequilibrium simulations are discussed, and some potential anomalies and critical pitfalls of using nonequilibrium molecular dynamics to determine transport properties are highlighted.

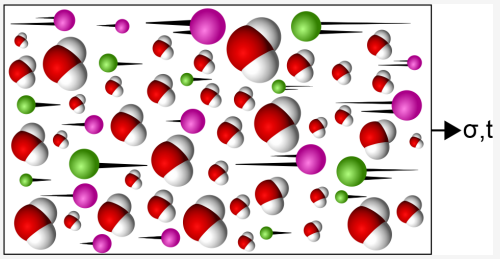

INTRODUCTION

Electrolytes have a central place in many disciplines, including electrochemistry, biology, and biomedical applications.[1] Technologies for energy production and storage are required to solve current challenges with global warming and the transition to sustainable energy sources.[2] The increased use of renewable and sustainable, but intermittent, energy sources depends on temporary storage of energy in batteries or hydrogen for fuel cells. Next-generation rechargeable batteries with high energy and power density require new electrode materials and new electrolytes with improved transport properties and improved electrochemical stability.[3−5]

Ionic conductivity and transport numbers are important with respect to charge transport in electrolytes. The ionic conductivity relates the ability of the electrolyte to carry electric charge through ionic motion,[1] while the ion transport number is defined as the fraction of the total current carried by the ionic species in question. Both properties are defined in the absence of concentration gradients.[1] For energy storage applications, e.g., a Li-ion battery electrolyte, the Li-ion transport number should preferably be as high as possible, ideally close to unity to improve the rate performance.[6]

Equilibrium or nonequilibrium molecular dynamics (MD) simulations can be used to compute ionic conductivity and transport numbers in complex mixtures. In nonequilibrium simulations, a flux of particles, energy, or charge is established by creating a gradient in the simulation box, or alternatively by applying an external field.[7] Ionic conductivity can be calculated directly from the particle displacements as a function of the gradient or field strength. From equilibrium simulations in the canonical or microcanonical ensemble, transport properties can be obtained by sampling the particle displacements, current density, or velocities, using the Einstein[8] or Green−Kubo[9] relations.

Several experimental methods exist for determining ionic conductivity and transport numbers of electrolytes. Typically, ionic conductivity is measured by electrochemical impedance spectroscopy. Transport numbers in liquid electrolytes can be measured by the Hittorf,[10] moving boundary,[11] emf,[12] or other methods. Transport numbers are always determined with respect to a reference frame. Different methods can employ different reference frames which requires caution when comparing values from different sources.

In this work, we have investigated and compared equilibrium and nonequilibrium MD simulation methods to compute ionic conductivity and transport numbers in model electrolytes. We have examined a benchmark electrolyte mixture which has been extensively studied experimentally: water with different concentrations of solvated NaCl. We have chosen the SPC/E[13] water model due to its computational efficiency and a force

Received: November 16, 2022
Revised: March 4, 2023
Published: March 15, 2023

https://doi.org/10.1021/acs.jpcb.2c08047
J. Phys. Chem. B 2023, 127, 2729−2738

field for solvated NaCl parametrized to reflect the microstructure of sodium chloride solutions.[14] Additionally, we have studied a polarizable water model, SWM4-NDP,[15] with polarizable NaCl.[16] A comparison is made to experimental data. We present potential challenges with using nonequilibrium MD simulations to obtain these quantities and discuss the implications.

THEORY

Charge transport properties can be obtained directly from equilibrium molecular dynamics simulations by sampling the particle displacements, i.e., the mean-squared displacement (MSD). The general equation for a transport coefficient D in three dimensions can be written:[17]

$$D = \frac{1}{6t}\langle(\mathbf{r}(t) - \mathbf{r}(0))^2\rangle \tag{1}$$

where t is time, $\mathbf{r}$ is the particle position vector, and $\langle\cdots\rangle$ denotes the ensemble average. For a multicomponent system, this can be generalized to the self-diffusion coefficient of a component i:[8]

$$D_{i,\mathrm{self}} = \frac{1}{6N_i}\lim_{t\to\infty}\frac{\mathrm{d}}{\mathrm{d}t}\left\langle\sum_{k=1}^{N_i}(\mathbf{r}_{k,i}(t) - \mathbf{r}_{k,i}(0))^2\right\rangle \tag{2}$$

where N_i is the number of particles of type i. The self-diffusion coefficient describes the motion of a single molecule of a specific type, describing the stochastic movements of individual particles, i.e., the movement of particles in the absence of a chemical potential gradient.

One way of computing ionic conductivity and transport numbers in electrolytes from equilibrium MD simulations is by employing the Nernst−Einstein (NE) approximation. The ionic conductivity is then related to the self-diffusion coefficients,[18−23] i.e., eq 2. The Nernst−Einstein approximations of the ionic conductivity and transport numbers are derived by substituting the expression for ionic mobility in the Nernst−Einstein equation into the equation for ionic conductivity. The Nernst−Einstein equation relates the ionic mobility to the diffusion coefficient:[24]

$$D_i = \frac{u_i RT}{z_i F} \tag{3}$$

where D_i is the diffusion coefficient of species i, u_i is the mobility of species i, R is the gas constant, T is the temperature, z_i is the charge valency of species i, and F is Faraday's constant. The derivation of the NE approximation of ionic conductivity is shown in the Supporting Information (SI). Since the NE approximations assume no correlations between particles of different species or particles of the same species in the electrolyte, they are intended for dilute or ideal systems. The NE approximation of the partial ionic conductivity of component i is

$$\sigma_i^{\mathrm{NE}} = \frac{z_i^2 e^2}{6k_{\mathrm{B}}TV}\lim_{t\to\infty}\frac{\mathrm{d}}{\mathrm{d}t}\left\langle\sum_{k=1}^{N_i}(\mathbf{r}_{k,i}(t) - \mathbf{r}_{k,i}(0))^2\right\rangle \tag{4}$$

in which k_{B} is the Boltzmann constant, V the system volume, and e is the elementary charge. The total ionic conductivity is the sum of all the partial conductivity contributions. In a binary electrolyte, the total ionic conductivity based on the NE approximation is

$$\sigma^{\mathrm{NE}} = \sigma_+^{\mathrm{NE}} + \sigma_-^{\mathrm{NE}} \tag{5}$$

in which σ_+^{NE} and σ_-^{NE} denote the partial conductivity contributions from cations and anions, respectively. The NE approximation of the ion transport number for species i is

$$t_i^{\mathrm{NE}} = \frac{\sigma_i^{\mathrm{NE}}}{\sum_i \sigma_i^{\mathrm{NE}}} = \frac{\sigma_i^{\mathrm{NE}}}{\sigma^{\mathrm{NE}}} \tag{6}$$

where we sum over all species in the denominator to obtain the total ionic conductivity, σ^{NE}.

In an electrolyte, multiple species are present and attractive, and repulsive interactions will influence the transport of each species. Concentrations deviating from the dilute limit will invalidate some of the assumptions used in the NE approximations. One way to characterize correlations and consider transport properties at higher concentrations is to compute the Onsager coefficients:[8]

$$L_{ij} = \frac{1}{6N}\lim_{t\to\infty}\frac{\mathrm{d}}{\mathrm{d}t}\left\langle\left(\sum_{k=1}^{N_i}[\mathbf{r}_{k,i}(t) - \mathbf{r}_{k,i}(0)]\right)\left(\sum_{l=1}^{N_j}[\mathbf{r}_{l,j}(t) - \mathbf{r}_{l,j}(0)]\right)\right\rangle \tag{7}$$

in which i and j are components, and N_i and N_j are the numbers of particles of components i and j, respectively. N is the total number of particles in the system. Note that i and j might denote the same component or different components, and $L_{ij} = L_{ji}$. L_{ij} describes the transport of component i in a chemical potential gradient of component j. When i and j are different components, L_{ij} describes the correlations between the different components. When i and j are the same component, L_{ii} includes the self-diffusion contribution but also describes how the motion of other particles of the same component influences the transport of component i. A system with n components can be described by $n(n-1)/2$ independent Onsager coefficients according to Onsager's reciprocal relations.[25] To characterize the transport properties of concentrated electrolytes, the Onsager theoretical framework is more appropriate because it takes into account the importance of coupling and deviations from infinite dilution. Onsager transport theory relates the driving forces acting on the electrolyte species to the flux of the species, with the Onsager coefficient acting as the proportionality constant. The derivation of the Onsager ionic conductivity is shown in the SI.

When we take ionic correlations into account, the partial ionic conductivity contribution from the correlation of species i and j is

$$\sigma_{ij} = \frac{e^2}{6k_{\mathrm{B}}TV}\lim_{t\to\infty}\frac{\mathrm{d}}{\mathrm{d}t}\left\langle\sum_{k=1}^{N_i}\sum_{l=1}^{N_j}z_i z_j[\mathbf{r}_{k,i}(t) - \mathbf{r}_{k,i}(0)]\cdot[\mathbf{r}_{l,j}(t) - \mathbf{r}_{l,j}(0)]\right\rangle \tag{8}$$

and the total ionic conductivity is[9,26]

$$\sigma = \sum_i\sum_j \sigma_{ij} \tag{9}$$

in which we sum over all ionic pairs in the system. In a binary electrolyte, the total ionic conductivity is

https://doi.org/10.1021/acs.jpcb.2c08047
J. Phys. Chem. B 2023, 127, 2729−2738

$$\sigma = \sigma_{++} + \sigma_{--} + 2\sigma_{+-} \tag{10}$$

in which σ_{++}, σ_{--}, and σ_{+-} denote the partial ionic conductivity contributions from cation−cation correlations, anion−anion correlations, and cation−anion correlations, respectively. In the dilute limit, there are no correlations, and σ_{+-} approaches zero, and σ_{++} and σ_{--} approach σ_+^{NE} and σ_-^{NE}, respectively. We then obtain the NE approximation of the ionic conductivity, σ^{NE}, in eq 5.

The transport number of an ionic species i is

$$t_i = \frac{\sum_j \sigma_{ij}}{\sigma} \tag{11}$$

where $\sum_j \sigma_{ij}$ is the sum of all the partial conductivity contributions of species i computed with eq 8. The cation transport number in a binary electrolyte is then:

$$t_+ = \frac{\sigma_{++} + \sigma_{+-}}{\sigma_{++} + \sigma_{--} + 2\sigma_{+-}} = \frac{\sigma_{++} + \sigma_{+-}}{\sigma} \tag{12}$$

METHOD

We conducted molecular dynamics simulations with the LAMMPS[27] software on a nonpolarizable model system composed of SPC/E[13] water with solvated NaCl[14] and a polarizable water model SWM4-NDP[15] with Na^+ and Cl^- ions.[16] To sample displacement of charged species, we have implemented the *order-n* algorithm of Dubbeldam et al.[28] as a fix in LAMMPS. In the SPC/E model, the water molecule is rigid with point charges at the atomic positions. The bond length and angle of the water molecule were fixed with the SHAKE algorithm.[29] The interactions of Na^+ and Cl^- ions were described using the parameters by Weerasinghe and Smith,[14] which was specifically developed to reproduce the properties of NaCl in water. Long-range Coulombic interactions were treated using standard Ewald summation with relative error in forces of 1×10^{-5}. Global cutoffs for the Lennard-Jones and Coulombic forces were set to 8 and 12 Å, respectively, and a Lennard-Jones tail correction to the energy and pressure was added.[24] Geometric mixing rules were used to determine the Lennard-Jones interactions between unlike atoms, except for a special scaled geometric mean of the Lennard-Jones energy parameter for water oxygen and Na^+. Periodic boundary conditions were applied in all directions. We varied salt concentration and system size to evaluate finite-size effects. Four different salt concentrations were studied, 0.5, 1.0, 2.5, 4.0 mol L^{-1}, and system sizes of 800, 3000, 10000, 20000 water molecules were investigated. Packmol[30] and fftool[31] were used to prepare initial configurations of pure water. Na^+ and Cl^- ions were placed randomly inside the box with a subsequent energy minimization employing the conjugate gradient algorithm to avoid initial overlap of particles.

Charge transport properties of the nonpolarizable model systems were calculated using equilibrium and nonequilibrium simulations. In the equilibrium simulations, the systems were first equilibrated in the isobaric−isothermal (NPT) ensemble at a temperature of 293 K and pressure of 1 atm for 3 ns with a time step of 1 fs. The Nosé−Hoover thermostat and barostat were used to control the temperature and pressure in the NPT ensemble.[32−34] The box volume was scaled according to the average volume during the equilibration to obtain correct density in the canonical (NVT) ensemble. After equilibration for 2 ns in the NVT ensemble, transport properties were sampled at a temperature of 293 K during production runs of 1 ns with a time step of 2 fs. The temperature was controlled with the Nosé−Hoover thermostat utilizing a time constant resulting in characteristic thermal fluctuations of 100 timesteps. We used the OCTP module for LAMMPS to compute self-diffusivities and Onsager coefficients of the solutions.[35] Ionic conductivity and transport numbers were calculated with the Nernst−Einstein and Onsager frameworks, using eqs 4, 6, 9, and 11. The Nernst−Einstein values were corrected for finite-size effects using the Yeh-Hummer correction for self-diffusion coefficients.[36−38] We made five replicas of each system. The replicas were prepared in the NPT ensemble by heating equilibrated systems from 293 K to 400 K during 10 ps, mixing for 20 ps at 400 K, cooling back to 293 K during 10 ps, and finally mixing at 293 K for 200 ps before saving the final configuration as a replica system. The velocities of all particles were reset before each replica run.

A rigid polarizable water model, SWM4-NDP,[15] together with polarizable Na^+ and Cl^- ions,[16] was also investigated to compare with the nonpolarizable model. The SWM4-NDP water model and associated ionic model utilize Drude particles to describe atomic polarizability. A negatively charged Drude particle is attached to the positively charged core particle by a harmonic spring. The polarizability of the atom or ion is adjusted by changing the charge of the Drude (and core) particle.[15] The original Na^+ and Cl^- ionic model[16] was parametrized against single ion properties, i.e., the hydration free energy at infinite dilution. Consequently, it did not describe the properties of concentrated solutions accurately. Particularly, the Na^+ and Cl^- interactions were too strong, favoring the formation of ionic clusters.[39] A later study sought to remedy this by optimizing the ionic parameters.[39] Two methods for optimizing the parameters are presented in ref 39: by adjusting the $R_{min}^{Na^+Cl^-}$ distance parameter in the Na^+-Cl^- Lennard-Jones potential or by introducing Thole damping of the Na^+-Cl^- interaction. We have chosen to use the adjusted $R_{min}^{Na^+Cl^-}$ value in this work. Note that the Lennard-Jones distance parameter σ as used in LAMMPS is equal to $R_{min}/2^{(1/6)}$. The Lennard-Jones ionic parameters are in Table 1.

Table 1. Lennard-Jones Parameters for the Polarizable Ions with the SWM4-NDP Water Model As Used in LAMMPS

ion(s)	ϵ (kcal/mol)	σ (Å)
Na^+	0.0315100	2.6044177
Cl^-	0.0719737	4.4208424
Na^+-Cl^-	0.0476224	3.6437758

The Langevin thermostat was used to control the temperature in the polarizable simulations. The center of mass of the Drude-core particles were set to 293 K and the Drude particles to 1 K. To minimize the effect on the particle dynamics, weak Langevin damping coefficients of 10 and 5 ps were used for the motions of the Drude-core center-of-mass and Drude particle relative to the core, respectively.[40] The Lennard-Jones and Coulombic forces were cut off at 12 Å and long-range Coulombic forces were computed by the particle−particle particle-mesh solver[41] with relative error in forces of 1×10^{-6}. A long-range Lennard-Jones tail correction was added to the energy and pressure. The water molecules were held rigid by a special fix in LAMMPS.[42] Lorentz−Berthelot mixing rules were

https://doi.org/10.1021/acs.jpcb.2c08047
J. Phys. Chem. B 2023, 127, 2729−2738

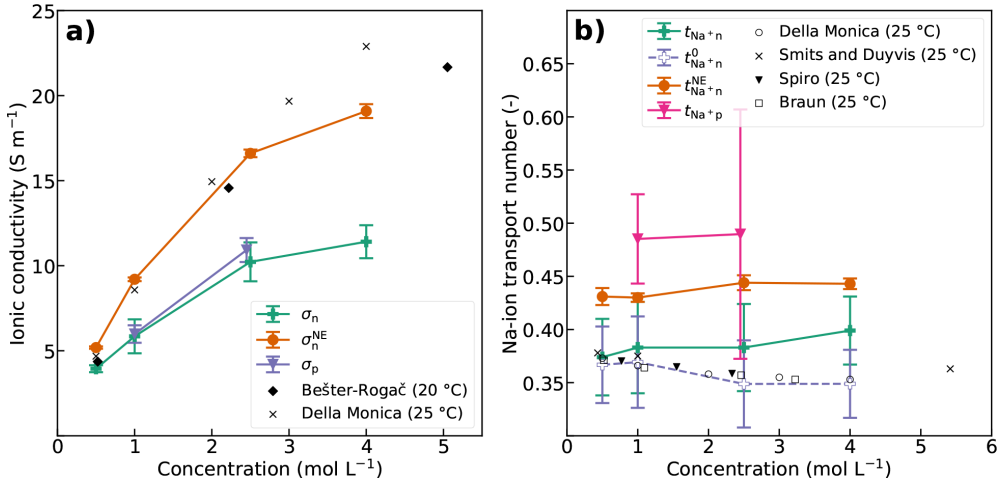

Figure 1. (a) Ionic conductivity and (b) Na-ion transport number as a function of salt concentration from equilibrium MD simulations on the systems with 10000 SPC/E and 9000 SWM4-NDP water molecules compared to experimental data. The results from nonpolarizable (SPC/E water) and polarizable (SWM4-NDP water) simulations are denoted with subscripts n and p, respectively. The computed ionic conductivities are compared to experimental data by Bešter-Rogač et al.[51] and Della Monica et al.[10] The computed transport numbers in the barycentric and solvent velocity reference frames are displayed, the latter denoted with superscript 0. The computed Na-ion transport numbers are compared to experimental data by Della Monica et al.,[10] Smits and Duyvis,[52] Spiro,[11] and Braun.[12]

applied for the interaction between the ions and the water oxygen. The bond between the Cl^- core and Drude particle included an anharmonic restoring force for bond lengths above 0.2 Å, as described in ref 16, to avoid the polarization catastrophe often encountered in highly polarizable ions. Initial configurations were prepared similarly to the nonpolarizable model, but without energy minimization after adding the ions. A time step of 0.5 fs was used in all the simulations with the polarizable model. Equilibration was performed in the isobaric−isothermal (NPT) ensemble at 293 K and 1 atm pressure. The Nosé−Hoover barostat controlled the pressure with a relaxation time of 500 time steps. Equilibration was performed for at least 500 ps, during which the box volume was sampled, and at the end adjusted to obtain correct density during sampling with constant volume. It was necessary to reset the linear momentum of the box during the equilibration to avoid the flying ice cube effect, but not during the constant volume simulations.[42] Sampling of charge transport properties was performed similarly to the nonpolarizable model in the NVT ensemble during simulations of at least 1 ns. Two polarizable systems were studied, with salt concentrations 1.0 and 2.45 mol L^{-1}, composed of 9000 water molecules and 167 and 417 NaCl, respectively. We made three replicas of both systems from different initial configurations.

In the nonequilibrium MD simulations (only nonpolarizable model), the systems were initially equilibrated in the NPT ensemble as described above. An external uniform electric field was applied in the x-direction after switching to the NVT ensemble. The electric field is invoked as a force $\mathbf{F} = ze\mathbf{E}$ that is applied to each particle in the box, where $\mathbf{E}$ is the electric field vector. The ions will begin to drift under the influence of the electric field. To avoid influencing the ionic fluxes caused by the electric field, the thermostat was applied to the two other directions than the applied field direction, i.e., the y- and z-directions, as done in previous studies.[43−45] The Nosé−Hoover thermostat was employed with a similar time constant as in the equilibrium simulations. After equilibration for 3 ns in the NVT ensemble, data was sampled over 15 ns with a time step of 2 fs to determine ionic conductivity and transport numbers. We applied the method explained by Shen and Hall in section 2 of the SI in ref 46 to compute the ionic conductivity and transport numbers in the nonequilibrium MD simulations. Here, the drift velocities of the ionic species are determined from the so-called field MSDs. The field MSD is the MSD due to the electric field. This is calculated by subtracting the MSD in a simulation without applied field from the MSD in a simulation with applied field. Alternatively, one can subtract the average MSD in the directions perpendicular to the field direction. The ionic drift velocity, v_d, is determined by fitting the field related MSD to a quadratic expression $a + bt^2$, where $v_d = \sqrt{b}$, as the field MSD has a slope of 2 in a log−log plot at long times.[46] The ionic mobility is

$$u = \frac{\langle v_d \rangle}{E} \tag{13}$$

where E is electric field strength. The total ionic conductivity is

$$\sigma = F \sum_i z_i c_i u_i \tag{14}$$

where c_i is the molar concentration of species i.

Several pitfalls of doing nonequilibrium MD simulations are discussed in the literature.[7,47−49] Notably, the transport properties might depend on the magnitude of the applied field due to nonlinearities. An example of such nonlinear behavior is the evolution of high-speed lanes for ionic species.[47] Ions then follow in the wake of other ions with similar charge where they experience less friction than outside the lane, and consequently the diffusivities become too large.[7] To establish if this influenced results to a large degree, we studied the effect of the electric field strength on the transport

https://doi.org/10.1021/acs.jpcb.2c08047
J. Phys. Chem. B 2023, 127, 2729−2738

properties by varying the field strength from 0.01 to 0.05 V Å^{-1} in steps of 0.01 V Å^{-1}. The response approaching the zero field limit was examined by evaluating field strengths of 0.005, 0.003, and 0.001 V Å^{-1}. Five replicas of the system with 3000 SPC/E water molecules and 140 NaCl were studied with nonequilibrium simulations at each field strength, using the same replicas as those prepared for the equilibrium MD simulations. We also performed nonequilibrium simulations of the systems with 10000 SPC/E water molecules and salt concentrations of 0.5, 1.0, 2.5, and 4.0 mol L^{-1} using an electric field strength of 0.03 V Å^{-1} to evaluate the effect of salt concentration. Three replicas were examined for each salt concentration.

All reported values and uncertainties were estimated by calculating the mean and standard deviations of the quantities obtained from the replicas. The standard deviations of the computed values in the replicas are denoted as error bars in the plots.

RESULTS AND DISCUSSION

Equilibrium Molecular Dynamics. The deviation between the ionic conductivity of the SPC/E model with NaCl computed with Onsager's theory and experimental data clearly increases with increasing salt concentration. This is not surprising, considering that SPC/E with NaCl is a nonpolarizable force field. It is well-known that nonpolarizable models significantly overestimate ion−ion correlations.[50] This is shown in Figure 1, which show the ionic conductivities and Na-ion transport numbers computed with the Nernst−Einstein approximation (eqs 4 and 6) and Onsager's theory (eqs 8, 9, and 11) as a function of salt concentration. The ionic motion and resulting ionic conductivity of the model is lower compared to experimental values, particularly at higher salt concentrations as seen in Figure 1a. A common way of reducing the ion−ion correlations in a nonpolarizable model to obtain more correct transport properties is to scale the ionic charges by a factor of 0.7 to 0.8.[50,53] We scaled the ionic charges by a factor of 0.8 in the system with 10000 SPC/E water molecules and 465 NaCl (2.5 mol L^{-1}) to study the effect on the charge transport properties. There were no substantial differences compared to the systems without charge scaling and the results are shown in the SI. Interestingly, the Nernst−Einstein approximation corresponds better with experimental data. However, this does not mean that the Nernst−Einstein approximation necessarily offers a better description of the ionic conductivity of the SPC/E water + NaCl model. We expect that the model underestimates the ionic conductivity at higher salt concentrations. At lower salt concentrations, both the Onsager and Nernst−Einstein methods are in better agreement with experimental data, as expected.

The polarizable model of SWM4-NDP water and Na^+ and Cl^- ions displays very similar ionic conductivity to the nonpolarizable model. This is surprising as we expect improved description of ion−ion interactions in the polarizable model would result in better agreement with experimental results. As mentioned earlier, the ionic parameters were initially parametrized against single ion properties and were not able to describe concentrated solutions correctly. Later, the interactions between Na^+ and Cl^- in SWM4-NDP water were adjusted to reproduce the osmotic pressure in concentrated solutions.[39] Obviously, this does not guarantee that transport properties, such as the ionic conductivity, and ionic correlations are perfectly described.

The computed ion transport numbers in the nonpolarizable model in Figure 1b are in good agreement with the experimental data at all salt concentrations studied. We observe a similar trend here as with the ionic conductivity, the discrepancy between the computed values and experimental values increase with increasing salt concentration. The transport numbers obtained by the Onsager equation agrees better with experimental data than the Nernst−Einstein approximation. Notably, the error bars for the Onsager ionic conductivity and transport numbers are significantly larger than the Nernst−Einstein approximations. The cause for this is clear when comparing the corresponding equations for ionic conductivity, eqs 9 and 4. In the equation for NE ionic conductivity, eq 4, we average over all ions of each kind, but the Onsager ionic conductivity, eq 9, is more susceptible to statistical noise and has less statistical data. The calculations of ion transport numbers are affected in the same way.

The Na-ion and Cl-ion transport numbers are almost equal, about 0.5, at both salt concentrations 1.0, 2.45 mol L^{-1} in the polarizable model. The polarizable model produces less correct transport numbers than the nonpolarizable model, compared to experimental data. The Na^+ and Cl^- ions apparently move almost equally fast in the polarizable model. We will not try to explain the reason for this behavior. Since the nonpolarizable model gives the most accurate results, we choose to focus on this model for the remainder of the article.

Determining ion transport numbers depends on the frame of reference, which will depend on the experimental or simulation method. The experimental values we compare our results with are obtained with different methods. For example, Della Monica et al.[10] and Smits and Duyvis[52] used the Hittorf and emf methods, respectively, which both employ the solvent velocity reference frame;[52,54] i.e., the transport numbers are determined with respect to the solvent. For MD simulations, the center of mass of all particles in the simulation box is the frame of reference, i.e., the barycentric reference frame. If the center of gravity of the electrolyte does not move relative to the solvent, the solvent velocity and barycentric reference frames are equivalent. This is likely the situation in dilute electrolytes, but it might not be the case in highly concentrated electrolytes where the ions make up a large part of the total mass. Either way, it is important to understand the significance of the reference frame when analyzing and comparing transport numbers. Barycentric transport numbers can be readily transformed to solvent velocity transport numbers.[55] We transformed the transport numbers from the nonpolarizable model computed with Onsager coefficients to the solvent velocity reference frame and obtained very good agreement with the experimental data which are mostly measured in this reference frame. The results are shown in Figure 1b. For a more extensive discussion on reference frames and how to transform between different reference frames, we refer the reader to refs 25 and 55.

Figure 2 shows the decomposed and total ionic conductivities as a function of salt concentration. A larger σ_{--} than σ_{++} means that the Cl^- ions will move further in the electrolyte than the Na^+ ions, and the Na-ion transport number is therefore below 0.5. We can explain this by considering ionic radii. Na^+ is a smaller ion than Cl^- and will have a higher charge density. In water the ions will be surrounded by a solvation shell of coordinating water molecules. Ions with

https://doi.org/10.1021/acs.jpcb.2c08047
J. Phys. Chem. B 2023, 127, 2729−2738

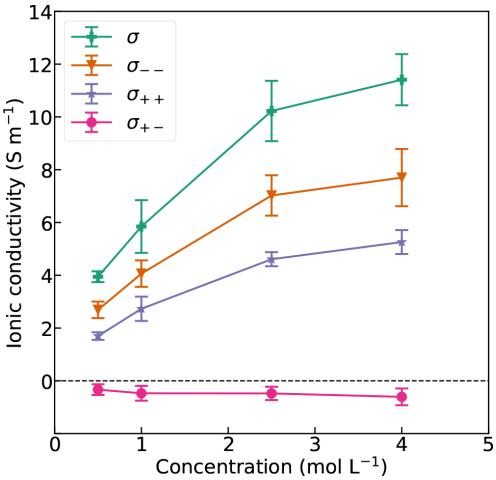

Figure 2. Ionic conductivity contributions as a function of salt concentration in the nonpolarizable model.

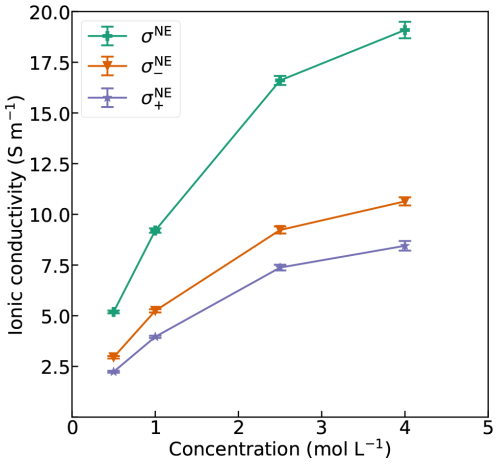

Figure 3. NE ionic conductivity contributions as a function of salt concentration in the nonpolarizable model.

higher charge density will be more strongly coordinated by more water molecules resulting in a larger effective radii which will reduce the ionic mobility compared to ions with lower charge density.[56] This is reflected in the respective radial distribution functions (RDF) of Na/Cl and oxygen from water, which are displayed in Figures S1 and S2, respectively. The RDF of Na and O displays a higher peak at a shorter interatomic distance than the RDF of Cl and O, which means that there are more water molecules closer to Na than Cl. The cross-correlation σ_{+-} is slightly negative and reduces the total ionic conductivity. The reason is that the oppositely charged Na^+ and Cl^- ions attract each other and will slow each other down when passing. The effect is rather small because of the surrounding water molecules which effectively screen the electrostatic charges due to the high relative permittivity (dielectric constant) of water.[57] The negative σ_{+-} explains why the Nernst−Einstein approximations of the cation transport number are larger than the corresponding Onsager values, as shown in Figure 1b. Since σ_{++} is smaller than σ_{--}, a negative σ_{+-} will cause a reduction of the cation transport number compared to the Nernst−Einstein approximation, according to eq 12.

The Nernst−Einstein approximations of decomposed and total ionic conductivities as a function of salt concentration are displayed in Figure 3. These data are based on the self-diffusion coefficients and describe the ionic conductivity assuming ideal conditions, but they do not provide any information about cross-correlations between the ions.

The finite-size effects on ionic conductivity and transport numbers were small and are shown in Figures S3 and S4. Example log−log plots of the NE conductivity MSDs; MSD_+^{NE}, and MSD_-^{NE}, and the conductivity MSDs; MSD_{++}, MSD_{--}, and MSD_{+-} obtained from equilibrium MD simulations are shown in Figures S5 and S6, respectively.

Nonequilibrium Molecular Dynamics. Nonequilibrium MD simulations to study the effect of electric field strength were conducted on the system with 3000 water molecules and 140 NaCl molecules, corresponding to a salt concentration of 2.5 mol L^{-1}. We confirmed that the simulations were done in the linear response regime by plotting the ion drift velocity against electric field strength. The plot verifies a linear relation and is presented in Figure S7. Ionic conductivity and transport numbers are strictly defined when the concentration is uniform. This might not be the case when an external electric field is applied to the simulation box. However, after a steady-state ionic drift is established, any concentration gradients will be small, and thus allow the use of this method with small electric fields. Figure 4 shows the computed ionic conductivity and Na-ion transport number as a function of the electric field strength. The ionic conductivity computed with the non-equilibrium method is lower than the equilibrium results. Additionally, the ionic conductivity decreases slightly with increasing electric field strength for field strenghts above 0.01 V $Å^{-1}$. The strength of the applied electric field is considerable, roughly 3 orders of magnitude higher than in for example a

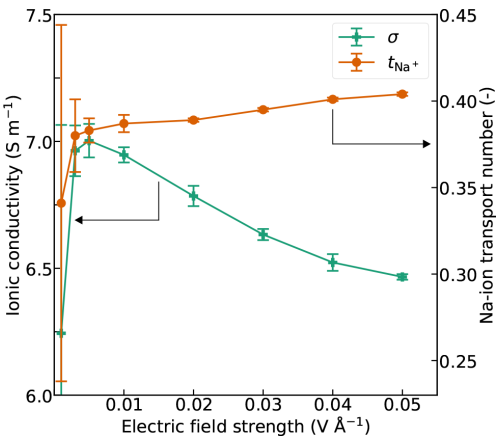

Figure 4. Ionic conductivity and Na-ion transport number as a function of electric field strength in the system with 3000 SPC/E water molecules and 140 NaCl.

https://doi.org/10.1021/acs.jpcb.2c08047
J. Phys. Chem. B 2023, 127, 2729−2738

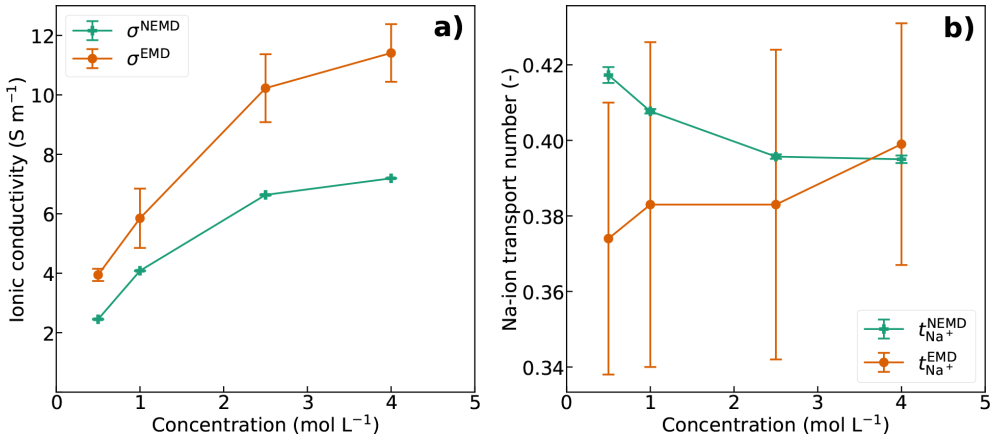

Figure 5. (a) Ionic conductivity and (b) Na-ion transport number as a function of salt concentration in the system with 10000 SPC/E water molecules in nonequilibrium simulations (NEMD) using an electric field strength of 0.03 V Å^{-1}. The values are compared to the equilibrium results (EMD) for the same systems.

typical battery electrolyte. The water molecule, due to its dipole moment, will likely be strongly polarized and aligned in the field, which will limit its self-diffusivity and rotational motion as shown in several studies.[58−62] This could in turn impede the mobility of the ions and reduce the ionic conductivity. The effect might be present also with other small polar solvent molecules in a simulated static electric field. The Na-ion transport number increases with increasing field strength but appears to approach the equilibrium value including uncertainty (Figure S4) upon extrapolation of the linear part of the curve to 0 V Å^{-1} field strength. As the Cl^- are heavier and move faster than the Na^+, the linear momentum due to the ionic fluxes will not cancel out. In order to compensate for this, the water molecules will gain a momentum in the same direction as the Na^+, which will increase with the magnitude of the field. The influence of water molecules moving in the same direction as the Na^+ could explain why the Na-ion transport number increases with increasing field strength. The ionic conductivity decreases when approaching the zero-field limit. Considerable field strengths are necessary to establish ionic fluxes at the time scales of nonequilibrium simulations.[7,49] The ionic fluxes will diminish as the slopes of the field MSDs approach 1 when the field becomes too weak, and consequently the ionic conductivity is reduced. The signal-to-noise ratio decreases and the uncertainty increases upon approaching 0 V Å^{-1} field strength. The linear part of the ionic conductivity curve does not approach the equilibrium value upon extrapolation to the zero-field limit which suggests that the field strength needed to establish ionic fluxes is larger than the field strength required to orient the water molecules.

The average temperature of the box, specifically the temperature in the direction of the field, went down with increasing field strength. This effect is displayed in Figure S8. The temperature drop in the field direction was about 11 K at the highest field strength (4 K average temperature drop), which might contribute to the reduced ionic conductivity with increasing field strength.[51] This is likely an anomaly due to the use of rigid molecules in an applied field. The number of degrees of freedom is reduced from nine to six in the rigid SPC/E water molecule, due to the two frozen bonds and frozen angle. When subjected to a field, we believe the rigidity or reduced number of degrees of freedom of the SPC/E water restricts its rotational motion in the direction of the field, which causes the temperature to decrease. The degrees of freedom removed by the SHAKE algorithm are accounted for in the temperature computation in equilibrium simulations. However, when an external field is applied in the non-equilibrium simulations, it appears the system is further constrained in the field direction which results in a temperature reduction.[63] With increasing field strength, the effective number of degrees of freedom removed increases causing the temperature to decrease proportionally to the field intensity, as shown in Figure S8. In order to test this hypothesis, we conducted similar simulations but used the flexible three-point SPC/Fw[64] and four-point TIP4P/2005f[65] water models instead of rigid SPC/E. The bonds and angles are described using harmonic potentials in SPC/Fw, and Morse and harmonic potentials, respectively, in TIP4P/2005f. We did not observe any temperature drop with increasing field strength using the TIP4P/2005f model and only a very slight temperature reduction with SPC/Fw of about 1 K in the field direction at the highest field strength. This strengthens our hypothesis that the temperature drop was due to the rigidity and reduced degrees of freedom of the SPC/E water molecule which artificially restricts its motion in the electric field direction. The observed temperature drop could be caused by reduced entropy in the field, a phenomenon also observed in other classes of materials, such as ferroics.[66,67] It is important to note that the temperature effect is different from the effect of limited diffusivity and rotational motion of the water molecules which we believe is the main factor reducing the ionic conductivity.

The ionic conductivity and Na-ion transport numbers as a function of salt concentration for the systems with 10000 water molecules in nonequilibrium simulations are displayed in Figure 5. Again, the ionic conductivity is lower than in the equilibrium simulations, due polarized water molecules aligned to the field that hinder the ionic motion. The relative deviation between the nonequilibrium and equilibrium results does not

https://doi.org/10.1021/acs.jpcb.2c08047
J. Phys. Chem. B 2023, 127, 2729−2738

change much with increasing salt concentration. The nonequilibrium Na-ion transport numbers decrease slightly with increasing salt concentration. As the number of ions increase, the effect of water molecules moving in the same direction as the Na^+ might be reduced.

It is not possible to obtain data on the main coefficients, σ_{++} and σ_{--}, or the ionic cross-correlation, σ_{+-}, directly from single field-driven nonequilibrium simulations as we have conducted here. An example log−log plot of MSDs from a nonequilibrium simulation is shown in Figure S9.

CONCLUSION

In this work, we have demonstrated that two methods employing equilibrium and nonequilibrium molecular dynamics, respectively, can be used to determine ionic conductivity and transport numbers in a model electrolyte of SPC/E water with NaCl. From both methods we find results that are comparable to experimental data. We have presented the Nernst−Einstein and Onsager frameworks for determining charge transport properties and discuss their advantages and disadvantages. We argue that the Onsager framework can be used to study concentrated electrolytes where ionic correlations are significant. We have shown how the data from these methods can be used to analyze the charge transport properties and relate them to molecular interactions. The importance of the reference frame when determining and comparing transport numbers is emphasized. To compare with the nonpolarizable model of SPC/E and NaCl, we performed equilibrium simulations with a polarizable model of SWM4-NDP water and polarizable Na^+ and Cl^- ions. The polarizable model did not display improved transport properties compared to the nonpolarizable model. Clearly, correctly modeling the charge transport properties in concentrated salt water solutions is challenging. Potential challenges and anomalies related to using nonequilibrium MD simulations to obtain these properties are discussed. Notably, in the SPC/E-NaCl system, the temperature drops with increasing electric field strength due to reduced degrees of freedom in the rigid water molecules. We recommend equilibrium simulations to investigate charge transport properties due to their simplicity relative to nonequilibrium simulations and the possibility of obtaining more information about ionic correlations.

ASSOCIATED CONTENT

Data Availability Statement

LAMMPS input-files and initial coordinates for the water/ion-mixtures used in this work can be found at: dx.doi.org/10.5281/zenodo.7691586.

Supporting Information

The Supporting Information is available free of charge at https://pubs.acs.org/doi/10.1021/acs.jpcb.2c08047.

Derivation of the Nernst−Einstein equation and the equation for Onsager ionic conductivity, as well as additional plots of radial distribution functions and mean squared displacements (PDF)

AUTHOR INFORMATION

Corresponding Author

Sondre Kvalvåg Schnell − *Department of Materials Science and Engineering, Norwegian University of Science and Technology, NTNU, Trondheim NO-7491, Norway;* orcid.org/0000-0002-0664-6756; Email: sondre.k.schnell@ntnu.no

Authors

Øystein Gullbrekken − *Department of Materials Science and Engineering, Norwegian University of Science and Technology, NTNU, Trondheim NO-7491, Norway;* orcid.org/0000-0002-2413-0120

Ingeborg Treu Røe − *Department of Materials Science and Engineering, Norwegian University of Science and Technology, NTNU, Trondheim NO-7491, Norway;* Present Address: SINTEF Energy Research, Trondheim NO-7036, Norway

Sverre Magnus Selbach − *Department of Materials Science and Engineering, Norwegian University of Science and Technology, NTNU, Trondheim NO-7491, Norway;* orcid.org/0000-0001-5838-8632

Complete contact information is available at: https://pubs.acs.org/10.1021/acs.jpcb.2c08047

Notes

The authors declare no competing financial interest.

ACKNOWLEDGMENTS

The simulations were performed on resources provided by Sigma2 - the National Infrastructure for High Performance Computing and Data Storage in Norway through the projects NN9264K and NN9414K, and on the NTNU IDUN/EPIC computing cluster. The Research Council of Norway is acknowledged for the support to the Norwegian Micro- and Nano-Fabrication Facility, NorFab, project number 295864. SKS acknowledges support through the NRC project 275754.

REFERENCES

(1) Newman, J. *Electrochemical Systems*, 2nd ed.; Prentice-Hall, 1991.
(2) Chu, S.; Cui, Y.; Liu, N. The path towards sustainable energy. *Nat. Mater.* **2017**, *16*, 16−22.
(3) Armand, M.; Tarascon, J.-M. Building better batteries. *Nature* **2008**, *451*, 652−657.
(4) Watanabe, M.; Dokko, K.; Ueno, K.; Thomas, M. L. From Ionic Liquids to Solvate Ionic Liquids: Challenges and Opportunities for Next Generation Battery Electrolytes. *Bull. Chem. Soc. Jpn.* **2018**, *91*, 1660−1682.
(5) Logan, E.; Dahn, J. Electrolyte Design for Fast-Charging Li-Ion Batteries. *Trends in Chemistry* **2020**, *2*, 354−366. Special Issue - Laying Groundwork for the Future.
(6) Doyle, M.; Fuller, T. F.; Newman, J. The importance of the lithium ion transference number in lithium/polymer cells. *Electrochim. Acta* **1994**, *39*, 2073−2081.
(7) Wheeler, D. R.; Newman, J. Molecular Dynamics Simulations of Multicomponent Diffusion. 2. Nonequilibrium Method. *J. Phys. Chem. B* **2004**, *108*, 18362−18367.
(8) Liu, X.; Schnell, S. K.; Simon, J.-M.; Krüger, P.; Bedeaux, D.; Kjelstrup, S.; Bardow, A.; Vlugt, T. J. H. Diffusion Coefficients from Molecular Dynamics Simulations in Binary and Ternary Mixtures. *Int. J. Thermophys.* **2013**, *34*, 1169−1196.
(9) Fong, K. D.; Bergstrom, H. K.; McCloskey, B. D.; Mandadapu, K. K. Transport phenomena in electrolyte solutions: Nonequilibrium thermodynamics and statistical mechanics. *AIChE J.* **2020**, *66*, e17091.
(10) Della Monica, M.; Petrella, G.; Sacco, A.; Bufo, S. Transference numbers in concentrated sodium chloride solutions. *Electrochim. Acta* **1979**, *24*, 1013−1017.
(11) Spiro, M. Volume Correction for the Indirect Moving-Boundary Method and the Transference Numbers of Concentrated

Aqueous Sodium Chloride Solutions. *J. Chem. Phys.* **1965**, *42*, 4060−4061.
(12) Braun, B. M. Transference numbers of aqueous NaCl and Na_2SO_4 at 25°C from EMF measurements with sodium-selective glass electrodes. *J. Solution Chem.* **1985**, *14*, 675−686.
(13) Berendsen, H. J. C.; Grigera, J. R.; Straatsma, T. P. The Missing Term in Effective Pair Potentials. *J. Phys. Chem.* **1987**, *91*, 6269−6271.
(14) Weerasinghe, S.; Smith, P. E. A Kirkwood-Buff derived force field for sodium chloride in water. *J. Chem. Phys.* **2003**, *119*, 11342−11349.
(15) Lamoureux, G.; Harder, E.; Vorobyov, I. V.; Roux, B.; MacKerell, A. D. A polarizable model of water for molecular dynamics simulations of biomolecules. *Chem. Phys. Lett.* **2006**, *418*, 245−249.
(16) Yu, H.; Whitfield, T. W.; Harder, E.; Lamoureux, G.; Vorobyov, I.; Anisimov, V. M.; MacKerell, A. D. J.; Roux, B. Simulating Monovalent and Divalent Ions in Aqueous Solution Using a Drude Polarizable Force Field. *J. Chem. Theory Comput.* **2010**, *6*, 774−786. PMID: 20300554.
(17) Metzler, R.; Jeon, J.-H.; Cherstvy, A. G.; Barkai, E. Anomalous diffusion models and their properties: non-stationarity, non-ergodicity, and ageing at the centenary of single particle tracking. *Phys. Chem. Chem. Phys.* **2014**, *16*, 24128−24164.
(18) Ebadi, M.; Eriksson, T.; Mandal, P.; Costa, L. T.; Araujo, C. M.; Mindemark, J.; Brandell, D. Restricted Ion Transport by Plasticizing Side Chains in Polycarbonate-Based Solid Electrolytes. *Macromolecules* **2020**, *53*, 764−774.
(19) Siqueira, L. J. A.; Ribeiro, M. C. C. Molecular dynamics simulation of the polymer electrolyte poly(ethylene oxide)/$LiClO_4$. II. Dynamical properties. *J. Chem. Phys.* **2006**, *125*, 214903.
(20) Fong, K. D.; Self, J.; McCloskey, B. D.; Persson, K. A. Ion Correlations and Their Impact on Transport in Polymer-Based Electrolytes. *Macromolecules* **2021**, *54*, 2575−2591.
(21) France-Lanord, A.; Wang, Y.; Xie, T.; Johnson, J. A.; Shao-Horn, Y.; Grossman, J. C. Effect of Chemical Variations in the Structure of Poly(ethylene oxide)-Based Polymers on Lithium Transport in Concentrated Electrolytes. *Chem. Mater.* **2020**, *32*, 121−126.
(22) Brooks, D. J.; Merinov, B. V.; Goddard, W. A.; Kozinsky, B.; Mailoa, J. Atomistic Description of Ionic Diffusion in PEO-LiTFSI: Effect of Temperature, Molecular Weight, and Ionic Concentration. *Macromolecules* **2018**, *51*, 8987−8995.
(23) Son, C. Y.; Wang, Z.-G. Ion transport in small-molecule and polymer electrolytes. *J. Chem. Phys.* **2020**, *153*, 100903.
(24) Frenkel, D.; Smit, B. *Understanding Molecular Simulation*, 2nd ed.; Academic Press: San Diego, 2002.
(25) Kjelstrup, S.; Bedeaux, D. *Non-Equilibrium Thermodynamics of Heterogeneous Systems*; World Scientific: Singapore, 2008.
(26) Fong, K. D.; Self, J.; Diederichsen, K. M.; Wood, B. M.; McCloskey, B. D.; Persson, K. A. Ion Transport and the True Transference Number in Nonaqueous Polyelectrolyte Solutions for Lithium Ion Batteries. *ACS Central Science* **2019**, *5*, 1250−1260.
(27) Thompson, A. P.; Aktulga, H. M.; Berger, R.; Bolintineanu, D. S.; Brown, W. M.; Crozier, P. S.; in 't Veld, P. J.; Kohlmeyer, A.; Moore, S. G.; Nguyen, T. D.; Shan, R.; Stevens, M. J.; Tranchida, J.; Trott, C.; Plimpton, S. J. LAMMPS - a flexible simulation tool for particle-based materials modeling at the atomic, meso, and continuum scales. *Comput. Phys. Commun.* **2022**, *271*, 108171.
(28) Dubbeldam, D.; Ford, D. C.; Ellis, D. E.; Snurr, R. Q. A new perspective on the order-n algorithm for computing correlation functions. *Mol. Simul.* **2009**, *35*, 1084−1097.
(29) Ryckaert, J.-P.; Ciccotti, G.; Berendsen, H. J. Numerical integration of the cartesian equations of motion of a system with constraints: molecular dynamics of n-alkanes. *J. Comput. Phys.* **1977**, *23*, 327−341.
(30) Martinez, L.; Andrade, R.; Birgin, E. G.; Martinez, J. M. PACKMOL: A Package for Building Initial Configurations for Molecular Dynamics Simulations. *J. Comput. Chem.* **2009**, *30*, 2157−2164.
(31) Padua, A. fftool. https://github.com/paduagroup/fftool, Accessed: June 2021.
(32) Shinoda, W.; Shiga, M.; Mikami, M. Rapid estimation of elastic constants by molecular dynamics simulation under constant stress. *Phys. Rev. B* **2004**, *69*, 134103.
(33) Hoover, W. G. Canonical dynamics: Equilibrium phase-space distributions. *Phys. Rev. A* **1985**, *31*, 1695−1697.
(34) Nosé, S. A molecular dynamics method for simulations in the canonical ensemble. *Mol. Phys.* **1984**, *52*, 255−268.
(35) Jamali, S. H.; Wolff, L.; Becker, T. M.; de Groen, M.; Ramdin, M.; Hartkamp, R.; Bardow, A.; Vlugt, T. J. H.; Moultos, O. A. OCTP: ATool for On-the-Fly Calculation of Transport Properties of Fluids with the Order-n Algorithm in LAMMPS. *J. Chem. Inf. Model.* **2019**, *59*, 1290−1294.
(36) Yeh, I.-C.; Hummer, G. System-Size Dependence of Diffusion Coefficients and Viscosities from Molecular Dynamics Simulations with Periodic Boundary Conditions. *J. Phys. Chem. B* **2004**, *108*, 15873−15879.
(37) Celebi, A. T.; Jamali, S. H.; Bardow, A.; Vlugt, T. J. H.; Moultos, O. A. Finite-size effects of diffusion coefficients computed from molecular dynamics: a review of what we have learned so far. *Mol. Simul.* **2021**, *47*, 831−845.
(38) Dünweg, B.; Kremer, K. Molecular dynamics simulation of a polymer chain in solution. *J. Chem. Phys.* **1993**, *99*, 6983−6997.
(39) Luo, Y.; Jiang, W.; Yu, H.; MacKerell, A. D.; Roux, B. Simulation study of ion pairing in concentrated aqueous salt solutions with a polarizable force field. *Faraday Discuss.* **2013**, *160*, 135−149.
(40) Jiang, W.; Hardy, D. J.; Phillips, J. C.; MacKerell, A. D. J.; Schulten, K.; Roux, B. High-Performance Scalable Molecular Dynamics Simulations of a Polarizable Force Field Based on Classical Drude Oscillators in NAMD. *J. Phys. Chem. Lett.* **2011**, *2*, 87−92. PMID: 21572567.
(41) Hockney, R. W.; Eastwood, J. W. *Computer simulation using particles*; Hilger: Bristol, 1988.
(42) Dequidt, A.; Devémy, J.; Pádua, A. A. H. Thermalized Drude Oscillators with the LAMMPS Molecular Dynamics Simulator. *J. Chem. Inf. Model.* **2016**, *56*, 260−268. PMID: 26646769.
(43) Ting, C. L.; Stevens, M. J.; Frischknecht, A. L. Structure and Dynamics of Coarse-Grained Ionomer Melts in an External Electric Field. *Macromolecules* **2015**, *48*, 809−818.
(44) Sampath, J.; Hall, L. M. Impact of ion content and electric field on mechanical properties of coarse-grained ionomers. *J. Chem. Phys.* **2018**, *149*, 163313.
(45) Shen, K.-H.; Hall, L. M. Ion Conductivity and Correlations in Model Salt-Doped Polymers: Effects of Interaction Strength and Concentration. *Macromolecules* **2020**, *53*, 3655−3668.
(46) Shen, K.-H.; Hall, L. M. Effects of Ion Size and Dielectric Constant on Ion Transport and Transference Number in Polymer Electrolytes. *Macromolecules* **2020**, *53*, 10086−10096.
(47) MacGowan, D.; Evans, D. J. Heat and matter transport in binary liquid mixtures. *Phys. Rev. A* **1986**, *34*, 2133−2142.
(48) Evans, D.J.; Lynden-Bell, R.M.; Morriss, G.P. Steady-state structure and dynamics of a two-dimensional conducting fluid. *Mol. Phys.* **1989**, *67*, 209−216.
(49) English, N. J.; Waldron, C. J. Perspectives on external electric fields in molecular simulation: progress, prospects and challenges. *Phys. Chem. Chem. Phys.* **2015**, *17*, 12407−12440.
(50) Leontyev, I.; Stuchebrukhov, A. Accounting for electronic polarization in non-polarizable force fields. *Phys. Chem. Chem. Phys.* **2011**, *13*, 2613−2626.
(51) Bešter-Rogač, M.; Neueder, R.; Barthel, J. Conductivity of Sodium Chloride in Water + 1,4-Dioxane Mixtures from 5 to 35°C II. Concentrated Solution. *J. Solution Chem.* **2000**, *29*, 51−61.
(52) Smits, L. J. M.; Duyvis, E. M. Transport Numbers of Concentrated Sodium Chloride Solutions at 25°. *J. Phys. Chem.* **1966**, *70*, 2747−2753.
(53) Youngs, T. G. A.; Hardacre, C. Application of Static Charge Transfer within an Ionic-Liquid Force Field and Its Effect on Structure and Dynamics. *ChemPhysChem* **2008**, *9*, 1548−1558.

https://doi.org/10.1021/acs.jpcb.2c08047
J. Phys. Chem. B 2023, 127, 2729−2738

(54) MacInnes, D. A.; Longsworth, L. G. Transference Numbers by the Method of Moving Boundaries. *Chem. Rev.* **1932**, *11*, 171−230.
(55) Shao, Y.; Gudla, H.; Brandell, D.; Zhang, C. Transference Number in Polymer Electrolytes: Mind the Reference-Frame Gap. *J. Am. Chem. Soc.* **2022**, *144*, 7583−7587.
(56) Nightingale, E. R. Phenomenological Theory of Ion Solvation. Effective Radii of Hydrated Ions. *J. Phys. Chem.* **1959**, *63*, 1381−1387.
(57) Malmberg, C. G.; Maryott, A. A. Dielectric Constant of Water from 0° to 100 °C. *Journal of Research of the National Bureau of Standards* **1956**, *56*, 1−8.
(58) Boyd, S. J.; Krishnan, Y.; Ghaani, M. R.; English, N. J. Influence of external static and alternating electric fields on self-diffusion of water from molecular dynamics. *J. Mol. Liq.* **2021**, *327*, 114788.
(59) Jung, D. H.; Yang, J. H.; Jhon, M. S. The effect of an external electric field on the structure of liquid water using molecular dynamics simulations. *Chem. Phys.* **1999**, *244*, 331−337.
(60) Cassone, G.; Sponer, J.; Trusso, S.; Saija, F. Ab initio spectroscopy of water under electric fields. *Phys. Chem. Chem. Phys.* **2019**, *21*, 21205−21212.
(61) English, N. J.; Mooney, D. A.; O'Brien, S. Ionic liquids in external electric and electromagnetic fields: a molecular dynamics study. *Mol. Phys.* **2011**, *109*, 625−638.
(62) English, N. J.; MacElroy, J. M. D. Hydrogen bonding and molecular mobility in liquid water in external electromagnetic fields. *J. Chem. Phys.* **2003**, *119*, 11806−11813.
(63) Xu, H.; Cabriolu, R.; Smit, B. Effects of Degrees of Freedom on Calculating Diffusion Properties in Nanoporous Materials. *J. Chem. Theory Comput.* **2022**, *18*, 2826−2835. PMID: 35438988.
(64) Wu, Y.; Tepper, H. L.; Voth, G. A. Flexible simple point-charge water model with improved liquid-state properties. *J. Chem. Phys.* **2006**, *124*, 024503.
(65) González, M. A.; Abascal, J. L. F. A flexible model for water based on TIP4P/2005. *J. Chem. Phys.* **2011**, *135*, 224516.
(66) Ram, N. R.; Prakash, M.; Naresh, U.; Kumar, N. S.; Sarmash, T. S.; Subbarao, T.; Kumar, R. J.; Kumar, G. R.; Naidu, K. C. B. Review on Magnetocaloric Effect and Materials. *Journal of Superconductivity and Novel Magnetism* **2018**, *31*, 1971−1979.
(67) Kumar, A.; Thakre, A.; Jeong, D.-Y.; Ryu, J. Prospects and challenges of the electrocaloric phenomenon in ferroelectric ceramics. *J. Mater. Chem. C* **2019**, *7*, 6836−6859.

https://doi.org/10.1021/acs.jpcb.2c08047
J. Phys. Chem. B 2023, 127, 2729−2738

Supporting Information: Charge Transport in Water-NaCl Electrolytes with Molecular Dynamics Simulations

Øystein Gullbrekken,[†] Ingeborg Treu Røe,[†,‡] Sverre Magnus Selbach,[†] and Sondre Kvalvåg Schnell[*,†]

†*Department of Materials Science and Engineering, Norwegian University of Science and Technology, NTNU, Trondheim NO-7491, Norway*

‡*Current address: SINTEF Energy Research, Trondheim NO-7036, Norway*

E-mail: sondre.k.schnell@ntnu.no

Derivation of the Nernst-Einstein ionic conductivity

The Nernst-Einstein equation for charged particles relates the diffusion coefficient to the mobility[S1]:

$$D_i = \frac{u_i RT}{z_i F}, \tag{1}$$

in which D_i is the diffusion coefficient of species i, R is the gas constant, T is absolute temperature, F is Faraday's constant, z_i is the charge valency of species i, and u_i is the mobility of species i, defined as:

$$u = \frac{\langle v_d \rangle}{E}, \tag{2}$$

where $\langle v_d \rangle$ is the average ionic drift velocity, and E is electric field strength. The partial ionic conductivity of species i in a material is[S2]:

$$\sigma_i = z_i F c_i u_i, \tag{3}$$

in which c_i is the molar concentration of species i. By substituting the expression for u_i in equation (1) into equation (3), we obtain the Nernst-Einstein approximation of the partial ionic conductivity of species i:

$$\sigma_i^{\mathrm{NE}} = \frac{z_i^2 F^2 c_i D_i}{RT}. \tag{4}$$

By substituting the expression for the self-diffusion coefficient into equation (4), we obtain the final expression for the NE approximation of partial ionic conductivity of species i:

$$\sigma_i^{\mathrm{NE}} = \frac{z_i^2 e^2}{6 k_{\mathrm{B}} T V} \lim_{t\to\infty} \frac{\mathrm{d}}{\mathrm{d}t} \left\langle \sum_{k=1}^{N_i} \left(\mathbf{r}_{k,i}(t) - \mathbf{r}_{k,i}(0)\right)^2 \right\rangle, \tag{5}$$

in which k_{B} is the Boltzmann constant, V is volume and e is the elementary charge. Here, we also utilized that $F = eN_A$ and $c_i = N_i/(N_A V)$, where N_A is Avogadro's constant. It is not uncommon to express the NE ionic conductivity in terms of the charge of species i, q_i, which is equal to $z_i e$. The total ionic conductivity is the sum of all the partial conductivity

contributions.

Derivation of the Onsager ionic conductivity

The flux of a species i is a linear combination of the forces acting on it[S3]:

$$J_i = \sum_j L_{ij} X_j, \tag{6}$$

in which X_j are the forces and L_{ij} are the Onsager coefficients. In an electrochemical cell, the force acting on the species is the negative gradient of the electrochemical potential, $\nabla\bar{\mu_j} = \nabla\mu_j + z_j F\nabla\phi$, where μ_j is chemical potential of species j and ϕ is electric potential[S4]. The ionic conductivity is defined in the absence of concentration gradients[S5]. Typically, the ionic conductivity of an electrolyte is measured using electrochemical impedance spectroscopy where the concentration is assumed to be uniform. We also assume no gradients in temperature or pressure. Hence, we assume no chemical potential gradient:

$$\nabla\bar{\mu_j} = \nabla\mu_j + z_j F\nabla\phi = z_j F\nabla\phi. \tag{7}$$

Substituting for the force X_j in equation (6)[S6]:

$$J_i = -\frac{1}{RT}\sum_j L_{ij}\nabla\bar{\mu_j} = -\frac{F}{RT}\sum_j L_{ij} z_j \nabla\phi. \tag{8}$$

The electric current density can be expressed in terms of the flux of ions:

$$j = F\sum_i c_i z_i J_i, \tag{9}$$

in which c_i is the molar concentration of species i and we sum over all species. Substituting for J_i:

$$j = -\frac{F^2}{RT}\sum_i\sum_j c_i z_i z_j L_{ij}\nabla\phi. \tag{10}$$

The ionic conductivity expressed by Ohm's law is[S5]:

$$j = -\sigma \nabla \phi, \tag{11}$$

where we also assume no concentration gradients. By substituting for j into equation (10):

$$\sigma = \frac{F^2}{RT} \sum_i \sum_j c_i z_i z_j L_{ij}, \tag{12}$$

$$\sigma = \frac{Ne^2}{k_\mathrm{B} T V} \sum_i \sum_j z_i z_j L_{ij}, \tag{13}$$

and we obtain an expression equivalent to equation (9) in the main text. N is the total number of particles in the system, equal to $\sum_i N_i$.

Effect of charge scaling

The effect of ionic charge scaling on the transport properties was tested on a system with 10 000 SPC/E water molecules and 465 NaCl ($2.5\,\mathrm{mol\,L^{-1}}$) by reducing the ionic charges to ± 0.8 in an equilibrium simulation. The resulting ionic conductivity was $10.96\,\mathrm{S\,m^{-1}}$ and the Na-ion transport number was 0.32. The ionic conductivity was the same as without charge scaling while the Na-ion transport number was a bit lower.

The error bars in the following figures denote the standard deviation of the computed quantities from five replicates.

Table S1: Systems studied with equilibrium molecular dynamics simulations. Concentration effects were evaluated for the system containing 10 000 SPC/E water molecules.

No of water molecules	No of NaCl	Salt concentration (mol L^{-1})	Polarizable
800	10	0.5	No
800	50	2.5	No
3000	28	0.5	No
3000	140	2.5	No
10 000	93	0.5	No
10 000	186	1.0	No
10 000	465	2.5	No
10 000	744	4.0	No
20 000	186	0.5	No
20 000	930	2.5	No
9000	167	1.0	Yes
9000	417	2.45	Yes

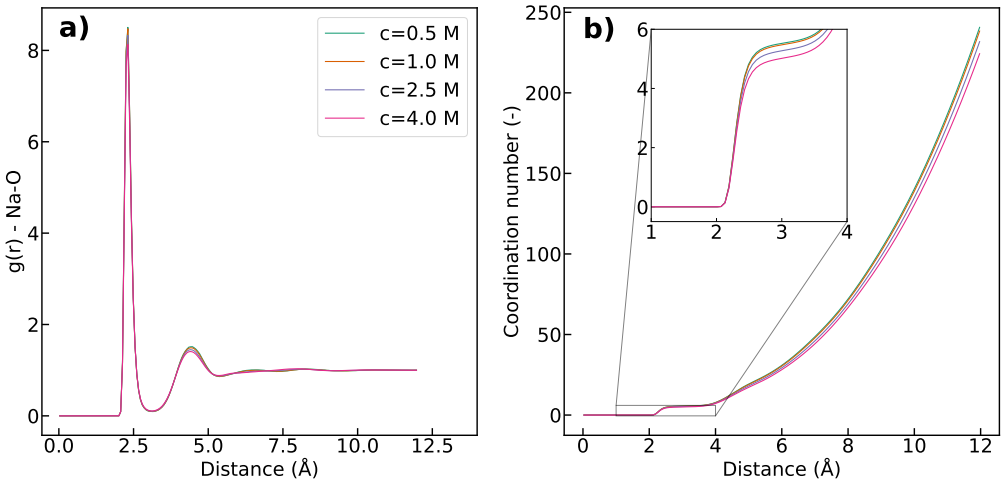

Figure S1: (a) Radial distribution functions and (b) coordination numbers of Na and water oxygen for the different salt concentrations. Data obtained from the systems with 10 000 SPC/E water molecules.

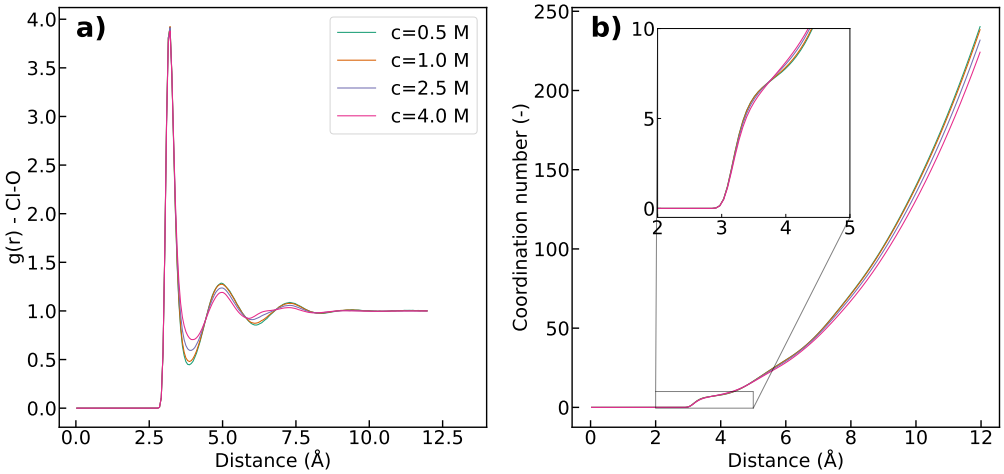

Figure S2: (a) Radial distribution functions and (b) coordination numbers of Cl and water oxygen for the different salt concentrations. Data obtained from the systems with 10 000 SPC/E water molecules.

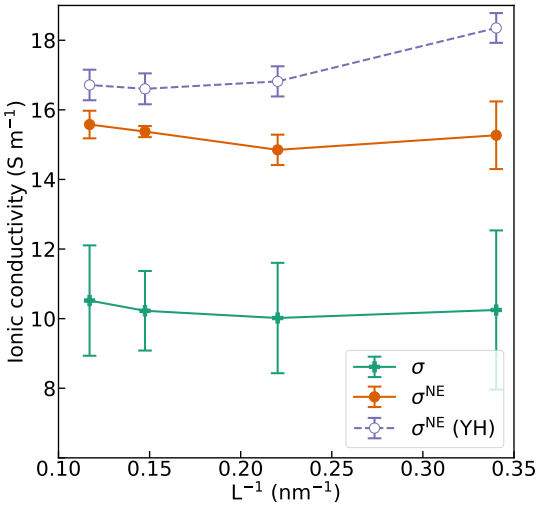

Figure S3: Ionic conductivity plotted against inverse of box length (cubic box). The data points from left to right correspond to the systems with 20 000, 10 000, 3000 and 800 SPC/E water molecules with salt concentration of 2.5 mol L^{-1}. Finite-size corrected values using the Yeh-Hummer (YH) correction are displayed.

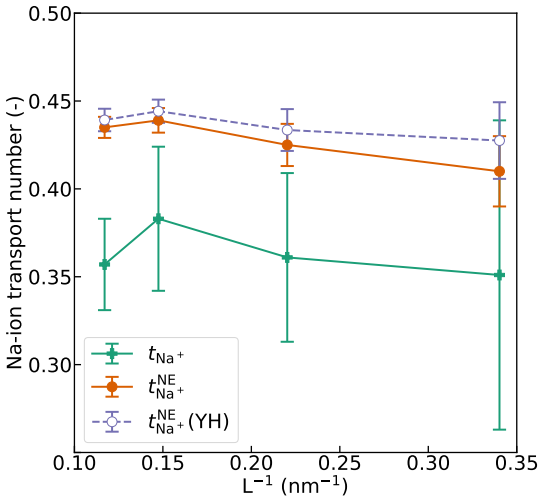

Figure S4: Na-ion transport numbers plotted against inverse of box length (cubic box). The data points from left to right correspond to the systems with 20 000, 10 000, 3000 and 800 SPC/E water molecules with salt concentration of 2.5 mol L^{-1}. Finite-size corrected values using the Yeh-Hummer (YH) correction are displayed.

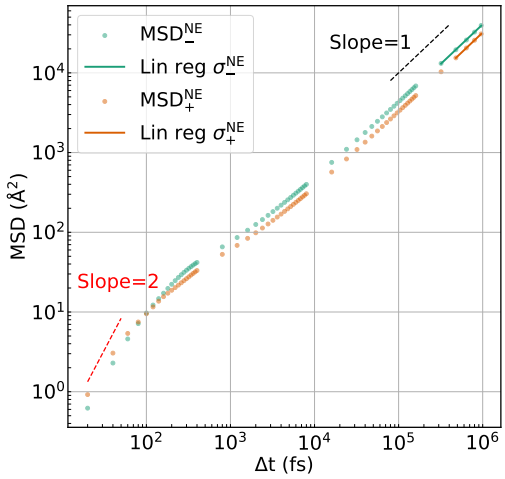

Figure S5: Example log-log plot of output NE conductivity MSD values from the equilibrium simulations. Note that Δt on the x axis denotes time difference, not simulation time. Linear regression to determine the σ^{NE} values is also shown. The data come from the system containing 10 000 SPC/E water molecules and 465 NaCl, corresponding to a concentration of 2.5 mol L^{-1}. Note the ballistic region with slope ~2 up to about 60 fs.

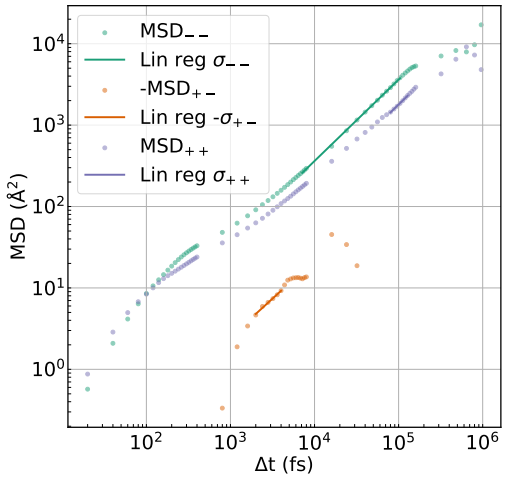

Figure S6: Example log-log plot of output conductivity MSD values from the equilibrium simulations. Linear regression to determine the σ values is also shown. The data come from the system containing 10 000 SPC/E water molecules and 465 NaCl, corresponding to a concentration of 2.5 mol L^{-1}.

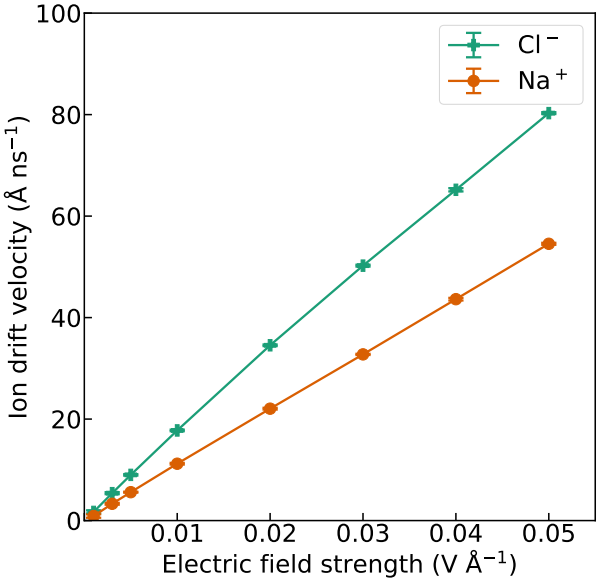

Figure S7: Ion drift velocity as function of electric field strength in the non-equilibrium simulations.

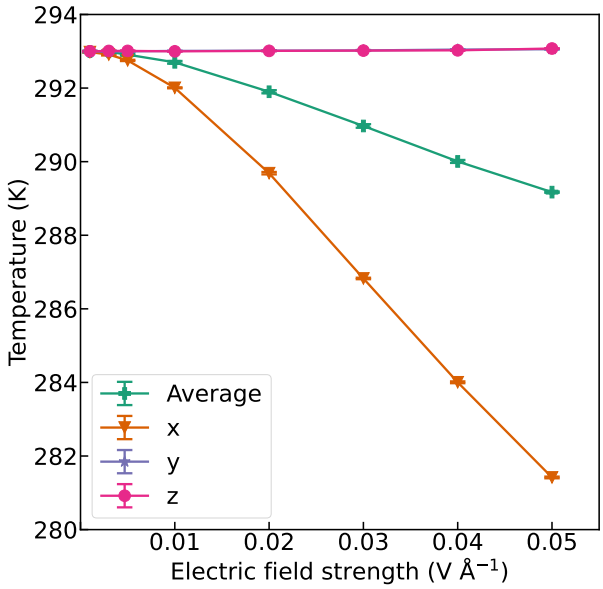

Figure S8: Average temperature and temperature in the three dimensions as function of electric field strength in the non-equilibrium simulations.

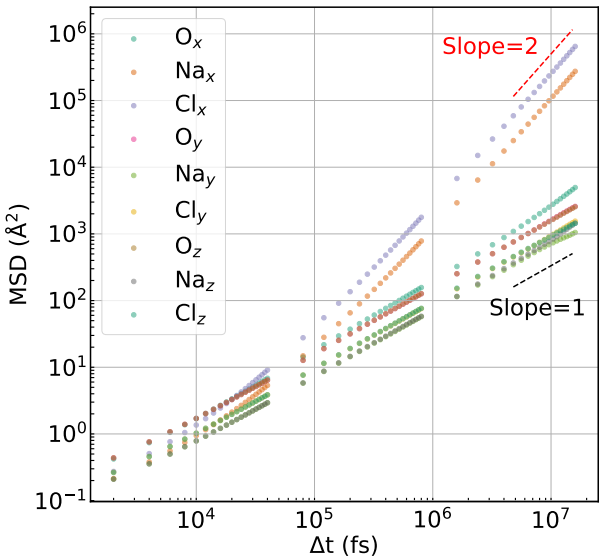

Figure S9: Example log-log plot of MSD values of each component in a non-equilibrium simulation with applied electric field. The data come from one of the replicates of the system containing 3000 SPC/E water molecules and 140 NaCl with an applied electric field of $0.03\,\mathrm{V\,Å^{-1}}$. O signifies the oxygen atom in water. MSD values are shown for each dimension, x, y and z, individually. The MSDs of Na^+ and Cl^- in the field direction have slope ∼2 at longer times while all the other MSDs have slope ∼1.

References

(S1) Frenkel, D.; Smit, B. *Understanding Molecular Simulation (Second Edition)*; Academic Press: San Diego, 2002.

(S2) Rao, C. N. R.; Gopalakrishnan, J. *New Directions in Solid State Chemistry*, 2nd ed.; Cambridge University Press, 1997.

(S3) Kjelstrup, S.; Bedeaux, D. *Non-Equilibrium Thermodynamics of Heterogeneous Systems*; World Scientific: Singapore, 2008.

(S4) Fong, K. D.; Bergstrom, H. K.; McCloskey, B. D.; Mandadapu, K. K. Transport phenomena in electrolyte solutions: Nonequilibrium thermodynamics and statistical mechanics. *AIChE Journal* **2020**, *66*, e17091.

(S5) Newman, J. *Electrochemical Systems*, 2nd ed.; Prentice-Hall, 1991.

(S6) Krishna, R.; Wesselingh, J. The Maxwell-Stefan approach to mass transfer. *Chemical Engineering Science* **1997**, *52*, 861–911.

Article II

Ø. Gullbrekken and S. K. Schnell

Coupled ion transport in concentrated PEO-LiTFSI polymer electrolytes,

New Journal of Chemistry **47**:44 20344-20357 (2023).
DOI: 10.1039/D3NJ04065H

Article II

Article II

NJC

ROYAL SOCIETY OF CHEMISTRY

PAPER

View Article Online
View Journal

Cite this: DOI: 10.1039/d3nj04065h

Coupled ion transport in concentrated PEO–LiTFSI polymer electrolytes†

Øystein Gullbrekken and Sondre Kvalvåg Schnell *

Received 30th August 2023,
Accepted 14th October 2023

DOI: 10.1039/d3nj04065h

rsc.li/njc

Understanding how microscopic mechanisms govern macroscopic transport properties is important for development of improved electrolytes for Li-ion batteries. The archetypal polymer electrolyte PEO–LiTFSI has been investigated for more than three decades, but the fundamental ion transport mechanisms are still elusive. Molecular Dynamics (MD) simulations enable us to determine transport properties by directly probing particle movements. Both transport properties and microscopic interactions that govern them can be studied simultaneously. In this work, ionic conductivity and transport numbers of PEO–LiTFSI electrolytes are computed as a function of salt concentration and PEO chain length. The values are obtained using the Nernst–Einstein approximation for dilute or ideal systems, in addition we determine the Onsager coefficients that take into account ionic correlations. We observe significant differences between the two methods, indicating non-ideality. The motion of Li and TFSI is anticorrelated, causing super-ionicity. We discuss the relevance of the frame of reference. The static and dynamic properties of Li-ion coordination environments are analyzed. The distributions of cation-solvent and cation–anion residence times are investigated and indicate that the TFSI facilitate Li transport and Li jumps in the polymer network. Finally, the thermodynamic factors are computed and used to quantify the non-ideality of the systems.

1 Introduction

Polymer electrolytes was initially introduced by Wright *et al.*[1,2] in the 1970s, where it was shown that poly(ethylene oxide) (PEO) had the ability of dissolving- and conducting alkali metal ions at close to ambient temperature. The metal cations are coordinated by units of Lewis base in the polymer, specifically by ether oxygen atoms in PEO.[3] Armand analyzed the properties of the new class of materials for electrochemical purposes in 1983,[4] and suggested lithium bis(trifluoromethanesulfonyl)-imide (LiTFSI) as a salt together with PEO[5] for use in Li-ion batteries. PEO–LiTFSI has since been widely investigated as a polymer electrolyte.[6] Li is typically coordinated by 5–6 ether oxygen atoms in PEO,[7] and the TFSI-anion is known for its plasticizing effect, arising due to the flexibility of the $-SO_2-N-SO_2-$ segment, which reduces the crystallinity of the PEO and thus increases the ionic conductivity. Additionally, LiTFSI dissociates easily due to the large size and low charge density of the anion.[3] However, the ionic conductivity of PEO–LiTFSI electrolytes is too low at room temperature for commercial applications, about 10^{-6} S cm^{-1} and the Li-ion transport number is found to be low in many studies, about 0.2 or lower.[3,6,8–10]

Li-ion transport in PEO-based electrolytes occurs by three main mechanisms: the Li-ions can jump from ether oxygen to ether oxygen along a PEO chain, called *intrachain* transport, or they can jump between PEO chains, called *interchain* transport.[11] Both of these transport mechanisms occur by changing coordination environment and are called structural diffusion.[12] Vehicular diffusion with the PEO chains, without changing coordination, is the third transportation mode of Li-ions. Consequently, the mobility of Li-ions is closely coupled to the motion of the polymer backbone and occurs in the amorphous phase where the polymer chains can move freely.[3]

Molecular dynamics (MD) simulations is a powerful tool to investigate transport properties in electrolytes and have been used in various studies.[11,13–22] Average charge transport properties, such as ionic conductivity and transport numbers, can be determined by studying equilibrium fluctuations in simulations.[21,23] Simultaneously, it is possible to analyze the molecular and ionic correlations that govern the average properties. The distribution of values beneath the averages can be exposed and examined as the trajectory of every particle is known. This combination is

Department of Materials Science and Engineering, Norwegian University of Science and Technology, NTNU, NO-7491 Trondheim, Norway.
E-mail: sondre.k.schnell@ntnu.no

† Electronic supplementary information (ESI) available: Finite size effects, coordination data, experimental ionic conductivity, Onsager coefficients involving solvent, Maxwell–Stefan coefficients, radial distribution functions, distribution of pair lifetime correlations at selected time intervals, and calculation of anion coordination of different parts of the distributions. See DOI: https://doi.org/10.1039/d3nj04065h. LAMMPS input-files, and relevant scripts can be found at DOI: https://doi.org/10.5281/zenodo.10000803

useful for a more complete understanding of the transport properties in electrolytes. It is common to utilize the Nernst–Einstein (NE) approximation, based on the self-diffusion coefficients, when analyzing the charge transport properties.[14–17,21,24] Nernst–Einstein is an approximation for dilute or ideal systems, where ionic correlations are neglected. Here, we analyze the transport properties both in terms of the self-diffusion coefficients and NE approximation, as well as in terms of the Onsager coefficients which takes ionic and molecular correlations into account.

In this work, we aim to understand the macroscopic ionic transport properties of PEO–LiTFSI polymer electrolytes from microscopic interactions. We show how to compute the ionic conductivity and transport numbers from equilibrium MD simulations using the NE approximation and the Onsager coefficients in the Theory section. The differences of the two methods are emphasized. The ionic conductivity and transport numbers of the PEO–LiTFSI systems computed with the NE approximation and Onsager coefficients are presented in the Results section. We observe significant differences between the two methods and discuss these. We discuss the significance of reference frame when analyzing and comparing transport numbers and transport coefficients. The static and dynamic properties of the Li coordination environments are characterized to understand the microscopic transport mechanisms of Li. Finally, we present the computed thermodynamic factor of the PEO–LiTFSI systems and relate it to the above findings.

2 Theory

Diffusion is potentially the limiting factor in transport of mass and charge in polymer electrolytes.[25] Transport and diffusion properties in electrolytes can be studied in equilibrium MD simulations by sampling the equilibrium fluctuations of particle displacements or velocities, or using the Einstein or Green–Kubo relations, respectively.[21] Both methods are in principle equivalent.[13] We used the Einstein relations to study the transport properties in this work, as plots of the mean squared displacement can indicate how well the system has converged.[26]

The Nernst–Einstein approximation or the Onsager coefficients can be used to examine the charge transport properties of electrolytes. The NE approximation is based on the Nernst–Einstein equation which relates the diffusion coefficient directly to the mobility of a species.[13] Hence, it is well suited for dilute and ideal systems. In MD simulations, the NE approximation is based on the self-diffusion coefficients,[14–17,21,24] which is calculated from the mean squared displacement or velocities of particles. The self-diffusion coefficients are defined when there is no chemical potential gradient influencing the transport, *i.e.* they describe the movements of individual particles in the absence of a field. The self-diffusion coefficient of component i is:

$$D_{i,\mathrm{self}} = \lim_{t\to\infty} \frac{1}{6N_i} \frac{\mathrm{d}}{\mathrm{d}t} \left\langle \sum_{k=1}^{N_i} \left(\mathbf{r}_{k,i}(t) - \mathbf{r}_{k,i}(0)\right)^2 \right\rangle, \qquad (1)$$

where t is time, $\mathbf{r}$ is the particle position vector, N_i is the number of particles of component i and the $\langle\cdots\rangle$ brackets denote an ensemble average. The resulting NE approximation of the partial ionic conductivity contribution by species i is:

$$\sigma_i^{\mathrm{NE}} = \frac{z_i e N_i D_{i,\mathrm{self}}}{k_{\mathrm{B}} T V}, \qquad (2)$$

where k_{B} is the Boltzmann constant, T is absolute temperature, V is system volume, z_i is the charge valency of species i, and e is the elementary charge. The NE total ionic conductivity is obtained by summing all partial ionic conductivity contributions: $\sigma^{\mathrm{NE}} = \sum_i \sigma_i^{\mathrm{NE}}$. The NE transport number of species i is:

$$t_i^{\mathrm{NE}} = \frac{\sigma_i^{\mathrm{NE}}}{\sum_i \sigma_i^{\mathrm{NE}}} = \frac{\sigma_i^{\mathrm{NE}}}{\sigma^{\mathrm{NE}}}. \qquad (3)$$

To study the transport properties of concentrated electrolytes, we need to include deviations from the NE approximation by evaluating the contributions from molecular and ionic correlations. These are included in the Onsager coefficients:

$$L_{ij} = \frac{1}{6N} \lim_{t\to\infty} \frac{\mathrm{d}}{\mathrm{d}t} \left\langle \left(\sum_{k=1}^{N_i} \left[r_{k,i}(t) - r_{k,i}(0)\right] \right) \left(\sum_{l=1}^{N_j} \left[r_{l,j}(t) - r_{l,j}(0)\right] \right) \right\rangle, \qquad (4)$$

in which N_i and N_j are the numbers of particles of component i and j, respectively, and N is the total number of particles in the system. Note that i and j might denote the same or different components. L is a general transport coefficient which gives the transport due to a gradient, *e.g.* an electric field or a thermal field. Here, L_{ij} describes the transport of species i in a chemical potential gradient of species j. L_{ii} describes the transport of species i in a chemical potential gradient of species i, which includes the self-diffusion contribution. An electrolyte with n species can be described by $n(n + 1)/2$ independent Onsager coefficients according to Onsager's reciprocal relations.[27] Thus, a binary electrolyte composed of a salt in a solvent has six independent Onsager coefficients.[27] The corresponding expression for the ionic conductivity contribution of the correlation between species i and j is:[23,28]

$$\sigma_{ij} = \frac{e^2}{6k_{\mathrm{B}} T V} \lim_{t\to\infty} \frac{\mathrm{d}}{\mathrm{d}t} \left\langle \sum_{k=1}^{N_i} \sum_{l=1}^{N_j} z_i z_j \left[r_{k,i}(t) - r_{k,i}(0)\right] \cdot \left[r_{l,j}(t) - r_{l,j}(0)\right] \right\rangle. \qquad (5)$$

The total ionic conductivity is obtained by summing over all ionic pairs:

$$\sigma = \sum_i \sum_j \sigma_{ij}, \qquad (6)$$

and we call this the Onsager ionic conductivity. The Onsager transport number of a species i is:

$$t_i = \frac{\sum_j \sigma_{ij}}{\sigma}, \qquad (7)$$

where we sum over all the partial conductivity contributions of species i computed with eqn (5) in the numerator.[29]

The effect of ionic correlations in an electrolyte can be quantified as the ionicity, also called the inverse Haven's ratio.[30] The ionicity is defined as the Onsager ionic conductivity divided by the Nernst–Einstein ionic conductivity. If ionic correlations decrease the ionic conductivity, the ionicity will be below one.

Residence time

The average residence time of two species pairs i and j is calculated using the normalized lifetime correlation function, $P_{ij}(t)$:[28,31]

$$P_{ij}(t) = \frac{\langle H_{ij}(t) H_{ij}(0) \rangle}{\langle H_{ij}(0) H_{ij}(0) \rangle}, \tag{8}$$

and $H_{ij}(t)$ which denotes whether the species are together or not:

$$H_{ij}(t) = \begin{cases} 1, & d_{ij}(t) \leq r_c \\ 0, & d_{ij}(t) > r_c \end{cases} \tag{9}$$

where $d_{ij}(t)$ is the distance between species i and j at time t and r_c is the specified cutoff distance. The $\langle \cdots \rangle$ brackets denote an ensemble average. The cutoff distance was chosen as the first minimum after the first peak in the radial distribution function (RDF) of i and j. The actual cutoffs for the different systems are given in Table S6 (ESI†). The lifetime correlation function in eqn (8) is computed using the total time that the species pairs i and j are closer than the specified cutoff distance. This means that if the pair separates and later joins back together, $P_{ij}(t)$ will continue to increase. Hence, we are computing the so-called intermittent residence time. The lifetime correlation function was fitted to the following equation:[32]

$$P_{ij}(t) = \sum_i a_i \exp\left(\frac{-t}{b_i}\right), \tag{10}$$

where a_i and b_i are fitting parameters and the number of terms in the summation was adjusted to optimize the fit such that the standard deviation of the parameters was below 6% of the values. The fitted function was integrated to determine the average residence time of species i and j:[32]

$$\tau_{ij} = \int_0^\infty P_{ij}(t) \mathrm{d}t. \tag{11}$$

Thermodynamic factor

The thermodynamic factor, Γ, is a way of quantifying the ideality of a mixture. In a binary electrolyte, it can be defined as:[9,33]

$$\Gamma = 1 + \frac{\mathrm{d} \ln \gamma_\pm}{\mathrm{d} \ln x}, \tag{12}$$

where $\gamma_\pm$ is the molar activity coefficient of the salt and x is the mole fraction of the salt. For an ideal mixture, $\gamma_\pm = 1$ and $\Gamma = 1$. Negative Γ indicates thermodynamically unstable mixtures of binary systems. Thermodynamic factors can be computed from MD simulations using Kirkwood–Buff integrals (KBI). Kirkwood–Buff theory relates the microscopic structure of isotropic liquids described by RDFs to their thermodynamic properties. We used the pseudo-binary approach to compute KBIs of the electrolyte systems where the anions and cations are treated as similar molecules, *i.e.* one component.[34–36] The ether oxygens were considered as the solvent. For a binary mixture consisting of species i and j, the Kirkwood–Buff integral of a finite spherical volume L is:[35]

$$G_{ij}^V = \int_0^L [g_{ij}(r) - 1] 4\pi r^2 \left(1 - \frac{3x}{2} + \frac{x^3}{2}\right) \mathrm{d}r, \tag{13}$$

where r is the radius, $x = r/L$ and the radial distribution functions, g_{ij}, of the pseudo-binary system are obtained from the RDFs of the ternary system.[35] Finally, the thermodynamic factor is computed by:[26,37,38]

$$\Gamma = 1 - \frac{x_i \rho_j (G_{ii} + G_{jj} - 2G_{ij})}{1 + \rho_j x_i (G_{ii} + G_{jj} - 2G_{ij})}, \tag{14}$$

where x_i is the mole fraction of species i and ρ_j is the average number density of species j. In an ideal mixture, the interactions between like and unlike components are equal, the expression $G_{ii} + G_{jj} - 2G_{ij}$ becomes zero and Γ becomes one.

3 Method

The transport properties were characterized by running MD simulations using the LAMMPS[39] software on all-atom PEO–LiTFSI polymer electrolyte systems with varying salt concentrations and PEO chain lengths. We used the OPLS-AA potential[40] to describe intra- and intermolecular interactions. The parameters for PEO were obtained from the Ligpargen web server,[41–43] the Li cation parameters from Jensen and Jorgensen,[44] and we used the parameters developed by Canongia Lopes and Pádua for the TFSI anion.[45] We used Moltemplate[46] to build longer polymer chains from the templates supplied by Ligpargen. Shorter template chains were joined together to create chains of the desired length. The assigned electric charges of the atoms near the template chain ends will differ from the more central atoms due to different chemical environments. The electric charge of the atoms near the interconnected chain sites were manually adjusted to obtain consistent charges of similar atom types and to achieve overall electroneutrality. The C–H bonds of the polymer were fixed at the equilibrium bond length using the SHAKE algorithm[47] with an accuracy tolerance of 1×10^{-6}. Intramolecular Lennard-Jones and coulombic forces between nearest and next-nearest neighbors were switched off while interactions between atoms separated by two atoms were halved, as is standard in OPLS.[40,41] Global cutoffs for the Lennard-Jones and coulombic forces were set to 11 Å. Geometric mixing rules were used to determine the Lennard-Jones interactions between unlike atoms. Long-range coulombic forces were solved using a particle–particle particle–mesh solver[48] with a relative error in forces of 1×10^{-6}. The ionic charges were scaled by a factor of 0.75 to account for the typical overestimation of coulombic interactions between ions in non-polarizable force fields.[49] Periodic boundary conditions were applied in all directions. Initial configurations of the most dilute systems were prepared by placing PEO chains, and Li and TFSI ions in a simulation box with the Packmol software.[50]

The equilibration and simulation details are described in the following. Firstly, the energy of the simulation box was minimized

to avoid particle overlap. Then, the systems were equilibrated to obtain probable local energy minimum structures of the polymer electrolytes. We adopted an equilibration routine composed of a series of annealing and compression/decompression steps, developed by Molinari *et al.*[20] In order for the density and potential energy of the systems to converge, additional equilibration at temperatures of 390 K and 400 K was performed in the isothermal–isobaric (*NPT*) ensemble with a pressure of 1 atm and a timestep of 1 fs. The final equilibration was done at 423 K and 1 atm with a timestep of 1.25 fs. The Nosé–Hoover thermostat and barostat[51–53] were used to control the temperature and pressure in the *NPT* ensemble with time constants resulting in characteristic thermal and pressure fluctuations of 100 and 1000 timesteps, respectively. The lengths of the box sides were relaxed to facilitate the equilibration procedure. When the density and potential energy of the systems were stabilized, we switched to the canonical (*NVT*) ensemble to conduct production simulation runs. The volume of the simulation box was scaled according to the average volume during the final equilibration at 423 K to obtain correct density in the *NVT* ensemble. The Nosé–Hoover thermostat with thermal fluctuations of 100 timesteps was used to control the temperature in the *NVT* ensemble. Production runs lasted for at least 100 ns, which was sufficient to reach the diffusive regime of most diffusion coefficients. It is noted in the text which coefficients are not computed from the diffusive regime. In order to achieve sufficiently fast dynamics and reduced simulation times, we ran simulations at a temperature of 423 K with a timestep of 1.25 fs. Simulating at this temperature should not dramatically influence the trends of the dynamic properties compared to the normal operating temperatures of these electrolytes of around 350 K. The systems with lowest salt concentration were prepared and sampled first. Then, the systems with higher salt concentrations were made consecutively by randomly placing more Li and TFSI to the configuration at the end of the production runs, followed by energy minimization and equilibration. The equilibration following salt addition was conducted by firstly running 5 million time steps of 1 fs at 390 K and 1 atm with a soft potential[54] utilizing a softness parameter of 0.5 to facilitate rapid mixing of polymer chains and ions. Next, the full potential was turned back on for 55 million time steps at 390 K and 1 atm, followed by at least 30 million time steps of 1.25 fs at 400 K and finally at least 20 million time steps of 1.25 fs at 423 K. The average box volume was sampled during the run at 423 K to adjust the box volume to the correct size before the production run in the *NVT* ensemble. The total energy of every system was sampled in the microcanonical (NVE) ensemble before the production run to check the stability of the systems. The change of total energy in the NVE ensemble was normally below 1 kcal mol^{-1} ns^{-1}, and always below 2 kcal mol^{-1} ns^{-1}, corresponding to less than 1% change of the total energy during 100 ns. The transport properties were sampled in the *NVT* ensemble.

The salt concentrations studied corresponded to ethylene oxide (EO) : Li ratios of 50, 20, 10, 6, 3, 2, or equivalently Li : EO ratios of 0.02, 0.05, 0.10, 0.17, 0.33, 0.50. We investigated the effect of PEO chain length on the ion dynamics. Two PEO chain lengths were investigated, 23, 100 monomers (EO) long. 172 chains of length 23 monomers or 40 chains of length 100 monomers were placed in the simulation box, giving about 4000 monomers of each. All PEO chains in each simulation box had the same length. The PEO chains were methoxy-/ethoxy-terminated with –O–CH_3 termination on one end and –O–CH_2–CH_3 on the other. We used the OCTP module[55] to calculate self-diffusivities and Onsager coefficients. The KBIs G_{ij} in the thermodynamic limit were estimated by plotting G_{ij}^{V} against $1/L$ where L is the radius of the volume and determining the intercept by extrapolating the linear range of the curve.[56] The nitrogen atom and the middle oxygen atom were chosen as tracer particles to compute transport properties of the TFSI anion and PEO chains, respectively. An in-house code was used to compute ionic conductivity and transport numbers based on the Nernst–Einstein approximation and the Onsager coefficients.[29] The configurations of the systems were stored every 125 ps for analyzing the coordination environments. We made three replicas of each system to analyze the statistical variation of the transport properties. The replica systems were prepared from different initial configurations with Packmol. Finite-size effects were evaluated by studying two systems with concentration r = 0.17 and PEO chain length of 100 monomers of double size.

The glass transition temperature in some selected systems was determined by cooling the systems with 5 K temperature intervals from 288 to 208 K at atmospheric pressure in the *NPT* ensemble. Each cooling was performed during 2 million time steps, and the temperature was then held constant at each temperature interval for 6 million time steps. The average density was calculated during the final 2 million time steps of each isothermal step. The glass transition temperature was determined from the change of the density as a function of temperature.[57,58] Three replica simulations were performed to determine averages and standard deviations for each system.

The reported values and uncertainties were estimated by calculating the mean and standard deviations of the quantities obtained from the simulations.

4 Results and discussion

The ionic conductivities and ionicities of all systems are presented in Fig. 1. The Nernst–Einstein approximations are denoted with superscript NE. n denotes the length of the PEO chains in number of ethylene oxide units. r denotes the salt concentration as defined by the number of Li divided by the number of EO units.

The ionic conductivities of all the systems increase with increasing salt concentration until reaching a maximum around a salt concentration of r = 0.17, corresponding to a fully saturated system (EO : Li = 6) where all ether oxygen atoms coordinate Li. Upon further increasing the salt concentration, the conductivities go down. The systems with shorter PEO chains, n = 23, display higher conductivities due to faster chain dynamics, as expected.[61–63] The glass transition temperatures of the short-chained systems appear to be slightly lower than in the long-chained systems, shown in Table S5 (ESI†), which could partially explain the higher

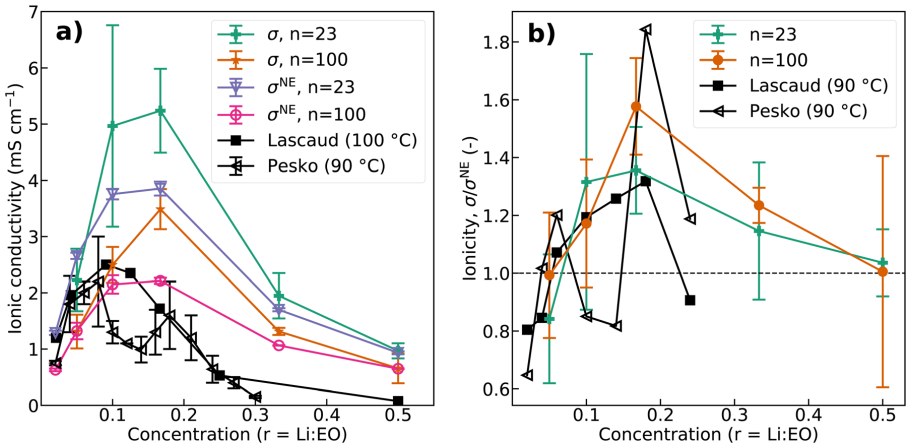

Fig. 1 (a) Ionic conductivity and (b) ionicity of PEO–LiTFSI systems as function of salt concentration and chain length. Experimental ionic conductivities by Lascaud *et al.*[59] measured at 100 °C and Pesko *et al.*[10] measured at 90 °C are shown for comparison. Ionicity $=\sigma/\sigma^{NE}$. The experimental ionicity values are calculated by dividing experimental ionic conductivities measured by electrochemical impedance spectroscopy[10,59] by conductivity values calculated using self-diffusion coefficients (NE approximation) from pulsed-field gradient nuclear magnetic resonance (pfg-NMR) data.[9,60]

conductivity of the short-chained systems, even though the variation in some systems is substantial. Surprisingly, the ionic conductivities computed from the Onsager coefficients taking ion–ion correlations into account are generally higher than the Nernst–Einstein approximations. This corresponds to ionicities above one, displayed in Fig. 1b, meaning that ionic correlations contribute to increasing the conductivity. This is an unexpected observation which we will discuss later.

Experimental ionic conductivities measured by Lascaud *et al.*[59] and Pesko *et al.*[10] are shown in Fig. 1a as comparison with the simulated values. Lascaud *et al.* used a PEO polymer with molecular weight M_n, of 3900–4500 g mol^{-1}, which is closest to the $n = 100$ system, which contains PEO chains with a molecular weight of 4420 g mol^{-1}. The experimental values measured at a temperature of 100 °C are expected to be lower than the simulated values obtained at 150 °C. However, the experimental conductivities are higher than the corresponding simulated values at salt concentrations below $r = 0.1$. Furthermore, the experimental values by Lascaud *et al.* reach a maximum and start to drop at a lower salt concentration of $r = 0.09$. At higher salt concentrations, above $r = 0.17$, the simulated conductivities are higher than the experimental values, as expected. The experimental ionic conductivity measured by Pesko *et al.* follow the same trend as the simulated data, except for a local minimum between $r = 0.10$ and $r = 0.18$. Despite these discrepancies, there is relatively good agreement between experimental and computed conductivities, and it seems that the model captures the overall trend of the ionic conductivity.

Fig. 2a shows the Li-ion transport numbers computed with the Nernst–Einstein approximation. The NE Li-ion transport numbers are quite low, below 0.3 for all salt concentrations except the highest, and decrease with increasing concentration until reaching a minimum of around 0.1/0.2 in the saturated system ($r = 0.17$). Apparently, the NE Li-ion transport number increases from $r = 0.02$ to $r = 0.10$ for the systems with chain length $n = 100$ but the error bars are too large in this range to conclude that this is the case. There are few ions in the simulated systems at the lowest concentrations, *e.g.* only 80 salt pairs at $r = 0.02$, and this increases the uncertainty due to limited data. In the super-saturated salt concentration region above $r = 0.17$, the NE Li-ion transport numbers increase again for both chain lengths. The polymer electrolytes composed of shorter chains display higher Li-ion transport numbers at all salt concentrations. The simulated NE values in Fig. 2a are compared to experimental values from a study by Pesko *et al.*,[9] which measured the Li-ion transport number in PEO–LiTFSI electrolytes using pulsed-field gradient nuclear magnetic resonance (pfg-NMR) probing the self-diffusion coefficients of the ions. The simulated values for the systems with chain length $n = 100$ are converted to steady-state Bruce-Vincent transport numbers using a recent method by Shao and Zhang,[65] and they are denoted as $t_{Li^+}^{SS}$ in Fig. 2a. These are comparable to experimental values obtained using the steady-state current method developed by Bruce and Vincent[66] from Pesko *et al.*[10] and Pożyczka *et al.*[8] on PEO–LiTFSI electrolytes. Hence, Fig. 2a compares data from methods for dilute or ideal electrolytes. We do not expect the pfg-NMR and steady-state methods to give equal results, but they are reasonably similar. We observe relatively good agreement between experimental and simulated data in Fig. 2a. The overall trend of a low and decreasing Li-ion transport number reaching a minimum at a salt concentration of $r = 0.17$, after which it increases again for higher salt concentrations, is present in both the experimental and simulated data. For the highest salt concentration, however, there is a significant deviation between the simulated data and experimental data by Pożyczka *et al.* Also, the steady-state converted simulated

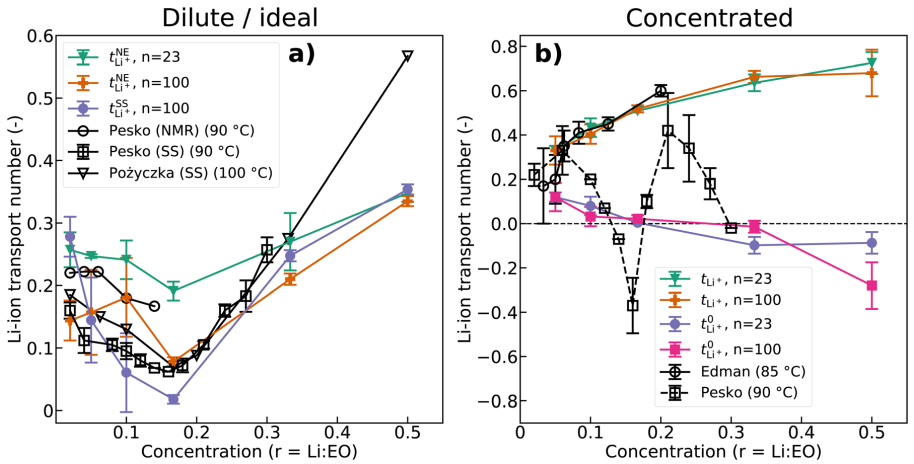

Fig. 2 Computed and experimental transport numbers of PEO–LiTFSI systems as function of salt concentration and PEO chain length. (a) Nernst–Einstein (NE) and steady-state (SS) converted transport numbers compared to pfg-NMR derived transport numbers[9] and experimental steady-state current transport numbers.[8,10] (b) Onsager transport numbers compared to experimental transport numbers from two studies using the Newman methods.[10,64] Onsager transport numbers converted to the solvent velocity reference frame are denoted with superscript 0.

transport number for the most dilute system deviates from the experimental data which can be explained by limited data as mentioned above.

Li-ion transport numbers computed using the Onsager coefficients, taking ion–ion correlations into account, are presented in Fig. 2b. The Onsager Li-ion transport numbers are quite high, above 0.3 for all salt concentrations, and increase with increasing salt concentration until a maximum value of above 0.6 in the most concentrated systems. There is negligible difference between the systems with short and longer PEO chains. Experimental data for the Li-ion transport numbers using methods for concentrated electrolytes are shown for comparison in Fig. 2b. Pesko *et al.*[9] and Edman *et al.*[64] measured the Li-ion transport number in PEO–LiTFSI electrolytes using two slightly different methods based on concentrated solution theory, both developed by Newman and colleagues.[10] The experimental data by Edman *et al.* deviates significantly when compared to the data by Pesko *et al.* for salt concentrations above $r = 0.05$. The main difference of the experimental work of Pesko and Edman was the length of the PEO chains used to prepare electrolytes. In the work by Pesko *et al.*, they used rather short PEO chains of molecular weight 5 kg mol^{-1}, while Edman and colleagues used high-molecular weight PEO with M_w= 5000 kg mol^{-1}. It is not clear why there are such large differences in the data of Edman and Pesko. The Newman method gives transport numbers in the solvent velocity reference frame while the MD simulations produce transport numbers in the barycentric reference frame. In order to properly compare the simulated and experimental transport numbers in similar reference frames, we converted the computed barycentric transport numbers to the solvent velocity reference frame[67,68] and these are also displayed in Fig. 2b. Notably, negative Li-ion transport numbers are observed both in the experimental data by Pesko *et al.* and in the simulated data in the solvent velocity reference frame.

There are significant differences between the rigorously computed transport numbers, obtained with Onsager coefficients, and the Nernst–Einstein approximations. This is a strong indication that ion–ion correlations are important in this system and that the system behaves far from ideally, particularly at higher salt concentrations, when $r \geq 0.1$. Both experimental and simulated data suggest that the Nernst–Einstein approximation is not valid at higher salt concentrations in this electrolyte system.

Frame of reference

Calculation of transport properties, such as diffusion coefficients and transport numbers, depends on the frame of reference. In our simulations, the center of mass of the particles in the simulation box is used as the frame of reference, *i.e.* the barycentric reference frame. All transport numbers and coefficients in this work are reported in the barycentric frame of reference unless otherwise specified. The computed Onsager transport numbers are compared to experimental data by Pesko *et al.*[10] and Edman *et al.*[64] in Fig. 2b. Both of these studies use the Newman method for determining transport numbers, which employ the solvent velocity as the frame of reference.[69] A recent study by Mistry *et al.*[70] reported that the solvent is not static in PEO–LiTFSI polymer electrolytes when a current is passed through, particularly not at higher salt concentrations. The driving force for the solvent motion was indicated to be the diffusion of charged species. By taking the moving electrode/electrolyte interface as the reference frame instead of the solvent velocity, they showed that the cations move in the same direction as the electric current, corresponding to a positive Li-ion transport number, in contrast to previous studies.[9,10]

This shows the importance of the choice of reference frame. When the solvent is the major component of a mixture, it is convenient to use it as the reference, but for highly concentrated systems it might not be the proper choice. Considering electrolytes for Li-ion batteries, we are normally interested in the motion of ions relative to the surface of the electrodes. If the center of gravity of the electrolyte is shifting relative to the electrodes during an experiment or practical use, our results might not be directly applicable to describing the transport properties of the electrolyte for use in Li-ion batteries.[71] Recently, Shao *et al.*[68] investigated the importance of reference frame in PEO–LiTFSI polymer electrolytes and also presented a method for transforming transport numbers and Onsager coefficients between the barycentric and solvent velocity reference frames. The authors found a reasonable correlation between experimental and simulated transport numbers after transforming the values to the same reference frame. Our results agree well with the results of Shao *et al.*

The analysis and understanding of transport coefficients and transport of species in multi-component mixtures becomes difficult if the motion of the reference frame is unknown. This can be the case for "internal" frames of reference which are part of the system, such as the barycentric or solvent velocity reference frames.[71] The laboratory frame of reference can be viewed as an "external" frame of reference which is outside the system and does not move with respect to an experimental apparatus containing an electrolyte. Therefore, it is convenient for analyzing transport during diffusion experiments.[72,73] The volume-fixed frame of reference is equivalent to the laboratory reference frame when the electrolyte mixture is incompressible, *i.e.* when the partial molar volumes are constant as a function of salt concentration.[72,74,75] Hence, we have converted the barycentric ionic Onsager transport coefficients to the volume-fixed reference frame to support our barycentric data and these will be presented in the next section. Various frames of reference and the transformations between them are further discussed in ref. 27 and 76.

To gain a deeper understanding of the ionic conductivities and transport numbers, we computed the Onsager coefficients and self-diffusion coefficients of the components in the systems and they are presented in Fig. 3. The self-diffusion coefficients are used to calculate the Nernst–Einstein values, while the Onsager coefficients are related to the Onsager ionic conductivity and transport numbers. The self-diffusion coefficients of all components in Fig. 3a decrease with increasing salt concentration. This is in good agreement with several studies[11,62,77] which suggest that the binding of Li-ions to the polymer decreases the polymer flexibility and increases the viscosity, which decreases the self-diffusivity of all components. The self-diffusion coefficients of Li and PEO follow each other quite closely, which is logical given that Li is coordinated by ether oxygen in PEO. The TFSI self-diffusion coefficients are significantly higher than the self-diffusion coefficients of Li and PEO. The simulated self-diffusion coefficients are compared to experimental data by Timachova[60] measured at 90 °C using pfg-NMR. D_{Li} was measured on lithium-containing species and D_F was measured on fluorine-containing species. These should be comparable to the self-diffusion coefficients of Li and TFSI obtained from the systems with chain length $n = 100$. The experimental D_F is lower than the simulated D_{TFSI} which is expected considering the lower temperature in the experiment, but both decrease with higher salt concentrations. The experimental D_{Li} is a bit higher than the simulated D_{Li} in the most dilute system, while at the higher concentrations the simulated values are higher, as expected. As mentioned, the limited number of ions in the simulated systems at the lowest concentrations increases the statistical uncertainty. Additionally, the simulated D_{Li} at $r = 0.02$ was calculated from the sub-diffusive regime. This could explain the unexpectedly low value at the lowest concentration. Apart from the data of the most dilute system, the trend of the simulated data is in good agreement with the experimental values. The trend of the simulated D_{Li} in the sub-saturated region is reflected in the NE Li-ion transport number in Fig. 2a.

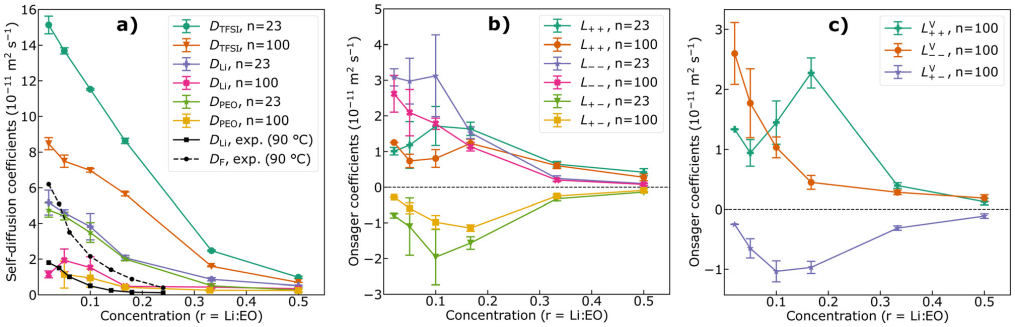

Fig. 3 (a) Self-diffusion coefficients, (b) Onsager coefficients in the barycentric reference frame, and (c) Onsager coefficients in the volume-fixed reference frame as function of salt concentration and chain length. The error in the volume-fixed coefficients was calculated using uncertainty propagation rules. Experimental self-diffusion coefficients by Timachova.[60] The self-diffusion coefficient of Li in the $n = 100$ system did not fully reach the diffusive regime at salt concentrations of $r = 0.02, 0.05, 0.10$. The self-diffusion coefficient of PEO in the $n = 100$ system did not fully reach the diffusive regime at salt concentrations of $r = 0.02, 0.05, 0.10, 0.33, 0.50$. L_{++} and L_{+-} for the $n = 100$ and $r = 0.02$ system were obtained in just one simulation and therefore have no error bars.

The barycentric Onsager coefficients in Fig. 3b provide information on the ionic correlations in the electrolyte systems. As an example, L_{--} describes the transport of anions in a chemical potential gradient of anions. L_{--} decreases with increasing salt concentration for the systems with chain length n = 100. The corresponding trend for the shorter chain systems is not so clear, particularly for low salt concentrations below r = 0.1 due to the large error bars. L_{++} seems to increase until a maximum at the salt concentration of r = 0.17 and then decrease at higher salt concentrations. This means that the Li-ions move more efficiently in a chemical potential gradient of Li-ions below the super-saturated concentrations than they do in the absence of such a gradient, as described by the self-diffusion coefficient. In the super-saturated region, L_{++} is higher than L_{--} which explains why the Onsager Li-ion transport numbers are above 0.5 in this region. The decreasing L_{--} with higher salt concentrations can be explained by considering the microscopic free volume in the electrolyte. The TFSI anion is believed to move in the free volume between the polymer chains, not directly coordinated by the polymer.[78] As the density of the electrolytes increase with increasing salt concentration, the free volume decreases which results in a reduction of the anion mobility.[64] The density of the systems as function of salt concentration is shown in Fig. S1 (ESI†). Interestingly, L_{+-} is negative at all concentrations and reaches a minimum at a salt concentration of r = 0.1–0.2. L_{++} reaching a maximum and L_{+-} reaching a negative minimum at the salt concentration r = 0.17 results in a maximum in the ionic conductivity and ionicity shown in Fig. 1a and b, respectively. The magnitude of the coupling coefficient L_{+-} is considerable relative to the main coefficients, L_{++} and L_{--}, when compared to common carbonate-based battery electrolytes.[33] However, the relation $L_{ii}L_{jj} \geq L_{ij}^2$ holds for all systems.[27] The trend of the ionic conductivity is a consequence of the balance between the number of free charge carriers and their mobility, which is tightly coupled to the polymer segmental motion, as shown in several studies.[25,79–81] Shao and Gudla *et al.* also found negative L_{+-} values in PEO–LiTFSI electrolytes in the barycentric frame of reference.[68,82] Negative L_{+-} values mean that the cation–anion correlation contributes to increasing the ionic conductivity of the system,[83] resulting in ionicities above 1. This is a counter-intuitive result. Firstly, it indicates that in this model, the TFSI anions bond weakly to the Li-ions, which we can justify given the bulky size of the TFSI anion and its highly delocalized charge.[3,81] Secondly, the TFSI anion is known to plasticize the polymer, *i.e.* increase polymer flexibility.[3] Hartree–Fock calculations have shown that the energy barrier for rotation about the S–N bonds in TFSI is comparable to the barriers for rotations of the C–C and C–O bonds in diglyme.[84,85] The corresponding dihedral interactions describing rotations in TFSI and PEO in the model we used are of similar magnitude. The plasticizing nature of the TFSI could thus facilitate and increase the Li-ion diffusion. In addition, it could increase diffusion of TFSI itself because enhanced polymer chain flexibility will create more voids for the anion to move into. The TFSI anion is illustrated in Fig. S2 (ESI†). Notably, the L_{+-} reaches a negative minimum at a quite high salt concentration (r = 0.1–0.2). The plasticization effect apparently increases with increasing salt concentration up to the saturated system due to the higher number of anions. At even higher concentrations, the effect is diminished which again reduces the ionicity. Ionicity values above one are rarely encountered in the literature, but they are not impossible.[79,86,87] The ionicity as a function of salt concentration calculated from experimental data for PEO–LiTFSI electrolytes is displayed in Fig. 1b and Fig. S3 (ESI†), and ionicities above one are evident for some salt concentrations, see also ref. 87. In electrolyte systems with shorter chains, *e.g.* triglyme or tetraglyme and LiTFSI salt, ionicity values below one have been found.[88,89] This suggests a change of the microscopic transport mechanisms and the significance of the cation–anion correlation upon increasing the chain length from glymes to PEO. It is also worth noting that in coarse-grained MD simulations of polymer electrolytes with monomers and ions described as spherical beads, ionicity values above one have not been observed,[80,81] which suggests that atomic resolution is necessary to detect this phenomenon.

The barycentric Onsager coefficients for the systems with long PEO chains were converted to the volume-fixed reference frame using the method explained in ref. 68, 73, 74 and 76, and these are shown in Fig. 3c. The partial molar volumes of the components are required to perform the conversion and these were obtained using Kirkwood–Buff integrals and the expressions of Ruckenstein and Shulgin.[90] The trends and values of the volume-fixed Onsager coefficients are mostly similar as the barycentric coefficients. Notably, the L_{+-} values are negative also in the volume-fixed reference frame. The partial molecular volumes of the neutral components, shown in Fig. S7 (ESI†), do not change dramatically with concentration which indicates that the assumption of incompressibility is acceptable. The volume-fixed Onsager coefficients are thus relevant also in an external frame of reference which supports our above argument concerning the barycentric Onsager coefficients. We note that the Li-ion transport number in the volume-fixed frame of reference display the same trend as in the barycentric frame of reference, shown in Fig. 2b.

We cannot avoid mentioning that the above findings contradict much of the literature published on this system which indicate that Li and TFSI tend to form mobile negatively charged clusters, *e.g.* two TFSI connected to one Li.[9,10,20,69,91] The two anions then drag the Li-ion away from the cathode towards the anode during discharge which causes negative Li-ion transport numbers. The remaining Li-ions not present in anion-dominated clusters are believed to be rather immobile compared to the clusters. This behavior does not seem to occur in our models. The Onsager coefficients involving the solvent (PEO) are presented in Fig. S4 (ESI†). We calculated the Maxwell–Stefan coefficients from the Onsager coefficients using the method developed by Krishna *et al.*[92] and they are displayed in Fig. S5 (ESI†). Transport properties for some selected systems were simulated at a reduced temperature of 353 K and these are shown in Table S4 (ESI†). The trends of the transport coefficients did not change dramatically compared to the simulations at 423 K, only their magnitudes due to slower dynamics.

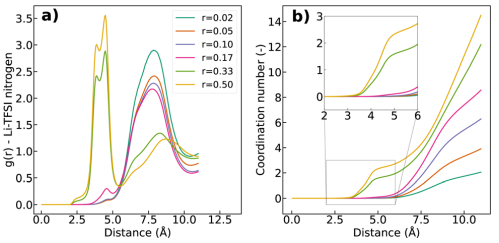

Fig. 4 (a) Radial distribution functions and (b) coordination numbers of Li and TFSI nitrogen for the different salt concentrations with chain length n = 100.

We analyzed the average static coordination environments around Li by computing the radial distribution functions and coordination numbers of Li and ether oxygen and Li and the central nitrogen of TFSI anions. The resulting plots for the Li-ether oxygen and Li–TFSI nitrogen coordination are presented in Fig. S6 (ESI†) and Fig. 4, respectively. More coordination data are presented in Table S3 (ESI†). Li is coordinated by 5–6 ether oxygen at salt concentrations up to r = 0.17. The RDFs for Li–TFSI show little sign of ion pairing closer than 5 Å for the concentrations lower than r = 0.17. This observation is in line with several spectroscopic and diffraction studies.[7,93–95] At the saturated concentration, r = 0.17, there is some indication of ion pairing and at higher concentrations there are clear signs of ion association. At the concentration r = 0.50, every Li is coordinated by more than two TFSI anions on average, meaning that ion clusters form throughout the material. Consequently, the average coordination number of ether oxygen is reduced to less than 2.5, as shown in Fig. S6b (ESI†). The total coordination number of oxygen is maintained at 5–6 but fluorine contacts are also observed in the super-saturated systems. Examples of Li coordination environments during the simulations are displayed in Fig. 5.

To obtain a better understanding of the significance of the coordination environment, it is necessary to examine the dynamic nature of the coordination.[82] We evaluated the dynamic properties of the coordination environments of Li by calculating the residence times of Li-ether oxygen, Li–PEO chain, and Li–TFSI nitrogen for the different salt concentrations and PEO chain lengths. The residence time is an estimate of the time that a pair of two species stay within a certain cutoff distance, as neighbors, before parting ways. Fig. 6 displays the average residence times.

The residence times of Li-ether oxygen and Li–PEO chain obviously follow the same trend. The Li-ether oxygen residence times are generally shorter than the Li–PEO chain residence times because Li normally moves a distance along a chain before jumping to the next chain. There is little dependence of chain length on the Li–ether oxygen residence times but the Li-ions sit slightly longer with the ether oxygen in the shorter chains than in the longer chains. The residence times of Li–ether oxygen are between 30 and 600 ns, indicating strong ion-solvent coordination. The residence times increase dramatically with increasing salt concentration until reaching a maximum in the saturated systems at concentration of r = 0.17. At higher salt concentrations, the residence times decrease again. As the Li concentration increases from the most dilute system, more ether oxygen atoms become coordinated to Li and fewer ether oxygen are uncoordinated/free. This increases the residence time as it becomes less likely for Li to find and jump to a free ether oxygen site. In the saturated system, at r = 0.17, all ether oxygen are in principle occupied and the residence time reaches a maximum. Li jumps must then occur by nearly all the Li jumping simultaneously in a collective manner which is a low-probability event. In the super-saturated systems, some Li are partly coordinated to anions and they can possibly move more freely between ether oxygens and PEO chains. This decreases the average residence time. The Li that only are coordinated to ether oxygen should still exhibit long residence times, leading us to believe there could be a distribution of residence times in these systems.

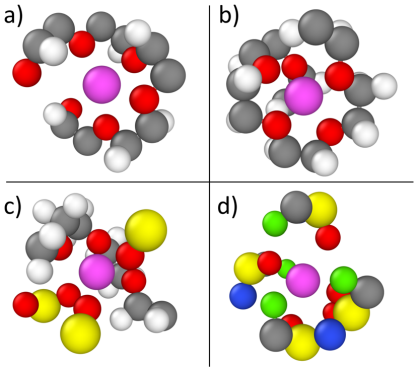

Fig. 5 Snapshots of Li coordination environments obtained with Ovito.[96] (a) Li coordinated by six ether oxygen, r = 0.17. (b) Li coordinated by five ether oxygen, r = 0.17. (c) Li coordinated by three ether oxygen and three oxygen from two TFSI anions, r = 0.33. (d) Li coordinated by oxygen from three TFSI anions, r = 0.50. Colors: carbon is grey, oxygen is red, hydrogen is white, sulphur is yellow, nitrogen is blue, fluorine is green and lithium is purple.

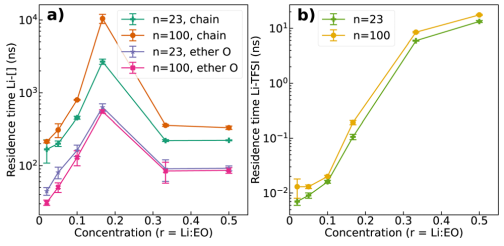

Fig. 6 Estimated average residence times for (a) Li-ether oxygen and Li–PEO chain and (b) Li–TFSI as function of salt concentration and chain length. Note logarithmic scale on the y axis. Note that some of the calculated residence times, particularly of Li–PEO chain, are much longer than the total simulation time. They might be more uncertain than reflected in the standard deviations (error bars), but we believe that the main trend of the data should hold.

To investigate this, we calculated the distribution of the pair lifetime correlation function for some selected systems at selected time intervals. The results for the system with longer PEO chains and the highest salt concentration are presented as violin plots in Fig. 7. Mean and extreme values are indicated in the violin plots. The mean values correspond to the pair lifetime correlation used to calculate average residence times in Fig. 6. The maximum and minimum values correspond to the individual pairs of Li–ether oxygen, Li–PEO chain, or Li–TFSI that exhibit the longest and shortest neighbor times, respectively. Wide pair lifetime correlation function distributions are observed for Li–ether oxygen and Li–PEO chain in the super-saturated system $r = 0.50$, supporting our hypothesis that some Li move quickly between ether oxygen atoms and PEO chains while others stay at the same site for much longer times. The bimodal distributions of Li–PEO chain indicates that some Li are coordinated to the same chain during the entire simulation time while others jump between chains more frequently. We also observe wide distributions in the other systems, particularly those close to the saturated concentration of $r = 0.17$, presented in Fig. S8 and S9 (ESI†). Even if the average Li–ether oxygen and Li–PEO chain residence time at the salt concentrations $r = 0.05$ and $r = 0.33/0.50$ are quite similar, the distributions are wider in the super-saturated systems than the sub-saturated system. This is an indication that the Li are changing coordination by different mechanisms in the different systems. We calculated the average number of anions coordinated to the Li exhibiting the longest and shortest Li–ether oxygen and Li–PEO chain residence times in Fig. 7. Details of the calculation are given in the ESI.† The Li displaying weaker correlation to ether oxygen and PEO chain, *i.e.* shorter residence times, were on average coordinated to more anions than the Li displaying stronger correlation to ether oxygen and PEO chain, *i.e.* longer residence times. Furthermore, the Li with shorter residence times (coordinated by more anions) moved faster and further than the Li with longer residence times (coordinated by fewer anions) in the most concentrated systems, see Table S8 (ESI†). This observation suggests that the Li–TFSI interaction facilitates Li jumps between ether oxygen and between PEO chains, which is in line with the negative L_{+-} in Fig. 3, meaning that the Li–TFSI correlation contributes to enhancing the Li transport and hence the ionic conductivity. Shen and Hall also hypothesized that the cation–anion interactions could increase diffusion in polymer electrolytes in specific situations.[80] The finding is however in contrast to the study by Molinari *et al.*[20] in which Li coordinated to more anions exhibited lower mobility. The systems with concentrations lower than $r = 0.33$ exhibit smaller differences with respect to anion coordination of the Li that are stronger and weaker correlated to ether oxygens and PEO chains, likely due to the generally low anion coordination numbers in these systems. The results are summarized in Tables S7–S9 (ESI†). The above analysis shows that the average residence time can hide interesting information about the distribution of pair lifetimes and generally about the dynamics of a system.

Notably, the systems with the longest residence time of Li to ether oxygen and PEO chain, at concentration $r = 0.17$, are also the systems with the highest ionic conductivity, see Fig. 1. A substantial contribution of the Li transport must then come from vehicular diffusion with the PEO chains. In fact, vehicular diffusion represents a significant part of the Li transport in all the systems, in agreement with previous studies.[61,81] The root-mean-square diffusion length of Li between each change of ether oxygen coordination can be estimated using the Einstein–Smoluchowski equation:[12]

$$\lambda_{\mathrm{Li}} = \sqrt{6 D_{\mathrm{Li}} \tau_{\mathrm{Li-etherO}}}, \qquad (15)$$

where D_{Li} is the self-diffusion coefficient of Li and $\tau_{\mathrm{Li-etherO}}$ is the average residence time of Li and ether oxygen. The mean diffusion length of Li between changing ether oxygen coordination is presented in Fig. S11 (ESI†). Longer mean diffusion lengths indicate that vehicular diffusion dominates the transport. As shown in Fig. S11 (ESI†), vehicular diffusion becomes more important with increasing salt concentration from the dilute systems to the saturated system. The drastic reduction of mean diffusion length in the super-saturated systems is due to significantly slower dynamics and a shift from vehicular to

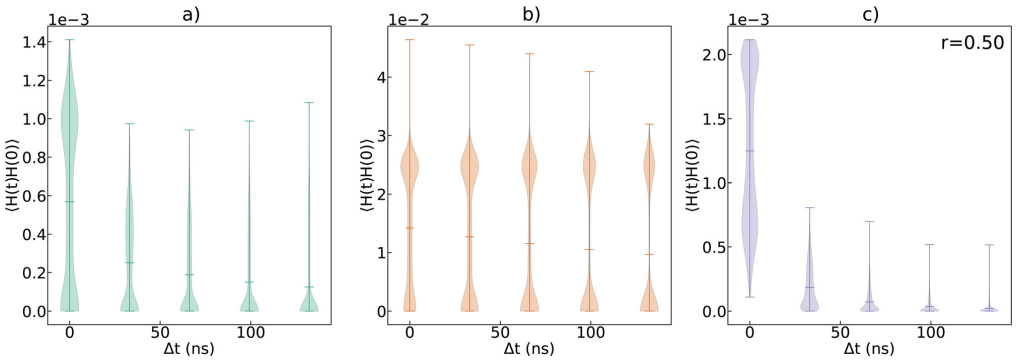

Fig. 7 Distribution of pair lifetime correlation functions at selected time intervals for (a) Li–ether oxygen, (b) Li–PEO chain, and (c) Li–TFSI for the system with chain length $n = 100$ and salt concentration $r = 0.5$. Mean and extreme values are marked in the violin plots.

structural diffusion. The Einstein–Smoluchowski equation is based on the three-dimensional random walk which might not be correct at all concentrations in these systems. However, the trend of the data appears plausible.

The residence times of Li and TFSI as function of salt concentration and PEO chain length are shown in Fig. 6b. For the most dilute systems, the residence times are very short, below 20 ps, indicative of very limited ion pairing. Upon increasing the concentration from $r = 0.10$ to 0.33, the residence time increases by about two orders of magnitude. At the highest concentrations, $r = 0.33$ and 0.50, Li–TFSI pairs are present and relatively long-lived, with a residence time on the order of 10 ns. During this time period, Li and TFSI acts as an electroneutral unit which does not carry electric charge. Combined with the decline of absolute values of the Onsager coefficients at the highest concentrations, this results in a decrease of ionic conductivity in the super-saturated regime, seen in Fig. 1a. From Fig. 7c we observe that some Li–TFSI pairs are stronger correlated, *i.e.* longer-lived, than the average and they will contribute more to reducing the ionic conductivity. The residence time at the concentration $r = 0.17$ is about 0.1–0.2 ns, too short to significantly influence the ionic conductivity.

The thermodynamic factor of the systems with chain length $n = 100$ calculated according to eqn (14) are presented in Fig. 8. A thermodynamic factor of one indicates an ideal mixture, and values away from one indicate non-ideality. Upon extrapolation to the dilute limit, $r = 0$, the thermodynamic factor approaches one as expected. The system becomes more non-ideal with increasing concentration, reaching a maximum in the saturated system, at $r = 0.17$. The thermodynamic factor is reduced to below one in the super-saturated systems indicating a change of the structure and interactions between the species, which corresponds to our previous discussions on the super-saturated systems. The data support our previous statement that PEO–LiTFSI electrolytes are generally non-ideal systems, even at quite low salt concentrations, most likely due to strong ion–ion correlations. The thermodynamic factor has been measured experimentally and calculated previously using simulations.[25,91,97] Our results agree reasonably well with the experimental data, also presented in Fig. 8, except for the highest concentrations where experimental data is lacking.

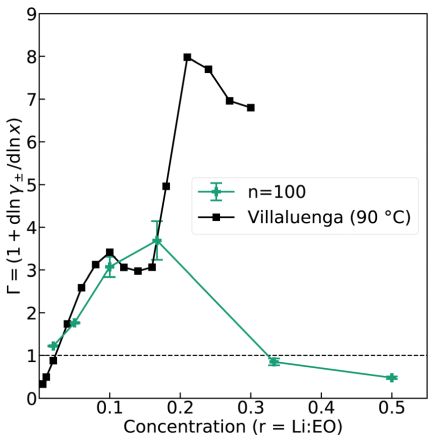

Fig. 8 Thermodynamic factor, Γ, of PEO–LiTFSI as function of salt concentration in the systems with chain length $n = 100$. Experimental values by Villaluenga *et al.*[25,91]

Deviations between experimental and simulated data

The deviation between the simulated ionic conductivity and experimental values warrants some discussion. In the simulations, the system with concentration $r = 0.17$ exhibits the highest ionic conductivity, while the experimental data suggest that the ionic conductivity is lower at this concentration than at $r = 0.1$. Obviously, there are substantial differences between simulations and experiments. Measuring ionic conductivity experimentally is usually done by performing electrochemical impedance spectroscopy on a sample of the electrolyte sandwiched between two blocking electrodes. Hence, interface effects might play a role. In our simulations, the systems are infinite with no interfaces. Furthermore, impurities and defects present in all real materials can influence experimental results, but are non-existent in the simulated systems. The fully saturated system where all ether oxygen are coordinated to Li is possibly a fragile system where local super-saturation and ion clustering might easily occur to create inhomogeneities, for example at interfaces.[98] This could explain the discrepancy between the simulated and experimental values. Additionally, it is possible that our charge-scaled non-polarizable model underestimates the degree of Li–TFSI ion pairing at the saturated concentration,[93] $r = 0.17$, which could result in too high ionic conductivity. Another possible explanation is finite-size effects, as the ionic conductivity at $r = 0.17$ was lower in a system of double size. The finite-size effects are presented in Table S2 (ESI†).

Li-ions acting as transient crosslinks between different PEO chains can reduce the polymer flexibility and decrease ionic conductivity.[62,77] The majority of Li-ions in our models are coordinated to just one PEO chain (Table S3, ESI†), limiting this effect. Several studies indicate that Li-ions prefer to coordinate to two PEO chains if possible.[11,18,99] Any lack of transient crosslinking in our systems compared to real-world electrolyte might cause the ionic conductivity to be artificially high. However, we believe this should not influence the main findings of the work.

Even though much work has been done to develop polymer electrolytes with improved transport properties, PEO–LiTFSI still exhibits some of the highest total and Li^+ partial conductivities of all polymer electrolytes.[100] We have proposed that the molecular character of the TFSI anion is important in PEO-based electrolytes and facilitates the transport of Li^+ by improving polymer segmental mobility. The LiTFSI salt reduces the crystallinity of neat PEO, making it more amorphous and increasing the chain flexibility. Electronic structure calculations suggest that the rotational flexibility around the S–N bonds is the main cause for this special behavior.[84,85] However, the size, shape and chemical character of TFSI could also contribute to breaking the crystalline domains of PEO and enhancing its flexibility. Compared to many anions, TFSI

clearly has unique properties and interact with PEO in a favorable way.[3] Nonetheless, other anions could potentially improve the transport properties of PEO-based electrolytes even further. Alternative polymer host materials with different chemical character than PEO could also potentially benefit from using salts with other anions than TFSI.[100] The cation–polymer interaction and coordination has been thoroughly studied in many polymer electrolytes.[101,102] We believe that a deeper understanding of the cation–anion and anion–polymer interactions are also useful for the development of next-generation polymer electrolytes and more effort should be directed towards engineering and developing new anions.

5 Conclusion

In this work, we have computed charge transport properties of PEO–LiTFSI polymer electrolytes, *i.e.* ionic conductivity and transport numbers, by equilibrium MD simulations. The results are comparable to experimental data, indicating that our models describe the real systems well. The values obtained using the NE approximation and Onsager coefficients and the significant differences between the results from the two methods suggest that the systems are non-ideal, which is further supported by our computation of thermodynamic factors. Therefore, we believe that determination of Onsager coefficients is necessary to understand the transport properties of these systems. Notably, negative L_{+-} values mean that Li and TFSI are anticorrelated, *i.e.* that their correlation contributes to increasing the ionic conductivity. This results in ionicity values above one, so-called superionicity. We attribute this effect to the rotational flexibility of the TFSI anion which plasticizes the PEO chains, facilitating Li transport. We observe that the Onsager coefficients L_{+-} and L_{++} reach absolute maxima at salt concentrations between $r = 0.10$ and $r = 0.17$, corresponding to maximum ionic conductivity and ionicity. The self-diffusivities, on the other hand, decrease monotonically with increasing salt concentration. Onsager coefficients converted to the volume-fixed reference frame agree well with the barycentric values obtained from simulations. The sum of the partial molar volumes of the components does not change much with increasing salt concentration, meaning that the volume-fixed frame of reference can be related to an external reference frame; the laboratory frame of reference. Both the volume-fixed and the barycentric frames of reference apparently move little relative to an external reference frame which simplifies the analysis of the Onsager transport coefficients. The absolute value of the coupling coefficient L_{+-} is remarkably large compared to the main coefficients, meaning that the cation–anion coupling is important in these electrolytes. The static and dynamic properties of the Li coordination environments were studied to understand the transport mechanisms of Li-ions. Very limited Li–TFSI ion pairing is observed for salt concentrations lower than $r = 0.17$. At the saturated concentration, $r = 0.17$, some Li–TFSI ion-pairing is observed but the residence time is too short to significantly influence the ionic conductivity. In the super-saturated systems, relatively long-lived ion-clusters are present throughout the material. The residence times of Li–ether oxygen and Li–PEO chains vary considerably with salt concentration, and are indeed very long at the saturated concentration, indicating that vehicular diffusion dominates the transport of Li. We observe a dramatic reduction of these residence times in the super-saturated systems, suggesting a change from vehicular to structural diffusion. The distribution of residence times provides more information on the variation of the dynamic properties of the Li environments. Bimodal distributions suggest that some Li quickly change coordination while others stay at the same site for longer times. The Li that display faster intrachain (Li–ether oxygen) and interchain (Li–PEO chain) jumps in the super-saturated systems are coordinated to more anions than the Li that are more strongly correlated to the coordination sites. This finding agrees well with the observation of negative L_{+-} values. We believe this implies that the TFSI anions facilitate Li jumps and Li transport, enhancing Li-ion conduction and the Li-ion transport number. Generally, we believe the anion is important for the transport properties of polymer electrolytes and a better understanding of its role in the charge transport is necessary.

The discrepancies that we observe between simulated and experimental data are discussed. Simulations and experiments are unavoidably fundamentally different and direct comparison between their results warrants caution and understanding of the inherent differences. One example is the frame of reference used to determine transport numbers, which is often different in experiments and in simulations. Nonetheless, we do believe our results are representative of real PEO–LiTFSI polymer electrolytes for use in Li-ion batteries and that the results will contribute to improved understanding of this fascinating class of materials.

Conflicts of interest

There are no conflicts to declare.

Acknowledgements

The simulations were performed on resources provided by Sigma2 – the National Infrastructure for High Performance Computing and Data Storage in Norway through the projects NN9264K and NN9414K, and on the NTNU IDUN/EPIC computing cluster. The Research Council of Norway is acknowledged for the support to the Norwegian Micro- and Nano-Fabrication Facility, NorFab, project number 295864. SKS acknowledges support through the NRC project 275754.

Notes and references

1 D. Fenton, J. Parker and P. Wright, *Polymer*, 1973, **14**, 589.
2 P. V. Wright, *Br. Polym. J.*, 1975, **7**, 319–327.
3 H. Zhang, C. Liu, L. Zheng, F. Xu, W. Feng, H. Li, X. Huang, M. Armand, J. Nie and Z. Zhou, *Electrochim. Acta*, 2014, **133**, 529–538.

4 M. Armand, *Solid State Ionics*, 1983, **9–10**, 745–754.
5 M. Armand, W. Gorecki and R. Andreani, *Proceedings of the 2nd International Meeting on Polymer Electrolytes*, 1989.
6 Z. Xue, D. He and X. Xie, *J. Mater. Chem. A*, 2015, **3**, 19218–19253.
7 G. Mao, M.-L. Saboungi, D. L. Price, M. B. Armand and W. S. Howells, *Phys. Rev. Lett.*, 2000, **84**, 5536–5539.
8 K. Pożyczka, M. Marzantowicz, J. Dygas and F. Krok, *Electrochim. Acta*, 2017, **227**, 127–135.
9 D. M. Pesko, K. Timachova, R. Bhattacharya, M. C. Smith, I. Villaluenga, J. Newman and N. P. Balsara, *J. Electrochem. Soc.*, 2017, **164**, E3569–E3575.
10 D. M. Pesko, S. Sawhney, J. Newman and N. P. Balsara, *J. Electrochem. Soc.*, 2018, **165**, A3014–A3021.
11 D. Diddens, A. Heuer and O. Borodin, *Macromolecules*, 2010, **43**, 2028–2036.
12 B. Dereka, N. H. C. Lewis, Y. Zhang, N. T. Hahn, J. H. Keim, S. A. Snyder, E. J. Maginn and A. Tokmakoff, *J. Am. Chem. Soc.*, 2022, **144**, 8591–8604.
13 D. Frenkel and B. Smit, *Understanding Molecular Simulation*, Academic Press, San Diego, Second edn, 2002.
14 M. Ebadi, T. Eriksson, P. Mandal, L. T. Costa, C. M. Araujo, J. Mindemark and D. Brandell, *Macromolecules*, 2020, **53**, 764–774.
15 L. J. A. Siqueira and M. C. C. Ribeiro, *J. Chem. Phys.*, 2006, **125**, 214903.
16 A. France-Lanord, Y. Wang, T. Xie, J. A. Johnson, Y. Shao-Horn and J. C. Grossman, *Chem. Mater.*, 2020, **32**, 121–126.
17 D. J. Brooks, B. V. Merinov, W. A. Goddard, B. Kozinsky and J. Mailoa, *Macromolecules*, 2018, **51**, 8987–8995.
18 O. Borodin and G. D. Smith, *Macromolecules*, 2006, **39**, 1620–1629.
19 L. T. Costa and M. C. C. Ribeiro, *J. Chem. Phys.*, 2007, **127**, 164901.
20 N. Molinari, J. P. Mailoa and B. Kozinsky, *Chem. Mater.*, 2018, **30**, 6298–6306.
21 K. D. Fong, J. Self, B. D. McCloskey and K. A. Persson, *Macromolecules*, 2021, **54**, 2575–2591.
22 H. Gudla, C. Zhang and D. Brandell, *J. Phys. Chem. B*, 2020, **124**, 8124–8131.
23 K. D. Fong, H. K. Bergstrom, B. D. McCloskey and K. K. Mandadapu, *AIChE J.*, 2020, **66**, e17091.
24 C. Y. Son and Z.-G. Wang, *J. Chem. Phys.*, 2020, **153**, 100903.
25 Y. Choo, D. M. Halat, I. Villaluenga, K. Timachova and N. P. Balsara, *Prog. Polym. Sci.*, 2020, **103**, 101220.
26 X. Liu, S. K. Schnell, J.-M. Simon, D. Bedeaux, S. Kjelstrup, A. Bardow and T. J. H. Vlugt, *J. Phys. Chem. B*, 2011, **115**, 12921–12929.
27 S. Kjelstrup and D. Bedeaux, *Non-Equilibrium Thermodynamics of Heterogeneous Systems*, World Scientific, Singapore, 2008.
28 K. D. Fong, J. Self, K. M. Diederichsen, B. M. Wood, B. D. McCloskey and K. A. Persson, *ACS Cent. Sci.*, 2019, **5**, 1250–1260.
29 Ø. Gullbrekken, I. T. Røe, S. M. Selbach and S. K. Schnell, *J. Phys. Chem. B*, 2023, **127**, 2729–2738.
30 V. Bocharova and A. P. Sokolov, *Macromolecules*, 2020, **53**, 4141–4157.
31 W. Zhao, F. Leroy, B. Heggen, S. Zahn, B. Kirchner, S. Balasubramanian and F. Müller-Plathe, *J. Am. Chem. Soc.*, 2009, **131**, 15825–15833.
32 Y. Zhang and E. J. Maginn, *J. Phys. Chem. Lett.*, 2015, **6**, 700–705.
33 S. Kjelstrup, A. F. Gunnarshaug, Ø. Gullbrekken, S. K. Schnell and A. Lervik, *J. Chem. Phys.*, 2023, **159**, 034104.
34 S. K. Schnell, P. Englebienne, J.-M. Simon, P. Krüger, S. P. Balaji, S. Kjelstrup, D. Bedeaux, A. Bardow and T. J. Vlugt, *Chem. Phys. Lett.*, 2013, **582**, 154–157.
35 P. Krüger, S. K. Schnell, D. Bedeaux, S. Kjelstrup, T. J. H. Vlugt and J.-M. Simon, *J. Phys. Chem. Lett.*, 2013, **4**, 235–238.
36 P. G. Kusalik and G. N. Patey, *J. Chem. Phys.*, 1987, **86**, 5110–5116.
37 A. Ben-Naim, *Molecular theory of solutions*, OUP Oxford, 2006.
38 X. Liu, S. K. Schnell, J.-M. Simon, P. Krüger, D. Bedeaux, S. Kjelstrup, A. Bardow and T. J. H. Vlugt, *Int. J. Thermophys.*, 2013, **34**, 1169–1196.
39 A. P. Thompson, H. M. Aktulga, R. Berger, D. S. Bolintineanu, W. M. Brown, P. S. Crozier, P. J. in 't Veld, A. Kohlmeyer, S. G. Moore, T. D. Nguyen, R. Shan, M. J. Stevens, J. Tranchida, C. Trott and S. J. Plimpton, *Comput. Phys. Comm.*, 2022, **271**, 108171.
40 W. L. Jorgensen, J. D. Madura and C. J. Swenson, *J. Am. Chem. Soc.*, 1984, **106**, 6638–6646.
41 W. L. Jorgensen and J. Tirado-Rives, *Proc. Natl. Acad. Sci. U. S. A.*, 2005, **102**, 6665–6670.
42 L. S. Dodda, J. Z. Vilseck, J. Tirado-Rives and W. L. Jorgensen, *J. Phys. Chem. B*, 2017, **121**, 3864–3870.
43 L. S. Dodda, I. Cabeza de Vaca, J. Tirado-Rives and W. L. Jorgensen, *Nucleic Acids Res.*, 2017, **45**, W331–W336.
44 K. P. Jensen and W. L. Jorgensen, *J. Chem. Theory Comput.*, 2006, **2**, 1499–1509.
45 J. N. Canongia Lopes and A. A. H. Pádua, *J. Phys. Chem. B*, 2004, **108**, 16893–16898.
46 A. I. Jewett, D. Stelter, J. Lambert, S. M. Saladi, O. M. Roscioni, M. Ricci, L. Autin, M. Maritan, S. M. Bashusqeh, T. Keyes, R. T. Dame, J.-E. Shea, G. J. Jensen and D. S. Goodsell, *J. Mol. Biol.*, 2021, **433**, 166841.
47 J.-P. Ryckaert, G. Ciccotti and H. J. Berendsen, *J. Comput. Phys.*, 1977, **23**, 327–341.
48 R. W. Hockney and J. W. Eastwood, *Computer simulation using particles*, Bristol, Hilger, 1988.
49 I. Leontyev and A. Stuchebrukhov, *Phys. Chem. Chem. Phys.*, 2011, **13**, 2613–2626.
50 L. Martinez, R. Andrade, E. G. Birgin and J. M. Martinez, *J. Comput. Chem.*, 2009, **30**, 2157–2164.
51 W. Shinoda, M. Shiga and M. Mikami, *Phys. Rev. B: Condens. Matter Mater. Phys.*, 2004, **69**, 134103.
52 W. G. Hoover, *Phys. Rev. A: At., Mol., Opt. Phys.*, 1985, **31**, 1695–1697.

53 S. Nosé, *Mol. Phys.*, 1984, **52**, 255–268.
54 T. C. Beutler, A. E. Mark, R. C. van Schaik, P. R. Gerber and W. F. van Gunsteren, *Chem. Phys. Lett.*, 1994, **222**, 529–539.
55 S. H. Jamali, L. Wolff, T. M. Becker, M. de Groen, M. Ramdin, R. Hartkamp, A. Bardow, T. J. H. Vlugt and O. A. Moultos, *J. Chem. Inf. Model.*, 2019, **59**, 1290–1294.
56 J.-M. Simon, P. Krüger, S. K. Schnell, T. J. H. Vlugt, S. Kjelstrup and D. Bedeaux, *J. Chem. Phys.*, 2022, **157**, 130901.
57 J. Han, R. H. Gee and R. H. Boyd, *Macromolecules*, 1994, **27**, 7781–7784.
58 K.-Q. Yu, Z.-S. Li and J. Sun, *Macromol. Theory Simul.*, 2001, **10**, 624–633.
59 S. Lascaud, M. Perrier, A. Vallee, S. Besner, J. Prud'homme and M. Armand, *Macromolecules*, 1994, **27**, 7469–7477.
60 K. Timachova, *PhD thesis*, University of California, Berkeley, 2018.
61 D. Devaux, R. Bouchet, D. Glé and R. Denoyel, *Solid State Ionics*, 2012, **227**, 119–127.
62 K. Timachova, H. Watanabe and N. P. Balsara, *Macromolecules*, 2015, **48**, 7882–7888.
63 M. P. Rosenwinkel, R. Andersson, J. Mindemark and M. Schönhoff, *J. Phys. Chem. C*, 2020, **124**, 23588–23596.
64 L. Edman, M. M. Doeff, A. Ferry, J. Kerr and L. C. De Jonghe, *J. Phys. Chem. B*, 2000, **104**, 3476–3480.
65 Y. Shao and C. Zhang, *J. Chem. Phys.*, 2023, **158**, 161104.
66 P. G. Bruce and C. A. Vincent, *J. Electroanal. Chem. Interfacial Electrochem.*, 1987, **225**, 1–17.
67 L. A. Woolf and K. R. Harris, *J. Chem. Soc., Faraday Trans. 1*, 1978, **74**, 933–947.
68 Y. Shao, H. Gudla, D. Brandell and C. Zhang, *J. Am. Chem. Soc.*, 2022, **144**, 7583–7587.
69 Y. Ma, M. Doyle, T. F. Fuller, M. M. Doeff, L. C. D. Jonghe and J. Newman, *J. Electrochem. Soc.*, 1995, **142**, 1859–1868.
70 A. Mistry, L. S. Grundy, D. M. Halat, J. Newman, N. P. Balsara and V. Srinivasan, *J. Electrochem. Soc.*, 2022, **169**, 040524.
71 M. Lorenz, F. Kilchert, P. Nürnberg, M. Schammer, A. Latz, B. Horstmann and M. Schönhoff, *J. Phys. Chem. Lett.*, 2022, **13**, 8761–8767.
72 Y. Zhou and G. H. Miller, *J. Phys. Chem.*, 1996, **100**, 5516–5524.
73 D. G. Miller, *J. Phys. Chem.*, 1986, **90**, 1509–1519.
74 J. G. Kirkwood, R. L. Baldwin, P. J. Dunlop, L. J. Gosting and G. Kegeles, *J. Chem. Phys.*, 1960, **33**, 1505–1513.
75 F. Kilchert, M. Lorenz, M. Schammer, P. Nürnberg, M. Schönhoff, A. Latz and B. Horstmann, *Phys. Chem. Chem. Phys.*, 2023, **25**, 25965–25978.
76 S. de Groot and P. Mazur, *Non-equilibrium Thermodynamics*, North-Holland Publishing Company, 1962.
77 R. He and T. Kyu, *Macromolecules*, 2016, **49**, 5637–5648.
78 G. Orädd, L. Edman and A. Ferry, *Solid State Ionics*, 2002, **152–153**, 131–136.
79 B. K. Wheatle, N. A. Lynd and V. Ganesan, *ACS Macro Lett.*, 2018, **7**, 1149–1154.
80 K.-H. Shen and L. M. Hall, *Macromolecules*, 2020, **53**, 3655–3668.
81 K.-H. Shen and L. M. Hall, *Macromolecules*, 2020, **53**, 10086–10096.
82 H. Gudla, Y. Shao, S. Phunnarungsi, D. Brandell and C. Zhang, *J. Phys. Chem. Lett.*, 2021, **12**, 8460–8464.
83 N. M. Vargas-Barbosa and B. Roling, *ChemElectroChem*, 2020, **7**, 367–385.
84 P. Johansson, S. P. Gejji, J. Tegenfeldt and J. Lindgren, *Electrochim. Acta*, 1998, **43**, 1375–1379.
85 R. Arnaud, D. Benrabah and J.-Y. Sanchez, *J. Phys. Chem.*, 1996, **100**, 10882–10891.
86 P. Nürnberg, J. Atik, O. Borodin, M. Winter, E. Paillard and M. Schönhoff, *J. Am. Chem. Soc.*, 2022, **144**, 4657–4666.
87 A. Mistry, Z. Yu, B. L. Peters, C. Fang, R. Wang, L. A. Curtiss, N. P. Balsara, L. Cheng and V. Srinivasan, *ACS Cent. Sci.*, 2022, **8**, 880–890.
88 K. Ueno, K. Yoshida, M. Tsuchiya, N. Tachikawa, K. Dokko and M. Watanabe, *J. Phys. Chem. B*, 2012, **116**, 11323–11331.
89 D. Dong, F. Sälzer, B. Roling and D. Bedrov, *Phys. Chem. Chem. Phys.*, 2018, **20**, 29174–29183.
90 E. Ruckenstein and I. Shulgin, *Fluid Phase Equilib.*, 2001, **180**, 345–359.
91 I. Villaluenga, D. M. Pesko, K. Timachova, Z. Feng, J. Newman, V. Srinivasan and N. P. Balsara, *J. Electrochem. Soc.*, 2018, **165**, A2766–A2773.
92 R. Krishna and J. M. van Baten, *Ind. Eng. Chem. Res.*, 2005, **44**, 6939–6947.
93 L. Edman, *J. Phys. Chem. B*, 2000, **104**, 7254–7258.
94 I. Rey, J. Lassègues, J. Grondin and L. Servant, *Electrochim. Acta*, 1998, **43**, 1505–1510.
95 A. Bakker, J. Lindgren and K. Hermansson, *Polymer*, 1996, **37**, 1871–1878.
96 A. Stukowski, *Modell. Simul. Mater. Sci. Eng.*, 2009, **18**, 015012.
97 C. Fang, W. S. Loo and R. Wang, *Macromolecules*, 2021, **54**, 2873–2881.
98 M. Rosso, T. Gobron, C. Brissot, J.-N. Chazalviel and S. Lascaud, *J. Power Sources*, 2001, **97–98**, 804–806.
99 A. G. Baboul, P. C. Redfern, A. Sutjianto and L. A. Curtiss, *J. Am. Chem. Soc.*, 1999, **121**, 7220–7227.
100 J. Mindemark, M. J. Lacey, T. Bowden and D. Brandell, *Prog. Polym. Sci.*, 2018, **81**, 114–143.
101 S. B. Aziz, T. J. Woo, M. Kadir and H. M. Ahmed, *J. Sci.: Adv. Mater. Dev.*, 2018, **3**, 1–17.
102 L. Long, S. Wang, M. Xiao and Y. Meng, *J. Mater. Chem. A*, 2016, **4**, 10038–10069.

Electronic Supplementary Information (ESI): Coupled Ion Transport in Concentrated PEO-LiTFSI Polymer Electrolytes

Øystein Gullbrekken and Sondre Kvalvåg Schnell*

Department of Materials Science and Engineering, Norwegian University of Science and Technology, NTNU, Trondheim NO-7491, Norway

E-mail: sondre.k.schnell@ntnu.no

Table S1: Number of salt molecules and salt concentration of simulated systems

n	r = Li:EO	No of salt molecules	Molar concentration (mol L^{-1})
23	0.02	80	0.42
23	0.05	200	0.95
23	0.10	400	1.66
23	0.17	666	2.36
23	0.33	1332	3.51
23	0.50	1998	4.17
100	0.02	80	0.43
100	0.05	200	0.98
100	0.10	400	1.70
100	0.17	666	2.40
100	0.33	1332	3.56
100	0.50	1998	4.23

Finite-size effects

Finite-size effects were evaluated by studying two systems with concentration r = 0.17 and PEO chain length of 100 monomers of double size. The ionic conductivity and ionicity

are lower in the bigger system compared to the normal system size. The Li-ion transport numbers are similar. The results are summarized in Table S2.

Table S2: Finite-size effects of transport properties in system with concentration r = 0.17 and PEO chain length of n = 100

System size	σ (mS cm^{-1})	σ^{NE} (mS cm^{-1})	t_{Li^+}	$t^{\mathrm{NE}}_{\mathrm{Li}^+}$	Ionicity
Normal size	3.49	2.21	0.52	0.078	1.58
Double size	2.73	2.10	0.52	0.063	1.30

Coordination data

Table S3: Fraction of free Li-ions (not coordinated by anions). Fraction of Li-ions coordinated to number of anions. Fraction of Li-ions coordinated to number of PEO chains

n	r = Li:EO	Free-Li ions	1 anion	2 anions	$\geq$3 anions	0 chains	1 chain	2 chains
23	0.02	0.99	0.01	0	0	0	0.96	0.04
23	0.05	0.99	0.01	0	0	0	0.97	0.03
23	0.10	0.98	0.02	0	0	0	0.98	0.02
23	0.17	0.91	0.09	0	0	0	0.99	0.01
23	0.33	0.25	0.27	0.22	0.26	0.23	0.77	0
23	0.50	0.14	0.17	0.20	0.49	0.44	0.56	0
100	0.02	0.99	0.01	0	0	0	0.96	0.04
100	0.05	0.99	0.01	0	0	0	0.98	0.02
100	0.10	0.98	0.02	0	0	0	0.99	0.01
100	0.17	0.91	0.09	0	0	0	0.99	0.01
100	0.33	0.25	0.24	0.24	0.27	0.22	0.78	0
100	0.50	0.14	0.16	0.21	0.49	0.43	0.57	0

Transport properties at 353 K

Table S4: Transport properties of systems with chain length $n = 100$ at 353 K. Average values from two simulations are provided.

r	L_{++} ($m^2\,s^{-1}$)	L_{--} ($m^2\,s^{-1}$)	L_{+-} ($m^2\,s^{-1}$)	σ ($mS\,cm^{-1}$)	σ^{NE} ($mS\,cm^{-1}$)	t_{Li^+} (-)	$t^{NE}_{Li^+}$ (-)	Ionicity (-)
0.10	1.5×10^{-13}	2.2×10^{-13}	-1.5×10^{-13}	0.25	0.25	0.47	0.38	1.00
0.17	2.5×10^{-13}	2.5×10^{-13}	-2.3×10^{-13}	0.37	0.24	0.51	0.15	1.53
0.33	8.4×10^{-14}	3.0×10^{-14}	-3.6×10^{-14}	0.056	0.029	0.73	0.32	1.95

Glass transition temperature

Table S5: Glass transition temperatures (T_g) of selected polymer electrolyte systems determined from simulations. Average values and standard deviation from three parallels are provided.

n	r = Li:EO	T_g (°C)
23	0.10	-26.6 ± 0.8
23	0.17	-22.0 ± 12.1
23	0.33	-21.1 ± 11.7
100	0.10	-17.7 ± 3.9
100	0.17	-24.0 ± 5.1
100	0.33	-10.2 ± 7.7

Table S6: Cutoff distances used to compute residence times for the different systems

n	r = Li:EO	Li-ether O cutoff (Å)	Li-TFSI N cutoff (Å)
23	0.02	3.68	5.00
23	0.05	3.66	5.00
23	0.10	3.71	5.00
23	0.17	3.71	5.00
23	0.33	3.60	5.42
23	0.50	3.62	5.47
100	0.02	3.66	5.00
100	0.05	3.66	5.00
100	0.10	3.69	5.00
100	0.17	3.71	5.00
100	0.33	3.60	5.42
100	0.50	3.62	5.47

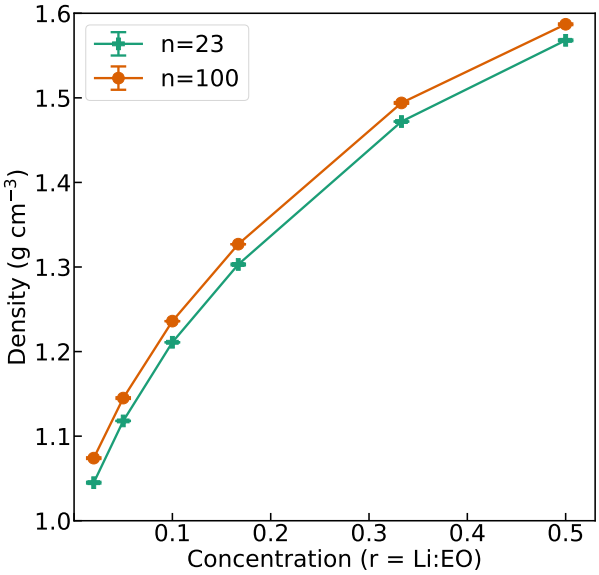

Figure S1: Density of systems as function of salt concentration.

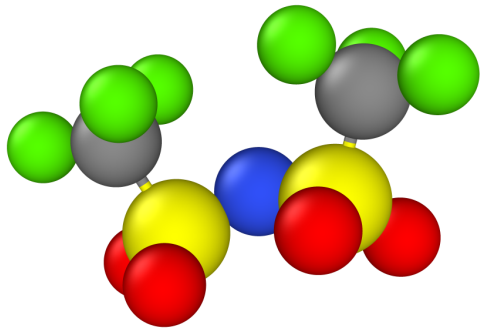

Figure S2: MD snapshot of TFSI anion. Fluorine is green, carbon is grey, sulphur is yellow, oxygen is red, nitrogen is blue.

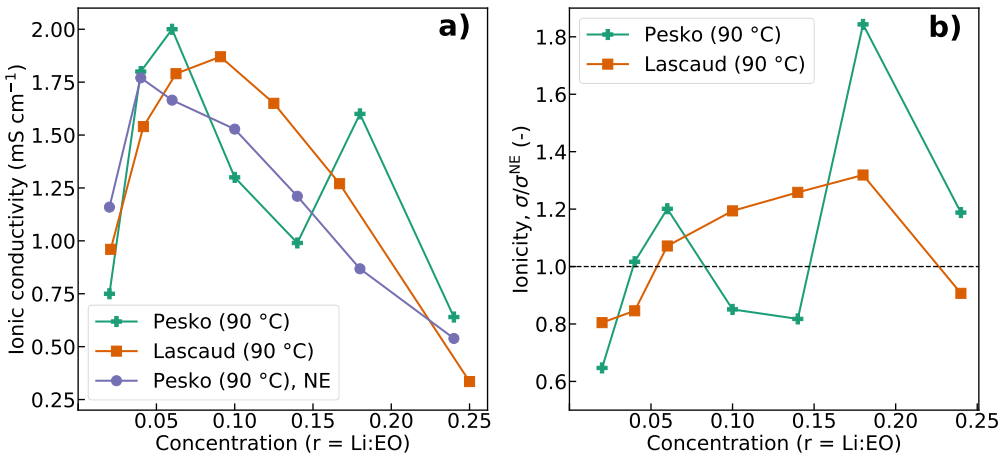

Figure S3: (a) Experimental ionic conductivity and (b) ionicity calculated from the data in (a) as function of salt concentration. The data labelled Pesko (90 °C), NE was calculated using the Nernst-Einstein approximation for ionic conductivity and the self-diffusion coefficients of Li and F species measured by Pesko and Timachova *et al.* using pfg-NMR[1,2]. The other experimental data was measured using electrochemical impedance spectroscopy (EIS)[3,4]. The ionicities in (b) were calculated by dividing the EIS data by the NE data. The ionicity of the Lascaud data was calculated by fitting a polynomial function to the data and dividing by the NE values of the same concentrations.

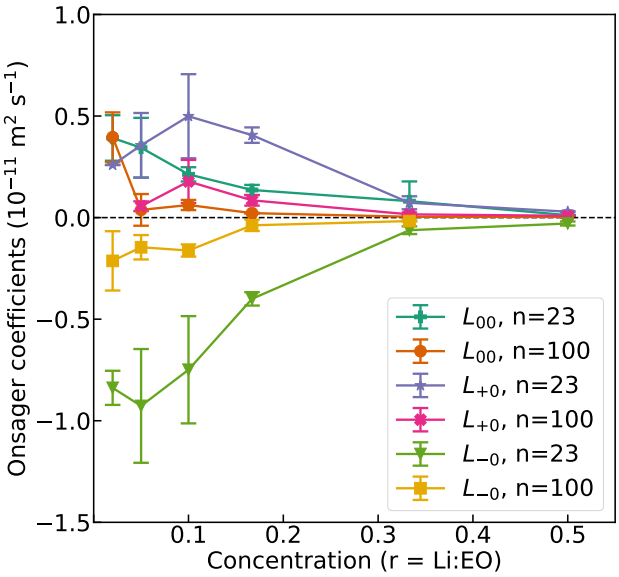

Figure S4: Onsager coefficients involving the solvent (PEO) as a function of salt concentration, denoted as 0 in the plot. These coefficients are dependent on the coefficients presented in the main part. Note that several of the L_{00} values did not reach the diffusive regime.

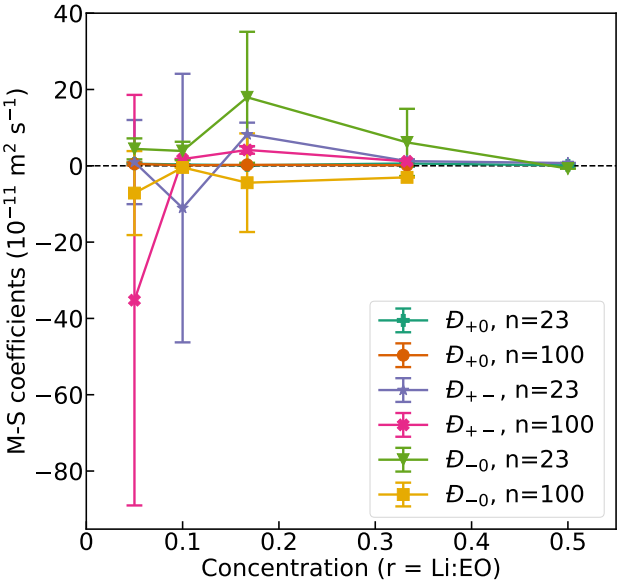

Figure S5: Maxwell-Stefan coefficients as a function of salt concentration. The solvent (PEO) is denoted as 0 in the plot.

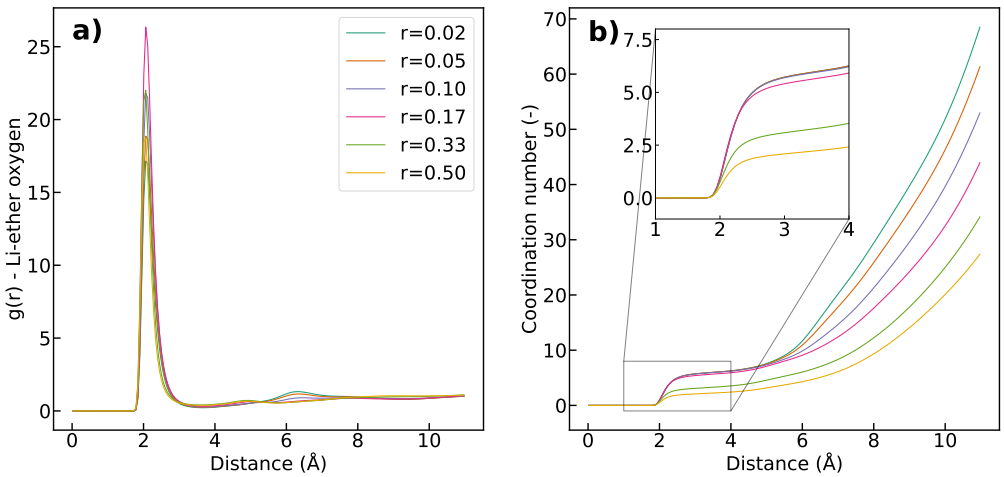

Figure S6: a) Radial distribution functions and b) coordination numbers of Li and ether oxygen for the different salt concentrations with chain length n = 100.

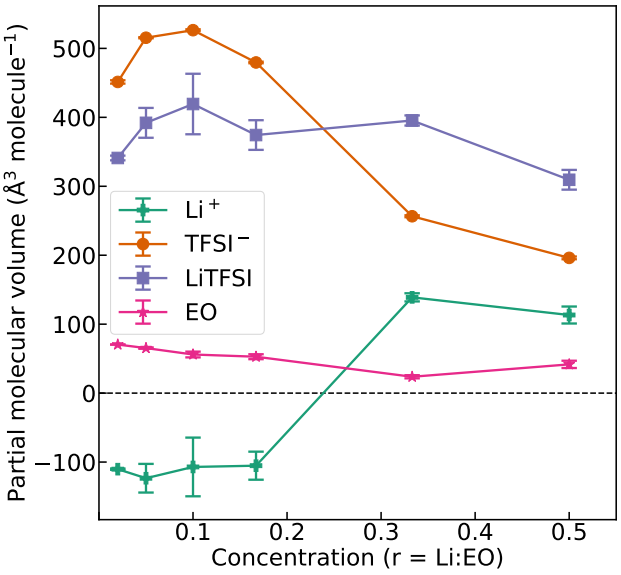

Figure S7: Partial molecular volumes of Li^+, $TFSI^-$ and ethylene oxide (EO) for the different salt concentrations with chain length n = 100. The partial molecular volume of LiTFSI is the sum of the volumes of Li^+ and $TFSI^-$.

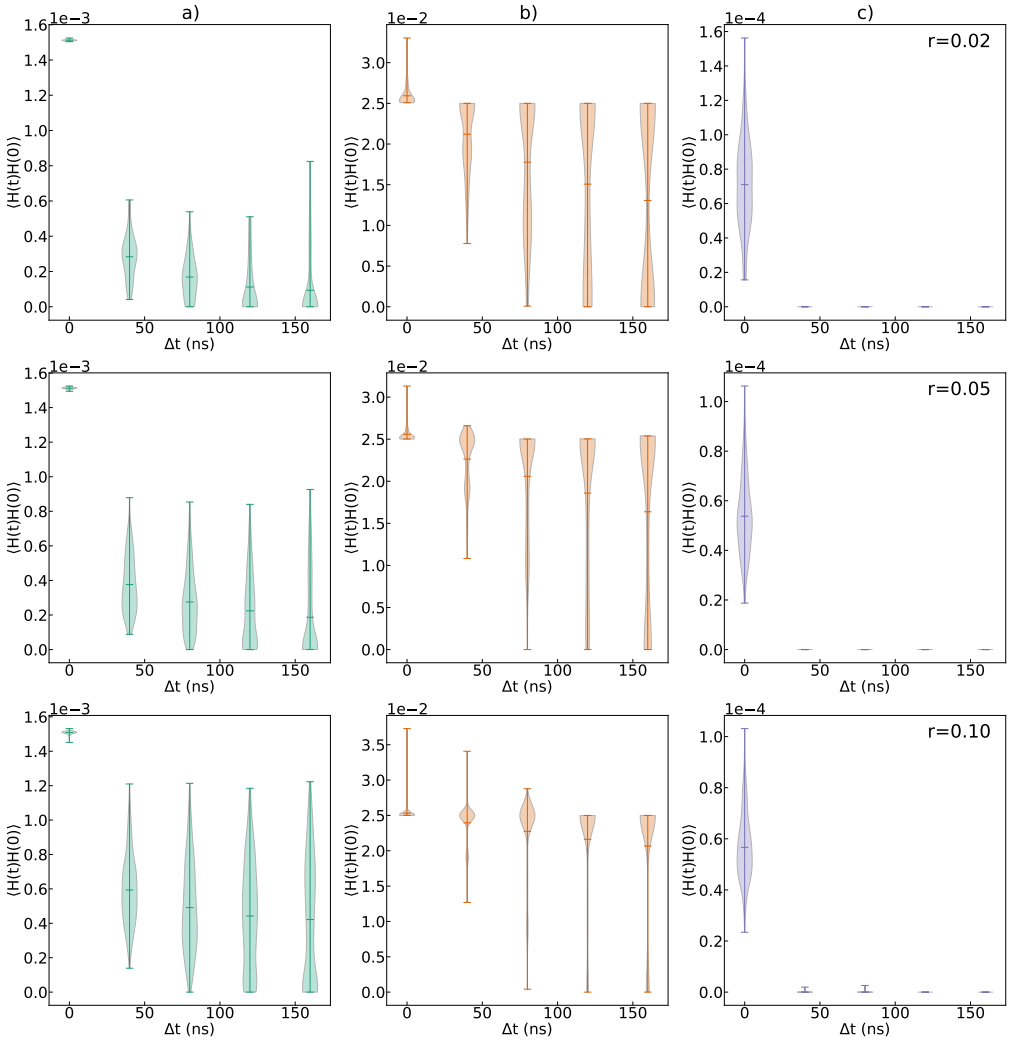

Figure S8: Distribution of the pair lifetime correlation functions at selected time intervals for (a) Li-ether oxygen, (b) Li-PEO chain, and (c) Li-TFSI for the systems with chain length n = 100. Salt concentrations are written in the rightmost plots. Mean and extreme values are marked in the violin plots.

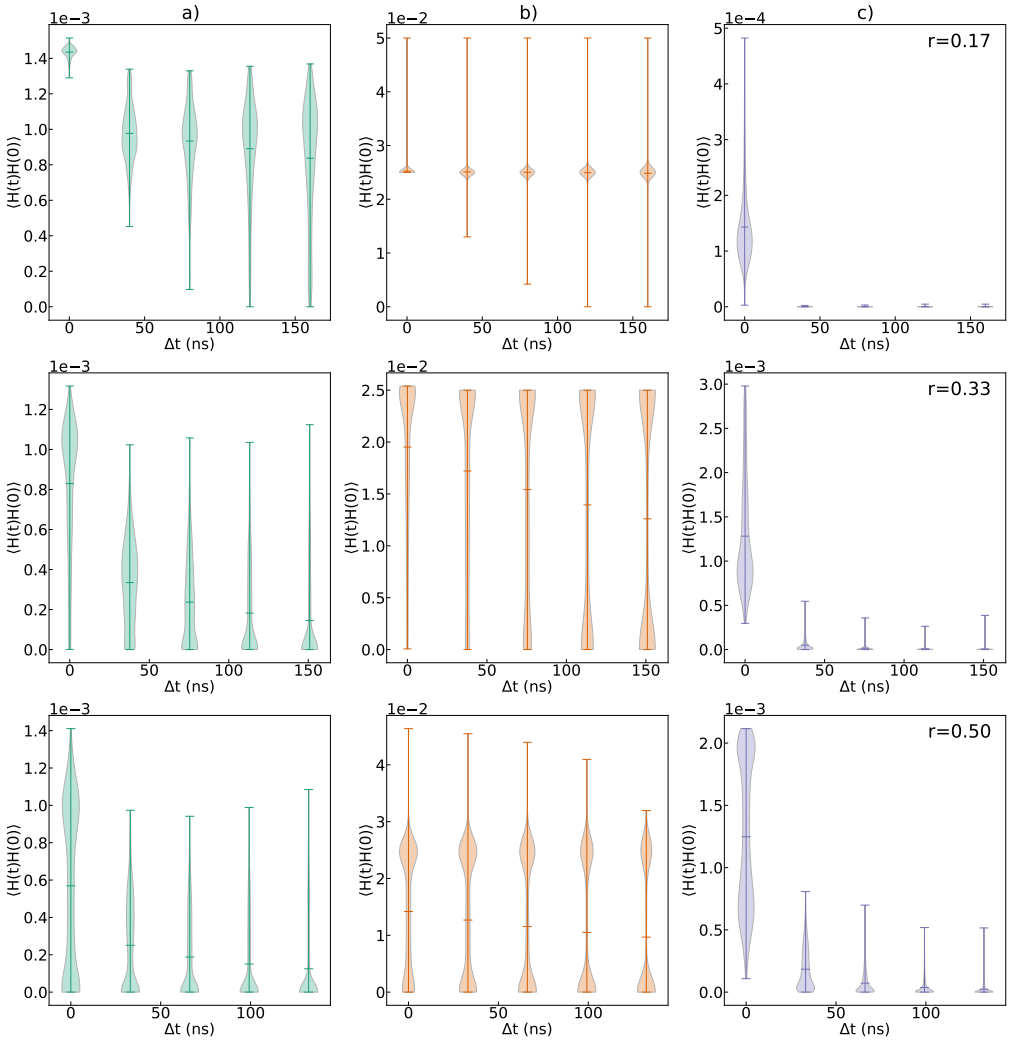

Figure S9: Distribution of the pair lifetime correlation functions at selected time intervals for (a) Li-ether oxygen, (b) Li-PEO chain, and (c) Li-TFSI for the systems with chain length n = 100. Salt concentrations are written in the rightmost plots. Mean and extreme values are marked in the violin plots.

Average number of anions coordinated to Li

The Li displaying strongest and weakest correlation to ether oxygen was determined from the distribution plots of the residence time in Figure S8 and S9. The upper and lower parts of the distributions, corresponding to the Li with stronger and weaker correlations, were determined manually to obtain enough data points.

Table S7: Average number of anions coordinated to Li strongly and weakly correlated to ether oxygen. Upper/lower fractions indicate the part of the distribution used to calculate anion coordination. 0 denotes the minimum and 1 denotes the maximum of the distribution

n	r = Li:EO	Upper fraction	Lower fraction	Average no of anions coordinated
100	0.02	0.6 to 1	-	<0.01
100	0.02	-	0 to 0.1	0.01
100	0.05	0.7 to 1	-	0.01
100	0.05	-	0 to 0.1	0.01
100	0.10	0.8 to 1	-	0.02
100	0.10	-	0 to 0.1	0.02
100	0.17	0.9 to 1	-	0.10
100	0.17	-	0 to 0.2	0.11
100	0.33	0.6 to 1	-	0.91
100	0.33	-	0 to 0.03	2.10
100	0.50	0.6 to 1	-	0.96
100	0.50	-	0 to 0.03	3.05

Examples of the parts of the distributions used to calculate the average anion coordination number are shown in Figure S10. We used the distribution at the longest time interval to calculate the anion coordination above, and mean squared displacement (MSD) and self-diffusion coefficients below.

Table S8: Mean squared displacement (MSD) and estimated self-diffusion coefficients of Li strongly and weakly correlated to ether oxygen in the two most concentrated systems

n	r = Li:EO	Fraction	MSD (Å^2)	Self-diffusion coefficient ($10^{-11}\,\mathrm{m^2\,s^{-1}}$)
100	0.33	0.6 to 1	135	0.382 (not diffusive)
100	0.33	0 to 0.03	242	0.573 (not diffusive)
100	0.50	0.6 to 1	88	0.142 (not diffusive)
100	0.50	0 to 0.03	213	0.438 (not diffusive)

Table S9: Average number of anions coordinated to Li strongly and weakly correlated to PEO chains. Upper/lower fractions indicate the part of the distribution used to calculate anion coordination. 0 denotes the minimum and 1 denotes the maximum of the distribution

n	r = Li:EO	Upper fraction	Lower fraction	Average no of anions coordinated
100	0.02	0.8 to 1	-	<0.01
100	0.02	-	0 to 0.2	<0.01
100	0.05	0.8 to 1	-	0.01
100	0.05	-	0 to 0.3	0.01
100	0.10	0.8 to 1	-	0.02
100	0.10	-	0 to 0.4	0.02
100	0.17	0.55 to 1	-	<0.01
100	0.17	-	0 to 0.4	0.11
100	0.33	0.7 to 1	-	1.11
100	0.33	-	0 to 0.3	2.35
100	0.50	0.6 to 1	-	1.27
100	0.50	-	0 to 0.3	3.29

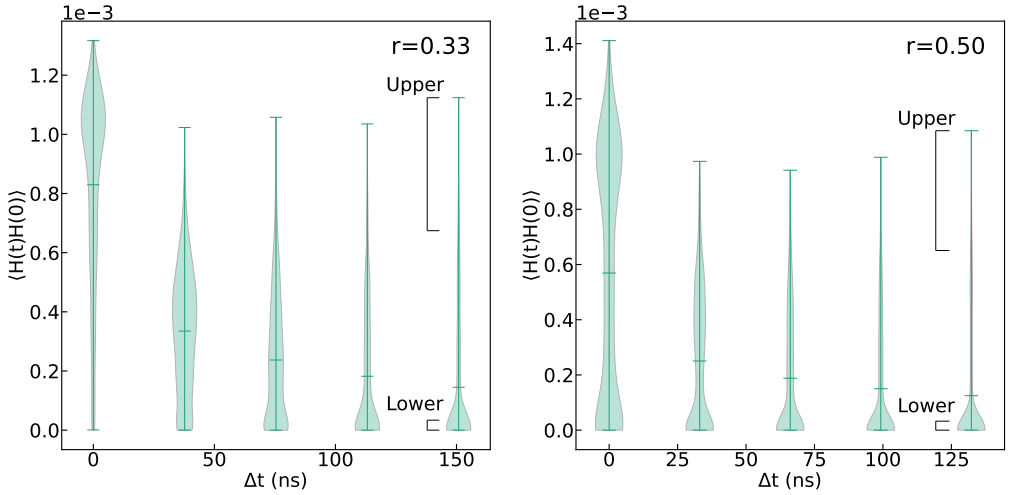

Figure S10: Example distribution plots showing the parts used to calculate average anion coordination number. The upper and lower fractions are marked. Salt concentrations are indicated in the plots.

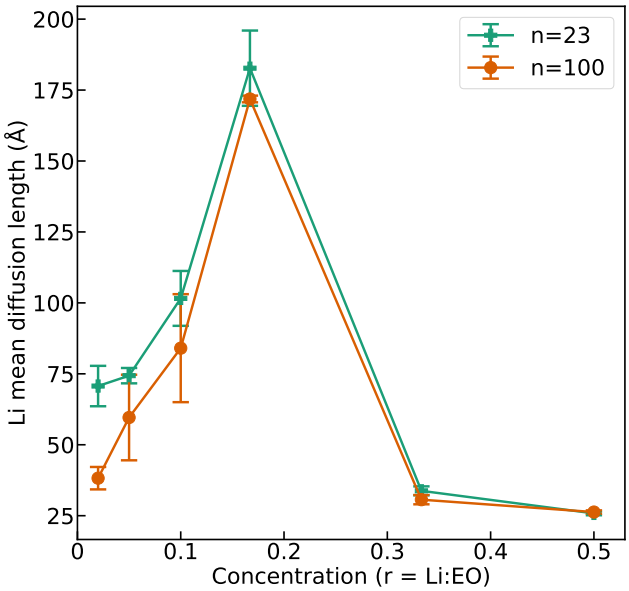

Figure S11: Li mean diffusion length between ether oxygen exchange as a function of PEO chain length and salt concentration.

References

(1) Pesko, D. M.; Timachova, K.; Bhattacharya, R.; Smith, M. C.; Villaluenga, I.; Newman, J.; Balsara, N. P. Negative Transference Numbers in Poly(ethylene oxide)-Based Electrolytes. *Journal of The Electrochemical Society* **2017**, *164*, E3569–E3575.

(2) Timachova, K. Ion Diffusion and Electrochemically Driven Transport in Homogenous and Nanostructured Polymer Electrolytes. Ph.D. thesis, University of California, Berkeley, 2018.

(3) Pesko, D. M.; Sawhney, S.; Newman, J.; Balsara, N. P. Comparing Two Electrochemical Approaches for Measuring Transference Numbers in Concentrated Electrolytes. *Journal of The Electrochemical Society* **2018**, *165*, A3014–A3021.

(4) Lascaud, S.; Perrier, M.; Vallee, A.; Besner, S.; Prud'homme, J.; Armand, M. Phase Diagrams and Conductivity Behavior of Poly(ethylene oxide)-Molten Salt Rubbery Electrolytes. *Macromolecules* **1994**, *27*, 7469–7477.

Article III

S. Kjelstrup, A. F. Gunnarshaug, Ø. Gullbrekken, S. K. Schnell, and A. Lervik

Transport coefficients for ion and solvent coupling. The case of the lithium-ion battery electrolyte,

The Journal of Chemical Physics **159**:3 034104 (2023).
DOI: 10.1063/5.0158623

Article III

Article III

The Journal of Chemical Physics ARTICLE pubs.aip.org/aip/jcp

Transport coefficients for ion and solvent coupling. The case of the lithium-ion battery electrolyte

Cite as: J. Chem. Phys. 159, 034104 (2023); doi: 10.1063/5.0158623
Submitted: 17 May 2023 • Accepted: 26 June 2023 •
Published Online: 17 July 2023

Signe Kjelstrup,[1] Astrid Fagertun Gunnarshaug,[1] Øystein Gullbrekken,[2] Sondre K. Schnell,[1,2] and Anders Lervik[1,a)]

AFFILIATIONS

[1] PoreLab, Department of Chemistry, Norwegian University of Science and Technology, NTNU, N-7491 Trondheim, Norway
[2] Department of Materials Science and Engineering, Norwegian University of Science and Technology, NTNU, N-7491 Trondheim, Norway

[a)] Author to whom correspondence should be addressed: anders.lervik@ntnu.no

ABSTRACT

Transport properties are essential for the understanding and modeling of electrochemical cells, in particular complex systems like lithium-ion batteries. In this study, we demonstrate how a certain degree of freedom in the choice of variables allows us to efficiently determine a complete set of transport properties. We apply the entropy production invariance condition to different sets of electrolyte variables and obtain a general set of formulas. We demonstrate the application of these formulas to an electrolyte typical for lithium-ion batteries, 1M lithium hexafluoro-phosphate in a 1:1 wt. % mixture of ethylene and diethyl carbonates. While simplifications can be introduced, they provide inadequate predictions of conductivity and transport numbers, and we argue that a full matrix of Onsager coefficients is needed for adequate property predictions. Our findings highlight the importance of a complete set of transport coefficients for accurate modeling of complex electrochemical systems and the need for careful consideration of the choice of variables used to determine these properties.

I. INTRODUCTION

Many central books in electrochemistry, e.g., Ref. 1, contain models for the transport of ions in an electrolyte. Models can also be found in books on irreversible thermodynamics,[2–4] and they are listed in Handbooks (cf. Ref. 5). In this work, we present a practical procedure, based on existing methods, to find general models for the transport of ions and solvents. Our goal is to provide useful procedures for modeling ion and solvent transport in different electrolyte systems for researchers and practitioners in electrochemistry. To demonstrate the procedures, we shall create a general transport model for the lithium-ion battery electrolyte.

Let us first recapitulate the main idea of the simplest model used to describe electrolyte transport with the example of a monovalent electrolyte. It is assumed that the two ions move independently of each other. The assumption means that the conductivity, κ, is a sum of the single contributions of the positive and negative ions. The mobility u_+ (u_-) of the cation (anion) is defined as the absolute velocity of the ion in a unit electric field (dimension $m^2\ V^{-1}\ s^{-1}$). For a fully dissociated monovalent electrolyte in water, the conductivity is

$$\kappa = Fc(u_+ + u_-). \tag{1}$$

Here F is Faraday's constant, and c is the electrolyte concentration (dimension mol m^{-3}). The conductivity, κ, has a dimension $\Omega^{-1}\ m^{-1}$. The dimensionless ion transport numbers are accordingly

$$\tau_+ = \frac{u_+}{u_+ + u_-}, \qquad \tau_- = \frac{u_-}{u_+ + u_-}, \tag{2}$$

where τ_i is the transport number of ion i, defined as the fraction of the electric current carried by i. These expressions result in the diffusion coefficient, D, of the salt in a dilute (ideal) solution,[2,6]

$$D = \frac{2RT}{F}\frac{u_+u_-}{u_+ + u_-}. \tag{3}$$

The dimension of D is m^2/s. Here, R is the gas constant, and T is the temperature in Kelvin. These equations have been used in numerous applications.

Cation–anion and ion–solvent coupling may, however, be significant, especially when the electrolyte solution is concentrated. The fluctuation-dissipation theorems (FDT), or Green–Kubo relations,[7–11] are then helpful. These relations take component-self as well as component-component interactions into account. The FDT constitute an essential part of nonequilibrium thermodynamics (NET)—they can be viewed as expressions of Onsager's regression hypothesis.[12] The expressions reflect the underlying symmetry implied by the time-reversal invariance of the processes at the particle level. The FDT offers a direct way to systematically extend the simple model of Eqs. (1)–(3), as ion–ion as well as solvent–ion interactions are included. Much work has thus been performed using FDT, particularly on diffusion in isothermal multi-component mixtures (see, e.g., Ref. 13). Work on thermal coupling effects is still scarce, however.

In an extended model,[2,6,14] the electric conductivity in Eq. (1) changes into

$$\kappa = F^2(L^{++} - L^{+-} - L^{-+} + L^{--}), \tag{4}$$

where L^{ij} is an Onsager coefficient (to be defined below). Superscript ij refers to the interaction of ions i and j, and Eq. (4) includes coupling between the two ions. The model of independent movement of cations and anions in Eq. (1) is recovered by neglecting cation–anion interactions, $L^{+-} = L^{-+} = 0$, and setting $L^{ii} = cu_i/F$. Introducing self-diffusion coefficients, $D_{i,\mathrm{self}} = u_iRT/F$, while still neglecting cation–anion interactions, the electric conductivity becomes

$$\kappa = F^2(c_+D_{+,\mathrm{self}} + c_-D_{-,\mathrm{self}})/RT. \tag{5}$$

The different formulas for κ have been shown to give very different results when compared to experimental results.[15,16] More sophisticated models are, therefore, of interest.[11]

In this work, we shall use the fact that the entropy production of the electrolyte is invariant to changes in the variable sets used to describe it and to the choice of frame of reference for the fluxes.[17] We shall find a set of rules that derive from this, connecting in a systematic way the transport properties of different variable sets. The purpose is to present practical procedures for the determination of two coefficient sets: The first set relates better to the electrolyte structure, while the second set addresses the measurement situation better. It is well known that a change in the frame of reference of fluxes creates a link between coefficient sets (see, e.g., Ref. 6). Here, we shall see that certain links also appear between different sets of electrolyte variables. These links can be combined with FDT to find transport properties in a systematic manner. By exploiting these links, or rules, as we shall call them, we hope to add deeper insight into the processes in a typical electrolyte and set the stage for modeling profiles in intensive and other variables across the electrolyte. As an example to illustrate the theoretical elaborations, we have chosen an important lithium-ion battery electrolyte.

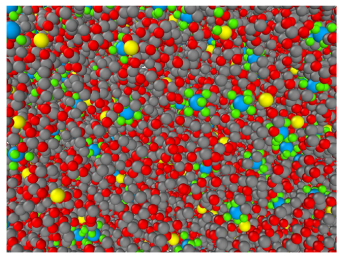

FIG. 1. Snapshot of the lithium battery electrolyte mixture consisting of the components shown in Fig. 2. The lithium-ions are colored yellow, the hexafluorophosphate ions are blue/green, the carbon atoms are gray, and the oxygen atoms are red. Hydrogen atoms are not shown. The carbonates shield lithium-ions, but a tendency to cluster positive and negative ions can also be seen.

The typical electrolyte consists of 1M of a lithium salt, here lithium hexafluorophosphate, and two solvent molecules, here ethylene carbonate and diethyl carbonate, in a weight ratio of 1:1%[18] in most cases. We will later in this paper present results from molecular dynamics simulations of this electrolyte, but a simulation snapshot of the complicated mixture is shown already in Fig. 1. As others have also observed, there is a tendency toward solvent-separated ion pairing.[19,20] Clearly, there are interactions of several sorts in the electrolyte.

Common acronyms for the carbonates are EC (ethylene carbonate) and DEC (diethyl carbonate) respectively, and we shall also use these. When used in subscripts, however, we shall shorten their names further to E and D. The salt as a component is denoted by L only to be distinguished from the single ions Li^+ and PF_6^-. The components of the electrolyte are illustrated in Fig. 2. We see that DEC is larger than EC. Both molecules have polar carbonate groups

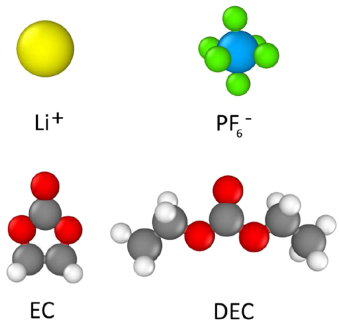

FIG. 2. Constituents of a typical lithium-ion battery electrolyte. The yellow lithium-ion to the left has the blue–green hexafluorophosphate ion as a counterion. The solvents are ethylene carbonate (EC) and diethyl carbonate (DEC). The carbonate group occupies the center of DEC. It is more exposed in the EC.

with one oxygen pointing out. The carbonates play different roles in the shielding of the lithium-ion. It is shielded by about three DEC molecules in this snapshot, and a relatively large distance between the cation and the anion is noticeable. At the same time, we also see tendencies toward clustering of the two ions.

There is a certain degree of freedom in the choice of variables that can be used to describe the electrolyte, and we consider two different variable sets for our purpose. The first set uses ions and neutral molecules mixed together. The components are Li^+, PF_6^-, EC, and DEC. The other set has only electroneutral components, namely components L, EC, and DEC.[17] The first set is more common. It connects more directly to the structure of the electrolyte and is suitable for use with FDT. The second set contains the independent components according to the phase rule.[21] This set is better connected to possible measurements, as their operational definitions demonstrate. We refer to the formulas derived for these two sets as the mixed component scenario and the neutral component scenario, respectively.

It is well known that mass transfer limitations and subsequent polarization can occur in the battery electrolyte.[16,22–25] Therefore, precise knowledge of coefficients for the transport of mass, charge, and heat is central to battery modeling. This work aims to demonstrate how we can find useful transport coefficients in a practical way using specific invariance criteria (rules). The procedure will be illustrated with data for the *isothermal electrolyte*. The principles are general in that the procedures should apply to other electrochemical systems, such as batteries or electrolysis cells. Nonisothermal results are presently unavailable from FDT; however,[26] we shall indicate how they can be included.

II. THEORETICAL BASIS

A. Entropy production in mixed and neutral component scenarios

We assume some familiarity with the theory of NET, the basis of our derivations. For more explanations, see Refs. 6 and 12. We repeat only the basic assumptions as follows:

- The theory of NET assumes that the system obeys local equilibrium, meaning that the Gibbs equation (the internal energy written as a total differential of the relevant extensive variables) applies locally to any volume element, even though the total system is not in global equilibrium.
- The balance laws for mass, energy, and momentum are written for the independent variables of interest and included in Gibbs' equation.
- The entropy production and the entropy flux are identified by comparing the result to the entropy balance.
- The linear laws of transport follow from the entropy production for any volume element in the system.
- The fluxes are related to the forces by a set of Onsager coefficients. The linear laws can be used to find the transport coefficients, but they can equally well be found from FDT, which is an integral part of NET.
- The entropy production is absolute, but there is a degree of freedom in the choice of variables used to describe it. In addition, the chosen set of fluxes depends on the frame of reference used in their determination.
- The NET theory, which originates from Onsager, assumes that particle fluctuations obey the regression hypothesis or, in essence, FDT. Onsager used microscopic reversibility to show that the matrix of coefficients, relating the fluxes to all forces, was symmetric.[6,12]

These premises have been shown to hold up exceptionally well. The assumption of local equilibrium was recently proven valid for shock waves.[27] The assumption can be formulated for reactions using mesoscopic variables.[28,29]

Electrochemical cells are heterogeneous, so a full system analysis starts by finding the entropy production of three bulk systems and two electrode interfaces. The bulk systems are the bulk of the electrodes and the bulk electrolyte. Kjelstrup and her co-workers showed how to integrate across the system.[6,17] Flux-force relations are obtained for each part. Electrolyte boundary conditions were given by the processes at the electrode surfaces.

Consider the electrolyte of a lithium battery in a cell with metal lithium electrodes. The electrolyte was pictured in Fig. 1. In the mixed component scenario (properties have a superscript C), there are four component fluxes in addition to the heat flux. The electric current is a dependent variable. In the neutral component scenario (properties have a superscript N), there are three component fluxes and one variable electric current. Its value is measured (and controlled) in the external circuit.[21] In addition, there is a heat flux. In both cases, there are five contributions to the entropy production of the electrolyte. These descriptions are equivalent in the sense that they give the same entropy production.

Here, we shall take advantage of this invariance of entropy production and examine the rules that bind the particular sets of coefficients together. We apply the condition to the two scenarios mentioned because one is practical for computational reasons (the mixed component scenario) and the other is suited to decompose experimental data (the neutral component scenario). There are rules connecting the sets of coefficients, which can help create models for transport coefficients.

In the mixed component scenario, the entropy production, σ, is[6]

$$\sigma = J_q'^{\mathrm{C}} \nabla \frac{1}{T} - J^{\mathrm{B}}_{\mathrm{Li}^+} \frac{1}{T} \nabla \tilde{\mu}_{\mathrm{Li}^+,T} - J^{\mathrm{B}}_{\mathrm{PF}_6^-} \frac{1}{T} \nabla \tilde{\mu}_{\mathrm{PF}_6^-,T} - J^{\mathrm{B}}_{\mathrm{D}} \frac{1}{T} \nabla \mu_{\mathrm{D},T} - J^{\mathrm{B}}_{\mathrm{E}} \frac{1}{T} \nabla \mu_{\mathrm{E},T}. \tag{6}$$

Table VI in Appendix A contains an overview of the quantities used, their symbols and their dimensions. The heat flux in this scenario is $J_q'^{\mathrm{C}}$ (dimension J m^{-2} s^{-1}), with conjugate force $\nabla(1/T)$. Component fluxes, indicated with subscripts Li^+ and PF_6^-, have as a driving force the negative electrochemical potential gradient divided by the temperature, i.e., $-\nabla\tilde{\mu}_{\mathrm{Li}^+,T}/T$ and $-\nabla\tilde{\mu}_{\mathrm{PF}_6^-,T}/T$,[2,3,21] where the electrochemical potential for ion i is defined by[30]

$$\tilde{\mu}_i \equiv \mu_i + z_i F \psi. \tag{7}$$

Here, z_i is the charge number of ion i, μ_i its chemical potential, and ψ is the Maxwell or electrostatic potential. The electrochemical potential gradients in Eq. (6) are all evaluated at a constant temperature. Superscript B indicates from now on that the barycentric frame of reference is used for the mixed component scenario. This choice

is natural when we want to use molecular dynamics simulations to provide the set of Onsager coefficients that belong to Eq. (6). Fong *et al.*[11] derived the same entropy production using a different set of premises.

In the neutral component scenario,[3,21] the five independent contributions to σ are

$$\sigma = J_q'^{\mathrm{N}}\nabla\frac{1}{T} - J_{\mathrm{L}}^{\mathrm{B}}\frac{1}{T}\nabla\mu_{\mathrm{L},T} - J_{\mathrm{D}}^{\mathrm{B}}\frac{1}{T}\nabla\mu_{\mathrm{D},T} - J_{\mathrm{E}}^{\mathrm{B}}\frac{1}{T}\nabla\mu_{\mathrm{E},T} - j\frac{1}{T}\nabla\varphi. \quad (8)$$

The electric current density, j, (in A/m^2) is the flux conjugate to $-\nabla\varphi/T$, where $\nabla\varphi$ is the electric potential gradient that we can measure with lithium-reversible electrodes (not to be confused with the Maxwell potential gradient). The heat flux in the neutral component scenario, $J_q'^{\mathrm{N}}$, is measurable and has, as the conjugate driving force, the gradient of the inverse temperature $1/T$. The driving force for components L, DEC, and EC, respectively, is the negative chemical potential gradient divided by the temperature, evaluated at constant temperature.

The measurable heat flux $J_q'^{\mathrm{N}}$ is defined as the energy flux J_q minus the latent heat, H_i (partial molar enthalpy), carried by the three components: $J_q'^{\mathrm{N}} = J_q - \sum_{j=1}^{3} J_j H_j$.[12] The heat fluxes in the two scenarios were shown to be related.[17] When lithium electrodes are used, we obtain $J_q'^{\mathrm{C}} = J_q'^{\mathrm{N}} + TS_{\mathrm{Li}^+}(j/F)$. The mass fluxes depend on the frame of reference.

Coefficients are generated with the barycentric frame of reference in simulation programs like the Large-scale Atomic/Molecular Massively Parallel Simulator (LAMMPS).[31] The FDT is well-defined in the mixed component scenario, where all component positions and velocities are uniquely defined. The FDT technique is well-established, but at present, only for isothermal systems. The system used in this work to give numerical insight is thus isothermal. In Appendix B and below, we explain how to find the Onsager coefficients Λ_{ij} that belong to the fluxes and forces of Eq. (6) by tracking particle positions and velocities. The coefficients have the dimension m^2 s^{-1}, typical for Fick's diffusion coefficients. This dimension can be converted to a dimension proper for the flux-force relations (see Appendix A) by multiplying with the factor c/R, as explained by Krishna and van Baten.[9] The data reduction procedure starts by computing the average component velocity $\mathbf{u}_i$ (in m/s) of all species i from the particle velocities $\mathbf{v}_{k,i}$. We have $N_i\mathbf{u}_i(t) = \sum_{k=1}^{N_i}\mathbf{v}_{k,i}(t)$. In the barycentric frame of reference, the isothermal flux of i obeys

$$x_i\mathbf{u}_i = -\frac{1}{RT}\sum_{j=1}^{n=4}\Lambda_{ij}\nabla\widetilde{\mu}_j, \quad (9)$$

where the summation is carried out over $n = 4$ components, and Λ_{ij} is an element in the matrix of Onsager coefficients. The molar flux of a component is found by multiplying Eq. (9) with c, the total concentration,

$$\mathbf{J}_i = x_i c\mathbf{u}_i = c_i\mathbf{u}_i = -\frac{c}{RT}\sum_{j=1}^{n=4}\Lambda_{ij}\nabla\widetilde{\mu}_j = -\frac{1}{T}\sum_{j=1}^{n=4}\Lambda^{ij}\nabla\widetilde{\mu}_j. \quad (10)$$

The coefficients Λ_{ij} have dimension m^2 s^{-1}, while the corresponding Λ^{ij} obtains the dimension needed in the thermodynamic flux-force relations of Appendix A when we multiply with the factor c/R,

$$\Lambda^{ij} = \frac{c}{R}\Lambda_{ij}. \quad (11)$$

In this manner, we find the $4 \times 4 = 16$ coefficients in the matrix that derive from Eq. (6) for a constant temperature. Six of them are dependent through the Onsager relations, leaving ten unknown coefficients to describe the isothermal system. Fortunately, the number of independent coefficients can be further reduced because the driving forces are dependent through Gibbs–Duhem's equation. We will reduce the coefficients from ten to six by choosing another frame of reference, and this reduction is our next step.

B. Reducing the number of variables: From the barycentric to the solvent frame of reference

Gibbs–Duhem's equation relates the chemical driving forces and offers the possibility of reducing the number of unknown coefficients from ten to six.[6] We want to study solvent segregation and choose one of the solvent components as the frame of reference: the EC component. We replace the chemical potential gradient of EC in both scenario formulations. In mixed as well as neutral component scenarios, Gibbs–Duhem's equation takes the form

$$\nabla\mu_{\mathrm{E},T} = -\frac{x_{\mathrm{L}}}{x_{\mathrm{E}}}\nabla\tilde{\mu}_{\mathrm{Li}^+,T} - \frac{x_{\mathrm{L}}}{x_{\mathrm{E}}}\nabla\tilde{\mu}_{\mathrm{PF}_6^-,T} - \frac{x_{\mathrm{D}}}{x_{\mathrm{E}}}\nabla\mu_{\mathrm{D},T}, \quad (12)$$

or

$$\nabla\mu_{\mathrm{E},T} = -\frac{x_{\mathrm{L}}}{x_{\mathrm{E}}}\nabla\mu_{\mathrm{L},T} - \frac{x_{\mathrm{D}}}{x_{\mathrm{E}}}\nabla\mu_{\mathrm{D},T}, \quad (13)$$

where x_i is the mole fraction of L or D. We introduce the respective expression in the corresponding expressions for the entropy production and obtain

$$\sigma = J_q'^{\mathrm{C}}\nabla\frac{1}{T} - J_{\mathrm{Li}^+}\frac{1}{T}\nabla\tilde{\mu}_{\mathrm{Li}^+,T} - J_{\mathrm{PF}_6^-}\frac{1}{T}\nabla\tilde{\mu}_{\mathrm{PF}_6^-,T} - J_{\mathrm{D}}\frac{1}{T}\nabla\mu_{\mathrm{D},T}, \quad (14)$$

or

$$\sigma = J_q'^{\mathrm{N}}\nabla\frac{1}{T} - J_{\mathrm{L}}\frac{1}{T}\nabla\mu_{\mathrm{L},T} - J_{\mathrm{D}}\frac{1}{T}\nabla\mu_{\mathrm{D},T} - j\frac{1}{T}\nabla\varphi. \quad (15)$$

All component fluxes are now in the E frame of reference (not indicated by a superscript). The number of flux-force products is reduced by one, and the flux-force relations have six independent coefficients. The entropy production is still the same, so a relation must exist between the Onsager coefficients in the E frame of reference and those in the B frame of reference.

The FDT is well defined in the mixed component scenario (see Sec. IV). Therefore, our primary target is this set of coefficients. The set is next transformed to the E frame of reference and to the operationally defined set. After some algebra, we find

$$L^{ij} = \frac{c}{R}\left(\Lambda^{ij} - \frac{x_j}{x_n}\Lambda^{in} - \frac{x_i}{x_n}\Lambda^{nj} + \frac{x_i x_j}{x_n^2}\Lambda^{nn}\right). \quad (16)$$

The matrix of any set of Onsager coefficients is symmetric because we have used independent variables in each set. The first coefficient set obtained with the help of FDT, Λ^{ij}, has the B-frame of reference. The set of L^{ij}-coefficients with the E frame of reference is computed from these.

C. Flux-force relations for mixed and neutral component scenarios

The Onsager coefficients are characteristic of the particular choice of variables. We proceed with the formulation that includes

the heat flux to provide a start for thermal transport modeling. The ionic variable set obtains flux equations in the E frame of reference defined by the entropy production in Eq. (14),

$$\begin{aligned} J_q'^{\mathrm{C}} &= L^{qq}\nabla\frac{1}{T} - L^{q+}\frac{1}{T}\nabla\tilde{\mu}_{\mathrm{Li}^+,T} - L^{q-}\frac{1}{T}\nabla\tilde{\mu}_{\mathrm{PF}_6^-,T} - L^{q\mathrm{D}}\frac{1}{T}\nabla\mu_{\mathrm{D},T},\\ J_{\mathrm{Li}^+} &= L^{+q}\nabla\frac{1}{T} - L^{++}\frac{1}{T}\nabla\tilde{\mu}_{\mathrm{Li}^+,T} - L^{+-}\frac{1}{T}\nabla\tilde{\mu}_{\mathrm{PF}_6^-,T} - L^{+\mathrm{D}}\frac{1}{T}\nabla\mu_{\mathrm{D},T},\\ J_{\mathrm{PF}_6^-} &= L^{-q}\nabla\frac{1}{T} - L^{-+}\frac{1}{T}\nabla\tilde{\mu}_{\mathrm{Li}^+,T} - L^{--}\frac{1}{T}\nabla\tilde{\mu}_{\mathrm{PF}_6^-,T} - L^{-D}\frac{1}{T}\nabla\mu_{\mathrm{D},T},\\ J_{\mathrm{D}} &= L^{\mathrm{D}q}\nabla\frac{1}{T} - L^{\mathrm{D}+}\frac{1}{T}\nabla\tilde{\mu}_{\mathrm{Li}^+,T} - L^{\mathrm{D}-}\frac{1}{T}\nabla\tilde{\mu}_{\mathrm{PF}_6^-,T} - L^{\mathrm{DD}}\frac{1}{T}\nabla\mu_{\mathrm{D},T}. \end{aligned} \tag{17}$$

A coefficient superscript indicates the interactions among the fluxes in question; cf. L^{ij}. The following dimensions apply to the Onsager coefficients in the mixed component scenario:

- L^{qq} has dimension K J m^{-1} s^{-1}, while the coupling coefficients L^{q+}, L^{q-}, and $L^{q\mathrm{D}}$ have dimension K mol m^{-1} s^{-1}.
- L^{++}, L^{+-}, $L^{+\mathrm{D}}$, L^{--}, $L^{-\mathrm{D}}$, and L^{DD} have dimensions K mol^2 J^{-1} m^{-1} s^{-1}.

Double superscripts indicate interacting phenomena. The matrix of coefficients is symmetric, according to Onsager. For isothermal systems, it is common to adsorb the constant $1/T$ into the coefficient.

In the neutral component scenario, the entropy production of an electrolyte in a cell with lithium electrodes [Eq. (15)] prescribes the following flux-force matrix:

$$\begin{aligned} J_q'^{\mathrm{N}} &= L_{qq}\nabla\frac{1}{T} - L_{q\mathrm{L}}\frac{1}{T}\nabla\mu_{\mathrm{L},T} - L_{q\mathrm{D}}\frac{1}{T}\nabla\mu_{\mathrm{D},T} - L_{q\varphi}\frac{1}{T}\nabla\varphi,\\ J_{\mathrm{L}} &= L_{\mathrm{L}q}\nabla\frac{1}{T} - L_{\mathrm{LL}}\frac{1}{T}\nabla\mu_{\mathrm{L},T} - L_{\mathrm{LD}}\frac{1}{T}\nabla\mu_{\mathrm{D},T} - L_{\mathrm{L}\varphi}\frac{1}{T}\nabla\varphi,\\ J_{\mathrm{D}} &= L_{\mathrm{D}q}\nabla\frac{1}{T} - L_{\mathrm{DL}}\frac{1}{T}\nabla\mu_{\mathrm{L},T} - L_{\mathrm{DD}}\frac{1}{T}\nabla\mu_{\mathrm{D},T} - L_{\mathrm{D}\varphi}\frac{1}{T}\nabla\varphi,\\ j &= L_{\varphi q}\nabla\frac{1}{T} - L_{\varphi\mathrm{L}}\frac{1}{T}\nabla\mu_{\mathrm{L},T} - L_{\varphi\mathrm{D}}\frac{1}{T}\nabla\mu_{\mathrm{D},T} - L_{\varphi\varphi}\frac{1}{T}\nabla\varphi. \end{aligned} \tag{18}$$

The dimensions are

- L_{qq} has dimension K J m^{-1} s^{-1}.
- $L_{q\mathrm{L}}$ and $L_{q\mathrm{D}}$ have dimensions K mol s^{-1} m^{-1}.
- $L_{q\varphi}$ has dimension K C m^{-1} s^{-1}.

The coefficient L_{qq} differs from L^{qq} because it refers to a different heat flux. The coefficients of the second and third rows have pairwise the same dimensions. The first pair $L_{\mathrm{L}q}$ and $L_{\mathrm{D}q}$ has dimension K mol m^{-1} s^{-1}. The second and third pairs, L_{LL}, L_{LD}, and L_{LD}, L_{DD}, have dimensions K mol^2 J^{-1} m^{-1} s^{-1}. The last coefficients, $L_{\mathrm{L}}\varphi$ and $L_{\mathrm{D}}\varphi$, have dimensions K C mol J^{-1} m^{-1} s^{-1}. The dimension of $L_{\varphi q}$ is K C m^{-1} s^{-1}, the dimension of $L_{\varphi\mathrm{L}}$ and $L_{\varphi\mathrm{D}}$ is K C mol J^{-1} m^{-1} s^{-1}, and the dimension of $L_{\varphi\varphi}$ is K C V^{-1} m^{-1} s^{-1} (see Appendix A). We include the common factor $1/T$ into the coefficients when the temperature is constant.

In order to distinguish the coefficients of the two scenarios, we have used subscripts for the interacting phenomena in the neutral component scenario rather than superscripts as in the mixed component scenario.

D. Operationally defined properties

The properties relevant for thermodynamic modeling of electrochemical systems are mostly obtained from experiments, i.e., they are operationally defined. The properties include diffusion coefficients, transference coefficients, electric conductivity, heats of transfer, Peltier coefficients, and the chemical potential. The operational definitions are, therefore, briefly recapitulated.

A basis for a definition of diffusion coefficients is obtained when we express $\nabla\varphi$ in terms of j with Eq. (18) and find

$$\begin{aligned} J_q'^{\mathrm{N}} &= \ell_{qq}\nabla\left(\frac{1}{T}\right) - \ell_{q\mathrm{L}}\frac{1}{T}\nabla\mu_{\mathrm{L},T} - \ell_{q\mathrm{D}}\frac{1}{T}\nabla\mu_{\mathrm{D},T} + \frac{L_{q\varphi}}{L_{\varphi\varphi}}j,\\ J_{\mathrm{L}} &= \ell_{\mathrm{L}q}\nabla\left(\frac{1}{T}\right) - \ell_{\mathrm{LL}}\frac{1}{T}\nabla\mu_{\mathrm{L},T} - \ell_{\mathrm{LD}}\frac{1}{T}\nabla\mu_{\mathrm{D},T} + \frac{L_{\mathrm{L}}\varphi}{L_{\varphi\varphi}}j,\\ J_{\mathrm{D}} &= \ell_{\mathrm{D}q}\nabla\left(\frac{1}{T}\right) - \ell_{\mathrm{DL}}\frac{1}{T}\nabla\mu_{\mathrm{L},T} - \ell_{\mathrm{DD}}\frac{1}{T}\nabla\mu_{\mathrm{D},T} + \frac{L_{\mathrm{D}}\varphi}{L_{\varphi\varphi}}j. \end{aligned} \tag{19}$$

The uppercase coefficient symbols of Eq. (18) and the lowercase coefficient symbols of Eq. (19) are related by

$$\ell_{ij} = L_{ij} - \frac{L_{i\varphi}L_{j\varphi}}{L_{\varphi\varphi}}. \tag{20}$$

We use this relation in Sec. V C to obtain the diffusion coefficients ℓ_{ij}. The coefficients are measured in the absence of j and $\nabla\varphi$[21] and with the E frame of reference.

The conductivity of the electrolyte is defined for a homogeneous, isothermal electrolyte and is obtained from the last row of Eq. (18) (Ohm's law),

$$\kappa = -\left(\frac{j}{\nabla\varphi}\right)_{\nabla T=0,\nabla\mu_{\mathrm{L}}=0,\nabla\mu_{\mathrm{D}}=0} = \frac{L_{\varphi\varphi}}{T}. \tag{21}$$

The transference coefficients, t_i, are defined by Hittorf experiments from Eq. (18),

$$t_i = \left(\frac{J_i}{j/F}\right)_{\nabla T=0,\nabla\mu_{\mathrm{L}}=0,\nabla\mu_{\mathrm{D}}=0} = F\frac{L_{i\varphi}}{L_{\varphi\varphi}}. \tag{22}$$

The transference coefficient expresses the movement of the component due to electric current, measured in the limit of zero concentration gradients.[21] It must not be confused with the transport number, cf. Eq. (2), the fraction of the electric current carried by one ion. For the co-solvent DEC, the transference coefficient describes the electro-osmosis of DEC and, therefore, solvent segregation. This coefficient is also accessible via Onsager relations and *emf*-measurements.[21]

The Peltier *coefficient*, π^{N}, is defined as the ratio of the heat flux and the electric current density,

$$\pi^{\mathrm{N}} \equiv \left(\frac{J_q'^{\mathrm{N}}}{j/F}\right)_{\nabla\mu_{i,T}=0,\nabla T=0} = \frac{L_{\varphi q}}{L_{\varphi\varphi}}. \tag{23}$$

The single Peltier coefficient cannot be measured in isolation. It is accessible from the combination of coefficients, the Peltier *heat* of the junction, which constitutes the electrode interface.[32] The Peltier heat is accessible via the Onsager relation and the Seebeck coefficient of the cell. The symmetry relation gives

$$\left(\frac{\pi^{\mathrm{N}}}{T}\right)_{\nabla T=0} = -\left(\frac{\Delta\varphi}{\Delta T}\right)_{j=0}.$$

The heat of transfer of components L and DEC, q_i^*, is best accessible via Onsager relations and the Soret coefficient of the cell; see the equation below. The heat of transfer can be computed from the gradient in chemical potential,

$$q_{\mathrm{L}}^* = \left(\frac{J_q^{\mathrm{N}}}{J_{\mathrm{L}}}\right)_{J_{\mathrm{D}}=0,\, j=0,\nabla T=0} = -T\left(\frac{\nabla\mu_{\mathrm{L},T}}{\nabla T}\right)_{J_{\mathrm{L}}=J_{\mathrm{D}}=0,\, j=0}. \tag{24}$$

An equivalent expression is obtained for component DEC. The temperature gradient, ∇T, can be determined in, for instance, nonequilibrium molecular dynamics simulations. The gradient in chemical potential, $\nabla\mu_{i,T}$ for i = L or DEC, can be found from knowledge of the composition c_i and the corresponding thermodynamic factor, cf. Eq. (27).

With knowledge of the above-mentioned quantities, we can model or measure the electric potential gradient across the electrolyte of the cell,

$$\nabla\varphi = -\frac{\pi}{T}\nabla T - t_{\mathrm{L}}\nabla\mu_{\mathrm{L},T} - t_{\mathrm{D}}\nabla\mu_{\mathrm{D},T} - j/\kappa. \tag{25}$$

The flux-force relations in Eq. (18) can be used to find the profiles of the variables that enter and the single contributions to the cell potential.

We have seen how the coefficients in the equations earlier are often determined. There are two major routes. In Subsection II B, we referred to the fluctuation-dissipation theorems (FDT) (available for isothermal systems; however, see Ref. 26). In this section, we have outlined how the coefficients can be obtained from their operational definitions. Both methods should give the same results, providing us with a useful check for consistency.

E. Fick's law's coefficients and the chemical potential

The symmetry of the Onsager coefficients on the macroscopic scale reflects the underlying symmetry on the molecular level and is an example of the many symmetry laws in physics.[8] Therefore, the Onsager coefficients are of primary interest, not only for the present case but for electrochemical systems in general. The diffusion coefficients of Fick are, however, more frequently used in practice,[13] and we will here comment on their relation to the Onsager coefficients.

The symmetric coefficient matrix can be related to Fick's diffusion matrix by using the invariance of the entropy production again. We apply the conditions $\nabla T = 0, j = 0$ to Eq. (19) and obtain

$$\begin{aligned} J_{\mathrm{L}} &= -\ell_{\mathrm{LL}}\frac{1}{T}\nabla\mu_{\mathrm{L},T} - \ell_{\mathrm{LD}}\frac{1}{T}\nabla\mu_{\mathrm{D},T},\\ J_{\mathrm{D}} &= -\ell_{\mathrm{DL}}\frac{1}{T}\nabla\mu_{\mathrm{L},T} - \ell_{\mathrm{DD}}\frac{1}{T}\nabla\mu_{\mathrm{D},T}. \end{aligned} \tag{26}$$

Next, we express the gradients in the chemical potential with the gradients in concentration using[12]

$$\nabla\mu_{i,T} = \sum_{j=1}^{2}\Gamma_{ji}\frac{RT}{c_j}\nabla c_j, \tag{27}$$

where c_j is the concentration of the (independent) components j = L and DEC. The non-ideality is expressed here using the thermodynamic factors Γ_{ij},[33–35]

$$\Gamma_{ij} = \frac{c_i}{RT}\left(\frac{\partial\mu_j}{\partial c_i}\right)_{T,V,\mathbf{c}_i}, \tag{28}$$

where the subscript $\mathbf{c}_i$ indicates that the derivative is taken while holding the concentrations of all components, except i, constant. The assumption of an ideal solution corresponds to $\Gamma_{ij} = \delta_{ij}$, where δ_{ij} is the Kronecker delta. Introducing the chemical potentials from Eq. (27) into Eq. (26) gives

$$\begin{aligned} J_{\mathrm{L}} &= -\frac{R}{c_{\mathrm{L}}}\nabla c_{\mathrm{L}}(\ell_{\mathrm{LL}}\Gamma_{\mathrm{LL}} + \ell_{\mathrm{LD}}\Gamma_{\mathrm{LD}}) - \frac{R}{c_{\mathrm{D}}}\nabla c_{\mathrm{D}}(\ell_{\mathrm{LD}}\Gamma_{\mathrm{DD}} + \ell_{\mathrm{LL}}\Gamma_{\mathrm{DL}}),\\ J_{\mathrm{D}} &= -\frac{R}{c_{\mathrm{L}}}\nabla c_{\mathrm{L}}(\ell_{\mathrm{DL}}\Gamma_{\mathrm{LL}} + \ell_{\mathrm{DD}}\Gamma_{\mathrm{LD}}) - \frac{R}{c_{\mathrm{D}}}\nabla c_{\mathrm{D}}(\ell_{\mathrm{DL}}\Gamma_{\mathrm{DL}} + \ell_{\mathrm{DD}}\Gamma_{\mathrm{DD}}). \end{aligned} \tag{29}$$

The factor $1/T$ from the force disappears from the coefficients of Eq. (22) when the concentration gradient is introduced. However, the introduction of the gradients in c_i and c_j and the corresponding thermodynamic factor Γ_{ij} means that the matrix of coefficients is no longer symmetric.[35] We obtain expressions for Fick's diffusion coefficients D_{ij},

$$\begin{aligned} D_{\mathrm{LL}} &= R(\ell_{\mathrm{LL}}\Gamma_{\mathrm{LL}} + \ell_{\mathrm{LD}}\Gamma_{\mathrm{LD}})/c_{\mathrm{L}},\\ D_{\mathrm{LD}} &= R(\ell_{\mathrm{LL}}\Gamma_{\mathrm{DL}} + \ell_{\mathrm{LD}}\Gamma_{\mathrm{DD}})/c_{\mathrm{D}},\\ D_{\mathrm{DL}} &= R(\ell_{\mathrm{DL}}\Gamma_{\mathrm{LL}} + \ell_{\mathrm{DD}}\Gamma_{\mathrm{LD}})/c_{\mathrm{L}},\\ D_{\mathrm{DD}} &= R(\ell_{\mathrm{DL}}\Gamma_{\mathrm{DL}} + \ell_{\mathrm{DD}}\Gamma_{\mathrm{DD}})/c_{\mathrm{D}}. \end{aligned} \tag{30}$$

The equations can be used to compute Fick's law's diffusion coefficients. The coefficients follow when the concentration gradients are used as driving forces. They need not obey the conditions for the determinant and the main coefficients: that $l_{ii}l_{jj} - l_{ij}l_{ji} \geq 0$, $l_{ii} > 0$. Knowledge of Γ_{ij}/c_i and ℓ_{ij} gives the matrix elements D_{ij}. In Appendix C, we describe how we calculate the thermodynamic factors Γ_{ij} from molecular dynamics simulations.

In the present case, it is practical to use FDT [Appendix B, Eq. (B1)] for the mixed component scenario (because all particle positions are well-definable). The target is the Onsager coefficients of the neutral component scenario. We shall next see how these can be obtained without the knowledge of Fick's coefficients.

III. IMPOSING ENTROPY PRODUCTION INVARIANCE

As pointed out earlier, the descriptions of the mixed and neutral component scenarios are equivalent, and relations exist due to entropy production invariance.[6,17,21] The supporting electrodes of the cell in question are both reversible to lithium. The relations follow from the expression for the electric current density:

$$j/F = J_{\mathrm{Li}^+} - J_{\mathrm{PF}_6^-}. \tag{31}$$

For lithium reversible electrodes, the observable salt flux is identified by the movement of the anion,

$$J_L = J_{PF_6^-}, \tag{32}$$

and the gradient in the measured electric potential is identified by the electrochemical potential gradient of the lithium-ion,

$$F\nabla\varphi = \nabla\tilde{\mu}_{Li^+}. \tag{33}$$

The gradient in the chemical potential of the salt is, furthermore, the sum of the electrochemical potential gradients of the ions,

$$\nabla\mu_L = \nabla\tilde{\mu}_{Li^+} + \nabla\tilde{\mu}_{PF_6^-}. \tag{34}$$

The last identity follows from the definition in Eq. (7).

A. Rules for coupling of fluxes

We introduce the expressions for the ionic fluxes, Eq. (17), into the right-hand side of the equation for the electric current density. Equation (31) gives

$$j/F = (L^{+q} - L^{-q})\nabla\frac{1}{T} - (L^{++} - L^{-+})\frac{1}{T}\nabla\tilde{\mu}_{Li^+,T} - (L^{+-} - L^{--})\frac{1}{T}\nabla\tilde{\mu}_{PF_6^-,T} - (L^{+D} - L^{-D})\frac{1}{T}\nabla\mu_{D,T}. \tag{35}$$

We introduce the expressions for forces in Eqs. (33) and (34) and compare the outcome to the bottom line of Eq. (18). The following relations are then obtained between the coefficients in the mixed (left-hand side) and neutral (right-hand side) component scenarios:

$$L_{\varphi\varphi} = (L^{++} - L^{+-} - L^{-+} + L^{--})F^2, \tag{36}$$

$$L_{\varphi L} = (L^{+-} - L^{--})F = L_{L\varphi} \tag{37}$$

$$L_{\varphi D} = (L^{+D} - L^{-D})F = L_D\varphi, \tag{38}$$

$$L_{\varphi q} = (L^{+q} - L^{-q})F = L_{q\varphi}. \tag{39}$$

Equations (36)–(39) describe coupling to charge transport, indicated by the subscript φ. For mixtures of multivalent electrolytes, the valency of the respective ion enters. For mass transport, the corresponding coefficient relations are

$$L_{LL} = L^{--}, \tag{40}$$

$$L_{LD} = L^{-D} = L_{DL}, \tag{41}$$

$$L_{DD} = L^{DD}. \tag{42}$$

Onsager relations have been used. The coefficient relations do not depend on the value of the driving forces. The relations follow from constant entropy production only and appear without assumptions. Approximations can be introduced, but not for one coefficient alone; the whole set must be considered. We have, therefore, given the set of equations the name "Rules for Coupling of Fluxes." They were derived here for a lithium battery-related case, but similar forms can be found for similar systems. However, they are rules that apply in the solvent E frame of reference.

B. Implications of the rules for coupling of fluxes

We can now use the Rules to generalize the formulas for the transport properties that appeared in Eqs. (1)–(3). The electric conductivity, κ, prescribed by the rules is the same. We repeat

$$\kappa = \frac{L_{\varphi\varphi}}{T} = F^2(L^{++} - 2L^{+-} + L^{--}). \tag{43}$$

The coupling coefficient L^{+-} can be positive or negative in sign. Coupling may, therefore, enhance or reduce κ.

Component transference coefficients follow. For the salt L,

$$t_L = F\frac{L_{\varphi L}}{L_{\varphi\varphi}} = \frac{L^{+-} - L^{--}}{L^{++} - 2L^{+-} + L^{--}}. \tag{44}$$

The transference coefficient is not equal to the transport number, and the transport number of ion i in Eq. (2) is the fraction of the electric current carried by the ion in question. In the presence of lithium-reversible electrodes, the transference coefficient of L can be understood as the negative transport number of the anion, PF_6^-. This expresses that salt accumulates on the left-hand side of the cell when a positive electric current is passing from left to right in the cell. Coupling can reduce or increase the transference coefficient. The transference coefficient applies to *neutral* components. For the DEC component, it becomes

$$t_D = F\frac{L_{\varphi D}}{L_{\varphi\varphi}} = \frac{L^{+D} - L^{-D}}{L^{++} - 2L^{+-} + L^{--}}. \tag{45}$$

The coefficient describes the transport of DEC that accompanies charge transport through the electrolyte. Depending on the sign of the coupling coefficients, it will lead to an accumulation of DEC to the right or left of the system. We see that it is zero when the co-solvent interacts equally with the cation and with the anion. In the present electrolyte, these coefficients are unknown. We know from ion-exchange membranes that the number of water molecules transported by cations or anions is high.[21] Therefore, coupling coefficients are likely to be significant in strong electrolyte solutions. The case of the independent movement of ions was referred to in the Introduction.[1,2,6] It is a limiting case, obtained by setting $L^{+-} = 0$, $L^{-D} = 0$, and $L^{+D} = 0$.

The first contribution to the main diffusion coefficient for the salt in Eq. (30) can be found in terms of Onsager coefficients,[6]

$$D_L = \frac{R}{c}\Gamma_{LL}\ell_{LL} = \left(L_{LL} - \frac{L_{\varphi L}^2}{L_{\varphi\varphi}}\right)\frac{1}{T}\frac{\partial\mu_L}{\partial c_L} = \left(L^{--} - \frac{(L^{+-} - L^{--})^2}{L^{++} - 2L^{+-} + L^{--}}\right)\frac{1}{T}\frac{\partial\mu_L}{\partial c_L}. \tag{46}$$

This is a common expression, but for binary mixtures. More general expressions can be developed using Eq. (30).

C. The nonisothermal case. An approximation

Consider again the coefficients that relate to heat transport. While the thermal conductivity of a system can be found with well-established techniques, experimental as well as computational, the procedure to find coupling coefficients for heat and mass and charge, heat, and mass is less well established. A complicating factor is the

definition of the heat flux. The heat flux $J_q'^{\mathrm{N}}$ is measurable in the neutral component scenario. From the discussion below Eq. (8), we understand that $J_q'^{\mathrm{C}}$ in the mixed component scenario is not measurable. Both scenarios are now discussed in view of the Rules for Coupling of Fluxes to gain more insight into the conditions for their determinations.

The heat of transfer is defined in the mixed component scenario,

$$q^*_{\mathrm{Li^+}} = \left(\frac{J_q'^{\mathrm{C}}}{J_{\mathrm{Li^+}}}\right)_{J_{\mathrm{D}}=0, J_{\mathrm{PF_6^-}}=0, \nabla T=0} = -T\left(\frac{\nabla \tilde{\mu}_{\mathrm{Li^+},T}}{\nabla T}\right)_{J_{\mathrm{D}}=0, J_{\mathrm{PF_6^-}}=0, J_{\mathrm{Li^+}}=0}, \quad (47)$$

$$q^*_{\mathrm{PF_6^-}} = \left(\frac{J_q'^{\mathrm{C}}}{J_{\mathrm{PF_6^-}}}\right)_{J_{\mathrm{D}}=0, J_{\mathrm{Li^+}}=0, \nabla T=0} = -T\left(\frac{\nabla \tilde{\mu}_{\mathrm{PF_6^-},T}}{\nabla T}\right)_{J_{\mathrm{D}}=0, J_{\mathrm{PF_6^-}}=0, J_{\mathrm{Li^+}}=0}. \quad (48)$$

From Eqs. (34) and (24), we obtain

$$q^*_{\mathrm{L}} = q^*_{\mathrm{Li^+}} + q^*_{\mathrm{PF_6^-}}. \quad (49)$$

In the mixed component scenario, the conditions for measurement are $J_{\mathrm{D}} = 0$ and $J_{\mathrm{PF_6^-}} = 0$. These stationary state conditions can be used to eliminate two driving forces from the flux equations. The heat flux of the mixed component description becomes

$$J_q'^{\mathrm{C}} = -\left(L^{q+} - L^{q-}K + L^{q\mathrm{D}}M\right)\frac{1}{T}\nabla\tilde{\mu}_{\mathrm{Li^+}}. \quad (50)$$

The cation flux that corresponds to these conditions is

$$J_{\mathrm{Li^+}} = -\left(L^{++} - L^{+-}K + L^{+\mathrm{D}}M\right)\frac{1}{T}\nabla\tilde{\mu}_{\mathrm{Li^+}}. \quad (51)$$

It is then possible to define the ratio of these fluxes as the *heat of transfer* of the lithium-ion in the mixed component scenario,

$$q^*_{\mathrm{Li^+}} = \left(\frac{J_q'^{\mathrm{C}}}{J_{\mathrm{Li^+}}}\right)_{J_{\mathrm{D}}=0, J_{\mathrm{PF_6^-}}=0, \nabla T=0} = \frac{\left(L^{q+} - L^{q-}K + L^{q\mathrm{D}}M\right)}{\left(L^{++} - L^{+-}K + L^{+\mathrm{D}}M\right)}. \quad (52)$$

Symbols K and M are lumped coefficients, which are functions of the Onsager coefficients,

$$K = \frac{L^{-+} - L^{-\mathrm{D}}L^{\mathrm{D}+}/L_{\mathrm{DD}}}{L^{--} - L^{-\mathrm{D}}L^{\mathrm{D}-}/L_{\mathrm{DD}}}, \quad (53)$$

$$M = -\frac{L^{\mathrm{D}+}}{L_{\mathrm{DD}}} + \frac{L^{\mathrm{D}-}}{L_{\mathrm{DD}}}K. \quad (54)$$

When the assumption of independent movement of ions applies, the complicated expressions reduce. We introduce $L^{+-} = 0$, $L^{-\mathrm{D}} = 0$, and $L^{+\mathrm{D}} = 0$, and obtain $K = 0$ and $M = 0$. The expressions for the heats of transfer simplify to

$$q^*_{\mathrm{Li^+}} = \left(\frac{J_q'^{\mathrm{C}}}{J_{\mathrm{Li^+}}}\right)_{J_{\mathrm{D}}=0, J_{\mathrm{PF_6^-}}=0, \nabla T=0} = \frac{L^{q+}}{L^{++}}, \quad (55)$$

and

$$q^*_{\mathrm{PF_6^-}} = \left(\frac{J_q'^{\mathrm{C}}}{J_{\mathrm{PF_6^-}}}\right)_{J_{\mathrm{D}}=0, J_{\mathrm{Li^+}}=0, \nabla T=0} = \frac{L^{q-}}{L^{--}}. \quad (56)$$

The transport numbers simplify accordingly. One of the Rules for Coupling of Fluxes, $L_{\varphi q} = L^{q+} - L^{q-}$, can now be applied. We divide both sides by $L_{\varphi\varphi}$ $(L^{++} + L^{--})$ and obtain

$$\pi^{\mathrm{N}} = \frac{L_{\varphi q}}{L_{\varphi\varphi}} = \frac{L^{q+}}{L^{++} + L^{--}} - \frac{L^{q-}}{L^{++} + L^{--}} = \tau_{\mathrm{Li^+}}q^*_{\mathrm{Li^+}} - \tau_{\mathrm{PF_6^-}}q^*_{\mathrm{PF_6^-}}. \quad (57)$$

The measurable Peltier heat may obtain a simplified contribution through this.

D. Summary of procedures for coefficient determinations

We have described the electrolyte in a concentration cell in two equivalent ways: as a set of mixed components and as a set of neutral components only. A procedure for determining practical transport properties has been outlined. A schematic illustration of the procedure is given in Fig. 3, and the procedure consists of four steps, as follows:

1. Determine the coefficients of the mixed component scenario with FDT in the barycentric frame of reference.
2. Reduce the number of coefficients by replacing the barycentric frame of reference with the (co-)solvent frame of reference.
3. Apply the Rules for Coupling of Fluxes to find the coefficients of the neutral component scenario from the coefficients of the mixed component scenario.
4. Finally, determine the set of practical transport properties by applying the operational definitions to the coefficients obtained in the previous step.

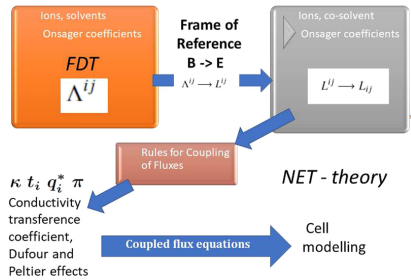

FIG. 3. Procedure for calculation of diffusion coefficients and electric- and thermal conductivities. Arrows show the sequence of steps. The procedure starts with the calculation of Onsager coefficients for the mixed component scenario using the fluctuation dissipation theorems (FDTs orange block). The coefficients for the mixed component scenario (gray block) are next obtained for the appropriate frame of reference. Using the Rules for Coupling of Fluxes, we next find properties that describe coupled transport of heat, mass, and charge (central block and left bottom corner). These steps will enable us to eventually model electrochemical cells in terms of nonequilibrium thermodynamics (NET).

In the following, we shall apply these theoretical steps and demonstrate how they apply to an example. As of yet, the set of Rules can only be used for isothermal systems. FDT for nonisothermal systems is still lacking in the practical literature.

IV. SIMULATION METHODS

To apply the theoretical framework, we have calculated transport coefficients with equilibrium molecular dynamics simulations, and we provide an overview of our simulation methodology in the following.

A. Electrolyte model and simulation set-up

The equilibrium MD simulations were performed using the LAMMPS[31] software. Atomic and molecular interactions were described by the OPLS-AA[36] potential. The parameters for the solvent molecules were obtained from the LigParGen web service,[37–39] and the parameters for Li^+ and PF_6^- were taken from Jensen and Jorgensen[40] and Acevedo *et al.*,[41,42] respectively. The real-space cutoff for the Lennard-Jones and Coulombic forces was set to 13 Å. A Lennard-Jones tail correction was added to the energy and pressure.[43] Electrostatic forces beyond the cutoff were computed using a particle–particle particle-mesh solver[44] with a maximum relative error in forces of 1×10^{-6}. The ionic charges were scaled by a factor of 0.75 to account for the overestimation of electrostatic interactions between ions in non-polarizable force fields.[45] Periodic boundary conditions were applied in all directions. Initial configurations of the systems were prepared by randomly placing solvent molecules, Li^+ and PF_6^-, in a simulation box with the Packmol software.[46] The composition of the electrolyte corresponded to the weight ratio EC:DEC = 1:1, which is a particle ratio of 5520:4116, and 920 particles of salt were added to reach a concentration of 1M.

The energies of the systems were minimized to avoid particle overlap. We used the routine developed by Molinari *et al.*[47] for initial equilibration. The systems were further equilibrated at a temperature of 350 K or higher and a pressure of 1 bar in the isobaric-isothermal (*NPT*) ensemble using a time-step of 1.25 fs in order for the potential energy and density of the systems to stabilize. The Nosé–Hoover thermostat and barostat[48–50] were used to control the temperature and pressure using time constants of 100 and 1000 time-steps, respectively. The final equilibration in the *NPT* ensemble was conducted at a temperature of 300 K while sampling the box volume. The simulation box size was adjusted (to the average volume) after equilibrium to obtain the correct density. The simulation boxes were cubic with sides of 115 Å.

B. Calculation of transport properties

We sampled the radial distribution functions (RDFs) and transport properties in the canonical ensemble (*NVT*) using a time-step of 1.25 fs during simulations lasting at least 80 ns. The Nosé–Hoover thermostat maintained the temperature, which was set to 300 K. Sampling transport properties in the *NVT* ensemble with the Nosé–Hoover thermostat produces transport properties that are statistically indistinguishable from those obtained using the *NVE* ensemble.[51] The average pressure was 0.4 bar for these simulations. All RDFs and coefficients were obtained from the OCTP code[52] by tracking the motion of the central atom of the various components.

We computed the coefficients L^{ij} of Eq. (17) in the mixed component scenario and the matrix of ℓ_{ij}-coefficients of Eq. (19) in the neutral component scenario. We have assumed monovalent ions in our theoretical framework, where the cation (anion) has a valency of +1 (−1). As described earlier, the ion charges are scaled to $z_+ = z = 0.75$ and $z_- = -z = -0.75$, respectively, in our simulations. This will modify the equations presented in Sec. III via the inclusion of the valency in Eqs. (31)–(34), as well as in the equations that follow. In particular, each term in the expression for $L_{\varphi\varphi}$ in Eq. (36) must be multiplied by z^2, while the terms in Eqs. (37)–(39) are multiplied by z. This also implies that the transference number in Eq. (44) should be divided by z. Finally, we calculate the transport numbers according to the derivation of Gullbrekken *et al.*,[53] which takes the charge into account.

To determine the thermodynamic factors, we evaluated the Kirkwood–Buff integrals[33] from the RDFs. The relations between the Kirkwood–Buff integrals and the thermodynamic factors are given in Appendix C. We used the finite-size correction of Ganguly and van der Vegt[54] for the RDFs and the integration procedure of Krüger *et al.*[55] in our computations. We refer to Milzetti *et al.* for further details on this procedure.[56]

V. RESULTS AND DISCUSSION

A. Equilibrium properties

The thermodynamic factors give information on attractive and repulsive forces in the electrolyte. Thermodynamic factors (based on mole fractions) of the example electrolyte are presented in Table I (see also Appendix C for a description of the calculation and the concentration-based thermodynamic factors). The thermodynamic factors for the salt and DEC indicate that there are repulsive forces between the components themselves. The conditions are far from ideal, with values for Γ_{LL} and Γ_{DD} of 1.5 and 1.2, respectively (see the two first rows of Table I). The cross terms Γ_{LD} and Γ_{DL} indicate that there are attractive forces between L and DEC embedded in co-solvent EC. It is known that DEC arranges itself around the lithium-ion,[19,20] as we noted in connection with Fig. 1. A clustering of ion pairs has also been observed. The results in Table I support this.

B. A comprehensive set of Onsager coefficients

Tables II–V present our comprehensive set of Onsager coefficients for the ternary lithium battery electrolyte that we have

TABLE I. Thermodynamic factors (based on mole fractions) of the lithium battery electrolyte from molecular dynamics simulations (at 300 K and an average pressure of 0.4 bar). The thermodynamic factors are calculated from the radial distribution functions, averaged over three independent simulations. The error estimates were obtained as the standard deviation of the thermodynamic factors calculated directly from the radial distribution functions (without averaging them).

Γ_{LL}	Γ_{DD}	Γ_{LD}	Γ_{DL}
1.50 ± 0.02	1.20 ± 0.04	−0.29 ± 0.02	−0.98 ± 0.03

TABLE II. Onsager diffusion coefficients for the mixed component scenario of the isothermal electrolyte obtained by molecular dynamics simulations (at 300 K and an average pressure of 0.4 bar). The coefficients are calculated using Eq. (B1) in the barycentric (B) frame of reference and converted to the solvent (E) frame of reference. Coefficients refer to Eq. (17) and are given in two sets of units for the E frame of reference (the total molar concentration, c, is used to convert the units). The values are averaged over three independent simulations, and the standard deviations are taken as the error estimate here.

	Frame of reference		
Coefficient	B $\times 10^{-11}$ m^2/s	E $\times 10^{-11}$ m^2/s	E $\times c/RT\ 10^{-11}$ mol^2/(J m s)
L^{++}	0.4 ± 0.04	0.8 ± 0.1	4.0 ± 0.3
L^{--}	0.7 ± 0.2	1.3 ± 0.2	6.2 ± 1.0
L^{+-}	0.1 ± 0.02	0.6 ± 0.05	2.8 ± 0.2
L^{D+}	0.5 ± 0.1	2.4 ± 0.2	12.1 ± 1.1
L^{D-}	−0.3 ± 0.1	1.8 ± 0.2	9.2 ± 0.9
L^{DD}	2.8 ± 0.2	11.3 ± 1.3	55.9 ± 6.2
L^{E+}	−0.9 ± 0.1		
L^{E-}	−1.0 ± 0.1		
L^{EE}	6.1 ± 0.9		
L^{ED}	−3.4 ± 0.4		

TABLE III. Onsager diffusion coefficients for the neutral component scenario of the isothermal electrolyte. The top six coefficients are computed from the Rules for Coupling of Fluxes using the indicated equation and values in Table II. The bottom three values are obtained from Eq. (20). Conditions are otherwise the same as for Table II.

Coefficient	Equation	Value	Unit
$L_{\varphi\varphi}$	(36)	0.23 ± 0.03	Ω^{-1} m^{-1}
$L_{\varphi L}$	(37)	−2.5 ± 0.8	10^{-6} mol C/(J m s)
$L_{\varphi D}$	(38)	2.1 ± 0.8	10^{-6} mol C/(J m s)
L_{LL}	(40)	6.2 ± 1.0	10^{-11} mol^2/(J m s)
L_{DL}	(41)	9.2 ± 0.9	10^{-11} mol^2/(J m s)
L_{DD}	(42)	55.9 ± 6.2	10^{-11} mol^2/(J m s)
ℓ_{LL}	(20)	3.7 ± 0.2	10^{-11} mol^2/(J m s)
ℓ_{DL}	(20)	11.3 ± 0.6	10^{-11} mol^2/(J m s)
ℓ_{DD}	(20)	53.7 ± 6.4	10^{-11} mol^2/(J m s)

considered. This set includes all coefficients for the isothermal electrolyte. Transport coefficients in the nonisothermal electrolyte are yet to be calculated, but we have provided preliminary expressions. Earlier studies have been less comprehensive.[16,23,57,58]

This paper's purpose is not to provide coefficients for a particular electrolyte but to present and document a convenient procedure for coefficient determination. As such, the physical-chemical meaning of the results and their application to battery modeling will not be the focus of our discussion here. However, using the lithium battery electrolyte as an example, we will now discuss the single steps of the new procedure and illustrate how they may be used. Most of the tools in this context are familiar and well-established, but a new item has been added: the Rules for Coupling of Fluxes. These Rules allow us to effectively predict measurable transport coefficients from

TABLE IV. Transport coefficients computed from the Rules for Coupling of Fluxes applied to the isothermal ternary battery electrolyte. The effect of neglecting cation–anion coupling, $L^{+-} = L^{-+} = 0$, is shown in the third column. The effect of using self-diffusion coefficients alone is shown in the fourth column. The results are computed from the values in Table III. Symbols are defined in the text in connection with the equations mentioned. Conditions are otherwise the same as for Table II.

Coefficient	All types of coupling	No cation–anion coupling	Self-diffusion coefficients
κ/Ω^{-1} m^{-1}	0.23 ± 0.03	0.27 ± 0.03	0.41 ± 0.01
t_L	−0.97 ± 0.12	−0.81 ± 0.07	−0.84 ± 0.01
t_D	0.90 ± 0.46	0.39 ± 0.17	0
τ_+	0.28 ± 0.09	0.39 ± 0.05	0.37 ± 0.01
τ_-	0.72 ± 0.09	0.61 ± 0.05	0.63 ± 0.01

sets of coefficients from FDT, which are relatively easy to compute and better related to electrolyte structure. In this manner, theory, simulation, and experiment go hand-in-hand in one tool.

The set of Onsager coefficients for isothermal conditions, presented in Tables II–V, demonstrate the advantages of such a tool. The first conclusion we can draw is that all coefficients in any of the matrices we have presented are significant. Coupling coefficients should, in general, be accounted for (see Table III).

C. Reducing the number of variables

The first dataset is the simulation results from FDT, obtained in the barycentric (B) frame of reference. They are listed in Table II, column one. We see a large number of coefficients—ten altogether. A large number of coefficients is clearly a disadvantage, and the first task is to reduce this number by transforming to the solvent (E) frame of reference; see the description in Sec. II B. Here, we choose the more mobile (which has less impact on the electrolyte structure) of the two organic solvents, EC, as the reference. After the change in frame of reference, we obtain the results in the second and third columns of Table II. The number of necessary coefficients changes

TABLE V. Onsager's ℓ_{ij}'s and Fick's interdiffusion coefficients, D_{ij}, and self-diffusion coefficients, D_j. The electrolyte conditions were described in Table II. The lithium salt L and its ions, and the co-solvent DEC, diffuse in a co-solvent of E.

Coefficient	Equation	Value $\times 10^{-11}$ m^2 s^{-1}	Value $\times 10^{11}$ mol^2 J^{-1} m^{-1} s^{-1}
ℓ_{LL}	(20)	0.7 ± 0.04	3.7 ± 0.2
ℓ_{DL}	(20)	2.3 ± 0.1	11.3 ± 0.6
ℓ_{DD}	(20)	10.8 ± 1.3	53.7 ± 6.4
D_{LL}	(29)	52.3 ± 2.6	
D_{LD}	(29)	309.4 ± 16.9	
D_{DL}	(29)	222.8 ± 22.4	
D_{DD}	(29)	1453.5 ± 170.2	
D_{Li^+}		7.2 ± 0.2	
$D_{PF_6^-}$		12.4 ± 0.2	
D_D		11.6 ± 0.1	
D_E		22.1 ± 0.1	

TABLE VI. Thermodynamic transport coefficients of the ternary electrolyte of components L, EC, and DEC and their dimensions according to the entropy production. Component EC serves as the frame of reference. Common for isothermal systems is to divide by the temperature T. Coefficient units are then multiplied by 1/K.

Name	Symbol	Dimension according to Eqs. (17) or (19)
Entropy production	σ	J K^{-1} m^{-3} s^{-1}
Heat flux	J'_q	J m^{-2} s^{-1}
Thermal force	$\nabla(1/T)$	K^{-1} m^{-1}
Mass flux	J_i	mol m^{-2} s^{-1}
Chemical force	$-\nabla\mu_i/T$	J K^{-1} mol^{-1} m^{-1}
Electric flux	j	C m^{-2} s^{-1}
Electric force	$-\nabla\varphi/T$	V K^{-1} m^{-1}
Main heat coefficient	L_{qq}	K J m^{-1} s^{-1}
Coupling coefficient, heat L	$L_{q\mathrm{L}} = L_{\mathrm{L}q}$	K mol m^{-1} s^{-1}
Coupling coefficient, heat D	$L_{q\mathrm{D}} = L_{\mathrm{D}q}$	K mol m^{-1} s^{-1}
Electric conductivity	$L_{\varphi\varphi}$	K C V^{-1} m^{-1} s^{-1}
Coupling coefficient, charge-heat	$L_{\varphi q} = L_{q\varphi}$	K C m^{-1} s^{-1}
Coupling coefficient, charge-mass L	$L_{\varphi\mathrm{L}} = L_{\mathrm{L}\varphi}$	K C mol J^{-1} m^{-1} s^{-1}
Coupling coefficient, charge-mass D	$L_{\varphi\mathrm{D}} = L_{\mathrm{D}\varphi}$	K C mol J^{-1} m^{-1} s^{-1}
Diffusion main coefficient L	ℓ_{LL}	K mol^2 J^{-1} m^{-1} s^{-1}
Diffusion main coefficient D	ℓ_{DD}	K mol^2 J^{-1} m^{-1} s^{-1}
Diffusion coupling coefficient LD	$\ell_{\mathrm{LD}} = \ell_{\mathrm{LD}}$	K mol^2 J^{-1} m^{-1} s^{-1}
Diffusion main coefficient ++	L^{++}	K mol^2 J^{-1} m^{-1} s^{-1}
Diffusion main coefficient −−	L^{--}	K mol^2 J^{-1} m^{-1} s^{-1}
Diffusion coupling coefficient +−	$L^{+-} = L^{-+}$	K mol^2 J^{-1} m^{-1} s^{-1}
Diffusion coupling coefficient D$^+$	$L^{\mathrm{D}+} = L^{+\mathrm{D}}$	K mol^2 J^{-1} m^{-1} s^{-1}
Diffusion coupling coefficient D−	$L^{\mathrm{D}-} = L^{-\mathrm{D}}$	K mol^2 J^{-1} m^{-1} s^{-1}
Diffusion main coefficient DD	L^{DD}	K mol^2 J^{-1} m^{-1} s^{-1}

from ten to six upon the shift to the E frame of reference, and the coefficient values change accordingly.

The frame of reference is always an issue when transport coefficients are concerned. Standard procedures are available on how to change from one frame to another (see, e.g., Ref. 6). Here, the choice of the frame of reference determines the contributions to the *emf* but not the (total) *emf* (which is invariant to the choice[17,59]).

The results presented in Table II have the same order of magnitude as those published in the literature, 10^{-10} m^2 s^{-1}.[58] So far, EC and DEC have been treated as one solvent (however, see Wang *et al.*[22]) while we distinguish between the co-solvents. A direct comparison of our results with those in the literature is thus not possible. However, all coupling coefficients are large in both frames of reference. This is an interesting point; it means that it will not be correct to neglect coefficients.

Return again to the two last columns of Table II for Onsager coefficients in the E frame of reference. The coefficients in the two columns are equivalent; they differ only by the factor that is used to convert between the dimensions used. The left column has dimensions m^2/s as they are directly derived from Eq. (B1). In order to obtain the coefficients with dimension mol^2/(J m s), which fit the flux Eq. (17), we have multiplied the left column with the factor c/RT. This unit gives the coefficient a dimension that fits with the thermodynamic description.

D. Diffusion and charge transfer

1. The mixed component scenario

In the E frame of reference, we find that the co-solvent DEC has the largest mobility of all components. All coefficients are positive, meaning that the movement of one constituent in the mixture always hampers the movement of others. This is intuitively obvious from a visual inspection of the simulation snapshot of the electrolyte in Fig. 1: The clustering tendency of ions and the structuring of DEC around the lithium-ions indicate that interactions obstruct rather than enhance the movements.

All Onsager coefficients are significant. Coupling coefficients have nearly the magnitude of the main coefficients (compare L^{+-} to L^{++} in Table II). The inequalities $L_{ii}L_{jj} > L_{ij}L_{ji}$ and $L_{ii} > 0$ are anyway obeyed. The physical picture that this conveys is clear: One ion does not move without significantly impacting the movement of other ions and other components. All components move significantly relative to one another when one ion moves. This means that the models that assume the independent movement of ions, Eqs. (1)–(3),

do not hold. They will, for instance, predict rather different electric conductivities when L^{+-} is significant. This is discussed further below.

2. The neutral component scenario

The coefficients $L_D\varphi$, $L_L\varphi$, and $L_{\varphi\varphi}$ were computed with input from Table II and the stated Rules for Coupling of Fluxes, Eqs. (36)–(42). We find $L_L\varphi = (-2.5 \pm 0.8) \times 10^{-6}$ mol C J^{-1} m^{-1} s^{-1}, $L_D\varphi = (2.1 \pm 0.8) \times 10^{-6}$ mol C J^{-1} m^{-1} s^{-1}, and $L_{\varphi\varphi} = 0.23 \pm 0.03$ Ω^{-1} m^{-1}. The results are also shown in Table III. Diffusion coefficients, ℓ_{ij}, were computed from Eq. (20). The results for ℓ_{LL}, ℓ_{LD}, and ℓ_{DD} are also shown in Table III (bottom rows). The coefficients that describe coupling to charge transport can now be computed from this input. These results are shown in Table IV. The results have numerical accuracy, obtained from three independent simulations.

Consider the first column of Table IV, where no approximations are applied (all types of coupling are considered). Our simulated value is 0.23 ± 0.03 Ω^{-1} m^{-1} (Table IV). Lundgren *et al.*[23] measured 0.7 Ω^{-1} m^{-1} for a similar electrolyte, while Morita *et al.*[18] measured 0.8 Ω^{-1} m^{-1}. Newman[57] measured a conductivity of 0.6 Ω^{-1} m^{-1} for $LiPF_6$ in a propylene carbonate electrolyte. Trends in data or ratios are better captured in simulations than absolute values. With the Rules for Coupling of Fluxes available, it is easy to compare the models that we addressed in the Introduction. The neglect of cation–anion coupling has not much to say for the electric conductivity (cf. the second column in Table IV), but there is a large impact on the transference coefficient for co-solvent when this approximation is used. The use of self-diffusion coefficients to estimate ionic transport properties is slightly worse (see the last column of data).

The transport number of Li^+ in the mixture was obtained from the transference coefficient of the salt.[53] It is rather small (0.28) for DEC:EC = 1:1. A value less than unity implies that there is always a build-up of salt during battery discharge close to the anode, followed by diffusion. Neglecting the coupling coefficient L^{+-} changes the transport number of Li^+ significantly, from 0.28 to 0.39. Clearly, a smaller value can lead to more concentration polarization at the electrode. The number may be essential for precise interpretations of electrolyte performance.

Using the self-diffusion coefficient rather than the coefficient that represents all interactions in the ternary mixture has a smaller impact on the transport number; see the last column of Table IV. The transport number changes to 0.37 in that case. Valøen and Reimers reported 0.38, Lundgren *et al.* 0.18, and Zugmann *et al.* 0.28, all values obtained from concentration cell experiments taking a solvent average frame of reference.[15,23,60] Neither these nor other authors considered the effect of co-solvent electro-osmosis or an impact on the emf by solvent polarization.

A large positive transference coefficient of D equal to 0.90 is found. This has not been reported before. The positive value means that the co-solvent is moving in the opposite direction of the salt. The solvent transference number is zero only when the coupling coefficients are neglected. On average, 0.90 mol D accumulates on the cathode side when one mol of electric charge passes the electrolyte during discharge. Clearly, the model that assumes independent movement of ions cannot predict the full impact of charge transfer; the fact is that D is carried along when the battery is in operation. The transport of D will cause its own polarization, which has only recently been recognized in the literature as a cause of segregation.[22]

The transport of EC with respect to the barycenter is opposite to that of DEC (cf. Table II). Large coefficients for solvents mean that the cell emf can have several significant contributions. Such contributions are presently neglected, say, in the formula for concentration polarization, which is used in the determination of transport numbers.

These points together underline once more that the assumption of independent movement of ions fails to describe component transport inside batteries. The neglected coefficients will lead to polarization, which eventually reduces cell efficiency. The assumption that the two solvents behave like one is also incorrect, and solvent segregation will reduce the cell voltage. These conclusions have been reached straightforwardly, using FDT and the Rules for Coupling of Fluxes.

3. Relation to Fick's law's coefficients

Fick's diffusion coefficients are used more frequently than the Onsager coefficients. They are often regarded as being more accessible than the cumbersome Onsager coefficients, so they deserve a special comment. Fick's law's coefficients for the present electrolyte, given by Eq. (29), are compared to the Onsager ℓ_{ij}-coefficients in Table V. We first note that these Onsager coefficients vary by one order of magnitude. Clearly, DEC is more mobile than salt. The self-diffusion coefficients (the four bottom rows of Table V) do not address inter-diffusion.

The set of Fick's coefficients describes the same reality as the Onsager coefficients. However, their interpretation is not as straightforward as for the Onsager coefficients. They contain part of the driving force, i.e., the thermodynamic factor. As described in Appendix C, the values of these factors depend on the chosen ensemble conditions and on the concentration metric used (e.g., mole fractions or molar concentrations). This is a source of some ambiguity, especially when comparing different works. In Appendix C, we provide the thermodynamic factors for *NVT* and *NPT* conditions and for using either molar concentration or mole fraction. The different factor sets lead to significantly different diffusion coefficients. Such ambiguities can be avoided using Onsager coefficients. Our aim has been to make the Onsager coefficients more accessible and avoid the ambiguities that arise with Fick's law.

4. Coupling to heat transport

One of the Rules for Coupling of Fluxes, presented in this work, connected the coupling coefficients for charge and heat transport for the mixed and neutral component scenarios. We have not been able to exploit this rule fully yet. Fluctuation-dissipation theorems have been formulated for this case but have been used less. Clearly, this opens the road for future work. The need for better methods and models to deal with thermal transport phenomena in electrochemical cells is evident and has been pointed out.[17] With the results of Table II, we can compute the value of K [see Eq. (53)] and find that the term $L^{+-} \times K$ is 20% of the value of L^{++}. In other words, the transport coefficients that describe thermal phenomena must also be taken into account to get a complete picture.

E. Conclusions and perspectives

A set of rules that connect the Onsager transport coefficients of a mixed component scenario to a neutral component description were obtained here for a ternary electrolyte mixture using entropy production invariance. No assumption was involved, and the rules are general in this sense. All types of coupling between ion and solvent transport processes were systematically accounted for. The relations could be reduced to well-known expressions for the independent movement of ions, Eqs. (1)–(3), when the interaction between particles was set to zero. The rules allow for the systematic introduction of assumptions when information is lacking. A coupling coefficient cannot be neglected without also neglecting its reciprocal Onsager coefficient. The main Onsager coefficients are always positive. All Onsager coefficients obey symmetry criteria, which reflect the nature of molecular fluctuations. Fick's law has its place, mostly for historical reasons.

We have obtained these results using a theoretical basis that takes advantage of NET for heterogeneous systems. Coupled transport phenomena in the example electrolyte were dealt with systematically. The procedure is applicable to electrochemical cells in general, and the Onsager coefficients play a central role. These coefficients have a solid foundation in the FDT and the entropy production of the system. Their symmetry property reflects the underlying molecular events, which should be brought out.

We have taken as an example the electrolyte of a typical lithium battery, containing a concentrated salt solution in two organic carbonate solvents, and presented in detail the rules that connect transport coefficients for a set of mixed variables, including ions, and a set of neutral variables that express coupled transport of heat, charge, and mass on a thermodynamic level. Solvent segregation, as well as concentration polarization, can now be described. The name "Rules for Coupling of Fluxes" has been used because the relations follow from entropy production invariance for the transformations in the (co-)solvent frame of reference.

ACKNOWLEDGMENTS

The Research Council of Norway is acknowledged for Project No. 262644, PoreLab, by S.K., A.F.G., S.K.S., and A.L. S.K.S. acknowledges financial support from the NRC through Project No. 275754. Ø.G. acknowledges the Research Council of Norway for its support of the Norwegian Micro- and Nano-Fabrication Facility, NorFab, Project No. 295864. Dick Bedeaux is acknowledged for a critical review of the manuscript in its last stages and for explicit formulations of the fluctuation dissipation theorems.

AUTHOR DECLARATIONS

Conflict of Interest

The authors have no conflicts to disclose.

Author Contributions

Signe Kjelstrup: Conceptualization (lead); Data curation (equal); Formal analysis (equal); Funding acquisition (lead); Investigation (equal); Methodology (equal); Supervision (equal); Validation (equal); Writing – original draft (lead); Writing – review & editing (equal). **Astrid Fagertun Gunnarshaug**: Conceptualization (equal); Data curation (equal); Formal analysis (equal); Investigation (equal); Methodology (equal); Validation (equal); Writing – original draft (equal); Writing – review & editing (equal). **Øystein Gullbrekken**: Conceptualization (equal); Data curation (equal); Formal analysis (equal); Investigation (equal); Methodology (equal); Software (equal); Validation (equal); Visualization (equal); Writing – review & editing (equal). **Sondre K. Schnell**: Conceptualization (equal); Formal analysis (equal); Methodology (equal); Supervision (equal); Validation (equal); Writing – review & editing (equal). **Anders Lervik**: Conceptualization (equal); Data curation (equal); Formal analysis (equal); Investigation (equal); Methodology (equal); Software (equal); Supervision (supporting); Validation (equal); Writing – original draft (supporting); Writing – review & editing (equal).

DATA AVAILABILITY

The data that support the findings of this study are available from the corresponding author upon reasonable request.

APPENDIX A: FLUXES, FORCES, TRANSPORT COEFFICIENTS, AND THEIR DIMENSIONS

Table VI summarizes the thermodynamic transport coefficients for the ternary electrolyte, consisting of components L (the lithium salt), EC (ethylene carbonate), and DEC (diethyl carbonate), along with their dimensions.

APPENDIX B: COEFFICIENTS FROM THE FLUCTUATION DISSIPATION THEOREMS

Krishna and van Baten[9] gave expressions for Onsager coefficients that are convenient for data reduction in molecular dynamics simulations at isothermal conditions. The Onsager coefficients Λ_{ij} were expressed in terms of particle position vectors $\mathbf{r}_{k,i}$, suitable for the simulation box,

$$\Lambda_{ij} = \frac{1}{6N}\lim_{\Delta t\to\infty}\frac{1}{\Delta t}\left\langle\left(\sum_{k=1}^{N_i}\left[\mathbf{r}_{k,i}(t+\Delta t)-\mathbf{r}_{k,i}(t)\right]\right)\cdot\left(\sum_{l=1}^{N_j}\left[\mathbf{r}_{l,j}(t+\Delta t)-\mathbf{r}_{l,j}(t)\right]\right)\right\rangle. \tag{B1}$$

The expression is called the Einstein approximation. Here, N_i and N_j are the particle numbers of components i and j, respectively, and N is the total number of particles. The particles can be charged or neutral. The $\langle\cdots\rangle$ brackets indicate an ensemble average, and the period $\cdot$ indicates a contraction of two vectors. The dimension of Λ_{ij} is m^2/s, and Onsager symmetry is obeyed $\Lambda_{ij} = \Lambda_{ji}$. The expression is particularly useful for the mixed component scenario, as particle positions are then well defined. Figure 4 displays the mean square displacements in Eq. (B1) from our simulations.

Equation (B1) can be derived from fluctuation-dissipation theorems. Consider isothermal conditions. The start is the entropy production of the isothermal system, obtained from Eq. (17) as $\sigma = -\frac{1}{T}\sum_{j=1}^{n}\mathbf{J}_i\cdot\nabla\widetilde{\mu}_j$. The fluctuation-dissipation theorem applies to

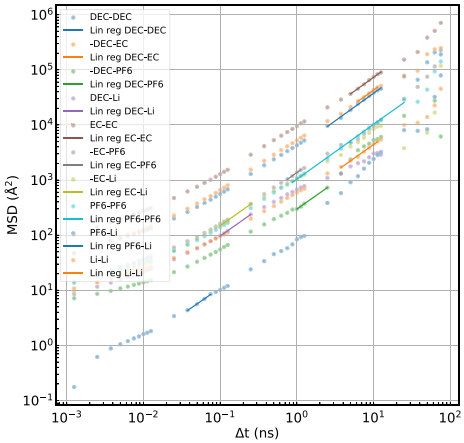

FIG. 4. Mean squared displacement (MSD) of the various molecular and ionic correlations as a function of time difference. The slopes of the curves are the Onsager diffusion coefficients in Table II. The region used for linear regression is chosen as the data points that are closest to a slope of 1 in the log–log plot. At least four data points are used in the linear regression. The time intervals used for linear regression will vary due to the different correlations between the species.

the *fluctuating contributions* to the molar fluxes that constitute entropy production. These give

$$\langle \mathbf{J}_{i,\mathrm{R}}(\mathbf{r},t)\mathbf{J}_{j,\mathrm{R}}(\mathbf{r}',t')\rangle = 2RL^{ij}\delta(\mathbf{r}-\mathbf{r}')\delta(t-t'). \tag{B2}$$

A bold symbol means a vector. The symbol δ is the Dirac delta function.

The displacements in Eq. (B1) are first written as integrals over the velocities. We find

$$\Lambda_{ij} = \frac{1}{6N}\lim_{\Delta t\to\infty}\frac{1}{\Delta t}\int_t^{t+\Delta t}dt\int_t^{t+\Delta t}dt' \times\left\langle\sum_{k=1}^{N_i}\mathbf{v}_{k,i}(t)\cdot\sum_{l=1}^{N_j}\mathbf{v}_{l,j}(t')\right\rangle. \tag{B3}$$

The fluctuating contributions to the velocities are the same in and away from equilibrium. The fluctuating contribution to the molar flux at position $\mathbf{r}$, $\mathbf{J}_{i,\mathrm{R}}(\mathbf{r},t)$, is given by

$$N_A\mathbf{J}_{i,\mathrm{R}}(\mathbf{r},t) = \sum_{k=1}^{N_i}\mathbf{v}_{k,i}(t)\delta(\mathbf{r}_{k,i}(t)-\mathbf{r}), \tag{B4}$$

where N_A is Avogadro's number. By introducing Eq. (B4) into Eq. (B3), we obtain

$$\Lambda_{ij} = \frac{N_A^2}{6N}\lim_{\Delta t\to\infty}\frac{1}{\Delta t}\int_t^{t+\Delta t}dt\int_t^{t+\Delta t}dt'\int_V d\mathbf{r}\int_V d\mathbf{r}' \times\langle\mathbf{J}_{i,\mathrm{R}}(\mathbf{r},t)\cdot\mathbf{J}_{j,\mathrm{R}}(\mathbf{r}',t')\rangle. \tag{B5}$$

We next introduce Eq. (B2) in this formula and find that

$$\Lambda^{ij} = \frac{R}{c}\Lambda_{ij}. \tag{B6}$$

This result is exactly the same that we find from the linear laws, see Eq. (11). We, therefore, confirm agreement with Eq. (B2), the fluctuation-dissipation theorem.

For the component velocities $\mathbf{u}_i$ in the E frame of reference, we obtain them for the $n-1$ components,

$$x_i\mathbf{u}_i = -\frac{1}{RT}\sum_{j=1}^{n-1}\left(\Lambda_{ij}-\frac{x_j}{x_n}\Lambda_{in}\right)\nabla\widetilde{\mu}_j. \tag{B7}$$

The summation is over $n-1$. By multiplication with c/R, we obtain the flux of component i,

$$\mathbf{J}_i = x_ic\mathbf{u}_i = c_i\mathbf{u}_i = -\frac{c}{RT}\sum_{j=1}^{n-1}\left(\Lambda_{ij}-\frac{x_j}{x_n}\Lambda_{in}\right)\nabla\widetilde{\mu}_j. \tag{B8}$$

This flux (in mol m^{-2} s^{-1}) relative to component E is then

$$\begin{aligned}\mathbf{J}_i^{\mathrm{E}} &= c_i(\mathbf{u}_i-\mathbf{u}_n)\\ &= -\frac{c}{RT}\sum_{j=1}^{n-1}\left(\Lambda_{ij}-\frac{x_j}{x_n}\Lambda_{in}-\frac{x_i}{x_n}\Lambda_{nj}+\frac{x_ix_j}{x_n^2}\Lambda_{nn}\right)\nabla\widetilde{\mu}_j\\ &= -\frac{1}{T}\sum_{j=1}^{n-1}L_{ij}^{\mathrm{E}}\nabla\widetilde{\mu}_j \quad \text{for } i=1,..,n-1.\end{aligned} \tag{B9}$$

These equations give the relation between L^{ij} and Λ_{ij} in the B- and E-frames of reference.

APPENDIX C: THE THERMODYNAMIC FACTORS

In the main text, we used the thermodynamic factors (Γ_{ij}) to account for non-ideality when expressing the chemical potential gradients as concentration gradients for the Fickian diffusion picture. The present section will explain how we calculated the thermodynamic factors from molecular dynamics simulations.

The thermodynamic factor is particular to the ensemble in question. In the present work, equilibrium molecular dynamics simulations are performed in the NVT ensemble, where[34,35]

$$\Gamma_{ij} \equiv \frac{c_i}{k_BT}\left(\frac{\partial\mu_j}{\partial c_i}\right)_{T,V,\mathbf{c}_i} = \frac{N_i}{k_BT}\left(\frac{\partial\mu_j}{\partial N_i}\right)_{T,V,\mathbf{N}_i}, \tag{C1}$$

and $c_i = N_i/V$ is the concentration of species i. This derivative is carried out at constant T, V, and concentrations of all components except i (indicated by the subscript "$\mathbf{c}_i$"), or equivalently, at constant particle numbers N_i for all components except i (indicated by the subscript "$\mathbf{N}_i$").

Kirkwood and Buff[33,34] related the thermodynamic factors to integrals of the radial distribution functions of the species. These Kirkwood–Buff integrals, G_{ij}, are

$$G_{ij} = 4\pi\int_0^\infty (g_{ij}(r)-1)r^2\,\mathrm{d}r, \tag{C2}$$

where g_{ij} is the radial distribution function for species i and j and they are related to the thermodynamic factors via

$$\frac{1}{k_B T}\left(\frac{\partial \mu_i}{\partial c_j}\right)_{T,V,\mathbf{c}_j} = \frac{C_{ij}}{\det(\mathbf{B})} = \frac{\Gamma_{ji}}{c_j}, \tag{C3}$$

where $\mathbf{B}$ is the matrix with elements $B_{ij} = c_i\delta_{ij} + c_i c_j G_{ij}$ and $C_{ij} = (-1)^{i+j}\det(\mathbf{B}_{ij})$ is the ij-cofactor in the cofactor expansion of the determinant of $\mathbf{B}$ ($\mathbf{B}_{ij}$ is obtained from $\mathbf{B}$ by deleting the ith row and the jth column). Since $G_{ij} = G_{ji}$, we have $\mathbf{B} = \mathbf{B}^{\top}$ and $C_{ij} = C_{ji}$ so that $\Gamma_{ij}c_j = \Gamma_{ji}c_i$. In practical applications, it might be more straightforward to calculate the thermodynamic factors directly from $\Gamma_{ij} = c_i A_{ij}$, where A_{ij} are the elements of the matrix $\boldsymbol{A} = \boldsymbol{B}^{-1}$. For a ternary system, we get

$$\begin{aligned}
\Gamma_{11}\zeta &= 1 + G_{22}c_2 + G_{33}c_3 + c_2c_3(G_{22}G_{33} - G_{23}G_{32}),\\
\Gamma_{12}\zeta &= c_1(-G_{12} + c_3(-G_{12}G_{33} + G_{13}G_{32})),\\
\Gamma_{13}\zeta &= c_1(-G_{13} + c_2(G_{12}G_{23} - G_{13}G_{22})),\\
\Gamma_{22}\zeta &= 1 + G_{11}c_1 + G_{33}c_3 + c_1c_3(G_{11}G_{33} - G_{13}G_{31}),\\
\Gamma_{23}\zeta &= c_2(-G_{23} + c_1(-G_{11}G_{23} + G_{13}G_{21})),\\
\Gamma_{33}\zeta &= 1 + G_{11}c_1 + G_{22}c_2 + c_1c_2(G_{11}G_{22} - G_{12}G_{21}),
\end{aligned} \tag{C4}$$

where

$$\zeta = \frac{\det(\mathbf{B})}{c_1c_2c_3}. \tag{C5}$$

For completeness, we will detail how we can adapt the thermodynamic factors to the isothermal-isobaric NPT ensemble and how we can introduce mole fractions. The transformation to NPT conditions is[33,34]

$$a_{ji} = \left(\frac{\partial \mu_i}{\partial N_j}\right)_{T,P,\mathbf{N}_j} = \left(\frac{\partial \mu_i}{\partial N_j}\right)_{T,V,\mathbf{N}_j} - \frac{\overline{V}_i\overline{V}_j}{V\kappa_T}, \tag{C6}$$

where $\overline{V}_i$ represents the partial molar volume of species i,

$$\overline{V}_i = \frac{\sum_k c_k C_{ki}}{\sum_{i,j} c_i c_j C_{ij}}, \tag{C7}$$

and κ_T denotes the isothermal compressibility,

$$\kappa_T = \frac{\det(\mathbf{B})}{k_B T\sum_{i,j} c_i c_j C_{ij}}. \tag{C8}$$

Together, these equations give

$$\begin{aligned}
a_{ji} &= \left(\frac{\partial \mu_i}{\partial N_j}\right)_{T,P,\mathbf{N}_j}\\
&= \frac{k_B T}{V\det(\mathbf{B})}\left(C_{ij} - \frac{\left(\sum_k c_k C_{ki}\right)\left(\sum_k c_k C_{kj}\right)}{\sum_{i,j} c_i c_j C_{ij}}\right).
\end{aligned} \tag{C9}$$

This equation can be employed to compute thermodynamic factors under NPT conditions (which are typically encountered in experimental settings). Analogous to Eq. (C1), we define a thermodynamic factor for NPT conditions as

$$\Gamma_{ij}^{\mathrm{NPT}} = \frac{N_i}{k_B T}\left(\frac{\partial \mu_j}{\partial N_i}\right)_{T,P,\mathbf{N}_i} = \frac{N_i}{k_B T}a_{ij}. \tag{C10}$$

From Eq. (C6), we have that $a_{ij} = a_{ji}$, which means that $\Gamma_{ij}^{\mathrm{NPT}}N_j = \Gamma_{ji}^{\mathrm{NPT}}N_i$, and from the Gibbs–Duhem relation at $\mathrm{d}T = 0$ and $\mathrm{d}P = 0$, we have

$$\sum_{i=1}^{n} c_i a_{ij} = 0, \tag{C11}$$

for all j. For a ternary system, with the following definitions:

$$\eta = \frac{1}{c_1c_2c_3}\sum_i\sum_j c_i c_j C_{ij}, \qquad \Delta_{ij} = G_{ii} + G_{jj} - 2G_{ij}, \tag{C12}$$

one may show that

$$\begin{aligned}
a_{11} &= \frac{k_B T}{V\eta}\left(\frac{c_2 + c_3 + c_2c_3\Delta_{23}}{c_1}\right),\\
a_{22} &= \frac{k_B T}{V\eta}\left(\frac{c_1 + c_3 + c_1c_3\Delta_{13}}{c_2}\right),\\
a_{33} &= \frac{k_B T}{V\eta}\left(\frac{c_1 + c_2 + c_1c_2\Delta_{12}}{c_3}\right),\\
a_{12} = a_{21} &= -\frac{k_B T}{V\eta}\left[1 + c_3(G_{33} + G_{12} - G_{13} - G_{23})\right],\\
a_{13} = a_{31} &= -\frac{k_B T}{V\eta}\left[1 + c_2(G_{22} + G_{13} - G_{12} - G_{23})\right],\\
a_{23} = a_{32} &= -\frac{k_B T}{V\eta}\left[1 + c_1(G_{11} + G_{23} - G_{12} - G_{13})\right].
\end{aligned} \tag{C13}$$

The relations in Eq. (C11) can be verified from these equations; for instance, $c_1a_{11} + c_2a_{21} + c_3a_{31} = 0$.

The thermodynamic factors are also commonly expressed as derivatives with respect to the mole fractions,[61]

$$\Gamma_{ij}^{x} = \frac{x_i}{k_B T}\left(\frac{\partial \mu_i}{\partial x_j}\right)_{T,P,\Sigma} = \delta_{ij} + x_i\left(\frac{\partial \ln \gamma_i}{\partial x_j}\right)_{T,P,\Sigma}, \tag{C14}$$

where γ_i is the activity coefficient, and we use the superscript "x" to indicate that Γ_{ij}^{x} is based on the mole fraction. The subscript Σ indicates that the derivative is taken with the constraint that the mole fractions sum to one, and it is carried out at a constant mole fraction for all components except the last (the nth). The required derivatives are[61–63]

$$\left(\frac{\partial \mu_i}{\partial x_j}\right)_{T,P,\Sigma} = N\left(\frac{\partial \mu_i}{\partial N_j}\right)_{T,P,\mathbf{N}_j} - N\left(\frac{\partial \mu_i}{\partial N_n}\right)_{T,P,\mathbf{N}_n}, \tag{C15}$$

and with Eqs. (C15) and (C14), explicit expressions for Γ_{ij}^{x} are[13,61,63]

$$\begin{aligned}
\Gamma_{11}^{x} &= \frac{1}{\eta}(c_1 + c_2 + c_3 + c_1c_2(-G_{12} + G_{13} + G_{22} - G_{23}) + c_2c_3\Delta_{23}),\\
\Gamma_{12}^{x} &= \frac{c_1}{\eta}(c_2(-G_{12} + G_{13} + G_{22} - G_{23}) + c_3(-G_{12} + G_{13} + G_{23} - G_{33})),\\
\Gamma_{21}^{x} &= \frac{c_2}{\eta}(c_1(G_{11} - G_{12} - G_{13} + G_{23}) + c_3(G_{13} + G_{23} - G_{12} - G_{33})),\\
\Gamma_{22}^{x} &= \frac{1}{\eta}(c_1 + c_2 + c_3 + c_1c_2(G_{11} - G_{12} - G_{13} + G_{23}) + c_1c_3\Delta_{13}),
\end{aligned} \tag{C16}$$

TABLE VII. Thermodynamic factors of the lithium battery electrolyte from molecular dynamics simulations (at 300 K and an average pressure of 0.4 bar). The thermodynamic factors are calculated from the radial distribution functions, averaged over three independent simulations. The error estimates were obtained as the standard deviation of the thermodynamic factors calculated directly from the radial distribution functions (without averaging them). The superscript "NPT" from Eq. (C10) and the superscript "x" from Eq. (C14) are excluded here.

Thermodynamic factor	*NVT* Eq. (C4)	*NPT* Eqs. (C10) and (C13)	*NPT* (mole fraction) Eq. (C16)
Γ_{LL}	1.678 ± 0.004	1.43 ± 0.02	1.50 ± 0.02
Γ_{DD}	47 ± 2	0.81 ± 0.03	1.20 ± 0.04
Γ_{EE}	18.7 ± 0.5	0.40 ± 0.01	⋯
Γ_{LD}	1.30 ± 0.02	−0.30 ± 0.01	−0.29 ± 0.02
Γ_{DL}	5.8 ± 0.1	−1.32 ± 0.04	−0.98 ± 0.03
Γ_{LE}	0.850 ± 0.008	−0.018 ± 0.005	⋯
Γ_{EL}	5.10 ± 0.05	−0.11 ± 0.03	⋯
Γ_{DE}	24.7 ± 0.7	−0.38 ± 0.01	⋯
Γ_{ED}	33 ± 1	−0.51 ± 0.02	⋯

TABLE VIII. Consistency check for the thermodynamic factors, $\Gamma_{ij}N_j = \Gamma_{ji}N_i$, numerical values from Table VII.

Γ_{ij}/Γ_{ji}	*NVT*	*NPT*	N_i/N_j
Γ_{LD}/Γ_{DL}	$\frac{1.30}{5.80} = 0.224$	$\frac{-0.30}{-1.32} = 0.227$	$N_L/N_D = \frac{920}{4116} = 0.223$
Γ_{LE}/Γ_{EL}	$\frac{0.85}{5.10} = 0.167$	$\frac{-0.018}{-0.11} = 0.164$	$N_L/N_E = \frac{920}{5520} = 0.167$
Γ_{DE}/Γ_{ED}	$\frac{24.7}{33} = 0.748$	$\frac{-0.38}{-0.51} = 0.745$	$N_D/N_E = \frac{4116}{5520} = 0.746$

where η is the same as defined in Eq. (C12). We refer to Ruckenstein and Shulgin[63] for the expressions for Γ^x_{31} and Γ^x_{32}.

The calculated thermodynamic factors from our simulations are given in Table VII. The salt is treated as one component, "L." In Table VIII, we examine the symmetry relations, $\Gamma_{ij}N_j = \Gamma_{ji}N_i$, and use the numerical values from Table VII to confirm the relations in Eq. (C11),

$$\begin{aligned}\Gamma^{NPT}_{LL} + \Gamma^{NPT}_{DL} + \Gamma^{NPT}_{EL} &= 1.43 - 1.32 - 0.11 \approx 0,\\ \Gamma^{NPT}_{LD} + \Gamma^{NPT}_{DD} + \Gamma^{NPT}_{ED} &= -0.30 + 0.81 - 0.51 \approx 0,\\ \Gamma^{NPT}_{LE} + \Gamma^{NPT}_{DE} + \Gamma^{NPT}_{EE} &= -0.018 - 0.38 + 0.40 \approx 0.002.\end{aligned} \tag{C17}$$

Regarding the last check, we note that the value of Γ^{NPT}_{LE} is on the same order of magnitude as the uncertainties in Γ^{NPT}_{DE} and Γ^{NPT}_{EE}.

REFERENCES

[1] J. S. Newman, *Electrochemical Systems*, 2nd ed. (Prentice Hall, 1991).
[2] R. Haase, *Thermodynamics of Irreversible Processes* (Addison-Wesley, 1969).
[3] A. Katchalsky and P. Curran, *Nonequilibrium Thermodynamics in Biophysics*, 2nd ed. (Harvard University Press, 1975).
[4] S. Kjelstrup, D. Bedeaux, E. Johannessen, and J. Gross, *Non-Equilibrium Thermodynamics for Engineers*, 2nd ed. (World Scientific, 2018).
[5] *CRC Handbook of Chemistry and Physics*, 96th ed., edited by W. Haynes (CRC Press, Boca Raton, 2015).
[6] S. Kjelstrup and D. Bedeaux, in *Non-Equilibrium Thermodynamics of Heterogeneous Systems*, 1st ed., Series on Advances in Statistical Mechanics (World Scientific, 2008), Vol. 16.
[7] R. Kubo, "The fluctuation-dissipation theorem," Rep. Prog. Phys. **29**, 255 (1966).
[8] H. Callen, "The fluctuation-dissipation theorems and irreversible thermodynamics," in *Fluctuation, Relaxation and Resonance in Magnetic Systems*, edited by D. ter Haar (Scottish Universities' Summer School, Oliver and Boyd, Edinburgh, 1962), pp. 15–23.
[9] R. Krishna and J. M. van Baten, "The Darken relation for multicomponent diffusion in liquid mixtures of linear alkanes: An investigation using molecular dynamics (MD) simulations," Ind. Eng. Chem. Res. **44**, 6939–6947 (2005).
[10] X. Liu, T. J. H. Vlugt, and A. Bardow, "Predictive Darken equation for Maxwell-Stefan diffusivities in multicomponent mixtures," Ind. Eng. Chem. Res. **50**, 10350–10358 (2011).
[11] K. D. Fong, H. K. Bergström, B. D. McClosky, and K. K. Mandadapu, "Transport phenomena in electrolyte solutions: Nonequilibrium thermodynamics and statistical mechanics," AIChE J. **66**, e17091 (2020).
[12] S. de Groot and P. Mazur, *Non-Equilibrium Thermodynamics* (Dover, London, 1984).
[13] X. Liu, A. Martín-Calvo, E. McGarrity, S. K. Schnell, S. Calero, J.-M. Simon, D. Bedeaux, S. Kjelstrup, A. Bardow, and T. J. H. Vlugt, "Fick diffusion coefficients in ternary liquid systems from equilibrium molecular dynamics simulations," Ind. Eng. Chem. Res. **51**, 10247–10258 (2012).
[14] J. Newman and T. W. Chapman, "Restricted diffusion in binary solutions," AIChE J. **19**, 343–348 (1973).
[15] S. Zugmann, M. Fleischmann, M. Amereller, R. M. Gschwind, H. D. Wiemhöfer, and H. J. Gores, "Measurement of transference numbers for lithium ion electrolytes via four different methods, a comparative study," Electrochim. Acta **56**, 3926–3933 (2011).
[16] M. Klett, M. Giesecke, A. Nyman, F. Hallberg, R. W. Lindström, G. Lindbergh, and I. Furó, "Quantifying mass transport during polarization in a Li ion battery electrolyte by in situ ^{7}Li NMR imaging," J. Am. Chem. Soc. **134**, 14654–14657 (2012).
[17] S. Kjelstrup, K. R. Kristiansen, A. F. Gunnarshaug, and D. Bedeaux, "Seebeck, Peltier and Soret effects: On different formalisms for transport equations in thermogalvanic cells," J. Chem. Phys. **158**, 020901 (2023).
[18] M. Morita, Y. Asai, N. Yoshimoto, and M. Ishikawa, "A Raman spectroscopic study of organic electrolyte solutions based on binary solvent systems of ethylene carbonate with low viscosity solvents which dissolve different lithium salts," J. Chem. Soc., Faraday Trans. **94**, 3451–3456 (1998).
[19] D. M. Seo, S. Reininger, M. Kutcher, K. Redmond, W. B. Euler, and B. L. Lucht, "Role of mixed solvation and ion pairing in the solution structure of lithium ion battery electrolytes," J. Phys. Chem. C **119**, 14038–14046 (2015).

[20]S.-K. Jeong, M. Inaba, Y. Iriyama, T. Abe, and Z. Ogumi, "Surface film formation on a graphite negative electrode in lithium-ion batteries: AFM study on the effects of co-solvents in ethylene carbonate-based solutions," Electrochim. Acta **47**, 1975–1982 (2002).
[21]K. Førland, T. Førland, and S. Kjelstrup Ratkje, *Irreversible Thermodynamics: Theory and Applications* (Wiley, Chichester, 1988).
[22]A. A. Wang, S. Greenbank, G. Li, D. A. Howey, and C. W. Monroe, "Current-driven solvent segregation in lithium-ion electrolytes," Cell Rep. Phys. Sci. **3**, 101047 (2022).
[23]H. Lundgren, M. Behm, and G. Lindbergh, "Electrochemical characterization and temperature dependency of mass-transport properties of $LiPF_6$ in EC:DEC," J. Electrochem. Soc. **162**, A413 (2015).
[24]R. Chandrasekaran, "Quantification of contributions to the cell overpotential during galvanostatic discharge of a lithium-ion cell," J. Power Sources **262**, 501–513 (2014).
[25]K. Shigenobu, F. Philippi, S. Tsuzuki, H. Kokubo, K. Dokko, M. Watanabe, and K. Ueno, "On the concentration polarisation in molten Li salts and borate-based Li ionic liquids," Phys. Chem. Chem. Phys. **25**, 6970–6978 (2023).
[26]S. Viscardy, J. Servantie, and P. Gaspard, "Transport and Helfand moments in the Lennard-Jones fluid. II. Thermal conductivity," J. Chem. Phys. **126**, 184513 (2007).
[27]T. W. Maltby, B. Hafskjold, D. Bedeaux, S. Kjelstrup, and Ø. Wilhelmsen, "Local equilibrium in liquid phase shock waves," Phys. Rev. E **107**, 035108 (2023).
[28]J. M. Rubi and S. Kjelstrup, "Mesoscopic nonequilibrium thermodynamics gives the same thermodynamic basis to Butler-Volmer and Nernst equations," J. Phys. Chem. B **107**, 13471–13477 (2003).
[29]S. Kjelstrup and A. Lervik, "The energy conversion in active transport of ions," Proc. Natl. Acad. Sci. U. S. A. **118**, e2116586118 (2021).
[30]E. A. Guggenheim, "The conceptions of electrical potential difference between two phases and the individual activities of ions," J. Phys. Chem. **33**, 842–849 (1929).
[31]A. P. Thompson, H. M. Aktulga, R. Berger, D. S. Bolintineanu, W. M. Brown, P. S. Crozier, P. J. in 't Veld, A. Kohlmeyer, S. G. Moore, T. D. Nguyen, R. Shan, M. J. Stevens, J. Tranchida, C. Trott, and S. J. Plimpton, "LAMMPS—A flexible simulation tool for particle-based materials modeling at the atomic, meso, and continuum scales," Comput. Phys. Commun. **271**, 108171 (2022).
[32]L. Spitthoff, A. F. Gunnarshaug, D. Bedeaux, O. Burheim, and S. Kjelstrup, "Peltier effects in lithium-ion battery modeling," J. Chem. Phys. **154**, 114705 (2021).
[33]J. G. Kirkwood and F. P. Buff, "The statistical mechanical theory of solutions. I," J. Chem. Phys. **19**, 774–777 (1951).
[34]A. Ben-Naim, *Molecular Theory of Solution* (OUP Oxford, 2006).
[35]D. Bedeaux, S. Kjelstrup, and S. K. Schnell, *Nanothermodynamics: Theory and Applications* (World Scientific, 2023).
[36]W. L. Jorgensen, J. D. Madura, and C. J. Swenson, "Optimized intermolecular potential functions for liquid hydrocarbons," J. Am. Chem. Soc. **106**, 6638–6646 (1984).
[37]W. L. Jorgensen and J. Tirado-Rives, "Potential energy functions for atomic-level simulations of water and organic and biomolecular systems," Proc. Natl. Acad. Sci. U. S. A. **102**, 6665–6670 (2005).
[38]L. S. Dodda, J. Z. Vilseck, J. Tirado-Rives, and W. L. Jorgensen, "1.14*CM1A-LBCC: Localized bond-charge corrected CM1A charges for condensed-phase simulations," J. Phys. Chem. B **121**, 3864–3870 (2017).
[39]L. S. Dodda, I. Cabeza de Vaca, J. Tirado-Rives, and W. L. Jorgensen, "LigParGen web server: An automatic OPLS-AA parameter generator for organic ligands," Nucleic Acids Res. **45**, W331–W336 (2017).
[40]K. P. Jensen and W. L. Jorgensen, "Halide, ammonium, and alkali metal ion parameters for modeling aqueous solutions," J. Chem. Theory Comput. **2**, 1499–1509 (2006).
[41]S. V. Sambasivarao and O. Acevedo, "Development of OPLS-AA force field parameters for 68 unique ionic liquids," J. Chem. Theory Comput. **5**, 1038–1050 (2009).
[42]B. Doherty, X. Zhong, S. Gathiaka, B. Li, and O. Acevedo, "Revisiting OPLS force field parameters for ionic liquid simulations," J. Chem. Theory Comput. **13**, 6131–6145 (2017).
[43]D. Frenkel and B. Smit, *Understanding Molecular Simulation*, 2nd ed. (Academic Press, San Diego, 2002).
[44]R. W. Hockney and J. W. Eastwood, *Computer Simulation Using Particles* (Hilger, Bristol, 1988).
[45]I. Leontyev and A. Stuchebrukhov, "Accounting for electronic polarization in non-polarizable force fields," Phys. Chem. Chem. Phys. **13**, 2613–2626 (2011).
[46]L. Martínez, R. Andrade, E. G. Birgin, and J. M. Martínez, "PACKMOL: A package for building initial configurations for molecular dynamics simulations," J. Comput. Chem. **30**, 2157–2164 (2009).
[47]N. Molinari, J. P. Mailoa, and B. Kozinsky, "Effect of salt concentration on ion clustering and transport in polymer solid electrolytes: A molecular dynamics study of PEO–LiTFSI," Chem. Mater. **30**, 6298–6306 (2018).
[48]W. Shinoda, M. Shiga, and M. Mikami, "Rapid estimation of elastic constants by molecular dynamics simulation under constant stress," Phys. Rev. B **69**, 134103 (2004).
[49]W. G. Hoover, "Canonical dynamics: Equilibrium phase-space distributions," Phys. Rev. A **31**, 1695–1697 (1985).
[50]S. Nosé, "A molecular dynamics method for simulations in the canonical ensemble," Mol. Phys. **52**, 255–268 (1984).
[51]J. E. Basconi and M. R. Shirts, "Effects of temperature control algorithms on transport properties and kinetics in molecular dynamics simulations," J. Chem. Theory Comput. **9**, 2887–2899 (2013).
[52]S. H. Jamali, L. Wolff, T. M. Becker, M. de Groen, M. Ramdin, R. Hartkamp, A. Bardow, T. J. H. Vlugt, and O. A. Moultos, "OCTP: A tool for on-the-fly calculation of transport properties of fluids with the order-*n* algorithm in LAMMPS," J. Chem. Inf. Model. **59**, 1290–1294 (2019).
[53]Ø. Gullbrekken, I. T. Røe, S. M. Selbach, and S. K. Schnell, "Charge transport in water–NaCl electrolytes with molecular dynamics simulations," J. Phys. Chem. B **127**, 2729–2738 (2023).
[54]P. Ganguly and N. F. A. van der Vegt, "Convergence of sampling Kirkwood–Buff integrals of aqueous solutions with molecular dynamics simulations," J. Chem. Theory Comput. **9**, 1347–1355 (2013).
[55]P. Krüger, S. K. Schnell, D. Bedeaux, S. Kjelstrup, T. J. H. Vlugt, and J.-M. Simon, "Kirkwood–Buff integrals for finite volumes," J. Phys. Chem. Lett. **4**, 235–238 (2013).
[56]J. Milzetti, D. Nayar, and N. F. A. van der Vegt, "Convergence of Kirkwood–Buff integrals of ideal and nonideal aqueous solutions using molecular dynamics simulations," J. Phys. Chem. B **122**, 5515–5526 (2018).
[57]J. Newman, K. E. Thomas, H. Hafezi, and D. R. Wheeler, "Modeling of lithium-ion battery," J. Power Sources **119–121**, 838–843 (2003).
[58]J. Landesfeind and H. A. Gasteiger, "Temperature and concentration dependence of the ionic transport properties of lithium-ion battery electrolytes," J. Electrochem. Soc. **166**, A3079–A3097 (2019).
[59]S. K. Ratkje, H. Rajabu, and T. Førland, "Transference coefficients and transference numbers in molten salt mixtures relevant for the aluminium electrolysis," Electrochim. Acta **38**, 415–423 (1993).
[60]L. O. Valøen and J. N. Reimers, "Transport properties of $LiPF_6$-based Li-ion battery electrolytes," J. Electrochem. Soc. **152**, A882 (2005).
[61]R. Fingerhut, G. Herres, and J. Vrabec, "Thermodynamic factor of quaternary mixtures from Kirkwood–Buff integration," Mol. Phys. **118**, e1643046 (2020).
[62]D. A. Jonah and H. D. Cochran, "Chemical potentials in dilute, multicomponent solutions," Fluid Phase Equilib. **92**, 107–137 (1994).
[63]E. Ruckenstein and I. Shulgin, "Entrainer effect in supercritical mixtures," Fluid Phase Equilib. **180**, 345–359 (2001).

Article IV

Ø. Gullbrekken, A. F. Gunnarshaug, A. Lervik, S. Kjelstrup, and S. K. Schnell

Effect of the Ion, Solvent, and Thermal Interaction Coefficients on Battery Voltage,

Journal of the American Chemical Society **146**:7 4592–4604 (2024).
DOI: 10.1021/jacs.3c11589

Article IV

Article IV

JACS
JOURNAL OF THE AMERICAN CHEMICAL SOCIETY
pubs.acs.org/JACS

Article

Effect of the Ion, Solvent, and Thermal Interaction Coefficients on Battery Voltage

Øystein Gullbrekken, Astrid Fagertun Gunnarshaug, Anders Lervik, Signe Kjelstrup, and Sondre Kvalvåg Schnell*

Cite This: J. Am. Chem. Soc. 2024, 146, 4592−4604

ABSTRACT: In order to increase the adoption of batteries for sustainable transport and energy storage, improved charging and discharging capabilities of lithium-ion batteries are necessary. To achieve this, accurate data that describe the internal state of the cells are essential. Several models have been derived, and transport coefficients have been reported for use in these models. We report for the first time a complete set of transport coefficients to model the concentration and temperature polarization in a lithium-ion battery ternary electrolyte, allowing us to test common assumptions. We include effects due to gradients in chemical potentials and in temperature. We find that the voltage contributions due to salt and solvent polarization are of the same order of magnitude as the ohmic loss and must be taken into account for more accurate modeling and understanding of battery performance. We report new Soret and Seebeck coefficients and find thermal polarization to be significant in cases relevant to battery research. The analysis is suitable for electrochemical systems, in general.

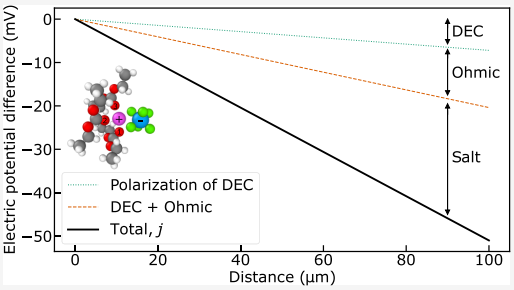

INTRODUCTION

It is generally known that charging or discharging of batteries may lead to concentration polarization, i.e., changes in electrolyte composition due to an electric field.[1] Thermal polarization, i.e., composition changes due to temperature gradients, may also play a role. The magnitudes of both follow from the transport of charge, mass, and heat in the electrolyte, including the coupling effects of these processes. The values of the coupling coefficients are central for the prediction of thermal and concentration polarization according to non-equilibrium thermodynamics, the method chosen for the present analysis.

A major part of the battery voltage is determined by the difference in electrode potentials between the cathode and the anode. In addition, ohmic resistance and polarization of the electrolyte contribute to the total cell voltage. At high charge and discharge rates, the polarization of the electrolyte can be significant and could dramatically influence the battery performance.[2] In the present work, we focus on such contributions that enable a more accurate and physical model of lithium-ion batteries.

As an important case of analysis, we have taken the well-studied lithium-ion battery with its electrolyte composed of a lithium salt ($LiPF_6$) and two organic carbonates as cosolvents, ethylene carbonate (EC) with either diethyl carbonate (DEC) or dimethyl carbonate (DMC). These components are typical in lithium battery research and in commercial batteries[3] and have not earlier been rigorously examined as an electrolyte mixture of independent components.

The polarization contributions are given by the gradient in the electric potential, $\nabla\varphi$, between two lithium metal electrodes. Here, we will only consider one-directional transport, i.e., $d\varphi/dx$, but this can be extended to two- or three-dimensional systems. We express the gradient in electric potential, $\nabla\varphi$, using nonequilibrium thermodynamics.[4] By choosing the cosolvent EC as frame of reference, we obtain

$$\nabla\varphi = -\frac{\pi}{FT}\nabla T - t_{\mathrm{L}}\frac{1}{FT}\nabla\mu_{\mathrm{L}} - t_{\mathrm{D}}\frac{1}{FT}\nabla\mu_{\mathrm{D}} - \frac{j}{\kappa} \qquad (1)$$

where the first term on the right-hand side is proportional to the temperature gradient, ∇T, via the Peltier coefficient π over the temperature T and Faraday's constant F. The second and third contributions contain the gradient in chemical potential of lithium salt, $\nabla\mu_{\mathrm{L,T}}$, (L is used as short-hand notation for the lithium salt here), and the gradient in chemical potential of the

Received: October 18, 2023
Revised: January 25, 2024
Accepted: January 29, 2024
Published: February 10, 2024

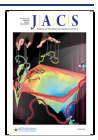

https://doi.org/10.1021/jacs.3c11589
J. Am. Chem. Soc. 2024, 146, 4592−4604

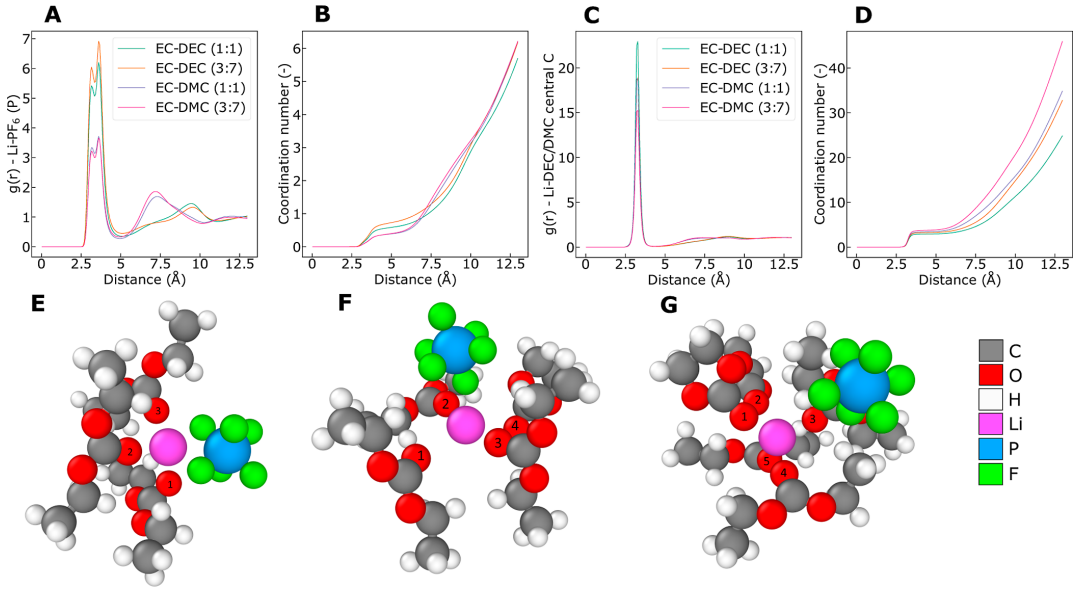

Figure 1. (a) RDFs of Li^+ and PF_6^- and corresponding (b) coordination numbers as a function of distance. (c) RDFs of Li^+ and DEC/DMC and corresponding (d) coordination numbers as a function of distance. (e) MD snapshot of Li^+ coordinated by three DECs and one PF_6^-, corresponding to the closest peak of the bimodal RDF of Li^+ and PF_6^-. (f) MD snapshot of Li^+ coordinated by three DECs, one EC, and one PF_6^-, corresponding to the second-closest peak of the bimodal RDF of Li^+ and PF_6^-. (g) MD snapshot of Li^+ coordinated by four DECs and one EC, the anion is outside the first solvation shell (solvent-separated ion-pair). The coordinating solvent carbonyl oxygen atoms are numbered. Particle colors are shown to the right.

cosolvent, $\nabla\mu_{D,T}$ (where D in this work can be DEC or DMC). Both gradients are evaluated at constant temperature, as indicated by subscript T. The transference coefficient of component i, t_i, is defined as the mass flux of i at a constant composition and temperature over the electric current density. It can be determined from, e.g., Hittorf experiments.[5] The ohmic potential drop is the fourth term, where the electric current density j is multiplied with the inverse electrolyte conductivity, $1/\kappa$.

The expression 1 originates in the entropy production of the cell, when neutral components are used to describe the entropy production. We describe transport in the bulk electrolyte under polarization conditions[6] by

$$
\begin{aligned}
J_q'^N &= l_{qq}\nabla\left(\frac{1}{T}\right) - l_{qL}\frac{1}{T}\nabla\mu_{L,T} - l_{qD}\frac{1}{T}\nabla\mu_{D,T} + \frac{L_{q\varphi}}{L_{\varphi\varphi}}j \\
J_L &= l_{Lq}\nabla\left(\frac{1}{T}\right) - l_{LL}\frac{1}{T}\nabla\mu_{L,T} - l_{LD}\frac{1}{T}\nabla\mu_{D,T} + \frac{L_{L\varphi}}{L_{\varphi\varphi}}j \\
J_D &= l_{Dq}\nabla\left(\frac{1}{T}\right) - l_{DL}\frac{1}{T}\nabla\mu_{L,T} - l_{DD}\frac{1}{T}\nabla\mu_{D,T} + \frac{L_{D\varphi}}{L_{\varphi\varphi}}j \\
\nabla\varphi &= \frac{T}{L_{\varphi\varphi}}\left(-j + L_{\varphi q}\nabla\left(\frac{1}{T}\right) - L_{\varphi L}\frac{1}{T}\nabla\mu_{L,T} - L_{\varphi D}\frac{1}{T}\nabla\mu_{D,T}\right),
\end{aligned}
\tag{2}
$$

where l_{ij} and L_{ij} are Onsager coefficients for the electrolyte mixture under different conditions. The large and small coefficient symbols are related by

$$
l_{ij} = L_{ij} - \frac{L_{i\varphi}L_{j\varphi}}{L_{\varphi\varphi}} \tag{3}
$$

where the coefficient $L_{\varphi\varphi} = \kappa T$. $J_q'^N$, J_L, J_D, and j are the measurable heat flux, mass fluxes of salt and cosolvent, and electric current density, respectively. The measurable heat flux and electric current density do not depend on the frame of reference. The mass fluxes do. They are here measured relative to EC. L_{ij} are coefficients for transport of heat, mass, and charge. The coefficients l_{ij} refer to diffusion in the absence of an electric current.[5] We observe that the value of $\nabla\varphi$ is equal to the ohmic potential drop in the absence of gradients in the composition and temperature. Transport in the electrolyte can be described in two ways, by the mixed (ions and solvents) or by the neutral (salt and solvents) component scenario.[6] The transport coefficients in the mixed component scenario (Λ^{ij}) are obtained directly from the fluctuation dissipation theorems using molecular dynamics (MD) simulations, see further explanation in the Supporting Information and in ref 6. The coefficients of the neutral component scenario, used in the equations above, can be obtained by converting the set of Λ^{ij} using the Rules for Coupling of Fluxes.[6]

The ability to accurately compute the potential profile in eq 1 has so far been much hampered by a lack of data. Properties of binary electrolytes are well studied e.g., by Newman et al.,[1,7] but most lithium-ion battery electrolytes are ternary or even

https://doi.org/10.1021/jacs.3c11589
J. Am. Chem. Soc. 2024, 146, 4592−4604

quaternary mixtures with more than one solvent. The transport properties of such complex mixtures are not fully known, and coupling of transport phenomena is therefore often neglected.[8] Assumptions have not been controlled, and little distinction has been made between descriptions with one or more solvent components. The mixture of solvents has often been considered as one component.[9−12] Recent studies indicate that solvent components separate in the cell.[13,14] The structure of the ternary electrolyte is, therefore, central for the description of components and their transport properties.

The aim of this work is thus to determine a complete set of transport properties obtained from MD simulations that enable us to compute all contributions to the electric potential at the stationary state. The transport coefficients are needed for battery modeling purposes. The frame of reference for t_i and the choice of components i will prove essential as the magnitude of the terms vary with the choice of the frame of reference.[15,16] The value of eq 1 is, however, independent of the frame of reference. We shall apply a method recently described by Kjelstrup et al., providing new relations for coefficient determinations, the so-called Rules for Coupling of Fluxes.[6] We start by describing the microstructure of the electrolyte at equilibrium. This is next used as a foundation for explaining thermodynamic and transport properties. A convenient choice of frame of reference will be explained based on the electrolyte microstructure and the diffusion coefficients in different frames of reference. We present and discuss first the effect of diffusion coefficients. The Seebeck coefficient and the heats of transfer will be reported, giving the coupling between the temperature gradient and the electric potential gradient. Finally, all determined parameters are used to estimate the impact of the temperature gradient and solve eq 1 in the stationary state. We can then evaluate how much each term in eq 1 contributes to the cell voltage.

RESULTS AND DISCUSSION

Equilibrium Structure of the Electrolyte. The structure information reported below suggests that the following exchange takes place in the presence of solvents DEC and EC at equilibrium

$$LiPF_6 + 3DEC \rightleftharpoons Li^+{\cdot}3DEC + PF_6^-$$

The reaction conveys two ways of viewing the electrolyte: as composed of a mixture of ionic and neutral components (right side) or as a mixture of neutral components only (left-hand side). The transport coefficients of the electrolyte can be formulated using either set of components, and they are connected via the Rules for Coupling of Fluxes, see Kjelstrup et al.[6] Both sets of components (of mixed and neutral components) were used to find the relevant sets of transport coefficients.

The coefficients of transport for the ternary electrolytes will be understood in terms of the electrolyte structure. We computed the radial distribution function (RDF) for Li^+ and DEC/DMC and PF_6^- in order to examine the electrolyte structure and the coordination environment of the Li^+ ions. The results are shown in Figure 1 and the results for Li^+ and EC are shown in SI, Figure S4. The residence time, i.e., the average time that two species stay together within a specified cutoff distance before parting, provides information about the dynamic properties of the coordination environments.[17−19] Coordination numbers and residence times are listed in Table 1.

Table 1. Coordination in Electrolytes. The Cutoff is Defined as the First Minimum after the First Peak in the RDF, i.e., the First Solvation Shell

electrolyte	pair	coordination number	residence time (ns)	cutoff (Å)
1:1 EC/DEC	Li-EC	1.40	0.42	4.52
1:1 EC/DEC	Li-DEC	2.92 ± 0.01	4.26 ± 0.06	4.45
1:1 EC/DEC	Li-PF_6	0.59	1.34 ± 0.12	5.08 ± 0.03
3:7 EC/DEC	Li-EC	0.81	0.54	4.52
3:7 EC/DEC	Li-DEC	3.23	3.82	4.45
3:7 EC/DEC	Li-PF_6	0.74	2.19	5.10
1:1 EC/DMC	Li-EC	1.01	0.18	4.45
1:1 EC/DMC	Li-DMC	3.42	1.87	4.39
1:1 EC/DMC	Li-PF_6	0.39	0.48	4.97
3:7 EC/DMC	Li-EC	0.59	0.17	4.52
3:7 EC/DMC	Li-DMC	3.74	1.35	4.39
3:7 EC/DMC	Li-PF_6	0.40	0.46	4.97

Figure 1 shows that each Li^+ on average is coordinated primarily by the linear carbonates in all electrolytes investigated, i.e., by DEC or DMC. The coordination numbers of DEC and of DMC in the first solvation shell range from 2.9 to 3.2 and 3.4 to 3.7, respectively. The corresponding numbers for EC range from 0.8 to 1.4 and 0.6 to 1.0 in the DEC- and DMC-containing electrolytes, respectively; see Figure S4. Additionally, from Table 1 we see that on average, the Li^+ spends about an order of magnitude longer time coordinated to DEC/DMC molecules than to EC molecules before changing coordination. All of the solvent molecules are facing Li^+ by the central carbonyl oxygen. The coordination of Li^+ in mixed carbonate electrolytes has been a point of discussion in the literature, but no consensus has been reached. Several studies indicate that Li^+ is preferentially coordinated by EC in electrolyte mixtures of EC and DEC/DMC[20−25] or that Li^+ is coordinated equally by EC and DEC/DMC,[26] but other studies indicate favored coordination by the linear carbonates.[27−29] There is less than one PF_6^- coordinating Li^+ on average in all electrolytes. The salt dissociation in the electrolytes containing DMC[30] is seemingly larger than in DEC. The RDFs of Li^+ and PF_6^- hint at the presence of ion clusters in the electrolyte. The fractions of ions in the ionic clusters are shown in Table 2. Ions are assumed to be part of a cluster if the interionic distance is less than 5 Å, the distance of the first minimum after the first peak of the Li^+-PF_6^- (P) RDF. More than 15% of the ions in the 1:1 wt % EC/DEC electrolyte are part of clusters with three or more ions. These clusters are dynamic and relatively short-lived, as indicated by the residence times in Table 1.

The equilibrium exchange reaction presented in the start of this section captures these findings. The reaction expresses

https://doi.org/10.1021/jacs.3c11589
J. Am. Chem. Soc. 2024, 146, 4592−4604

Table 2. Ionic Clusters in the Electrolytes. Fraction of Free Ions and Fraction of Ions in Different Sized Clusters

electrolyte	free ions	2 ions	3 ions	4 ions	≥5 ions
1:1 EC/DEC (1)	0.49	0.34	0.11	0.04	0.02
1:1 EC/DEC (2)	0.48	0.34	0.11	0.04	0.02
1:1 EC/DEC (3)	0.49	0.34	0.11	0.04	0.02
3:7 EC/DEC	0.37	0.40	0.13	0.06	0.03
1:1 EC/DMC	0.64	0.28	0.06	0.02	0.00
3:7 EC/DMC	0.63	0.30	0.05	0.01	0.00

how DEC or DMC can shield the ions from each other. DMC does this more readily than DEC. The reaction is slightly shifted to the right in the presence of DMC. It is therefore likely that the charge transport involves solvent transport. We will see later that this can be confirmed.

The thermodynamic factors, which describe deviations from ideal mixture theory, were calculated from Kirkwood-Buff integrals (Supporting Information) and are presented in Table 3. A main factor Γ_{ii} equal to one and a cross factor Γ_{ij} equal to zero means that the mixture is ideal, cf. Simon et al.[31] The values of the main factors Γ_{LL} and Γ_{DD} are clearly above one in all electrolytes, indicating the presence of repulsive forces. The cross-terms Γ_{LD} and Γ_{DL} are smaller than the corresponding main factors, indicating more attractive forces between polar DEC/DMC molecules and the ions. The thermodynamic factors involving the solvent are sensitive to the solvent composition of the electrolytes.

Table 3. Thermodynamic Factors (Γ_{ij}, L = $LiPF_6$, D = DEC or DMC) Calculated Using Concentrations[6]

system	Γ_{LL}	Γ_{LD}	Γ_{DL}	Γ_{DD}
1:1 EC/DEC +1 M $LiPF_6$	1.68	1.30	5.80	47.0
3:7 EC/DEC +1 M $LiPF_6$	1.65	1.42	7.72	58.0
1:1 EC/DMC +1 M $LiPF_6$	1.66	0.84	4.89	28.6
3:7 EC/DMC +1 M $LiPF_6$	1.63	0.94	7.21	36.8

From the Barycentric to the Cosolvent Frame of Reference. The frame of reference is central when transport of components in multicomponent mixtures is measured. The transport coefficients depend on the frame of reference. The Onsager coefficients from the simulations were obtained in the barycentric (or wall) frame of reference. The flux−force matrix of the isothermal system in this frame of reference has 10 coefficients, but we can reduce this number, using the fact that the driving forces are dependent through Gibbs−Duhem's equation, cf. Ref 6. Two possibilities for elimination of driving forces are then possible: EC or DEC. To help in that decision, we provide Onsager coefficients in Supporting Information Table S1 for the barycentric, EC-, and DEC frames of reference.

Consider first $L^{++} = (0.35 \pm 0.04) \times 10^{-11}$ m^2 s^{-1} in the barycentric frame of reference. Upon transformation to the EC frame of reference, L^{++} becomes $(0.8 \pm 0.1) \times 10^{-11}$ m^2 s^{-1} and in the DEC frame of reference, L^{++} is $(0.3 \pm 0.1) \times 10^{-11}$ m^2 s^{-1}. The coefficient L^{++} is larger when measured relative to EC than to DEC because Li^+ is less strongly coordinated to EC than to DEC. Both EC and DEC move with respect to the center of mass frame of reference, and they also move relative to one another. To treat the solvent as one component only, as is done in the literature,[32] means to neglect these relative movements. Furthermore, L^{--} is $(0.7 \pm 0.2) \times 10^{-11}$ m^2 s^{-1} in the barycentric frame of reference, $(1.3 \pm 0.2) \times 10^{-11}$ m^2 s^{-1} in the EC frame of reference, and $(1.0 \pm 2) \times 10^{-11}$ m^2 s^{-1} in the DEC reference frame. The PF_6^- anion is weakly coordinated by solvent molecules and moves more independently of the solvent, resulting in a smaller difference between the EC- and DEC frames of reference. The coefficient L^{ED}, which is present only in the barycentric frame of reference, is negative. This suggests that EC and DEC tend to move away from one another. In fact, EC moves away from all the other components in the barycentric reference frame and apparently is not much directly involved in charge transport. This gives arguments in favor of choosing the cosolvent EC as frame of reference for a reduced set of coefficients.[7,9,10,33,34] To use a mixture of solvents as the frame of reference gives fewer components transported and less variables. We have chosen to use EC alone as a frame of reference for the mass fluxes. The number of unknown coefficients is reduced from ten to six with this choice. We will have the possibility to study solvent segregation, which has recently been observed experimentally.[13] The choice for component EC is thus motivated by EC being less involved in structure-making than DEC as well as in the transport of Li^+ and charge. Note, however, that upon going from the barycentric to a cosolvent as frame of reference, some information about the system is lost, e.g., the correlation of the solvent components EC and DEC, L^{ED}. Moreover, if the motion of the cosolvent chosen as frame of reference is unknown, the interpretation of the transport coefficients becomes less transparent.[35,36]

Coefficients for Isothermal Diffusion. As mentioned, the electrolyte can be equivalently described by the mixed component or the neutral-only component scenario. At isothermal conditions, molecular simulations naturally produce transport coefficients in the mixed component scenario. But operationally defined, experimentally obtained properties are usually related to neutral components.[5,37] The Rules for Coupling of Fluxes provide links between the two scenarios and thus between simulations and experiments. The set of transport coefficients of the neutral component scenario is our target, to be used for thermodynamic modeling of the battery electrolyte.

Onsager Coefficients. The Onsager coefficients for the mixed component scenario obtained from the fluctuation−dissipation theorems, as shown in the Supporting Information, are presented in Table 4. The Onsager coefficients for the neutral components scenario were computed from these to finally give the electrolyte conductivity plus the transference coefficients for the salt and the cosolvent in the 1:1 EC/DEC with 1 M $LiPF_6$ electrolyte. The last properties were obtained using the Rules for Coupling of Fluxes[6] and are presented in the lower part of Table 4.

We see from the table that L^{--} is larger than L^{++}, which means that PF_6^- will move faster than Li^+. This is also reflected in the low Li^+ transport number (τ_+) of 0.28. This value is comparable to experimental values for the Li^+ transport number in EC/DEC + $LiPF_6$ electrolytes reported by, e.g., Lundgren et al.[11] and Landesfeind and Gasteiger.[10] These studies report transport numbers relative to the solvent mixture (as most experimenters do), while our results are relative to the EC. In other words, we assume that $J_{EC} = 0$. Notably, τ_+ in the DEC frame of reference is only 0.12 as Li^+ and DEC move together. A positive L^{+-} means that the cation and anion movements are positively correlated; i.e., they tend to move together and reduce ionic conductivity. This is reflected in the

https://doi.org/10.1021/jacs.3c11589
J. Am. Chem. Soc. 2024, 146, 4592−4604

Table 4. Diffusion Coefficients of the 1:1 wt.% EC/DEC + 1 M $LiPF_6$ Electrolyte in the Mixed Component Scenario, Derived from Equations in the Supporting Information and ref 6., and Converted to the EC and DEC Frames of Reference. Transference Coefficients, t_L, t_D, and t_E, and Transport Numbers, τ_+ and τ_-, are Dimensionless. The Coefficients in the Mixed Scenario L^{ij} Have Dimension m^2 s^{-1}. The Dimension Needed for eq 2 Is Obtained by Multiplication with c/R and These Coefficients Are Shown in the Rightmost Column

frame of reference	EC	DEC	EC
coefficient	value $\times 10^{-11}$ m^2 s^{-1}	value $\times 10^{-11}$ m^2 s^{-1}	value $\times 10^{-9}$ K mol^2 J^{-1} m^{-1} s^{-1}
L^{++}	0.8 ± 0.1	0.3 ± 0.1	12.1 ± 0.9
L^{--}	1.3 ± 0.2	1.0 ± 0.2	18.7 ± 3.0
L^{+-}	0.56 ± 0.05	0.2 ± 0.1	8.4 ± 0.7
L^{D+}	2.4 ± 0.2		36.4 ± 3.2
L^{D-}	1.8 ± 0.2		27.5 ± 2.7
L^{DD}	11.3 ± 1.3		167.8 ± 18.7
L^{E+}		0.1 ± 0.3	
L^{E-}		0.9 ± 0.1	
L^{EE}		20.3 ± 2.3	
$L_{\varphi\varphi} = \kappa T$	(69.3 ± 10.4) K S m^{-1}		
$L_{\varphi L}$	$(-7.5 \pm 2.3)\times 10^{-4}$ K mol C J^{-1} m^{-1} s^{-1}		
$L_{\varphi D}$	$(6.4 \pm 2.5)\times 10^{-4}$ K mol C J^{-1} m^{-1} s^{-1}		
$\kappa = L_{\varphi\varphi}/T$	(0.23 ± 0.03) S m^{-1}		
t_L	−0.97 ± 0.12	−1.17 ± 0.06	
t_D	0.90 ± 0.46		
t_E		−1.21 ± 0.62	
τ_+	0.28 ± 0.09	0.12 ± 0.04	
τ_-	0.72 ± 0.09	0.88 ± 0.04	

RDF values of Li^+ and PF_6^- in Figure 1a and in Tables 1 and 2. The L^{D+} is quite large and positive, which means that there is a strong tendency for correlated motion of Li^+ and DEC, as reflected in the corresponding RDF in Figure 1c and the residence times. Interestingly, L^{D-} is positive and significant but smaller than L^{D+}, so DEC will mostly follow Li^+. Generally, the coupling coefficients, L^{ij}, are of the same order of magnitude as the main coefficients, L^{ii}. They should hence not be neglected, as is now common. A large L^{DD} indicates that DEC is moving quickly relative to EC, indicating again that the assumption of the solvent mixture moving as one component is not true. Already from the results under isothermal conditions, we see that gradients in salt concentration and solvent composition will evolve in the electrolyte during charge or discharge of the battery. This will affect the battery voltage and will be demonstrated later. The transference coefficients t_L and t_D define the amount of salt and DEC transferred when 1 F of positive charges is passing the electrolyte from left to right.

In particular, 0.90 mol of DEC is transferred with the passage of 1 F of electric charge through the electrolyte. Consequently, DEC will move toward the cathode side, when measured relative to EC. This finding is not in agreement with a recent experimental study by Wang et al.[13] They showed that the linear carbonate cosolvent, ethyl methyl carbonate (EMC), in an electrolyte mixture with EC and $LiPF_6$ accumulated on the anode side upon passage of current. If the Li^+ were primarily coordinated by EC molecules in the simulations, we expect that EC would follow Li^+ and accumulate on the cathode side, and the linear carbonate DEC would move toward the anode side to fill the remaining void, as in the experiment. This deviation between our simulations and experimental results points to a potential inaccuracy of the force field that in reality, Li^+ is primarily coordinated by the cyclic carbonate EC and not by the linear carbonate. Our results for the salt transference coefficient mean that salt accumulates on the anode side. The electrodes are reversible to Li^+ ions and produce 1 F of lithium ions in the adjacent electrolyte, while only a fraction of 0.28 leaves the electrolyte chamber.

The ionic conductivity of the simulated electrolyte is 0.23 S m^{-1}, which is below the measured value of about 0.8 S m^{-1} by Lundgren et al.[11] However, even though the absolute values of the transport coefficients are lower than the experimentally measured values, the ratios expressed as transference coefficients are seemingly correct. The $L_{\varphi L}$ and $L_{\varphi D}$ coefficients describe how the components move in the electric field or respond to the net electric current. Their sign gives the direction of transport, positive when the movement follows positive charges and vice versa for the opposite sign. The transference coefficient is given by the ratio of this coefficient and the ionic conductivity multiplied by Faraday's constant.[6]

Fick's Diffusion Coefficients. Fick's diffusion coefficients are more frequently measured than the Onsager coefficients since there is easier access to gradients in concentration than to the gradients in chemical potential. The set of Fick's coefficients describes the same reality as the Onsager coefficients. The two sets are therefore related by entropy production invariance. The Fick's law coefficients were computed using the equations in ref 6, and the results are shown in Table 5. For example, D_{LL} is the diffusion of salt due to a concentration gradient of salt, and D_{LD} is the diffusion of salt due to a concentration gradient of DEC. The symmetry of the Onsager coefficient matrix is no longer present in Fick's diffusion coefficients, meaning that four rather than three coefficients are needed. There is also no

Table 5. Diffusion Coefficients of the Isothermal 1:1 wt.% EC/DEC + 1 M $LiPF_6$ Electrolyte in the EC Reference Frame. The Six Top Values for the Neutral Component Scenario Are Computed from the Coefficients in Table 4 Using the Generalized Transport Model and Equations in ref 6. The Four next Values Are Diffusion Coefficients from Fick's Extended Law, Equations in ref 6. The Four Bottom Values Are the Self-Diffusion Coefficients. Conditions Are the Same as for Table 4

coefficient	value $\times 10^{-11}$ m^2 s^{-1}	value $\times 10^{-9}$ K mol^2 J^{-1} m^{-1} s^{-1}
L_{LL}	1.3 ± 0.2	18.7 ± 3.0
L_{DL}	1.8 ± 0.2	27.5 ± 2.7
L_{DD}	11.2 ± 1.3	167.8 ± 18.7
l_{LL}	0.74 ± 0.04	11.0 ± 0.6
l_{DL}	2.3 ± 0.1	33.8 ± 1.9
l_{DD}	10.8 ± 1.3	161.0 ± 19.2
D_{LL}	52.3 ± 2.6	
D_{LD}	309.4 ± 16.9	
D_{DL}	222.8 ± 22.4	
D_{DD}	1453.5 ± 170.2	
D_{Li^+}	7.2 ± 0.2	
$D_{PF_6^-}$	12.4 ± 0.2	
D_D	11.6 ± 0.1	
D_E	22.1 ± 0.1	

https://doi.org/10.1021/jacs.3c11589
J. Am. Chem. Soc. 2024, 146, 4592−4604

requirement that Fick's main diffusion coefficients must be positive like for the Onsager main coefficients. The thermodynamic factor relates the chemical potential gradient and concentration gradient and is used to convert Onsager coefficients to Fick's diffusion coefficients. The values of the thermodynamic factors depend on the ensemble conditions and concentration units used. Performing the conversion increases the potential error and the method for computing thermodynamic factors could be a source of ambiguity.[6]

The advantage of Fick's diffusion coefficients is that they can be compared to experimental results. Lundgren et al.[11] obtained Fick's diffusion coefficients in electrolytes containing $LiPF_6$ in EC/DEC by measuring the relaxation of the open circuit potential after applying a small current for a certain time through the electrolyte sandwiched by Li electrodes. They calculated an effective diffusion coefficient of the salt in the mixed solvent frame of reference for the mixture of 1.5×10^{-10} $m^2\ s^{-1}$ for a salt concentration of 1 M. This value is of the same order of magnitude as the calculated Fick's diffusion coefficients in Table 5. Unlike in the above-mentioned experiment, simulations give four Fick's diffusion coefficients in a ternary mixture. The four coefficients are not separable in the experiments, so the experimental result can be viewed as an effective diffusion coefficient composed of four contributions. The disadvantage of a description using Fick's coefficients is that the driving forces are not fully captured by the concentration gradients.

Self-Diffusion Coefficients. Self-diffusion coefficients of all components are also provided in Table 5. These values can be compared to measurements, e.g., to nuclear magnetic resonance (NMR) spectroscopy. Hayamizu[38] measured the self-diffusion coefficients of all components of a 1 M $LiPF_6$ in 4:6 EC/DEC electrolyte at 303 K. The self-diffusion coefficients of EC, DEC, Li^+, and PF_6^- were (3.5, 3.60, 1.70 and 2.61) $\times 10^{-10}$ $m^2\ s^{-1}$. Notably, EC and DEC move almost equally fast in the experimental setup while in our simulations, EC moves faster than DEC. The experimental and simulated values can only be expected to be of the same order of magnitude.

Composition Dependence. The transport coefficients under isothermal conditions for the 1:1 EC/DMC with the 1 M $LiPF_6$ electrolyte are presented in Table 6. All transport coefficients in the 1:1 EC/DMC system are larger than the corresponding coefficients in the 1:1 EC/DEC electrolyte (Table 4). The resulting ionic conductivity of 1:1 EC/DMC is about twice as high as in the 1:1 EC/DEC electrolyte due to faster dynamics and improved salt dissociation with the shorter DMC molecule.

Transport coefficients for the 3:7 EC/DEC and EC/DMC systems are provided in Tables S2 and S3. By increasing the concentration of the linear carbonate, we generally obtain larger transport coefficients and increased electric conductivity. There are no dramatic changes in the transference coefficients, however.

Table 6. Transport Coefficients of the 1:1 wt.% EC/DMC + 1 M $LiPF_6$ Electrolyte in the Mixed Component Scenario Using the EC Frame of Reference. Transference Coefficients, t, and Transport Numbers, τ, Are Dimensionless

coefficient	value $\times 10^{-11}$ $m^2\ s^{-1}$	value $\times 10^{-9}$ K $mol^2\ J^{-1}\ m^{-1}\ s^{-1}$
L^{++}	1.1	18.8
L^{--}	1.9	33.4
L^{+-}	0.6	10.9
L^{D+}	4.2	72.6
L^{D-}	3.2	54.8
L^{DD}	26.9	464.5
κ	0.48 S m^{-1}	
t_L	−0.99	
t_D	0.78	
τ_+	0.26	

Thermal Polarization of the Electrolyte. We have discussed above that concentration polarization takes place in the isothermal electrolyte. In the presence of a temperature gradient, we need to include thermal polarization. When a temperature difference is applied or arises between the electrodes of an electrochemical cell, we can observe a distribution of components in the thermal field (a Soret effect) as well as migration of charges to produce a cell voltage (a Seebeck effect). The two effects are superimposed. Both effects affect the cell voltage.

Seebeck Coefficients. The Seebeck coefficient is defined as the cell potential difference measured by two identical electrodes caused by an applied temperature difference under reversible conditions with a uniform electrolyte composition. The cell potential, obtained by integrating eq 1, includes also a Soret effect via the change in the chemical potential gradients in this equation. Through the Onsager reciprocal relations, the Peltier heat of the electrode surface and from it the Peltier coefficient of the electrolyte can be computed from the Seebeck coefficient, cf. eq 11 in the Supporting Information.

The Seebeck coefficient was measured in a symmetric Li−Li cell. In these experiments, the cell was sandwiched between two copper plates; see Figure 2a for a sketch. The high temperature at the top copper plate and the low temperature at the bottom copper plate were controlled by thermostated water flowing from a water reservoir to the copper plate in question. Each copper plate with its electrode was insulated from the surroundings. The temperature difference between the electrodes was measured or computed from a calibration experiment and the temperature difference of the copper plates, cf. Figure 2b. See ref[39] for more details. The electric potential difference was measured as a function of the temperature difference between the copper plates,[4,40] see Figure 2c,d.

Figure 2d shows a typical plot of $\Delta\varphi$ as a function of ΔT for the present choice of electrolyte. From the slope of the curve in Figure 2d, we computed the Seebeck coefficient first due to thermal polarization at the start of the experiment (t = 0), when the electrolyte is still homogeneous. The slope that we derived from three measurements gave the value 1.15(20) mV K^{-1} at 300 K for the 1 M $LiPF_6$ in 1:1 (vol) EC/DEC electrolyte. The Seebeck coefficient with the 1:1 wt % EC/DMC electrolyte was determined to 1.1(1) mV K^{-1} at 300 K based on 14 measurements,[39] equal to the DEC-containing electrolyte within experimental uncertainty. This value translates into a Peltier heat of 300 K × $1.15 \times 10^{-3} \times 1 \times 10^5$ V C K mol = −34.5 kJ mol^{-1}. This is the reversible heat that is generated or absorbed at the electrode surface, here being a source at the anode boundary and a sink at the cathode boundary during operation of the battery. By subtracting the electrode contribution to the Peltier heat (S^0_{Li} = 29 J K^{-1} mol^{-1}), we computed the Peltier coefficient of the electrolyte to be 300 K × $0.86 \times 10^{-3} \times 1 \times 10^5$ V C K^{-1} mol^{-1} = −24.7

https://doi.org/10.1021/jacs.3c11589
J. Am. Chem. Soc. 2024, 146, 4592−4604

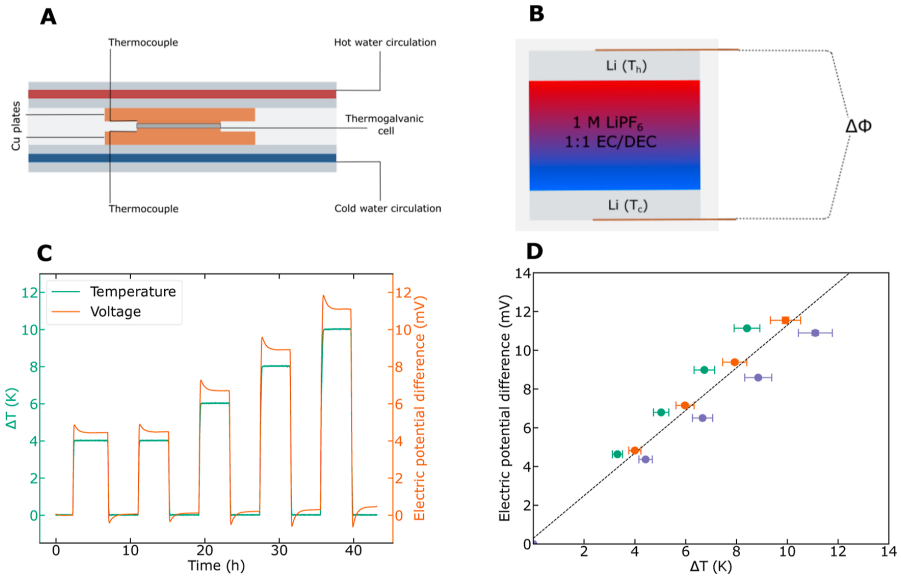

Figure 2. (a) Schematic diagram of the experimental setup for measuring Seebeck coefficients in electrolytes. (b) Close-up view of the electrolyte between hot and cold Li electrodes. (c) Temperature difference between Li electrodes and electric potential difference as a function of time in the 1 M $LiPF_6$ in 1:1 EC/DEC electrolyte. (d) Electric potential difference as a function of temperature difference in three parallel experiments on the 1 M $LiPF_6$ in 1:1 EC/DEC electrolyte. The slope of the linear line is the Seebeck coefficient.

kJ mol^{-1} using eq 12 in the Supporting Information, employing a Seebeck coefficient for the bulk electrolyte of 0.86 mV K^{-1}.

We shall see below that this Seebeck coefficient has a small contribution from the Soret effect (the heat of transfer of the salt and of DEC is small). We see from Figure 2c that the temperature difference establishes itself within minutes and that the potential difference responds uniquely to the applied temperature difference. In the present case, the initial time value did not change significantly over time, giving a first indication that the Soret effect was indeed small. The prediction was verified below.

Soret Effect. Nonequilibrium molecular dynamics (NEMD) simulations gave results for Soret equilibrium, when the thermal driving force balances the chemical driving forces or the gradients in mole fraction of the different components. The balance of forces occurs at the stationary condition ($t = \infty$) and provides the impact of thermal polarization via gradients in chemical potential, which further adds to eq 1.

We calculated the chemical potential gradients and the heats of transfer by eqs 10 and 9 in the Supporting Informtion. The gradients (and the accompanying heat flux) are given in Table 7 and example profiles are shown in Figure 3. The thermal conductivity (calculated from the heat flux and temperature gradient for the sake of completeness) is approximately 0.2 W K^{-1} m^{-1} in all cases. We find (Table 7) that the heat of transfer of the salt, q_L^*, is small (about 1 to 2 kJ mol^{-1}), which supports the fact that the first terms of π in eq 12 in the Supporting Information dominate $(\Delta\varphi/\Delta T)_{j=0}$. The heat of transfer of component DEC, q_D^*, is even smaller than q_L^* ($\leq$0.3 kJ mol^{-1}) and is not shown in Table 7. The corresponding composition profiles in Figure 3 do not deviate significantly from the equilibrium profiles obtained without a temperature gradient.

Table 7. Heat Flux and Gradients in Mole Fraction (x_i) from the NEMD Simulations. The Value of q_L* Is Evaluated at the Mean Temperature in the NEMD Simulations (330 K). The Thermodynamic Factors Γ_{Ij}^{x} Used to Calculate q_i* Are Provided in Table S1

	$J_q'\times10^{-9}$	$\partial T/\partial z$	$\partial x_i/\partial z \times 10^4$ (Å^{-1})				q_L*
system	(W m^{-2})	(K Å^{-1})	$LiPF_6$	DEC	EC	DMC	(kJ mol^{-1})
1:1 EC/DEC	2.8	−1.39	1.5	0.55	−2.1		1.6
3:7 EC/DEC	3.0	−1.45	1.3	−0.66	−0.69		1.1
1:1 EC/DMC	2.8	−1.36	1.01		0.42	−1.4	1.2
3:7 EC/DMC	3.0	−1.43	2.1		0.50	−2.6	2.2

The Soret effect is reflected in the time-dependence of the electric potential difference, when the force balance of thermal and chemical forces establishes itself; see Figure 2c. We see that the Soret effect seems to give a negative contribution to the electric potential difference. The observed effect is the sum of products of heat of transfer and transference coefficient of the independent electrolyte components times the inverse temperature.[40] The difference in the initial and stationary state values of the Seebeck coefficient was here smaller than the experimental uncertainty; therefore, no value could be extracted from the experimental data. A contribution to the relaxation from phase-change phenomena in the electrode has also been suggested.[39] For our purpose, to compute the thermal polarization, we conclude that the Soret coefficient or the heat of transfer in the present case is so small that it has a negligible impact on the gradients in chemical potential and

https://doi.org/10.1021/jacs.3c11589
J. Am. Chem. Soc. 2024, 146, 4592−4604

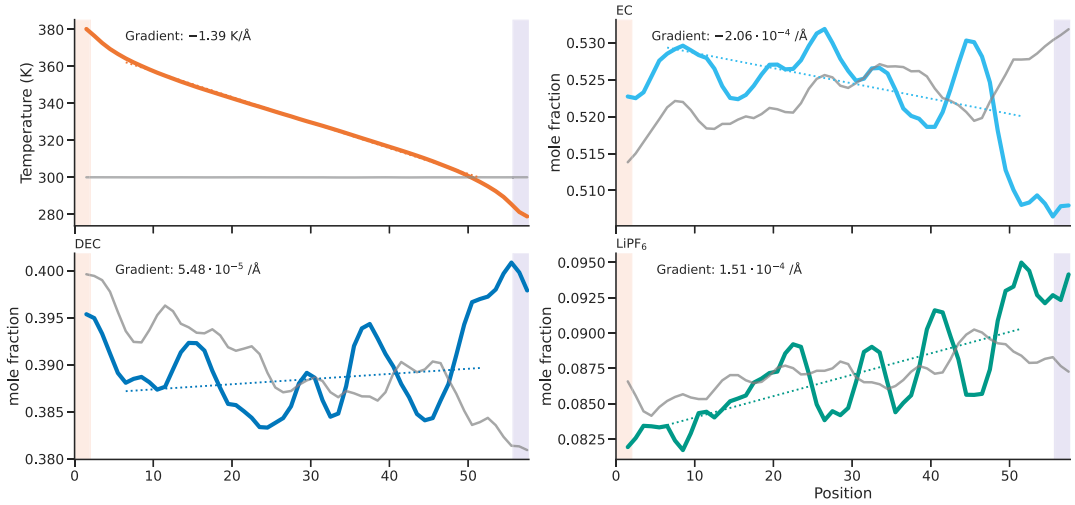

Figure 3. Profiles from the NEMD simulations of the 1 M $LiPF_6$ in the 1:1 EC/DEC system for the temperature and the mole fractions of EC, DEC, and $LiPF_6$. The gray lines show the profiles from corresponding equilibrium simulations, and the dotted lines show linear fits to the profiles used to determine the gradients. The thermostated regions are highlighted as blue (cold) and red (hot).

therefore on the thermal polarization. In a good approximation, the thermal polarization is due to the Seebeck coefficient alone. The contribution can simply be added to the concentration polarization of the cell voltage.

Total Polarization of Lithium-Ion Battery Electrolytes. We can now return to the question raised upfront; how large can we expect the concentration polarization and the thermal polarization to be in a lithium-ion battery, i.e., what are the contributions on the right-hand side of eq 1 to the battery voltage? The coefficients that entered the equation have now been defined and determined.

Consider first the events that take place when an electric current is passing through the isothermal electrolyte. Charge is transported and solvent DEC/DMC (D) is carried along, leading to the buildup of a gradient in chemical potential of both salt along with accumulation of cosolvent D. Mass transfer, or reaction heat sinks and sources, will eventually also lead to a temperature gradient. We are interested in both types of polarization, and can now compute them at the stationary state operation, when $J_D = 0$ and $J_L = 0$.

Concentration Polarization. Consider first isothermal conditions: $\nabla T = 0$. We apply eqs 2 and 3 and use one of the conditions to express the other chemical potentials.

$$0 = -l_{LL}\frac{1}{T}\nabla\mu_{L,T} - l_{LD}\frac{1}{T}\nabla\mu_{D,T} + \frac{L_{L\varphi}}{L_{\varphi\varphi}}j \tag{4}$$

$$0 = -l_{DL}\frac{1}{T}\nabla\mu_{L,T} - l_{DD}\frac{1}{T}\nabla\mu_{D,T} + \frac{L_{D\varphi}}{L_{\varphi\varphi}}j \tag{5}$$

$$\nabla\varphi = -\frac{1}{FT}t_L\nabla\mu_L - \frac{1}{FT}t_D\nabla\mu_D - j/\kappa \tag{6}$$

We introduce the transference coefficients into the flux conditions, and obtain

$$0 = -l_{LL}\frac{1}{T}\nabla\mu_{L,T} - l_{LD}\frac{1}{T}\nabla\mu_{D,T} + t_L j/F \tag{7}$$

$$0 = -l_{DL}\frac{1}{T}\nabla\mu_{L,T} - l_{DD}\frac{1}{T}\nabla\mu_{D,T} + t_D j/F \tag{8}$$

The last equation is used to express $\nabla\mu_{L,T}$, which we introduce in the equation above to give

$$A\nabla\mu_{D,T} = B\frac{j}{F} \tag{9}$$

where

$$A = \left(l_{LD} - \frac{l_{LL}l_{DD}}{l_{DL}}\right)\frac{1}{T} \tag{10}$$

and

$$B = \left(t_L - \frac{l_{LL}}{l_{DL}}t_D\right) \tag{11}$$

The solution for the isothermal electric potential difference of the cell with two lithium-reversible electrodes at stationary state becomes

$$\nabla\varphi = -\frac{t_L}{F}\left(-\frac{B}{A}\frac{l_{DD}}{l_{DL}} + t_D\frac{T}{l_{DL}}\right)\frac{j}{F} - \frac{t_D B j}{F^2 A} - \frac{j}{\kappa} \tag{12}$$

The equation describes the three types of losses described above, in electric potential on the right-hand side. All of them are proportional to the electric current density, j. The last term on the right side represents the potential ohmic loss; the central term represents loss due to a gradient in D (concentration polarization due to D), and the first term on the right side is due to the accumulation of salt at the anode, producing a peak in the chemical potential gradient of salt at this location. At the stationary state, the isothermal electric potential gradient depends only on the transport properties. This is the solution in the absence of a temperature gradient. In the presence of a temperature gradient, there is one more term, here computable from the Seebeck coefficient; see below.

https://doi.org/10.1021/jacs.3c11589
J. Am. Chem. Soc. 2024, 146, 4592−4604

For the relevant concentration polarization, we know all coefficients involved and can compute A and B in the equation above. Their values in the different electrolytes are given in Table S4. The contributions to cell voltage from salt polarization, polarization of solvent D, and ohmic loss in the different electrolytes are presented in Table 8. They are also visualized in Figure 4a.

Table 8. Potential Contributions to Cell Voltage in the Isothermal Case

electrolyte	$1/\kappa$ (Ω m)	tDF2BA (Ω m)	tLF2(−BAlDDlDL + tDTlDL) (Ω m)
1:1 EC/DEC	4.4 ± 0.7	2.4 ± 1.7	10.2 ± 4.6
3:7 EC/DEC	4.0	0.8	9.3
1:1 EC/DMC	2.2	0.7	5.3
3:7 EC/DMC	1.9	0.7	3.3

The equations and data presented enable us to evaluate the effect of concentration gradients on battery performance under operation. In order to obtain numerical insights, the typical current density j = 30 A m^{-2} used by Spitthoff et al. is considered.[41] This is a current density that can be expected when a fully charged cell is discharged within an hour (1 C rate). The current density gives $j/F = 3 \times 10^{-4}$ mol m^{-2} s^{-1}. We are now ready to calculate the various contributions to the cell voltage under isothermal conditions.

The conductivity of the 1:1 EC/DEC electrolyte is 0.23 S m^{-1} (from Table 4), resulting in an ohmic voltage drop of 132 V m^{-1}. The distance between the electrode interfaces is given by the separator thickness, which is about 20 μm.[42] In addition, the electrodes in typical commercial batteries are typically 50 to 60 μm thick.[43] For the present calculations, we assume a total distance between the electrodes of 100 μm, which is relevant for research cells. Electrodes and the separator are soaked in the electrolyte.[43] We did not evaluate the effect of porous electrodes and separator in this work but note that they will increase the concentration polarization.[2,44] This analysis assumes flat and thin Li electrodes. A gradient of 132 V m^{-1} gives a difference of 13.2 mV over 100 μm. Other contributions are of the same order of magnitude. Tables 4 and 5 give for the 1:1 EC/DEC electrolyte, $t_L = -0.97$, $t_D = 0.90$ and the diffusion coefficient ratio $l_{LD}/l_{LL} = 33.8/11.0 = 3.07$, giving $B = -1.3$. The term t_D adds to the potential drop. The coefficients of Table 4 have the common factor $\times 10^{-9}$ K mol^2 J^{-1} m^{-1} s^{-1}. With this factor, we obtain $A = -6.3 \times 10^{-11}$ mol^2 J^{-1} m^{-1} s^{-1} for the 1:1 EC/DEC electrolyte. The gradient in chemical potential of D becomes $Bj/AF = 7.17 \times 10^6$ J mol^{-1} m^{-1}, which means that there is a 717 J mol^{-1} difference in chemical potential of DEC over 100 μm. The difference amounts to 7.2 mV over this distance. The chemical potential gradients of the three components are displayed in Figure 4b. Polarization of the salt contributes between two and three times more to the voltage than the ohmic resistance. Polarization of component DEC/DMC contributes more than 10% of the total potential contributions, which is in accordance with a recent experimental study on the overpotential due to solvent polarization.[45]

We have thus computed the first, second, and third terms on the right-hand side of eq 12 to combine to (−132−72−306) V m^{-1} = −510 V m^{-1}. This gives an electric potential difference at the stationary state of 51.0 mV over the distance between the electrodes (100 μm) in the 1:1 EC/DEC electrolyte for a current density of 30 A m^{-2}, disregarding all effects due to electrodes and the separator, see Figure 4.

The potential ohmic loss is smaller in DMC-containing electrolytes due to their higher ionic conductivity. The potential contribution due to polarization of the salt in the DMC containing electrolytes is about half of the corresponding values in the DEC containing electrolytes. The relative contribution from component DMC is smaller than the contribution from component DEC.

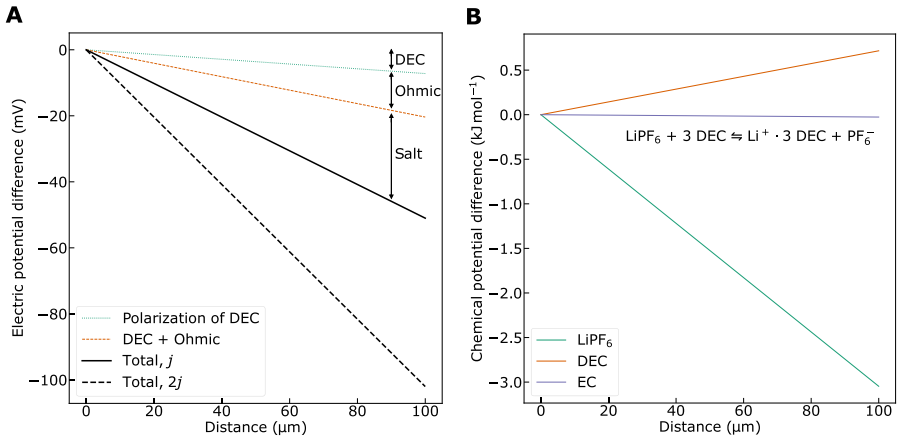

Figure 4. (a) Isothermal electrolyte contributions to electric potential difference in the stationary state as a function of distance from the anode during discharge. Contributions are shown for a current density corresponding to a discharge time of 1 h (1 C). The total polarization for a current density corresponding to a discharge time of 0.5 h (2 C) is also shown. Interface resistances are not taken into account. (b) Chemical potential gradients of the three components in the stationary state as a function of distance from the anode during discharge. The chemical potential gradient of $LiPF_6$ is negative and it is slightly positive for DEC. In the EC frame of reference, the chemical potential of EC is constant. Only relative differences matter, i.e., the starting point is arbitrary. Interface resistances are neglected.

https://doi.org/10.1021/jacs.3c11589
J. Am. Chem. Soc. 2024, 146, 4592−4604

Thermal Polarization. In this investigation, the Seebeck coefficient was 0.86 mV K^{-1} in both 1:1 EC/DEC/DMC electrolytes, while the Soret coefficient gave a negligible contribution to the cell potential at the stationary state. The thermal polarization in volt at stationary state is therefore equal to the Seebeck coefficient times the temperature gradient and the electrolyte thickness. A difference of 40 K is used here, motivated by accelerated aging experiments with externally applied thermal gradients,[46] where a severe increase in lithium plating was observed for a battery cycled under a thermal gradient. Knowledge of the temperature difference across the electrolyte is necessary to determine thermal polarization. This is difficult to measure directly due to the very short distance (~20 μm) between the anode and cathode interfaces in a battery cell. Moreover, the temperature measurement itself could potentially influence the result. Our selected temperature difference of 40 K is likely too large for normal battery operation but enables a calculation of the thermal polarization in the special case of an applied interelectrode thermal force. The contribution due to a temperature difference between the electrode surfaces to the electric potential is important but is not taken into account here.[41] The results are compared to the other contributions in Table 9. With DEC as the cosolvent, the total polarization amounts to 85.4 mV under these operating conditions. The corresponding value for DMC is 59.1 mV. This is 30% lower compared to when DEC is used and gives a clear advantage to DMC. This cosolvent leads to smaller polarization of salt and component D and a smaller ohmic loss. A concentration variation of EC/DEC/DMC from 1:1 to 3:7 will reduce the ohmic loss, salt polarization, and polarization of component DEC/DMC.

Table 9. Electrolyte Potential Contributions to Cell Voltage Assuming a Current Density of 30 A m^{-2} (1 C Rate), 100 μm Distance between Electrodes and Temperature Difference of 40 K between Flat and Thin Electrodes (Average Temperature 300 K). Conductivity and Transference Coefficients Are Assumed to Be Constant in This Temperature Range. Interface Effects Are not Considered

lectrolyte	ohmic loss (mV)	polarization of D (mV)	salt polarization (mV)	thermal polarization (mV)	sum (mV)
1:1 EC/DEC	13.2	7.2	30.6	34.4	85.4
3:7 EC/DEC	12.0	2.3	27.8		
1:1 EC/DMC	6.7	2.0	16.0	34.4	59.1
3:7 EC/DMC	5.6	2.0	9.8		

The potential contributions to the cell voltage reported in Table 9 likely depend on the temperature. The temperature dependence of the transference coefficients and the conductivity was examined by conducting equilibrium simulations of the 1:1 EC/DEC electrolyte at 280 and 320 K. The results are summarized in Table S6. The transference coefficients vary little in the temperature interval (within uncertainty). The conductivity increases nearly linearly with the temperature in the temperature interval. The potential contributions due to salt and solvent polarization decrease almost linearly with increasing temperature, so it is appropriate to use the values at 300 K as we have done above. The Seebeck coefficient shows a similar temperature dependence as entropy, which is usually small over such a limited temperature interval. We measure a linear relation between the electric potential difference and temperature in Figure 2d across a wide temperature interval, indicating a small temperature dependence of the Seebeck coefficient. We do not expect the temperature dependence to differ for the electrolyte compositions that we have studied.

CONCLUSIONS

This article presents for the first time a full set of transport coefficients needed to model the concentration and temperature polarization in a lithium-ion battery-relevant electrolyte. The coefficients were determined using a practical procedure recently established to link coefficients under two types of scenarios; for the case that ions are used as electrolyte components and for the case that there are neutral components only. In addition, we report a Seebeck coefficient of 0.86 mV K^{-1} and heats of transfer for the salt varying with concentration from 1.1 to 2.2 kJ mol^{-1}, which are small values compared to the Peltier heat. The coefficients allow us to test assumptions that are common in the literature. In the nonisothermal system, all coefficients except the Soret coefficient are significant. The Soret effect can be neglected without a loss of precision in the computation of stationary state polarization under battery operation.

The equilibrium studies of the electrolyte have confirmed earlier results on pair correlation distributions and the electrolyte structure. Diffusion coefficients are supported by less detailed observations in the literature; they have the same order of magnitude. The transport number of the lithium ion in the EC frame of reference is comparable to literature values, about 0.3, but earlier investigations did not include solvent segregation and transport of DEC. Polarization of the salt is the largest contributor to the battery voltage in the stationary state, followed by potential ohmic loss, polarization of component D, and finally thermal polarization. Regarding the alternative cosolvents, we find that DMC produces half the potential loss of DEC, giving in particular a much smaller salt polarization and ohmic loss. Regarding the solvent composition, a higher fraction of component DEC or DMC seems favorable. All terms in eq 1 contributing to the electric potential are relevant and should be taken into account for better battery modeling and understanding. We believe the framework presented here represents an improved starting point for cell-level models (which include porous electrodes and the separator) compared to current state-of-the-art physics-based models.[8,47]

EXPERIMENTAL SECTION

Equilibrium MD Simulations. All MD simulations were performed using the LAMMPS[48] code. Atomic and ionic interactions were described by the OPLS-AA[49] potential. The parameters for the solvent molecule atoms were obtained from Ligpargen.[50−52] The ionic parameters for Li^+ and PF_6^- ions were taken from Jensen et al.[53] and Acevedo et al.,[54,55] respectively. This force field has been thoroughly investigated for modeling of lithium-ion battery electrolytes and is a good compromise of accuracy and computational efficiency. Real-space Lennard-Jones and Coulombic forces were cutoff at 13 Å. A Lennard-Jones tail correction was added to the energy and pressure.[56] Coulombic forces beyond the cutoff were computed in reciprocal space using a particle−particle particle-mesh solver[57] with a relative error in forces of 10^{-6}. The ionic charges were scaled by a factor of 0.75 to correct for the overestimation of electrostatic interactions

https://doi.org/10.1021/jacs.3c11589
J. Am. Chem. Soc. 2024, 146, 4592−4604

between ions in nonpolarizable force fields.[58] Packmol and Moltemplate were used to prepare initial configurations of the systems by randomly placing solvent molecules Li^+ and PF_6^- in a simulation box. The 1:1 wt % EC/DEC +1 M $LiPF_6$ model electrolyte contained 5520 EC molecules, 4116 DEC molecules, and 920 $LiPF_6$. Periodicity was applied in all dimensions.

The equilibration procedure is described in the following. First, the energies of the systems were minimized to avoid particle overlap. Initial equilibration was performed according to the method developed by Molinari et al.[59] The systems were further equilibrated at a temperature of 350 K or higher and a pressure of 1 atm in the isobaric−isothermal (*NPT*) ensemble using a time step of 1.25 fs in order for the potential energy and density of the systems to stabilize. The temperature and pressure were controlled by the Nosé-Hoover thermostat and barostat[60−62] using time constants resulting in characteristic fluctuations of 100 and 1000 time steps, respectively. The final equilibration in the *NPT* ensemble was conducted with a temperature of 300 K and pressure of 1 atm while sampling the box volume, and the simulation box size was scaled to the average volume at the end to obtain the correct density. The transport properties were sampled in the canonical ensemble (*NVT*) at 300 K using a time step of 1.25 fs in simulations running for at least 80 ns, which was sufficient to reach the diffusive regime. The Nosé-Hoover thermostat was used in the *NVT* ensemble. The Onsager coefficients of Tables 4 and 6 for the ions and the solvent (mixed component scenario), L^{++}, L^{+-}, L^{--}, L^{+D}, L^{-D}, and L^{DD}, and the RDFs for computing Kirkwood-Buff integrals were obtained using the OCTP module[63] for LAMMPS. The Onsager coefficients shown in Table 4 and 5 for the salt and the solvents (neutral component scenario), L_{LL}, L_{LD}, L_{DL}, and L_{DD}, were computed from the set of coefficients in Table 4. The Fickian coefficients in Table 5 were computed using equations in ref[6]. Three parallel simulations were performed from independent starting configurations for the 1:1 EC/DEC +1 M $LiPF_6$ system. Data are presented as the mean of three values with the standard deviation. The other systems were simulated only once.

Nonequilibrium MD Simulations. In order to obtain heats of transfer, a temperature gradient was set up in the *z*-direction by thermostatting the center and edge regions of the simulation box to 280 and 380 K, respectively. Both regions were 4 Å thick, and they were spanning the whole box in the two other dimensions. The edge region was placed such that its center was at the box boundary. The thermostatting was conducted by explicitly rescaling the atom velocities every 10 timesteps. The system was allowed to equilibrate for at least 30 ns using a time step of 1 fs to ensure that a stationary state was reached before sampling the composition profile of the components in the box. The linear momentum of all particles in the box was reset every time step to avoid drift. The volume of the box was held constant during the nonequilibrium simulations. Composition profiles of the components in the simulation box were calculated by sampling the number of the various components in layers of 1 Å thickness. The number of salt molecules inside a layer was defined as the number of cations and anions divided by two.

Determination of Seebeck Coefficients. *Cell Assembly.* The thermogalvanic cells were assembled as pouch-cells in an argon-filled glovebox. A PC8 pouch-cell laminate from Targray was used as the cell housing. The thermogalvanic cells had a symmetric electrode arrangement, using lithium-chips from Tmax (0.25 mm thick and with a diameter of 15.6 mm). Copper foil was used as a tab for electric potential difference measurements with one part embedded in the cell on the backside of the lithium chips and the other part outside the pouch. A polypropylene tape film was used to reinforce the seal around the tab. A stack of 4 Whatman Glass Microfibre Filters GF/D (no 1823070, pore diameter of 2.7 μm) were used as a separator. The stack was sandwiched between the two electrodes and had a thickness of 1.8 mm after vacuum sealing. The electrolyte was 1 M $LiPF_6$ in a 1:1 wt % EC/DEC (LP40) from Gotion. Electrolyte was added to the separators until the separators were soaked but not dripping, approximately 1 mL per cell. The pouch cells were sealed with an Audion VMS 53 Vacuum Chamber. The lowest pressure was reached after 15 s, and the cells spent 25−45 s at this pressure before the cells were sealed. We found no dependence on the time spent under vacuum.

Thermogalvanic Cell Measurements. Prior to measurement, the cells were equilibrated by short-circuiting and allowed to reach a stable electric potential difference at isothermal conditions. The thermogalvanic cell was sandwiched between two copper plates within a frame of two aluminum plates (see Figure 2a). A temperature gradient was applied by circulating water in the aluminum frames (see Figure 2a) using two water baths (Grant Ecocool 150R) set to different temperatures. Hot water was circulating in the top plate and cold water in the bottom plate. The electric potential difference between the hot electrode (defined as the positive electrode) and the cool electrode (defined as the negative) was recorded with an Agilent 34970A Data acquisition/Switch unit. A bias potential of typically ±0.3 mV was recorded prior to and in-between the measurements and subtracted from the reading. Type K thermocouples were placed between the copper plates to measure the external temperature difference during the experiment.

The internal temperature difference was found from a calibration experiment with thermocouples embedded in the pouch, cf. ref 39. The temperature between the cell housing and the lithium electrode was measured by two type K thermocouples stripped of the insulation in three Li-symmetric cells. At the same time, the external temperature difference was controlled. The ratio of the two differences was 0.66 ± 0.06.[39]

■ ASSOCIATED CONTENT

Supporting Information

The Supporting Information is available free of charge at https://pubs.acs.org/doi/10.1021/jacs.3c11589.

Calculation of thermodynamic factors from Kirkwood-Buff integrals; determination of heats of transfer and Seebeck coefficients; and isothermal diffusion coefficients for the additional electrolyte systems (PDF)

■ AUTHOR INFORMATION

Corresponding Author

Sondre Kvalvåg Schnell − *Department of Materials Science and Engineering, Norwegian University of Science and Technology, NTNU, N-7491 Trondheim, Norway;* orcid.org/0000-0002-0664-6756; Email: sondre.k.schnell@ntnu.no

Authors

Øystein Gullbrekken − *Department of Materials Science and Engineering, Norwegian University of Science and Technology, NTNU, N-7491 Trondheim, Norway;* orcid.org/0000-0002-2413-0120

Astrid Fagertun Gunnarshaug − *PoreLab, Department of Chemistry, Norwegian University of Science and Technology, NTNU, N-7491 Trondheim, Norway*

Anders Lervik − *PoreLab, Department of Chemistry, Norwegian University of Science and Technology, NTNU, N-7491 Trondheim, Norway*

Signe Kjelstrup − *PoreLab, Department of Chemistry, Norwegian University of Science and Technology, NTNU, N-7491 Trondheim, Norway;* orcid.org/0000-0003-1235-5709

Complete contact information is available at: https://pubs.acs.org/10.1021/jacs.3c11589

Notes

The authors declare no competing financial interest.

https://doi.org/10.1021/jacs.3c11589
J. Am. Chem. Soc. 2024, 146, 4592−4604

■ ACKNOWLEDGMENTS

A.F.G., S.K., S.K.S., and A.L. are grateful to the Norwegian Research Council Center of Excellence Funding Scheme, for project no 262644 Porelab. ØG acknowledges the Research Council of Norway for the support to the Norwegian Micro- and Nano-Fabrication Facility, NorFab, project number 295864. S.K.S. acknowledges financial support from NRC through project 275754. The simulations were performed on resources provided by Sigma2 - the National Infrastructure for High Performance Computing and Data Storage in Norway through the projects NN9264K and NN9414K.

■ REFERENCES

(1) Newman, J.; Bennion, D.; Tobias, C. W. Mass Transfer in Concentrated Binary Electrolytes. *Ber. Bunsenges. Phys. Chem.* **1965**, *69*, 608−612.
(2) Chandrasekaran, R. Quantification of contributions to the cell overpotential during galvanostatic discharge of a lithium-ion cell. *J. Power Sources* **2014**, *262*, 501−513.
(3) Xu, K. Li-ion battery electrolytes. *Nat. Energy* **2021**, *6*, 763.
(4) Gunnarshaug, A. F.; Vie, P. J. S.; Kjelstrup, S. ReviewReversible Heat Effects in Cells Relevant for Lithium-Ion Batteries. *J. Electrochem. Soc.* **2021**, *168*, 050522.
(5) Førland, K.; Førland, T.; Kjelstrup Ratkje, S. *Irreversible Thermodynamics. Theory and Applications*; Wiley: Chichester, 1988.
(6) Kjelstrup, S.; Gunnarshaug, A. F.; Gullbrekken, Ø.; Schnell, S. K.; Lervik, A. Transport coefficients for ion and solvent coupling. The case of the lithium-ion battery electrolyte. *J. Chem. Phys.* **2023**, *159*, 034104.
(7) Newman, J. *Electrochemical Systems*, 2nd ed.; Prentice-Hall, 1991.
(8) Wang, A. A.; O'Kane, S. E. J.; Brosa Planella, F.; Houx, J. L.; O'Regan, K.; Zyskin, M.; Edge, J.; Monroe, C. W.; Cooper, S. J.; Howey, D. A.; Kendrick, E.; Foster, J. M. Review of parameterisation and a novel database (LiionDB) for continuum Li-ion battery models. *Prog. Energy* **2022**, *4*, 032004.
(9) Valøen, L. O.; Reimers, J. N. Transport Properties of $LiPF_6$-Based Li-Ion Battery Electrolytes. *J. Electrochem. Soc.* **2005**, *152*, A882.
(10) Landesfeind, J.; Gasteiger, H. A. Temperature and Concentration Dependence of the Ionic Transport Properties of Lithium-Ion Battery Electrolytes. *J. Electrochem. Soc.* **2019**, *166*, A3079−A3097.
(11) Lundgren, H.; Behm, M.; Lindbergh, G. Electrochemical Characterization and Temperature Dependency of Mass-Transport Properties of $LiPF_6$ in EC:DEC. *J. Electrochem. Soc.* **2015**, *162*, A413−A420.
(12) Newman, J.; Thomas, K. E.; Hafezi, H.; Wheeler, D. R. Modeling of lithium-ion batteries. *J. Power Sources* **2003**, *119*−*121*, 838−843.
(13) Wang, A. A.; Greenbank, S.; Li, G.; Howey, D. A.; Monroe, C. W. Current-driven solvent segregation in lithium-ion electrolytes. *Cell Rep. Phys. Sci.* **2022**, *3*, 101047.
(14) Mistry, A.; Srinivasan, V. Do we need an accurate understanding of transport in electrolytes? *Joule* **2021**, *5*, 2773−2776.
(15) Ratkje, S. K.; Rajabu, H.; Førland, T. Transference coefficients and transference numbers in salt mixtures relevant for the aluminium electrolysis. *Electrochim. Acta* **1993**, *38*, 415−423.
(16) Shao, Y.; Gudla, H.; Brandell, D.; Zhang, C. Transference Number in Polymer Electrolytes: Mind the Reference-Frame Gap. *J. Am. Chem. Soc.* **2022**, *144*, 7583−7587.
(17) Zhao, W.; Leroy, F.; Heggen, B.; Zahn, S.; Kirchner, B.; Balasubramanian, S.; Müller-Plathe, F. Are There Stable Ion-Pairs in Room-Temperature Ionic Liquids? Molecular Dynamics Simulations of 1-n-Butyl-3-methylimidazolium Hexafluorophosphate. *J. Am. Chem. Soc.* **2009**, *131*, 15825−15833.
(18) Fong, K. D.; Self, J.; Diederichsen, K. M.; Wood, B. M.; McCloskey, B. D.; Persson, K. A. Ion Transport and the True Transference Number in Nonaqueous Polyelectrolyte Solutions for Lithium Ion Batteries. *ACS Cent. Sci.* **2019**, *5*, 1250−1260.
(19) Zhang, Y.; Maginn, E. J. Direct Correlation between Ionic Liquid Transport Properties and Ion Pair Lifetimes: A Molecular Dynamics Study. *J. Phys. Chem. Lett.* **2015**, *6*, 700−705.
(20) Morita, M.; Asai, Y.; Yoshimoto, N.; Ishikawa, M. A Raman spectroscopic study of organic electrolyte solutions based on binary solvent systems of ethylene carbonate with low viscosity solvents which dissolve different lithium salts. *J. Chem. Soc., Faraday Trans.* **1998**, *94*, 3451−3456.
(21) Borodin, O.; Olguin, M.; Ganesh, P.; Kent, P. R. C.; Allen, J. L.; Henderson, W. A. Competitive lithium solvation of linear and cyclic carbonates from quantum chemistry. *Phys. Chem. Chem. Phys.* **2016**, *18*, 164−175.
(22) Xu, K.; Lam, Y.; Zhang, S. S.; Jow, T. R.; Curtis, T. B. Solvation Sheath of Li^+ in Nonaqueous Electrolytes and Its Implication of Graphite/Electrolyte Interface Chemistry. *J. Phys. Chem. C* **2007**, *111*, 7411−7421.
(23) Uchida, S.; Kiyobayashi, T. What differentiates the transport properties of lithium electrolyte in ethylene carbonate mixed with diethylcarbonate from those mixed with dimethylcarbonate? *J. Power Sources* **2021**, *511*, 230423.
(24) von Wald Cresce, A.; Borodin, O.; Xu, K. Correlating Li^+ Solvation Sheath Structure with Interphasial Chemistry on Graphite. *J. Phys. Chem. C* **2012**, *116*, 26111−26117.
(25) Yang, L.; Xiao, A.; Lucht, B. L. Investigation of solvation in lithium ion battery electrolytes by NMR spectroscopy. *J. Mol. Liq.* **2010**, *154*, 131−133.
(26) Tenney, C. M.; Cygan, R. T. Analysis of Molecular Clusters in Simulations of Lithium-Ion Battery Electrolytes. *J. Phys. Chem. C* **2013**, *117*, 24673−24684.
(27) Seo, D. M.; Reininger, S.; Kutcher, M.; Redmond, K.; Euler, W. B.; Lucht, B. L. Role of Mixed Solvation and Ion Pairing in the Solution Structure of Lithium Ion Battery Electrolytes. *J. Phys. Chem. C* **2015**, *119*, 14038−14046.
(28) Skarmoutsos, I.; Ponnuchamy, V.; Vetere, V.; Mossa, S. Li^+ Solvation in Pure, Binary, and Ternary Mixtures of Organic Carbonate Electrolytes. *J. Phys. Chem. C* **2015**, *119*, 4502−4515.
(29) Borodin, O.; Smith, G. D. Quantum Chemistry and Molecular Dynamics Simulation Study of Dimethyl Carbonate: Ethylene Carbonate Electrolytes Doped with $LiPF_6$. *J. Phys. Chem. B* **2009**, *113*, 1763−1776.
(30) Lee, H.; Hwang, S.; Kim, M.; Kwak, K.; Lee, J.; Han, Y.-K.; Lee, H. Why Does Dimethyl Carbonate Dissociate Li Salt Better Than Other Linear Carbonates? Critical Role of Polar Conformers. *J. Phys. Chem. Lett.* **2020**, *11*, 10382−10387.
(31) Simon, J.-M.; Krüger, P.; Schnell, S. K.; Vlugt, T. J. H.; Kjelstrup, S.; Bedeaux, D. KirkwoodBuff integrals: From fluctuations in finite volumes to the thermodynamic limit. *J. Chem. Phys.* **2022**, *157*, 130901.
(32) Thomas, K. E.; Newman, J.; Darling, R. M. *Mathematical Modeling of Lithium Batteries*; Springer, 2002.
(33) Ma, Y.; Doyle, M.; Fuller, T. F.; Doeff, M. M.; De Jonghe, L. C.; Newman, J. The Measurement of a Complete Set of Transport Properties for a Concentrated Solid Polymer Electrolyte Solution. *J. Electrochem. Soc.* **1995**, *142*, 1859−1868.
(34) Pesko, D. M.; Sawhney, S.; Newman, J.; Balsara, N. P. Comparing Two Electrochemical Approaches for Measuring Transference Numbers in Concentrated Electrolytes. *J. Electrochem. Soc.* **2018**, *165*, A3014−A3021.
(35) Mistry, A.; Grundy, L. S.; Halat, D. M.; Newman, J.; Balsara, N. P.; Srinivasan, V. Effect of Solvent Motion on Ion Transport in Electrolytes. *J. Electrochem. Soc.* **2022**, *169*, 040524.
(36) Gullbrekken, Ø.; Kvalvåg Schnell, S. Coupled ion transport in concentrated PEO-LiTFSI polymer electrolytes. *New J. Chem.* **2023**, *47*, 20344−20357.
(37) Kjelstrup, S.; Kristiansen, K. R.; Gunnarshaug, A. F.; Bedeaux, D. Seebeck, Peltier, and Soret effects: On different formalisms for transport equations in thermogalvanic cells. *J. Chem. Phys.* **2023**, *158*, 020901.

https://doi.org/10.1021/jacs.3c11589
J. Am. Chem. Soc. 2024, 146, 4592−4604

(38) Hayamizu, K. Temperature Dependence of Self-Diffusion Coefficients of Ions and Solvents in Ethylene Carbonate, Propylene Carbonate, and Diethyl Carbonate Single Solutions and Ethylene Carbonate + Diethyl Carbonate Binary Solutions of $LiPF_6$ Studied by NMR. *J. Chem. Eng. Data* **2012**, *57*, 2012−2017.
(39) Gunnarshaug, A. F.; Burheim, O. S.; Kjelstrup, S. Reversible heat effects of lithium metal- and porous lithium iron phosphate electrodes. *Electrochim. Acta* **2023**, *462*, 142739.
(40) Gunnarshaug, A. F.; Kjelstrup, S.; Bedeaux, D.; Richter, F.; Burheim, O. S. The reversible heat effects at lithium iron phosphate- and graphite electrodes. *Electrochim. Acta* **2020**, *337*, 135567.
(41) Spitthoff, L.; Gunnarshaug, A. F.; Bedeaux, D.; Burheim, O.; Kjelstrup, S. Peltier effects in lithium-ion battery modeling. *J. Chem. Phys.* **2021**, *154*, 114705.
(42) Parikh, D.; Christensen, T.; Hsieh, C.-T.; Li, J. Elucidation of Separator Effect on Energy Density of Li-Ion Batteries. *J. Electrochem. Soc.* **2019**, *166*, A3377−A3383.
(43) Singh, M.; Kaiser, J.; Hahn, H. Thick Electrodes for High Energy Lithium Ion Batteries. *J. Electrochem. Soc.* **2015**, *162*, A1196−A1201.
(44) Thorat, I. V.; Stephenson, D. E.; Zacharias, N. A.; Zaghib, K.; Harb, J. N.; Wheeler, D. R. Quantifying tortuosity in porous Li-ion battery materials. *J. Power Sources* **2009**, *188*, 592−600.
(45) Jung, T.; Wang, A. A.; Monroe, C. W. Overpotential from Cosolvent Imbalance in Battery Electrolytes: $LiPF_6$ in EMC:EC. *ACS Omega* **2023**, *8*, 21133−21144.
(46) Carter, R.; Love, C. T. Modulation of Lithium Plating in Li-Ion Batteries with External Thermal Gradient. *ACS Appl. Mater. Interfaces* **2018**, *10*, 26328−26334.
(47) Andersson, M.; Streb, M.; Ko, J. Y.; Löfqvist Klass, V.; Klett, M.; Ekström, H.; Johansson, M.; Lindbergh, G. Parametrization of physics-based battery models from inputoutput data: A review of methodology and current research. *J. Power Sources* **2022**, *521*, 230859.
(48) Thompson, A. P.; Aktulga, H. M.; Berger, R.; Bolintineanu, D. S.; Brown, W. M.; Crozier, P. S.; in 't Veld, P. J.; Kohlmeyer, A.; Moore, S. G.; Nguyen, T. D.; Shan, R.; Stevens, M. J.; Tranchida, J.; Trott, C.; Plimpton, S. J. LAMMPS - a flexible simulation tool for particle-based materials modeling at the atomic, meso, and continuum scales. *Comput. Phys. Commun.* **2022**, *271*, 108171.
(49) Jorgensen, W. L.; Madura, J. D.; Swenson, C. J. Optimized intermolecular potential functions for liquid hydrocarbons. *J. Am. Chem. Soc.* **1984**, *106*, 6638−6646.
(50) Jorgensen, W. L.; Tirado-Rives, J. Potential energy functions for atomic-level simulations of water and organic and biomolecular systems. *Proc. Natl. Acad. Sci. U.S.A.* **2005**, *102*, 6665−6670.
(51) Dodda, L. S.; Vilseck, J. Z.; Tirado-Rives, J.; Jorgensen, W. L. 1.14*CM1A-LBCC: Localized Bond-Charge Corrected CM1A Charges for Condensed-Phase Simulations. *J. Phys. Chem. B* **2017**, *121*, 3864−3870.
(52) Dodda, L. S.; Cabeza de Vaca, I.; Tirado-Rives, J.; Jorgensen, W. L. LigParGen web server: an automatic OPLS-AA parameter generator for organic ligands. *Nucleic Acids Res.* **2017**, *45*, W331−W336.
(53) Jensen, K. P.; Jorgensen, W. L. Halide, Ammonium, and Alkali Metal Ion Parameters for Modeling Aqueous Solutions. *J. Chem. Theory Comput.* **2006**, *2*, 1499−1509.
(54) Sambasivarao, S. V.; Acevedo, O. Development of OPLS-AA Force Field Parameters for 68 Unique Ionic Liquids. *J. Chem. Theory Comput.* **2009**, *5*, 1038−1050.
(55) Doherty, B.; Zhong, X.; Gathiaka, S.; Li, B.; Acevedo, O. Revisiting OPLS Force Field Parameters for Ionic Liquid Simulations. *J. Chem. Theory Comput.* **2017**, *13*, 6131−6145.
(56) Frenkel, D.; Smit, B. *Understanding Molecular Simulation*, 2nd ed.; Academic Press: San Diego, 2002.
(57) Hockney, R. W.; Eastwood, J. W. *Computer Simulation Using Particles*; Hilger: Bristol, 1988.
(58) Leontyev, I.; Stuchebrukhov, A. Accounting for electronic polarization in non-polarizable force fields. *Phys. Chem. Chem. Phys.* **2011**, *13*, 2613−2626.
(59) Molinari, N.; Mailoa, J. P.; Kozinsky, B. Effect of Salt Concentration on Ion Clustering and Transport in Polymer Solid Electrolytes: A Molecular Dynamics Study of PEO-LiTFSI. *Chem. Mater.* **2018**, *30*, 6298−6306.
(60) Shinoda, W.; Shiga, M.; Mikami, M. Rapid estimation of elastic constants by molecular dynamics simulation under constant stress. *Phys. Rev. B* **2004**, *69*, 134103.
(61) Hoover, W. G. Canonical dynamics: Equilibrium phase-space distributions. *Phys. Rev. A* **1985**, *31*, 1695−1697.
(62) Nosé, S. A molecular dynamics method for simulations in the canonical ensemble. *Mol. Phys.* **1984**, *52*, 255−268.
(63) Jamali, S. H.; Wolff, L.; Becker, T. M.; de Groen, M.; Ramdin, M.; Hartkamp, R.; Bardow, A.; Vlugt, T. J. H.; Moultos, O. A. OCTP: A Tool for On-the-Fly Calculation of Transport Properties of Fluids with the Order-n Algorithm in LAMMPS. *J. Chem. Inf. Model.* **2019**, *59*, 1290−1294.

https://doi.org/10.1021/jacs.3c11589
J. Am. Chem. Soc. 2024, 146, 4592−4604

Supporting Information: The effect of ion-, solvent- and thermal interaction coefficients on battery voltage

Øystein Gullbrekken,[†] Astrid Fagertun Gunnarshaug,[‡] Anders Lervik,[‡] Signe Kjelstrup,[‡] and Sondre Kvalvåg Schnell[*,†]

[†]*Department of Materials Science and Engineering, Norwegian University of Science and Technology, NTNU, N-7491 Trondheim, Norway*

[‡]*PoreLab, Department of Chemistry, Norwegian University of Science and Technology, NTNU, N-7491 Trondheim, Norway*

E-mail: sondre.k.schnell@ntnu.no

Electrolyte thermodynamic factors

The thermodynamic factor is a way to describe deviations from ideality of a mixture. The relation between the common activity coefficient and the thermodynamic factor is unique, and a transformation from one set of coefficients to another can be done. The thermodynamic factors are defined by,

$$\Gamma^{x}_{ij} = \delta_{ij} + x_i \left(\frac{\partial \ln \gamma_i}{\partial x_j} \right)_{T,p,\sum} \tag{1}$$

where δ_{ij} is the Kronecker delta, γ_i the activity coefficient of component i, and the subscript $\sum$ indicates that the partial derivative is taken at constant mole fraction of all components, except for the nth one. Superscript x indicates that the thermodynamic factors are calculated using mole fractions. Thermodynamic factors can also be calculated using the concentration

as a basis[S1]. Γ^x_{ij} is determined from the equilibrium simulations by evaluating the Kirkwood-Buff integrals[S2,S3]:

$$G_{ij} = 4\pi \int_0^\infty (g_{ij}(r) - 1)\, r^2 \mathrm{d}r, \tag{2}$$

where $g_{ij}(r)$ is the pair distribution function. The radial distribution functions were calculated using the OCTP plugin[S4] for LAMMPS with the finite-size correction method of van der Vegt et al.[S5,S6]. For evaluating the integrals in Eq. (2), we have used the finite-size correction of Krüger et al.[S7] and one example of the extrapolation is shown in Figure S1 for the 1 M $LiPF_6$ in EC:DEC system.

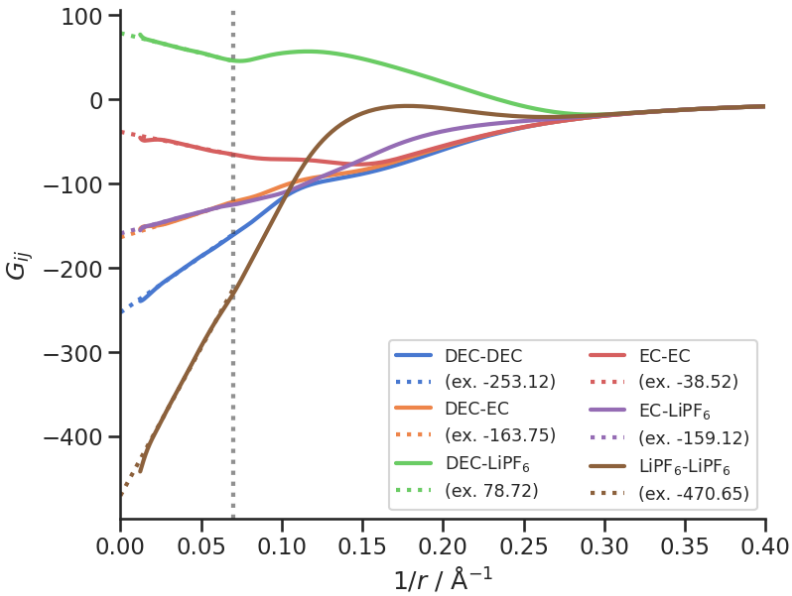

Figure S1: Calculation of G_{ij} by linear extrapolation for the 1 M $LiPF_6$ in EC:DEC system. The dotted vertical line shows the start of the linear extrapolation and the extrapolated values are given in the legend (as the values following "ex.").

Relations between G_{ij} and Γ^x_{ij} for a ternary system are given by Liu et al.[S3] and Krishna

et al.[S8]:

$$\Gamma^x_{11} = -\frac{1}{\eta}\big(- c_2c_3G_{22} - c_2 + 2c_2c_3G_{23} - c_2c_3G_{33} - c_3 + c_1\left(c_2G_{12} - c_2G_{22} - 1 + c_2G_{23} - c_2G_{13}\right)\big), \tag{3}$$

$$\Gamma^x_{12} = -\frac{c_1}{\eta}\big(c_2G_{12} + c_3G_{12} - c_2G_{13} - c_3G_{13} - c_2G_{22} + c_2G_{23} - c_3G_{23} + c_3G_{33}\big), \tag{4}$$

$$\Gamma^x_{21} = \frac{c_2}{\eta}\big(c_1G_{11} - c_1G_{12} - c_3G_{12} - c_1G_{13} + c_3G_{13} + c_1G_{23} + c_3G_{23} - c_3G_{33}\big), \tag{5}$$

$$\Gamma^x_{22} = \frac{1}{\eta}\big(c_1c_3G_{11} + c_1 - 2c_1c_3G_{13} + c_1c_3G_{33} + c_3 + c_2\left(c_1G_{11} - c_1G_{12} - c_1G_{13} + 1 + c_1G_{23}\right)\big), \tag{6}$$

where c_i is the molar concentration of i and,

$$\begin{aligned}\eta =& c_1 + c_2 + c_3 + c_1c_2\Delta G_{12} + c_2c_3\Delta G_{23} + c_1c_3\Delta G_{13} \\ &- \frac{1}{4}c_1c_2c_3\big(\Delta G^2_{12} + \Delta G^2_{23} + \Delta G^2_{13} - 2\Delta G_{13}\Delta G_{23} \\ &- 2\Delta G_{12}\Delta G_{13} - 2\Delta G_{12}\Delta G_{23}\big),\end{aligned} \tag{7}$$

and,

$$\Delta G_{ij} = G_{ii} + G_{jj} - 2G_{ij}. \tag{8}$$

For the evaluation of the thermodynamic factors, EC has been taken as the reference (component 3).

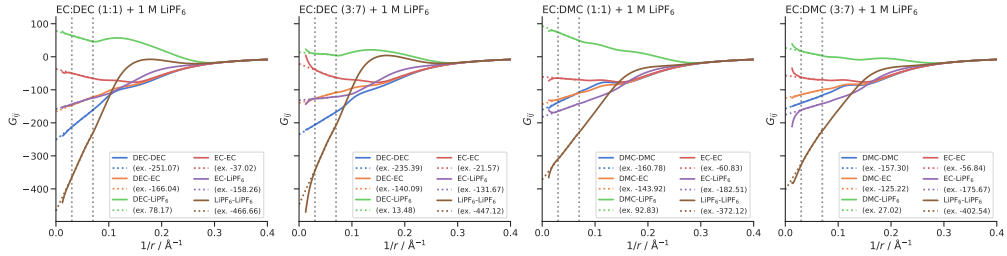

Figure S2: Kirkwood-Buff integrals as a function of inverse distance for the four electrolytes studied. The regions used for linear regression to find the intercepts of the curves are displayed by dotted vertical lines.

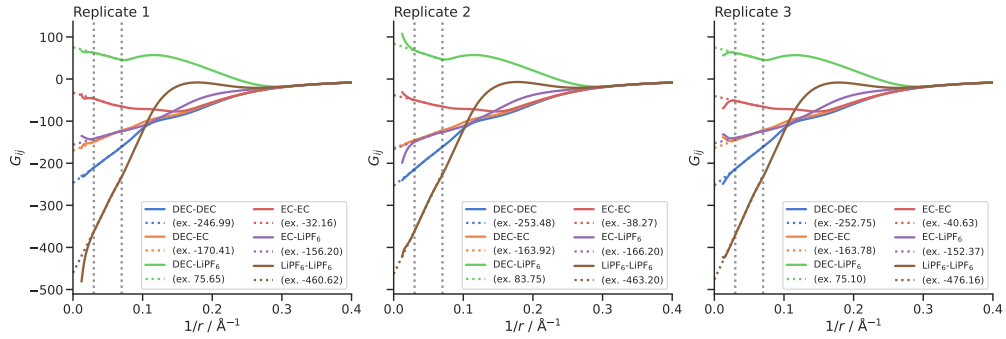

Figure S3: Kirkwood-Buff integrals as a function of inverse distance for the three replicates of the 1:1 EC:DEC electrolyte. The regions used for linear regression to find the intercepts of the curves are displayed by dotted vertical lines.

Thermal coefficients

The heat of transfer can be computed from composition gradients once we have the thermodynamic factors, Γ^x_{ij}. In the stationary state for transport of salt, we obtain

$$q^*_{\mathrm{L}} = \left(\frac{J'^N_q}{J_{\mathrm{L}}}\right)_{J_{\mathrm{D}}=0,j=0,dT=0} = -T\left(\frac{\nabla\mu_{\mathrm{L},T}}{\nabla T}\right)_{J_{\mathrm{L}}=J_{\mathrm{D}}=0,j=0} \tag{9}$$

An equivalent expression can be found for D. In both cases, ∇T is directly measured and $\nabla \mu_{\mathrm{i},T}$ for $i = \mathrm{L}$ or D is determined from

$$\nabla \mu_{i,T} = \sum_{j=1}^{2} \Gamma_{ij}^{x} \frac{RT}{x_j} \nabla x_j, \tag{10}$$

where R is the gas constant and x_j is the mole fraction of (independent) components $j = \mathrm{L}$ or D. The gradient in the mole fraction ∇x_j is determined in non-equilibrium simulations, and Γ_{ij}^{x} is determined from equilibrium simulations by evaluating equation (2).

The aim of the present investigation is to compute the electric potential gradient across the electrolyte from the last line in equation 2 in the main text. This can be done with knowledge of the conductivity $L_{\varphi\varphi}/T$ and the transference coefficients $t_i = F(L_{i\varphi}/L_{\varphi\varphi})$. These coefficients can be obtained from equilibrium simulations, using fluctuation-dissipation theorems. The heat of transfer can be determined from non-equilibrium simulations by setting up a heat flux and measuring the resulting composition gradients.

The Peltier coefficient on the other hand is not directly obtainable from simulations. It will here be determined from Seebeck coefficient measurements. By using the Onsager relations, we obtain the identity

$$\left(\frac{\pi}{T}\right)_{dT=0,d\mu_i=0} = -F \left(\frac{\Delta\varphi}{\Delta T}\right)_{j=0,d\mu_i=0}. \tag{11}$$

The expression applies to a subsystem as well as to the whole measuring cell. The single contributions to the Peltier heat was obtained for this cell from the entropy balance[S9]:

$$\pi = T \left(S^*_{\mathrm{Li}^+} + S^*_{\mathrm{e}^-} - S_{\mathrm{Li}}\right) + \sum_{i=1}^{2} t_i q_i^* \tag{12}$$

Here S_i^* are transported entropies of the lithium ion and the electron, respectively, S_{Li} is the entropy of lithium. The heat of transfer and the transference coefficients were defined above. The transported entropy of the electron is assumed to be small.

Table S1: Thermodynamic factors (Γ^x_{ij}, L = $LiPF_6$, D = DEC or DMC) used to calculate heats of transfer.

System	Γ^x_{LL}	Γ^x_{LD}	Γ^x_{DL}	Γ^x_{DD}
1:1 EC:DEC + 1 M $LiPF_6$	1.45	−0.28	−0.94	1.19
3:7 EC:DEC + 1 M $LiPF_6$	1.41	−0.22	−0.72	1.20
1:1 EC:DMC + 1 M $LiPF_6$	1.40	−0.26	−1.00	1.16
3:7 EC:DMC + 1 M $LiPF_6$	1.35	−0.21	−0.75	1.16

The equilibrium structure of the electrolyte

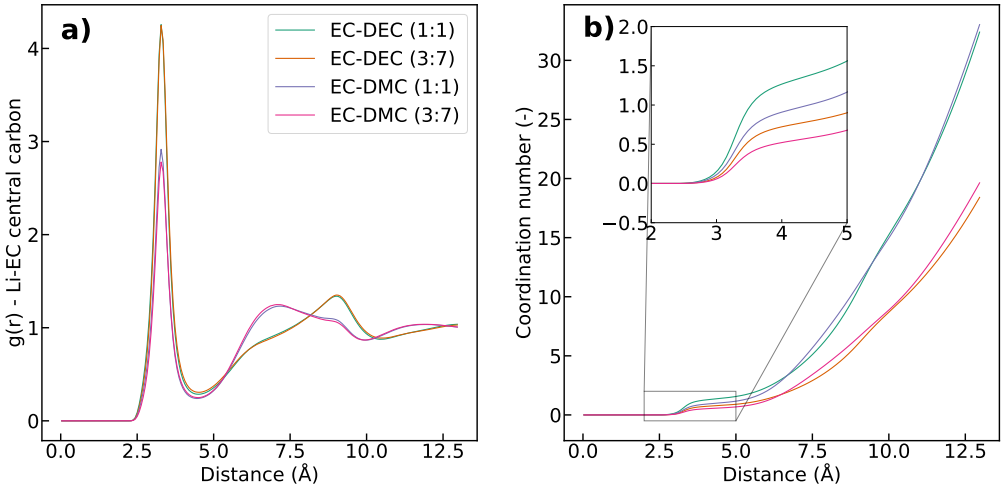

Figure S4: (a) Radial distribution functions and (b) coordination numbers of the central carbon atom of EC around Li.

In Tables S2, S3 and S4, the coefficients are obtained using Eq. (13) in the barycentric (B) frame of reference, and converted to the EC- and DEC frames of reference. The conversion is shown in Ref. S1. As described by Liu et al.[S3], the barycentric Onsager coefficients, Λ_{ij}, can be directly obtained in MD simulations from the particle displacements as a function of

time,

$$\Lambda_{ij} = \frac{1}{6} \lim_{m\to\infty} \frac{1}{N} \frac{1}{m\Delta t} \langle (\sum_{l=1}^{N_i} (r_{l,i}(t+m\Delta t) - r_{l,i}(t))) \times (\sum_{k=1}^{N_j} (r_{k,j}(t+m\Delta t) - r_{k,j}(t))) \rangle, \tag{13}$$

where Δt is the simulation time step, N the total number of molecules, and $r_{l,k}(t)$ the position of molecule/particle l of species k at time t.

Table S2: Diffusion coefficients for the mixed component scenario of the isothermal electrolyte of 1:1 wt.% EC:DEC + 1 M $LiPF_6$ using the barycentric (B), EC- and DEC frames of reference.

Frame of reference	B	EC	DEC
Coefficient	Value × $10^{-11}\,\mathrm{m^2/s}$	Value × $10^{-11}\,\mathrm{m^2/s}$	Value × $10^{-11}\,\mathrm{m^2/s}$
L^{++}	0.35 ± 0.04	0.8 ± 0.1	0.3 ± 0.1
L^{--}	0.7 ± 0.2	1.3 ± 0.2	1.0 ± 0.2
L^{+-}	0.08 ± 0.02	0.56 ± 0.05	0.2 ± 0.1
$L^{\mathrm{D}+}$	0.5 ± 0.1	2.4 ± 0.2	
$L^{\mathrm{D}-}$	-0.3 ± 0.1	1.8 ± 0.2	
L^{DD}	2.8 ± 0.2	11.3 ± 1.3	
$L^{\mathrm{E}+}$	-0.9 ± 0.1		0.1 ± 0.3
$L^{\mathrm{E}-}$	-1.0 ± 0.1		0.9 ± 0.1
L^{EE}	6.1 ± 0.9		20.3 ± 2.3
L^{ED}	-3.4 ± 0.4		

When formulated with fluxes and forces, as defined by the entropy production, eq. 1 in the main text, the fluctuation dissipation theorem refers to coefficients of the flux-force matrix, eq. 2 in the main text. The coefficients dimension in eq. 2 follow, also for isothermal systems, when the factor $1/T$ is contained in the force.

Table S3: Diffusion coefficients for the mixed component scenario of the isothermal electrolyte of 3:7 wt.% EC:DEC + 1 M $LiPF_6$ using the EC frame of reference. Transference coefficients, t, and transport numbers, τ, are dimensionless.

Coefficient	Value ($\times 10^{-11}\,\mathrm{m^2/s}$)	Value ($\times 10^{-9}\,\mathrm{K\,mol^2/(J\,m\,s)}$)
L^{++}	1.1	14.9
L^{--}	1.6	21.4
L^{+-}	0.9	12.3
$L^{\mathrm{D}+}$	4.4	60.0
$L^{\mathrm{D}-}$	4.1	55.9
L^{DD}	24.9	341.9
κ	0.25 S/m	
t_{L}	−1.04	
t_{D}	0.47	
τ_+	0.22	

Table S4: Diffusion coefficients for the mixed component scenario of the isothermal electrolyte of 3:7 wt.% EC:DMC + 1 M $LiPF_6$ using the EC frame of reference. Transference coefficients, t, and transport numbers, τ, are dimensionless.

Coefficient	Value ($\times 10^{-11}\,\mathrm{m^2/s}$)	Value ($\times 10^{-9}\,\mathrm{K\,mol^2/(J\,m\,s)}$)
L^{++}	1.8	31.1
L^{--}	2.3	38.7
L^{+-}	1.3	22.1
$L^{\mathrm{D}+}$	9.5	159.1
$L^{\mathrm{D}-}$	8.0	134.4
L^{DD}	71.8	1205.8
κ	0.54 S/m	
t_{L}	−0.87	
t_{D}	1.29	
τ_+	0.35	

Table S5: Potential contributions to cell voltage in the isothermal case

Electrolyte	A ($10^{-11}\,\mathrm{mol^2/(J\,m\,s)}$)	B	$1/\kappa$ ($\Omega\,\mathrm{m}$)	$\frac{t_{\mathrm{D}}}{F^2}\frac{B}{A}$ ($\Omega\,\mathrm{m}$)	$\frac{t_{\mathrm{L}}}{F^2}\left(-\frac{B}{A}\frac{l_{\mathrm{DD}}}{l_{\mathrm{DL}}}+t_{\mathrm{D}}\frac{T}{l_{\mathrm{DL}}}\right)$ ($\Omega\,\mathrm{m}$)
1:1 EC:DEC	-6.3 ± 2.6	-1.3 ± 0.1	4.4 ± 0.7	2.4 ± 1.7	10.2 ± 4.6
3:7 EC:DEC	−7.8	−1.2	4.0	0.8	9.3
1:1 EC:DMC	−14.7	−1.2	2.2	0.7	5.3
3:7 EC:DMC	−23.0	−1.1	1.9	0.7	3.3

Table S6: Diffusion coefficients for the mixed component scenario of the isothermal electrolyte of 1:1 wt.% EC:DEC + 1 M $LiPF_6$ using the EC frame of reference at 280 and 320 K. Transference coefficients, t, and transport numbers, τ, are dimensionless. Potential contributions to cell voltage in the bottom section. Mean values and standard deviations from two replicas.

Temperature	280 K	320 K
Coefficient	Value ($\times\ 10^{-11}\,\mathrm{m^2/s}$)	Value ($\times\ 10^{-11}\,\mathrm{m^2/s}$)
L^{++}	0.4	1.8
L^{--}	0.5 ± 0.1	2.5
L^{+-}	0.2	1.2
$L^{\mathrm{D}+}$	1.0 ± 0.3	5.3 ± 0.4
$L^{\mathrm{D}-}$	0.6	3.9 ± 0.2
L^{DD}	5.1 ± 1.6	25.2 ± 1.0
κ	$(0.14 \pm 0.04)\,\mathrm{S/m}$	$(0.50 \pm 0.01)\,\mathrm{S/m}$
t_{L}	-0.90 ± 0.12	-0.92
t_{D}	1.31 ± 1.11	0.88 ± 0.13
τ_+	0.33 ± 0.09	0.31 ± 0.01
Potential contributions to cell voltage		
$1/\kappa\ (\Omega\,\mathrm{m})$	7.8 ± 2.4	2.0
$\frac{t_{\mathrm{D}}}{F^2}\frac{B}{A}\ (\Omega\,\mathrm{m})$	5.8 ± 6.1	0.8 ± 0.2
$\frac{t_{\mathrm{L}}}{F^2}\left(-\frac{B}{A}\frac{l_{\mathrm{DD}}}{l_{\mathrm{DL}}} + t_{\mathrm{D}}\frac{T}{l_{\mathrm{DL}}}\right)\ (\Omega\,\mathrm{m})$	15.5 ± 3.5	3.9 ± 0.5

References

(S1) Kjelstrup, S.; Gunnarshaug, A. F.; Gullbrekken, Ø.; Schnell, S. K.; Lervik, A. Transport coefficients for ion and solvent coupling. The case of the lithium-ion battery electrolyte. *The Journal of Chemical Physics* **2023**, *159*, 034104.

(S2) Kirkwood, J. G.; Buff, F. P. The Statistical Mechanical Theory of Solutions. I. *The Journal of Chemical Physics* **1951**, *19*, 774–777.

(S3) Liu, X.; Martín-Calvo, A.; McGarrity, E.; Schnell, S. K.; Calero, S.; Simon, J.-M.; Bedeaux, D.; Kjelstrup, S.; Bardow, A.; Vlugt, T. J. H. Fick Diffusion Coefficients in Ternary Liquid Systems from Equilibrium Molecular Dynamics Simulations. *Industrial & Engineering Chemistry Research* **2012**, *51*, 10247–10258.

(S4) Jamali, S. H.; Wolff, L.; Becker, T. M.; de Groen, M.; Ramdin, M.; Hartkamp, R.; Bardow, A.; Vlugt, T. J. H.; Moultos, O. A. OCTP: A Tool for On-the-Fly Calculation of Transport Properties of Fluids with the Order-n Algorithm in LAMMPS. *Journal of Chemical Information and Modeling* **2019**, *59*, 1290–1294.

(S5) Ganguly, P.; van der Vegt, N. F. A. Convergence of Sampling Kirkwood–Buff Integrals of Aqueous Solutions with Molecular Dynamics Simulations. *Journal of Chemical Theory and Computation* **2013**, *9*, 1347–1355, PMID: 26587597.

(S6) Milzetti, J.; Nayar, D.; van der Vegt, N. F. A. Convergence of Kirkwood–Buff Integrals of Ideal and Nonideal Aqueous Solutions Using Molecular Dynamics Simulations. *The Journal of Physical Chemistry B* **2018**, *122*, 5515–5526, PMID: 29342355.

(S7) Krüger, P.; Schnell, S. K.; Bedeaux, D.; Kjelstrup, S.; Vlugt, T. J. H.; Simon, J.-M. Kirkwood–Buff Integrals for Finite Volumes. *The Journal of Physical Chemistry Letters* **2013**, *4*, 235–238, PMID: 26283427.

(S8) Krishna, R.; van Baten, J. M. The Darken Relation for Multicomponent Diffusion in Liquid Mixtures of Linear Alkanes: An Investigation Using Molecular Dynamics (MD) Simulations. *Industrial & Engineering Chemistry Research* **2005**, *44*, 6939–6947.

(S9) Spitthoff, L.; Gunnarshaug, A. F.; Bedeaux, D.; Burheim, O.; Kjelstrup, S. Peltier effects in lithium-ion battery modeling. *The Journal of Chemical Physics* **2021**, *154*, 114705.

ISBN 978-82-326-7966-9 (printed ver.)
ISBN 978-82-326-7965-2 (electronic ver.)
ISSN 1503-8181 (printed ver.)
ISSN 2703-8084 (online ver.)

NTNU

Norwegian University of
Science and Technology